8th International Conference on

ENVIRONMENTAL EFFECTS ON BUILDINGS AND PEOPLE:

ACTIONS, INFLUENCES, INTERACTIONS, DISCOMFORT

EEBP8

OCTOBER 3-5, 2018, CRACOW, POLAND

Book of Keynote Lectures and Abstracts

EDITORS: TOMASZ LIPECKI, ANDRZEJ FLAGA

Polish Association for Wind Engineering
Cracow-Lublin 2018

AUSPICES:

- Science Committee of the Polish Association of the Civil Engineers and Technicians;
- Polish Society of Bridge Engineers;
- Civil Engineering Committee of the Cracow Branch of the Polish Academy of Science;
- Chamber of Civil Engineers of Małopolska District;
- Cracow University of Technology;
- Lublin University of Technology;
- AMC – Andrzej M. Chołdzyński Sp. z o. o. - Sp.k.

in cooperation with:

- International Association for Wind Engineering

SPONSORS:

CONFERENCE ORGANIZERS:

- Polish Association for Wind Engineering, Member Organization of the International Association for Wind Engineering
  ul. Warszawska 24, 31-155 Kraków, www.psiw.org.pl, liwpk@pollub.pl, t.lipecki@pollub.pl

ORGANIZING COMMITTEE:

- Chairman: Andrzej Flaga
- Secretary: Tomasz Lipecki, Łukasz Flaga
- Members: Ewa Błazik-Borowa, Jerzy Podgórski, Jarosław Bęc, Agata Szeląg, Paulina Jamińska-Gadomska, Renata Kłaput, Agnieszka Kocoń, Piotr Krajewski

SCIENTIFIC COMMITTEE:

- Chairman Tadeusz Chmielewski (Poland)

MEMBERS:

- Alexandru Aldea (Romania)
- Jan Benčat (Slovakia)
- Claudio Borri (Italy)
- Philippe Delpech (France)
- Richard Flay (New Zealand)
- Adam Goliger (RSA)
- Yoshiomi Ito (Japan)
- Roman Kinash (Poland/Ukraine)
- Holger Koss (Denmark)
- Zhu Le-Dong (China)
- Acir M.Loredo-Souza (Brazil)
- Hans J. Niemann (Germany)
- Jerzy Podgórski (Poland)
- Jonas Snaebjörnsson (Iceland)
- Mark Sterling (United Kingdom)
- Thomas Thiis (Norway)
- Takuya Tsutsumi (Japan)
- Hitosi Yamada (Japan)
- Srinvasan Arunachalan (India)
- Bert Blocken (The Netherlands)
- Shuyang Cao (China)
- Andrzej Flaga (Poland)
- Yaojun Ge (China)
- Piotr Górski (Poland)
- José Angel Jurado (Spain)
- Katarzyna Klemm (Poland)
- Hrvoje Kozmar (Croatia)
- Chris W. Letchford (USA)
- Mariusz Maślak (Poland)
- John Owen (United Kingdom)
- Stanislav Pospišil (Czech Republic)
- Giovanni Solari (Italy)
- Krzysztof Szilder (Canada)
- Yoshihide Tominaga (Japan)
- Yasushi Uematsu (Japan)
- Alberto Zasso (Italy)
- Chris Baker (United Kingdom)
- Ewa Błazik-Borowa (Poland)
- Ashraf El Damatty (Canada)
- Olivier Flamand (France)
- Chris Geurts (The Netherlands)
- Geetha Rajasekharan Sabareesh (India)
- Ahsan Kareem (USA)
- Gregory A. Kopp (Canada)
- Kenny Kwok (Australia)
- Tomasz Lipecki (Poland)
- Jiři Náprstek (Czech Republic)
- Siergiej Piczugin (Ukraine)
- Francesco Riccardelli (Italy)
- Ted Stathopoulos (Canada)
- Yukio Tamura (China)
- Tim K. Tse (Hong Kong)
- Wojciech Węgrzyński (Poland)
- Xuanyi Zhou (China)

Polish Association for Wind Engineering, Cracow-Lublin 2018
ISBN 978-83-932544-2-2

Preface

The 8th International Conference on *Environmental Effects on Buildings and People: Actions, Influences, Interactions, Discomfort* (EEBP8) held in Tyniec, Poland, 3-5 October 2018, has been organized by: Polish Association for Wind Engineering, in cooperation with Wind Engineering Laboratory of Cracow University of Technology and Department of Structural Mechanics of Lublin University of Technology under the auspices of:

- Science Committee of the Polish Association of the Civil Engineers and Technicians;
- Polish Society of Bridge Engineers;
- Civil Engineering Committee of the Cracow Branch of the Polish Academy of Science;
- Chamber of Civil Engineers of Małopolska District;
- Cracow University of Technology;
- Lublin University of Technology;
- AMC – Andrzej M. Chołdzyński Sp. z o. o. - Sp.k.

in cooperation with:

- International Association for Wind Engineering.

Seven previous symposia held in Lublin (1994), Kazimierz Dolny (1997), Zwierzyniec (2001), Susiec (2004), Kazimierz Dolny (2007), Tomaszowice near Cracow (2010) and Cracow (2014) were successful, therefore the general subject and particular topics of the 8th Conference have been retained. The three-day conference is filled with a variety of session formats, with a balance of research and practice to permit the widest possible participation, providing an excellent forum to exchange ideas and to progress the scientific field.

The EEBP8 Conference deals primarily with the following topics:

- Environmental effects on buildings and structures (*wind action, snow load, ice accretion and ice load, thermal action of climatic and technological origin, etc.*);
- Wind flows over complex terrain;
- Smog and air pollution reduction and urban ventilation;
- Tornadoes and other nonstationary winds;
- Pedestrian wind comfort and environmental comfort of people in buildings and their surroundings;
- Applied buildings and environmental acoustics;
- Thermal influences on buildings and structures;
- Interactions between environmental actions;
- Ways of reduction of excessive environmental effects on buildings and people;
- CFD applications in environmental actions;
- Wind power plants;
- Problems of standardization of environmental effects on buildings and people;
- New measuring techniques of environmental effects on buildings and people.

The proceedings published in the book of keynote lectures and extended summaries of the papers have been elaborated by people working professionally in many different scientific and scientific-research institutions. The papers are divided into the following thematic groups:

- Aerodynamics of buildings and structures;
- Wind flows over complex terrain and extreme winds;
- Pedestrian wind comfort and environmental comfort;
- Smog reduction and urban ventilation;
- Snow and ice loads;
- Applied building and environmental acoustics;
- Thermal and fire influences on buildings and structures;
- Miscellaneous.

The Conference is addressed to researchers, designers, building experts, consulting workers, students and people involved in measurements and measurement techniques, working in the field of problems comprised by the Conference.

We hope that the Conference will be fruitful for all of the participants and that discussions during the Conference will be continued in the future during the next periodic meetings within the subject.

Last but not least, we would like to thank all the sponsors for their financial support, without which it would not be possible to organize the Conference.

Secretary of the Organizing Committee

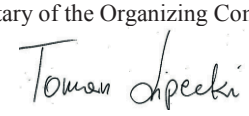

Prof. Tomasz Lipecki

Chairman of the Organizing Committee

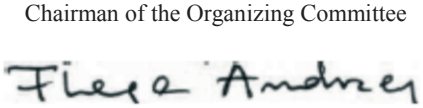

Prof. Andrzej Flaga

Distinguished invited Speakers

Ashraf El Damatty

Department of Civil and Environmental Engineering
Faculty of Engineering
The University of Western Ontario, London, Ontario
Canada
e-mail: damatty@uwo.ca

Dr. Ashraf El Damatty, Professor and Chair of the Department of Civil and Environmental Engineering at the University of Western Ontario, London, Ontario, Canada. He is a Fellow of the Canadian Society of Civil Engineering and the Engineering Institute of Canada. He is a Research Director at the Wind Engineering, Energy and Environment (WindEEE) Research Institute and Co-Editor-in-Chief of the Journal of Wind and Structures. He holds the title of High End Expert at Tongji University, China. He obtained a BSc. and M.Sc. from Cairo University in 1986 and 1991, Ph.D. in Structural Engineering from McMaster University, Canada, in 1995, and an MBA in 2016 in Higher Education Management from University College, London, UK. He is the founder of the Canadian Society of Civil Engineers (CSCE) Steel Structures Committee and serves currently as the Chair of the CSCE Structures Division. He has consulted on many projects in North America and the Middle East He has written over 200 publications and has secured research funding exceeding $15.0 M. He has supervised more than 30 Ph.D. and 20 M.Sc. students and has been invited as keynote speaker in many countries around the globe. He received several awards including the Alan Yorkdale Award by ASTM, Best Paper Award at the Canadian Conference on Effective Design of Structures, Honourable Mention in 2014 Casimir Gzowski Medal Competition, 2015 CSCE Whitman Wright Award, 2016 CSCE Horst Leipholz Medal, Western University Faculty Scholar Award, and the 2018 Ontario Professional Engineers Medal for Research and Development. His research work has influenced the international codes and the Engineering practice worldwide.

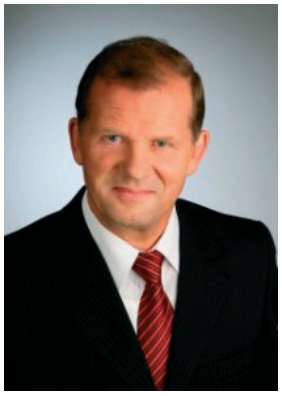

Andrzej Flaga

Institute of Structural Mechanics
Cracow University of Technology
Poland
e-mail: liwpk@windlab.pl

Full Professor at Cracow University of Technology. Outstanding specialist and creator of a Polish school of science in an interdisciplinary field comprising wind engineering, building aerodynamics, environmental effects on buildings and people, snow engineering and structural dynamics. Author or coauthor of 13 books and monographs and over 300 scientific publications. Author of 11 invited/keynote lectures presented on abroad universities and international conferences. Author, coauthor or chief of teams of over 100 scientific-research works, some tens of expert opinions, scientific-technical opinions and 15 grants. Head initiator, designer, implementer, organizer and chief of the world-famous Wind Engineering Laboratory with a boundary layer wind tunnel at the Cracow University of Technology. Head organizer and, for nineteen years, chief of the Chair of Structural Mechanics at Lublin University of Technology. Supervisor of 12 Ph.D. theses and of 90 M.Sc. diploma works. Cofounder and chairman of the Polish Association for Wind Engineering – a member organization of the International Association for Wind Engineering. Member of the scientific committees of many international conferences and symposia. Initiator and chairman of the organizing committees for eight editions of the symposium Environmental effects on buildings and people – actions, influences, interactions, discomfort. Licensed construction engineer. Expert on building techniques and expert of Polish Association of Civil Engineers and Technicians. For the achievements in scientific and scientific-research works awarded with numerous prizes and distinctions by the government ministers and the university rectors.

Mark Sterling

School of Engineering
University of Birmingham, Edgbaston, Birmingham
UK
e-mail: m.sterling@bham.ac.uk

Professor Mark Sterling is Beale Professor of Civil Engineering at the University of Birmingham and has undertaken research in the area of applied fluid mechanics for over 20 years. Within the wind engineering field, Mark's research has focused on transient winds, particularly the effects of extreme winds on infrastructure, vehicles and plants. He has published over 150 peer reviewed journal and conference papers, supervises a large research team and leads a number of international collaborations. He is currently involved in two large multi-disciplinary projects involving biologists, geographers and farmers. He is also co-chair of the upcoming 9th International Colloquium on Bluff Body Aerodynamics and Applications, which will be held in Birmingham in 2020. In addition to his research, Mark is also the Head of the School of Engineering, one of the largest Schools at the University of Birmigham. In a recent National Student Survey, the School was ranked first in the Russell Group for Teaching, first for Assessment and Feedback and first for Overall Satisfaction. The School also holds a prestigious Queen's Anniversary Prize for Higher Education.

Yukio Tamura

School of Civil Engineering
Chongqing University, Chongqing
China
e-mail:yukio@arch.t-kougei.ac.jp

Professor Yukio Tamura has conducted long-term, systematic and in-depth research in all aspects of wind-resistant design of building structures including basic theory of bluff body aerodynamics, rational determination of design wind speed, provision of structural wind loading and calculation of structural equivalent static wind loading, evaluation of structural aerodynamic stability, compilation and revision of the wind resistant design code for building structures, wind hazard mitigation and so on. Professor Yukio Tamura served as the President of the International Association for Wind Engineering (IAWE) for eight years from 2007 to 2015. He has received many awards including the American Society of Civil Engineers (ASCE) Jack E. Cermak Medal in 2004, the ASCE Robert H. Scanlan Medal in 2016, as well as the IAWE Alan Davenport Medal in 2016. Professor Yukio Tamura is a member of the Engineering Academy of Japan, a Foreign Fellow of the Indian National Academy of Engineering, and a Foreign Member of Chinese Academy of Engineering.

Alberto Zasso

Department of Mechanical Engineering
Politecnico Milano
Italy
e-mail: alberto.zasso@polimi.it

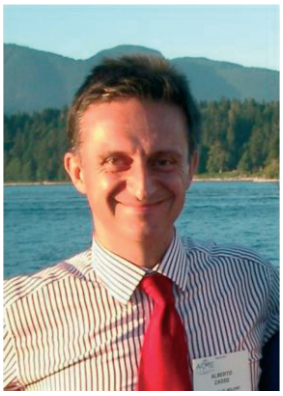

Full Professor in 2008 in Applied Mechanics at Dipartimento di Meccanica-POLIMI. Research activity on the Wind Engineering and Wind Energy fields: 1) fluid-structure interaction of long-span suspension bridges; 2) modal and aeroelastic parameters identification of slender structures under wind action; 3) bluff body fluid-dynamics and vortex shedding induced vibrations of circular and rectangular section cylinders; 4) high rise buildings fluid-structure interaction; 5) wind energy: wind tunnel tests on horizontal axis (scaled models) and vertical axis (scale models & full scale prototypes) wind turbines; 6) CFD modelling of the wind tunnel simulated atmospheric boundary layer (LES Open Foam environment on HPC) for applications on the built environment and on wind turbines. The scientific activity resulted in more than 100 publications at National and International level. President of ANIV, the Italian Wind Engineering Association, member of the Steering Committee of EERA Joint Programme Wind Energy, local coordinator of the two Horizon 2020 Projects CL-Windcon "Closed loop wind farm control" and LIFES50+ "Qualification of innovative floating substructures for 10MW wind turbines and water depths greater than 50m". Responsible for the design and realization of the Boundary Layer Wind Tunnel at Campus Bovisa POLIMI, nowadays the most significant facility for Wind Engineering applications in Europe, Prof. A. Zasso is at present the Director of the Wind Tunnel facility. Concerning the participation to international relevant projects, Prof. Zasso is at present external advisor concerning aerodynamics within the going on construction of the Canakkale world longest span Bridge (Turkey), has been Member of the Panel of Specialists (Expert for Aerodynamics and Aeroelasticity of the bridge) for the P.M.C. Advisory Activity concerning Stretto di Messina Suspension Bridge, member of the research team in charge of the aerodynamic design of the Messina Bridge (Italy Since 1989), member of the design team concerning aerodynamics and Wind Tunnel Tests for BB3 Third Bosphorous Bridge project (Turkey 2013), the Forth Replacement Crossing project (UK 2011), City Life project (Milano 2008). Consultant of leading design and construction companies ARUP (UK), PARSONS (USA), Salini Impregilo (ITALY), ENEL Green Power (ITALY).

Ledong ZHU

State Key Laboratory of Disaster Reduction in Civil Engineering
Department of Bridge Engineering
College of Civil Engineering
Key Laboratory for Wind Resistance Technology of Bridges
(Ministry of Transport)
Tongji University
China
e-mail: Ledong@tongji.edu.cn

Prof. Ledong ZHU graduated from Tongji University and got his bachelor degree in engineering in 1986 and his master degree in engineering in 1989. He studied in the Civil and Structural Department of Hong Kong Polytechnic University during Aug. 1998 and Apr. 2002 and was awarded the degree of doctor of philosophy in Nov. 2002. He has engaged in the wind engineering research for over thirty years, and Up to now, he has published about 140 journal papers . As the project leader, he has finished many wind-resistant projects of long-span bridges, high-rise and super high-ride buildings and TV tower, large span structures, etc. He has also charged or taken part in many wind engineering-related research projects granted by China government departments, such as China Natural Science Foundation, Ministry of Science and Technology, Ministry of Education, etc. In recent years, he has been mainly focused on investigating the theory and wind tunnel test technology related to the nonlinear unsteady self-excited vibration of long-span bridges and bluff bodies, such as flutter, galloping, vortex-induced vibration. He is now the director of Research Division for Wind-resistance of Bridges and Structures of Department of Bridge Engineering of Tongji University, the deputy director of Key Laboratory of Wind Resistance Technology of Bridges (Shanghai) of China Ministry of Transport, one of the core members of State Key Laboratory of Disaster Reduction in Civil Engineering of China. Currently, he acts as the chairman of Wind Engineering Group of China Civil Engineering Society, and is a senior member of China Vibration Engineering Society, a member of International Association for Bridge and Structural Engineering.

Contents

Keynote Lectures:

Aerodynamics of buildings and structures:

Wind flows over complex terrain and extreme winds:

Pedestrian wind comfort and environmental comfort:

Smog reduction and urban ventilation:

Miscellaneous:

Snow and ice loads:

Applied building and environmental acoustics:

Thermal and fire influences on buildings and structures:

Research for adaptive and sustainable structures

Ashraf El Damatty[1], Ahmed Shehata[1], Adnan Enajar[1], Joshua Rosenkrantz[2] and Fouad Elezaby[3]

[1]Department of Civil and Environmental Engineering, Faculty of Engineering, The University of Western Ontario, London Ontario Canada
e-mail: damatty@uwo.ca
[2]Thornton Tomasetti, Toronto, ON, Canada
[3]T.Y Lin International, Miami, Florida, USA

Abstract: Despite the advancement in the fields of Wind and Structural Engineering, the performance of many structures under severe wind storms indicate an inability to adapt to such events. Among structures that have shown to exhibit poor performances are transmission lines especially under high intensity wind (HIW) localized events such as tornadoes and downbursts. An extensive research program was conducted during the past fifteen years at the University of Western Ontario attempting to solve this problem. While it is difficult to prevent failures of all the towers of a line during such events, the research currently assesses the response of an entire line under HIW with aim to minimize the consequences on a grid system. Another type of structures that exhibited a poor performance under hurricanes is twooden houses. The research assesses the structures behaviour of such structures using the finite element method and a probabilistic approach that takes into account the variability in the connection strength. A retrofit technique that was tested using a one third scale of a house at the WindEEE dome is presented. On the other hand, high rise buildings can be overdesigned under wind loads resulting in unsustainable design. The study investigates the use of ductility in the design of high rise buildings under wind loads similar to the approach adopted for years in seismic design.

Keywords: wind engineering, transmission lines, tornadoes, downbursts, wood houses, roofs, high-rise buildings.

1. Introduction

This presentation highlight three research topics in Wind and Structural Engineering that demonstrate the need for development of procedures to improve the adaptation of various structures to severe wind events using sustainable approaches. The first topic considers transmission line structures under High Intensity Wind (HIW) localized events in the form of tornadoes and downbursts. This a significant problem facing the electrical utility industries all over the world as it was reported by Dempsey (1996) that 80% of weather-related transmission line failures worldwide resulted from those events. A brief review of the outcomes of more than 15 years of research conducted at the University of Western Ontario on this subject will be presented. This is followed by a presentation for the current research progress which involves studying the post failure behaviour of a tower and its effect on the progression of failure of the entire line in an attempt to establish a sustainable design since preventing failures of all towers might not be feasible economically under extreme events. The second problem deals with low-rise wood houses subjected to extreme wind events. The research addresses particularly a common type of failure observed extensively during all strong hurricanes and typhoons, which is the de-attachment of the trusses of the roofs of wooden houses from the supporting walls as a result of the uplift pressure acting on the roofs. Full-scale mechanical testing under simulated wind loads and reduced scale wind testing have been conducted at the Insurance Research Lab for Better Homes (IRLBH) and the WindEEE Research Institute, respectively. Detailed non-linear finite element modelling has been conducted as well using both a deterministic and a probabilistic approach. In addition a practical retrofitting technique has been developed and tested. A summary of this research program aiming to make wood houses more adaptable to severe wind storms will be presented. The third study considers high-rise buildings, which had been historically designed to remain elastic under severe wind loads. The modern seismic design codes rely on ductility and allow inelastic actions to happen under severe earthquakes. With the increase in return period of design wind loads, approaching the return periods typically used in seismic design, the authors believes that a similar approach relying on ductility needs to be adopted in wind design for sustainable use of materials. In seismic design, this is achieved through applying a load reduction factor, which needs to be compensated with an equivalent amount of structural ductility. A similar approach is adopted through a case study conducted on a real high rise building tested at the wind tunnel. Here, the reduction factor is applied only to the resonant component and the nonlinear behaviour of the building designed under reduced wind loads is assessed.

2. Transmission Line Structures under HIW events

Failures of transmission lines structures under HIW events have been occurring very frequently during the past two decades. Examples include failures in Australia (Hawes and Dempsey (1993) and Li (2000)), Slovakia (Kanak et al. (2007)), China (Zhang (2006)) and Canada (McCarthy and Melsness (1996)). The first author and his research collaborators started working on this subject more than fifteen years ago. The research used various tools and covered various aspects including computational fluid dynamics simulations of the downburst and tornado wind fields (Aboshosha et al. (2015) and Kim and Hangan (2007)), development of nonlinear finite element models (Shehata et al. (2005), Hamada et al. (2010) and Ibrahim et al. (2017)) and development of semi-analytical solutions for the conductors' behaviour under HIW fields (Aboshosha and El Damatty (2014) and Aboshosha and El Damatty (2015a)). One specific feature about the analysis of transmission line structures under HIW events results from their localized nature. The forces acting on the line depends on the location of the event. As such the prediction of the internal forces in members of a transmission tower requires conducting a large parametric study in which the location of the event is varied, which was incorporated in the developed numerical models. The research also included assessment of structural and failure behaviour of the towers (Shehata and El Damatty (2007), Shehata and El Damatty (2008), Shehata et al. (2008), Hamada and El Damatty (2011), Darwish and El Damatty (2011), ladubec et al.(2012), Altalmas et al. (2012), Hamada and El Damatty (2011) and Hamada and El Damatty (2016)), aero-elastic testing of line systems at both the Boundary Layer Wind Tunnel (BLWT) and at the Wind Engineering, Energy and Environment (WindEEE) laboratories (Hamada et al.(2017), Elawady et al. (2016) and Elawady et al. (2018)), assessment of dynamic behaviour of the

towers and the lines (Darwish et al (2010) and Aboshosha and El Damatty(2015)), and the development of design load cases for the ASCE-74 that simulate the critical effects of downbursts and tornadoes on transmission line structures (Elawady and El Damatty (2016), Elawady and El Damatty (2018) and El Damatty et al. (2015) and El Damatty and Hamada (2016)). A photo of the aero-elastic test conducted at WindEEE is presented in Fig.1. A major outcome of this research program was the development of a unique structural Software, called "HIW", which can predict the behaviour of TL structures under downbursts and tornadoes. The research is currently progressing by extending this numerical model to be able to predict the behaviour of an entire line before and after the collapse of an individual tower. This is important since it is not sustainable to design all towers to resist extreme downburst and tornado events. In the same time, the failure of a significant portion of a line can be very devastating. As such, a performance based design needs to be adopted such that the negative consequences of a tower failure are minimized while considering the importance of the line. The challenge in the development of such a model that it requires the prediction of the post failure behaviour of a tower and its effect, through the conductors' behaviour, on the adjacent towers. Various steps as well as the challenges involved in the development of a numerical model that can predict the response of an entire transmission line system under HIW events will be presented.

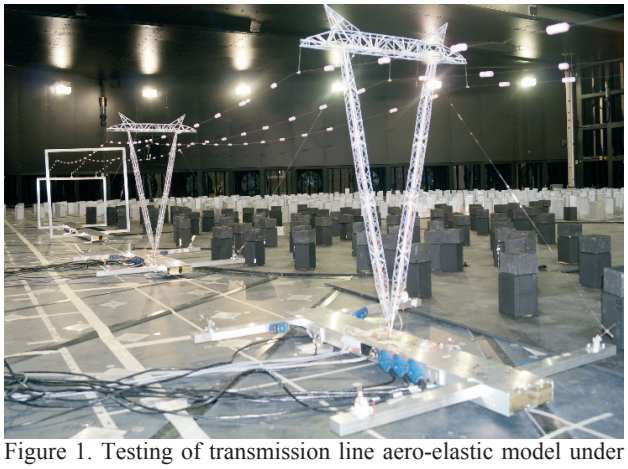

Figure 1. Testing of transmission line aero-elastic model under downburst.

3. Wood Houses

Tremendous losses has been observed in wood frame houses during major hurricane and typhoon events (Li and Ellingwood, 2005). A dominant type of failure extensively occurred at the roof-to-wall connections (RTWCs) as a result of the suction pressure. This leads to the de-attachment of the roof trusses from the supporting walls, which becomes unsupported and eventually collapse. A research facility was established of Western Ontario, called the Insurance Research Lab for Better Homes (IRLBH). This facility allows testing up to two-story full-scale houses under simulated uplift wind load through the use of large number of pressure boxes that can be controlled separately. During the past ten years, the first author and his coworkers have conducted an extensive research program on this subject. A test of a full-scale house roof previously conducted at the IRLBH (Morrison et al. (2012)) was numerically simulated using a non-linear finite element model. The comparison was carried out at wind speed of 35 m/sec during which the nails connecting the trusses to the walls exhibit non-linear hysteresis behavior. Compared to the experimental results, the numerical model was able to predict accurately the non-linear cyclic behavior of roof. Details of the numerical model and comparisons of its prediction with experimental results can be found in (Jacklin et al. (2014) and Enajar et al. (2018)). The research also proceeded by developing a retrofit technique that allows existing houses to adapt to severe wind storms. The advantage of this retrofit scheme is that it does not require expensive alteration for an existing house. It consists of wires that rest on the roof and are attached to rigid bar which is connected to external cables supported by micro-piles permanently embedded in the ground. This allows the suction loading to have an alternative path rather than being transferred through the RTWC connections. The adequacy of this retrofit was assessed through various research stages. First, it was assessed numerically using finite element modeling. Second, it was examined experimentally by conducting structural tests of a number of full-scale trusses with and without the retrofit technique. The third stage was conducted also experimentally at the WindEEE research facility using a one-third scale of an entire house. The tests indicated an excellent performance and the results have shown that a full-scale house can be upgraded from category I to category IV resistant hurricanes. A photo of the test conducted at WindEEE is shown in Fig.2. Coupling the Genetic Algorithm approach with the Finite Element Method, a numerical tool was developed for optimizing the design of various components of the retrofit system for any roof shape under a certain design wind speed. An important accomplishment in this research was the development of a semi-analytical solution that can predict accurately the uplift response of roof with and without the retrofit system.

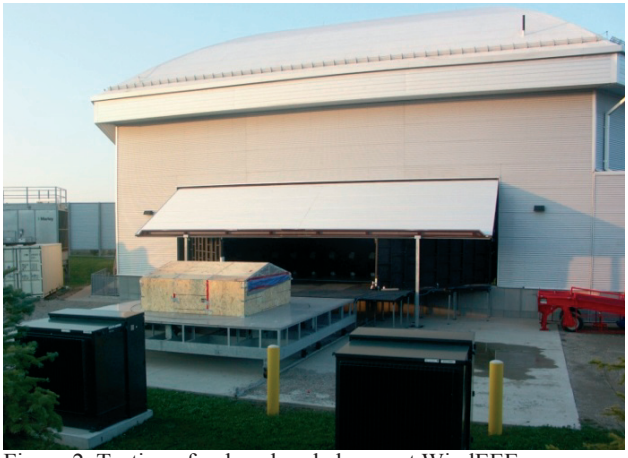

Figure 2. Testing of reduced scale house at WindEEE.

4. Non-Linear Design of Buildings

The design of buildings under wind loads had been always conducted such that the structures are expected to behave elastic under the specified loads. This in unlike the design under seismic loads in which modern building codes allow inelastic action to happen under large return period earthquake loads. In this approach, the seismic demand on the structures is modified by reducing the seismic elastic loads by large load reduction factors. The structures rely on their ductility to dissipate the energy of the strong earthquakes through inelastic actions. A survival limit state is adopted under such severe earthquakes such that the building might suffer from damage but no collapse. The recent design winds in many specifications are based on an increased return periods approaching the return periods of the earthquakes. The study poses the question if this approach used in seismic design can be adopted in wind design. A case study of a real high rise previously tested at the Boundary Layer Wind Tunnel Laboratory at the University of Western Ontario is considered to assess the implications of considering a nonlinear design under wind loads. The resonant component of the building is evaluated based on wind tunnel pressure measurements and finite element modelling. A load reduction factor is applied to

the resonant component only and the building is re-designed under the reduced set of loading. Wind loads are then re-calculated due to the change in the building period resulting from the reduction in the building cross sections. Non-linear push over analyses are then conducted to assess the expected performance level of the building designed to behave inelastically under the extreme wind loads. The results indicate a very promising behaviour for the considered case. Future studies needed for the establishment of a nonlinear design procedure of buildings under wind loads are discussed.

Figure 3. Wind tunnel test for a tall building.

5. Acknowledgments

This work was sponsored by the Natural Science and Engineering Research Council of Canada, the Ontario Centre of Excellence and the two companies Hydro One, and Steelcon Engineering.

6. References

Aboshosha H., El Damatty A.A. *Effective technique to analyze transmission line conductors under high intensity winds.* Wind and Structures, An International Journal 18 (2014) 235–252.

Aboshosha H., El Damatty A. *Engineering method for estimating the reactions of transmission line conductors under downburst winds*. Engineering Structures 99 (2015a) 272–284.

Aboshosha H., El Damatty A.A. *Span reduction factor of transmission line conductors under downburst winds*. Journal of Wind and Engineering 11(1) (2014) 13-22.

Aboshosha H., Bitsuamlak G., El Damatty A.A. *Turbulence characterization of downbursts using LES*. Journal of Wind Engineering and Industrial Aerodynamics 136 (2015) 44-61.

Aboshosha H., El Damatty A.A. *Dynamic response of transmission line conductors under downburst and synoptic winds*. Wind and Structures, an International Journal 21(2015) 241-272.

Altalmas A., El Damatty A.A., Hamada A. *Progressive failure of transmission towers under tornado loading*. Proceedings of the 3rd International Structural Specialty Conference (CSCE), Edmonton, Canada, 2012.

Darwish M.M., El Damatty A.A., Hangan H. *Dynamic characteristics of transmission line conductor and behaviour under turbulent downburst loading*. Wind and Structures, an International Journal 13(4) (2010) 327-346.

Darwish M.M., El Damatty A.A. *Behaviour of self-supported transmission line towers under stationary downburst loading*. Wind and Structures, an International Structure 14(5) (2011) 481-498.

Dempsey D., White H. *Winds wreak havoc on lines*. Transmission and Distribution World 48(6) (1996) 32–37.

Elawady A., El Damatty A.A. *Longitudinal force on transmission towers due to non-symmetric downburst conductor load*. Engineering Structures 127 (2016) 206-226.

Elawady A., Aboshosha H., El Damatty A.A., Bitsuamlak G., Hangan H., Elatar A. *Aeroelastic testing of multi-spanned transmission line subjected to downbursts*. Journal of Wind Engineering and Industrial Aerodynamics 169 (2017) 194-216.

Elawady A., El Damatty A.A. *Critical load cases for lattice transmission line structures subjected to downbursts: economic implications for design of transmission lines*. Engineering Structures 159 (2018) 213-226.

Elawady A., Aboshosha H., El Damatty A.A. *Aero-elastic response of transmission line system subjected to downburst wind: validation of numerical model using experimental data*. Wind and Structures, an International Journal, (Accepted 2018).

El Damatty A.A., Hamada M., Hamada A. *Load cases for transmission line structures*. 14th International Conference on Wind Engineering (ICWE14), Brazil, 2015.

El Damatty A.A., Hamada A. *F2 tornado velocity profiles critical for transmission line structures*. Engineering Structures 106 (2016) 436–449.

Enajar F.E., Jacklin R.B., El Damatty A.A. *Nonlinear modeling of roof to wall connections in a gable-roof structure under uplift wind loads*. Submitted to Wind and Structures (2018).

Hamada A., El Damatty A.A., Hangan H., Shehata A.Y. *Finite element modelling of transmission line structures under tornado wind loading*. Wind and Structures, an International Journal 13 (2010) 451–469.

Hamada A., El Damatty A.A. *Behaviour of guyed transmission line structures under tornado wind loading*. Computers and Structures, 89(11-12) (2011) 986-1003.

Hamada A., El Damatty A.A. *Behaviour of transmission line conductors under tornado wind loads.* Wind and Structures, an International Journal 22(3) (2016) 369-391.

Hamada A., El Damatty A.A. *Failure analysis of guyed transmission lines under F2 tornado event*. Engineering Structures 85 (2015) 11-25.

Hamada A., King J.P.C., El Damatty A.A., Bitsuamlak G., Hamada M. *The response of a guyed transmission line system to boundary layer wind*. Engineering Structures 139 (2017) 135-152.

Hawes H., Dempsey D. *Review of recent Australian transmission line failures due to high intensity winds*. Proceedings of the Task Force of High Intensity Winds on Transmission Lines, Buenos Aires, 1993.

Ibrahim A., El Damatty A.A., El Ansary A. *Finite element modelling of pre-stressed concrete poles under downbursts and tornados*. Engineering Structures 153 (2017) 370-382.

Jacklin R.B., El Damatty A.A., Dessouki A.A. *Finite-element modeling of a light-framed wood roof structure*. Wind and Structures 19(6) (2014) 603-621.

Kanak, J., Benko, M., Simon, A., and Sokol, A., *Case study of the 9 May 2003 windstorm in southwestern Slovakia*. Atmos. Res. 83 (2007)162-175.

Kim J., Hangan H., *Numerical simulations of impinging jets with application to downbursts*. Journal of Wind Engineering and Industrial Aerodynamics, 95(4) (2007) 279-298.

Ladubec C., El Damatty A.A., El Ansary A.M. *Effect of geometric nonlinear behaviour of guyed transmission tower under downburst loading*. Applied Mechanics and Materials 226-228 (2012) 1240-124.

Li C.Q. *Stochastic model of severe thunderstorms for transmission line design*. Probabilistic Engineering Mechanics 15(4) (2000) 359-364.

Li Y., Ellingwood B.R. *Hurricane damage to residential construction in the US: Importance of uncertainty modelling in risk assessment*. Engineering Structures 28(7) (2006) 1009-1018.

McCarthy P., Melsness M. *Severe weather elements associated with September 5, 1996 hydro tower failures near Grosse Isle, Manitoba, Canada*. Manitoba Environmental Service Centre, Environment Canada, 1996.

Morrison M.J., Henderson D.J., Kopp G.A. *The response of a wood-frame, gable roof to fluctuating wind loads*. Engineering Structures 41 (2012) 498-509.

Shehata A.Y., El Damatty A.A., Savory E. *Finite element modelling of transmission line under downburst wind loading*. Journal of Finite Element in Analysis and Design 42(1) (2005) 71-89.

Shehata A.Y., El Damatty A.A. *Behaviour of guyed transmission line structures under downburst wind loading*. Winds and Structures, an International Journal 10(3) (2007) 249-268.

Shehata A.Y., El Damatty, A.A. *Failure analysis of a transmission tower during a microburst*. Wind and Structures, an International Journal 11(3) (2008)193-208.

Shehata A.Y., Nassef A.O., El Damatty A.A. *A coupled finite element-optimization technique to determine critical microburst parameters for transmission towers.* Journal of Finite Element in Analysis and Design 45(1) (2008) 1-12.

Zhang Y. *Status quo of wind hazard prevention for transmission lines and countermeasures*. East China Electric Power, 34(3) (2006) 28-31.

Dynamic action on atmospheric boundary layer as an effective method of improving the urban areas ventilation with similarity criteria of the problem

Andrzej Flaga

Institute of Structural Mechanics, Cracow University of Technology, Poland,
e-mail: liwpk@windlab.pl

1. Introduction

On 14th May 2016 the World Health Organization issued a report [1] of air pollution in urban areas. This illustrates the problem of smog and decreasing level of ventilation conditions faced by modern towns, cities and urban areas all over the Europe. These problems are very important and serious in many towns, cities and villages in Poland, especially located in mountain valleys (e.g. Żywiec, Nowy Sącz, Zakopane) and troughs (e.g. Cracow) (Fig. 1). It is similar in many other countries all over the world. Deterioration of air quality is caused not only by the growth of industry, communication or population, but also by blocking of natural ventilation channels.

Hence, an idea came up to improve the conditions of urban areas ventilation by forcing dynamically the movement of air masses in urban areas assuming the following ways of moving the air masses:

S1. Mechanical generation of additional horizontal air streams in parallel configurations of stream generation points (Fig. 2a) as well as additional horizontal vortex air streams in circulating configurations of stream generation points (Fig. 2b);

S2. Mechanical generation of additional horizontal radial air streams in concentric configurations of stream generation points cooperating with central ventilation vertical exhaust system (Fig. 3).

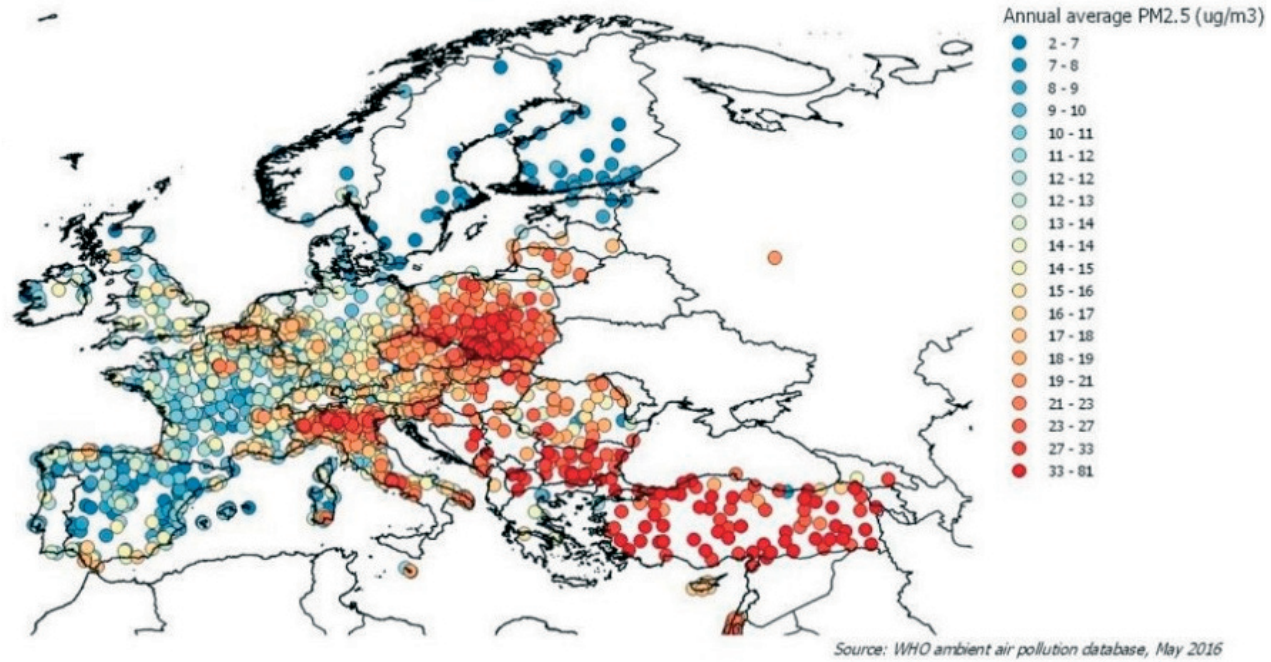

Figure 1. Average air pollution levels in European cities [1].

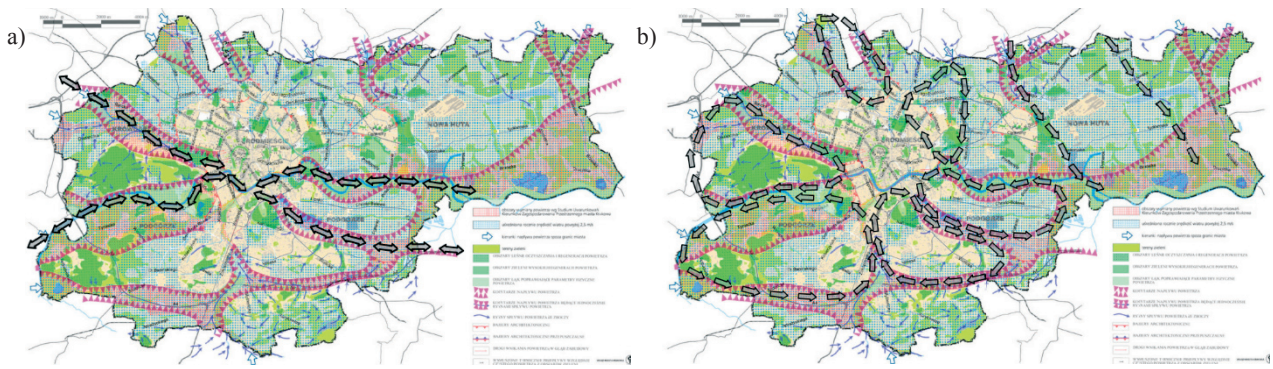

Figure 2. Concept sketch of additional air streams generated mechanically on the example of air exchange and regeneration system for Cracow [2]: a) horizontal air streams in parallel configuration of stream generation points; b) horizontal vortex air streams in circulating configurations of stream generation points.

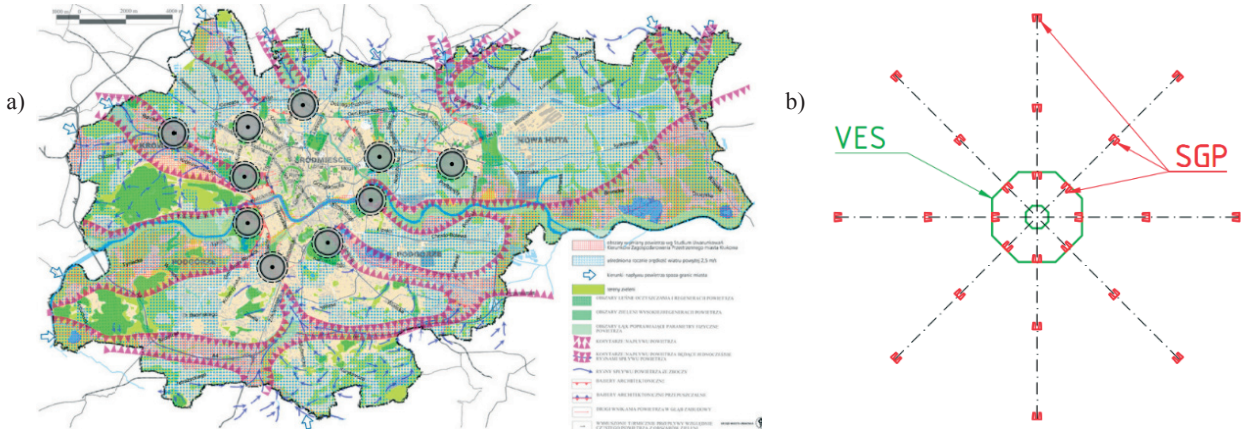

Figure 3. Concept sketch for: a) locating the areas for horizontal radial air streams generation and the central ventilation vertical exhaust systems – on the example of air exchange and regeneration system for Cracow [2]; b) single radial system of stream generation points (SGP) cooperating with central ventilation vertical exhaust system (VES).

It is worth mentioning that the team from Wind Engineering Laboratory of the Cracow University of Technology, chaired by the Author, submitted two solutions considering this problem to the Patent Office, i.e.:

- System of the linear configuration ventilation towers for forcing the air masses movements over open spaces, especially for generating and maintaining air streams over urban areas. Submission No.: **P.424785** [WIPO ST 10/C PL424785];
- System of the concentric configuration of ventilation towers with a central ventilation chimney for forcing the air masses movements over open spaces. Submission No.: **P.424786** [WIPO ST 10/C PL424786].

The idea of two systems for forcing the air masses movements over urban areas are presented in Fig. 4 and 5.

To investigate the phenomenon of dynamic action on atmospheric boundary layer one should analyse some individual items that affect the final result, especially:

- a method of horizontal and vertical air streams generation;
- forming air streams (turbulence reduction, flow rate control, elimination of local losses);
- aerodynamic interference between generated air streams;
- parameters that affect the movement of air streams, i.e. terrain roughness, flow resistance, distribution of pressure, temperature and density of the air in atmospheric boundary layer.

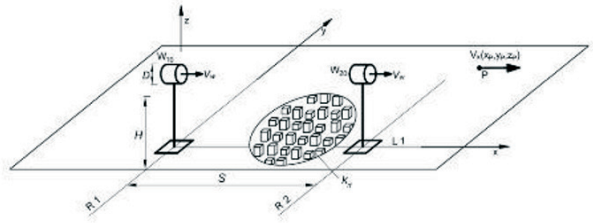

Preliminary test results: single row of 3 fans separated by a distance of 3 diameters and two rows located 370 cm apart from each other of 3 fans separated by a distance of 3 diameters (empirically determined the most efficient of the tested configurations in the scale of 1:833).

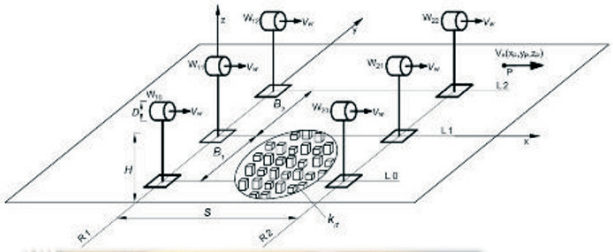

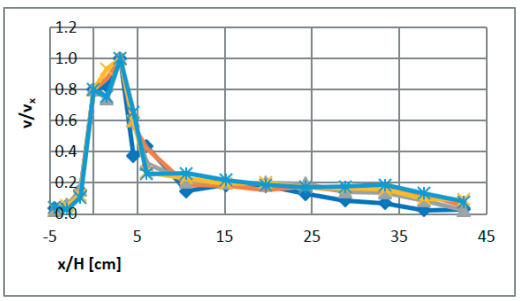

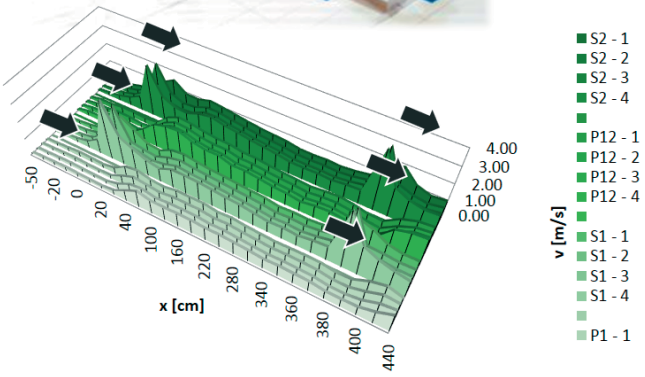

Figure 4. Idea of the system of linear configuration for forcing the air masses movements over urban areas.

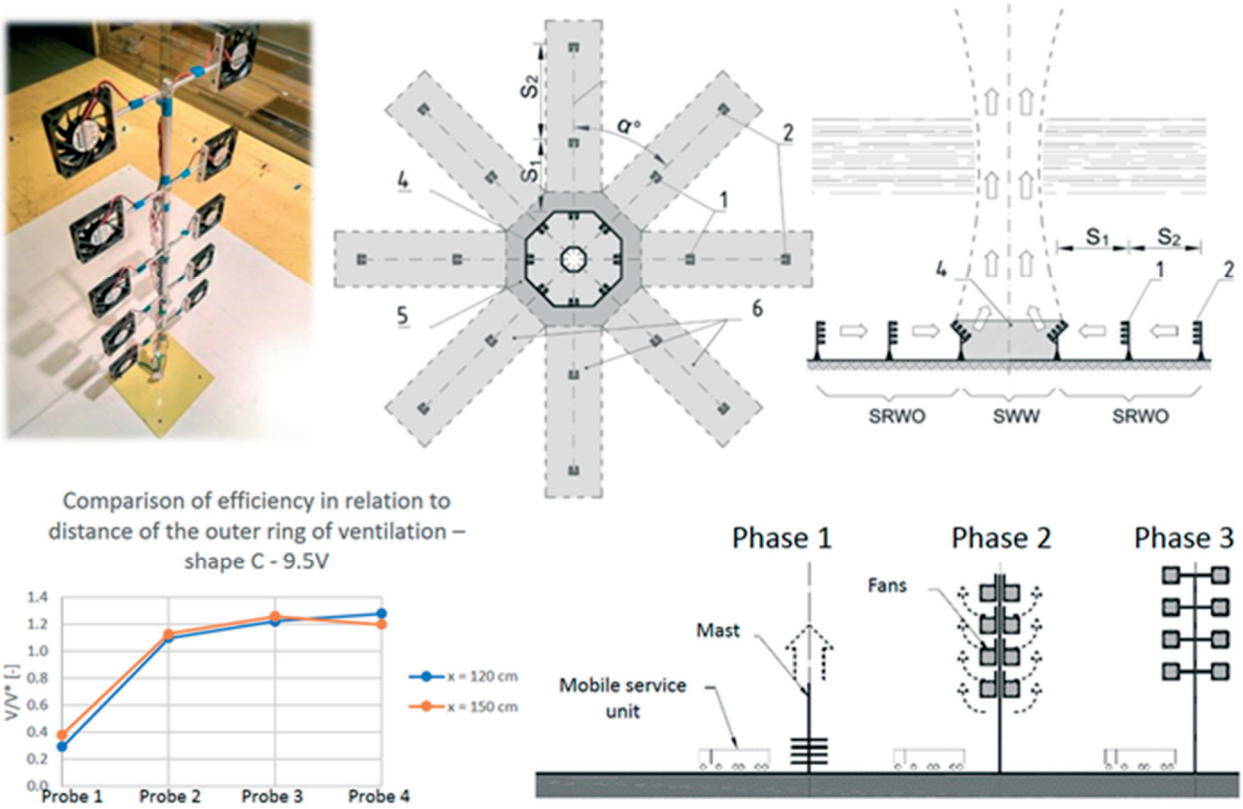

Figure 5. Idea of the system of concentric configuration for forcing the air masses movements over urban areas.

In order to verify the possibility of the solutions success, preliminary model works and studies were carried out in the Wind Engineering Laboratory at the Cracow University of Technology. The whole work entitled „Preliminary investigations of the possibility of dynamic action on the atmospheric ground level" contain 3 stages: Stage 1 - Measurements of flow velocity fields and ranges of the air streams generated by the models of fans / ventilation towers in different variants of their parallel configurations [36]; Stage II - Measurements of flow velocity fields and ranges of air streams generated by models of system of fans/ventilation towers in different variants of their concentric configurations with a ventilation chimney located in the centre [37]. Stage III - Measurements of selected issues from stages I and II, taking into account the influence of terrain roughness (urban development) [38]. These stages were done within the grant founded by the Civil Engineering Faculty of the Cracow University of Technology.

2. Relevant studies and papers connected with the problem

Current solutions used to improve the ventilation conditions in urban areas mainly relate to application of preventive measures such as:

- reduction of pollution sources [3, 4] based on air quality monitoring [5];
- urban planning for the purpose of ensuring adequate ventilation conditions [6, 7].

These actions are passive in nature, i.e. they are only suitable for prevention of unfavourable ventilation conditions in urban areas. This is certainly the best way to act against bad ventilation conditions, but not always sufficient.

The ventilation system sometimes requires some support. For this purpose, active actions are required, which may improve the existing conditions. The use of air purifiers may be such an active solution [8, 9, 10]. There is also the idea to create barriers in the form of water walls to block the flow of pollution from industrial areas [11]. Nevertheless, the territorial range of all these actions is rather local. Therefore, paper [12] suggests using an air exchange and regeneration system as a global active measure against bad aero-sanitary conditions in urban areas. Hitherto, such a system has not been created and applied. What is more, it has not been investigated whether it would be physically possible to create such a system as well as whether the system would be economically justified.

The research, that is the subject of this request, will cover the study of the phenomenon of dynamic action on atmospheric boundary layer. The authors aim to investigate whether it is possible to force the movement of air mass on such a large scale. The study will also include an analysis of this phenomenon effectiveness. To emphasise the pioneering nature of this type of research, it is worthwhile to analyse the current state of knowledge in the field of the urban ventilation as well as the phenomenon of forced air masses movements. Thus, these are some relevant studies that have been conducted and described so far:

- studies of natural ventilation channels in the urban areas: CFD simulations of air pollution dispersion in urban areas [13,14], wind tunnel tests of wind conditions in urban areas [15], comparisons of CFD results with wind tunnel measurements [14], influence of the terrain (buildings, roughness, etc.) on natural ventilation channels [16, 17, 18, 19];
- influence of wind conditions on the transport of air pollution outside the urban areas as well as on change of urban microclimatic conditions [20];
- study on the phenomenon of forced air movement on a small scale (home ventilation) [21, 22];

- study of natural vertical air movement: impact of cities thermal conditions on their ventilation [23,24, 25];
- study of forced vertical air movement: increasing the efficiency of small-scale ventilation by creating a tornado-like artificial vortex [26]; patent for the cooling tower with forced ventilation and natural draft [27] or cooling tower discharging the polluted air after breaking through the inversion layer [28, 29]; study of the process for reducing smog by the chimney inversion/injector effect – sucking warmer and cleaner air from the higher layers towards the ground by pipelines [30];
- aerodynamic interference test: mainly aerodynamic interference study of buildings, objects [31]; investigation of generated air streams interference only in vertical direction and on a small scale [32];
- similarity criteria for the phenomenon of dynamic action on atmospheric boundary layer: only own works discussed in the pre-test section.

Summing up the above literature review, it is evident that there are many gaps in the state of knowledge about the phenomenon of dynamic action on atmospheric boundary layer. First of all, no one has ever thoroughly investigated the mechanical movements of air masses on such a large scale. Moreover, the effectiveness of such a dynamic action is not known. So far, there is also little information about the aerodynamic interference of the generated air streams. This phenomenon is particularly important since, as a result of air streams interference, the efficiency of the system can be dramatically improved or deteriorated. Another issue that requires extensive research is a penetration through the inversion layer and throwing the previously sucked air (for example polluted air) over this layer. It is necessary to answer the question whether such action is physically feasible and economically justified.

All of the aforementioned shortcomings and doubts are the subject of the presented authorial research works as well as research works planned in the near future. Hence, it is clear that the done and planned studies are reasoned and pioneering. What is more, the research results will have a significant impact on the development of a scientific discipline that is environmental engineering, especially dynamics of atmospheric boundary layer. The detailed analysis of the phenomenon of dynamic action on atmospheric boundary layer makes it possible to fully describe all factors that may affect the feasibility and effectiveness of such dynamic action. In the longer term, this phenomenon could be used to improve the aero-sanitary conditions of many urban areas if their natural ventilation is insufficient.

3. General description of the model tests and assumed similarity criteria

At the beginning, it was necessary to adopt a model of stream generation points (SGP) and vertical exhaust system (VES) for all conducted tests. It was assumed that SGP would be modelled in the form of a ventilation towers each equipped with several single fans. The assumed dimensions of such a tower in real scale are shown in Fig. 6a. Furthermore, a vertical exhaust system was modelled as a chimney assisted by ventilation towers. The dimensions and position of the chimney were related to the thickness and height of the inversion layer (Fig. 6b).

It was assumed that most of the tests would be conducted on scale models. Model tests reflect the reality with satisfactory accuracy if the basic relations in analysed phenomenon are preserved. Hence, the first key step in initial test was to define these relations, i.e. similarity criteria, which must be fulfilled during investigations. The following elements of the system were analysed, from the most basic to the more complex sets [33-38]:

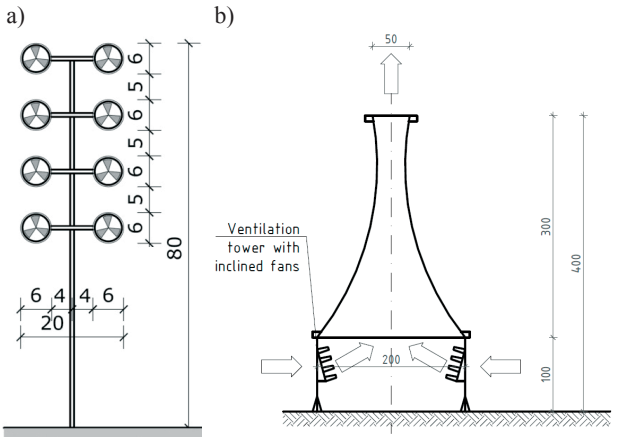

Figure 6. Sketch and dimensions in [m] of assumed system elements in real scale: a) stream generation point as a tower equipped with several fans; b) vertical exhaust system as a chimney supported by ventilation towers

A. Single ventilation tower with multiple parallel similar fans

As first, a ventilation tower equipped with multiple parallel similar fans was studied. Its concept scheme showing the relevant parameters is shown in Fig. 7.

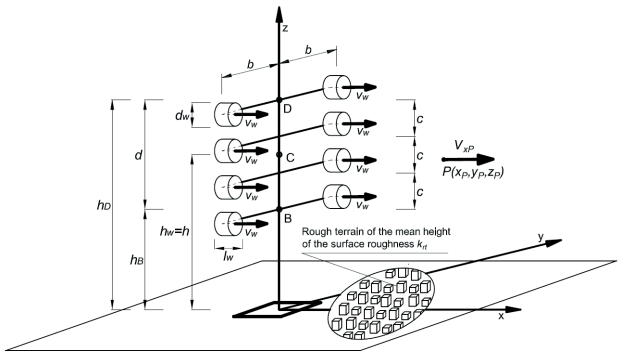

Figure 7. Sketch of ventilation tower equipped with eight fans; each fan generates an air stream of mean outlet velocity v_w.

The x-component of the mean air stream velocity at point P (x_P, y_P, z_P) marked as V_{xP} is a function dependent on the following factors: geometric parameters of a ventilation tower (h_B, d, h, h_D, c, b), geometric parameters of a single fan (d_w, l_w, …) = (g_w), mean outlet air velocity (v_w), coordinates of point P: (x_P, y_P, z_P), physical characteristics of air (ρ – mass density, μ – dynamic viscosity, $\nu = \mu/\rho$ – kinematic viscosity), terrain roughness parameters (k_{rt} – mean height of the surface irregularity – assuming quite uniformly rough terrain). Based on all above parameters, the undermentioned functional relationship can be stated:

$$V_{xP} = F[h_B, d, h, h_D, c, b; (g_w); (x_P, y_P, z_P); v_w, \rho, \mu; k_{rt}]. \quad (1)$$

Assuming the dimensional base of the problem as (ρ, v_w, h) and using the Π (Buckingham) theorem that concerns the dimensional analysis, the following dimensionless function is defined:

$$\check{V} = \frac{V_{xP}}{v_w} = \check{F}[\frac{h_B}{h}, \frac{d}{h}, \frac{h}{h}, \frac{h_D}{h}, \frac{c}{h}, \frac{b}{h}; (\check{g}_w); \left(\frac{x_P}{h}, \frac{y_P}{h}, \frac{z_P}{h}\right); Re^*; \check{k}_{rt}], \quad (2)$$

where $Re^* = \frac{v_w h \rho}{\mu} = \frac{v_w h}{\nu}$ is a Reynolds number, $\check{k}_{rt} = \frac{k_{rt}}{h}$ is a dimensionless roughness of the surface.

From above relations it follows that at given dimensionless geometric parameters of ventilation tower and fans, dimensionless velocity $\check{V}$ depends on: dimensionless coordinates of point P $\left(\frac{x_P}{h}, \frac{y_P}{h}, \frac{z_P}{h}\right)$, Reynolds number *Re* and dimensionless roughness of the surface $\check{k}_{rt}$. The easiest method of achieving the individual values of the function $\check{F}$ is conducting series of model tests.

B. Single ventilation tower with one substitutive fan

Stream generation point can be modelled in a simpler way as a single ventilation tower with one substitutive fan (Fig. 8) generating air stream of a mass flow rate Q_w equal to the sum of mass flow rates $\sum q_w$ of eight (or, in the general, n_w) fans mounted on the ventilation tower presented in Fig.4.

In this case:

$$Q_w = \rho A_w V_w = \rho \frac{\pi D_w^2}{4} V_w,$$
$$q_w = \rho a_w v_w = \rho \frac{\pi d_w^2}{4} v_w, \tag{3-5}$$
$$Q_w = n_w q_w = 8 q_w,$$

where A_w is an area of substitutive fan, a_w is an area of each single fan and V_w is a mean outlet velocity of a substitutive fan. Therefore:

$$A_w V_w = 8 a_w v_w \text{ or } D_w^2 V_w = 8 d_w^2 v_w, \tag{6}$$

$$V_w = 8 \frac{a_w}{A_w} v_w \text{ or } V_w = 8 \left(\frac{d_w}{D_w}\right)^2 v_w. \tag{7}$$

Assuming $V_w = v_w$, we obtain that: $A_w = 8 a_w$ or $D_w = \sqrt{8} d_w$. Dimensionless functional relationship for ventilation tower with one substitutive fan can be defined as follows:

$$\check{V}^* = \frac{V_{xP}{}^*}{V_w} = \check{F}^* \left[\frac{D}{H}; (\check{G}_w); \left(\frac{x_P}{H}, \frac{y_P}{H}, \frac{z_P}{H}\right); Re; \check{k}_{rt}\right], \tag{8}$$

where: $Re = \frac{V_w H}{\nu}$.

For comparable parameters of both functions $\check{F}$ and $\check{F}^*$ it can be stated that $\check{V}^* = \check{V}$. For further considerations of similarity criteria for different set-ups of stream generation points, it was assumed that they are modelled as a ventilation towers with individuals substitutive fans.

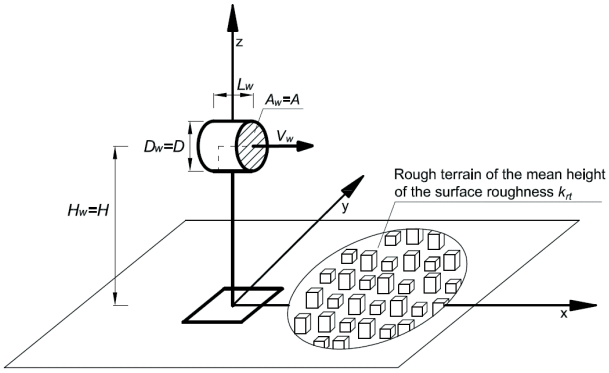

Figure 8. Sketch of single ventilation tower with one substitutive fan.

C. Array of substitutive ventilation towers

Now, let us consider a general case for a system of multiple substitutive ventilation towers located at the nodes of a regular mesh where towers are located side-by-side in rows in the *y*-direction and one-by-one in lines in the *x*-direction as shown in Fig. 9. Additional parameters of this issue are: distances between rows L; distances between the lines B; number of rows n_y; number of lines n_x.

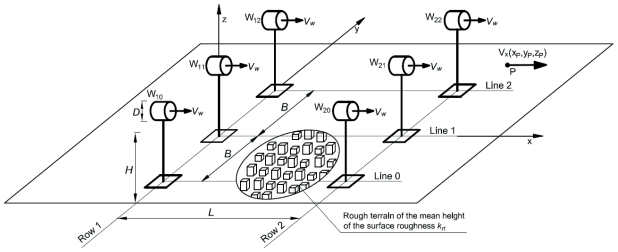

Figure 9. Six substitutive ventilation towers on a meshed system of two rows and three lines.

By conducting a dimensional analysis as above, the resulting functional relationship is [33]:

$$\check{V}^{**} = \frac{V_{xP}{}^{**}}{V_w} = \check{F}^{**}\left[\frac{D}{H}, \frac{L}{H}, \frac{B}{H}; (\check{G}_w); \left(\frac{x_P}{H}, \frac{y_P}{H}, \frac{z_P}{H}\right); Re; \check{k}_{rt}\right]. \tag{9}$$

D. Ventilation chimney with concentric configuration of substitutive ventilation towers

The last element of the examined system is a ventilation chimney. For similarity analysis, it was considered a set consisting of a chimney, two rows of substitutive ventilation towers arranged concentrically around the chimney (cf. Fig.3b) as well as a relevant section of atmospheric boundary layer. Fig.10 shows the most important dimensional and dimensionless parameters of this set in its vertical plane [34]. The whole set, marked as V, is divided into four subsystems I – IV. In addition, in Fig.10 there are marked vertical distribution of static pressure p, mass density ρ and absolute temperature T throughout the analysed atmospheric boundary layer.

Ventilation towers which are a part of the set are arranged regularly around the chimney once every β angle. Towers located in the inlet row – round about the chimney – generate an air streams of velocity V_{wo}, whilst towers in the first row generate an air streams of velocity V_w.

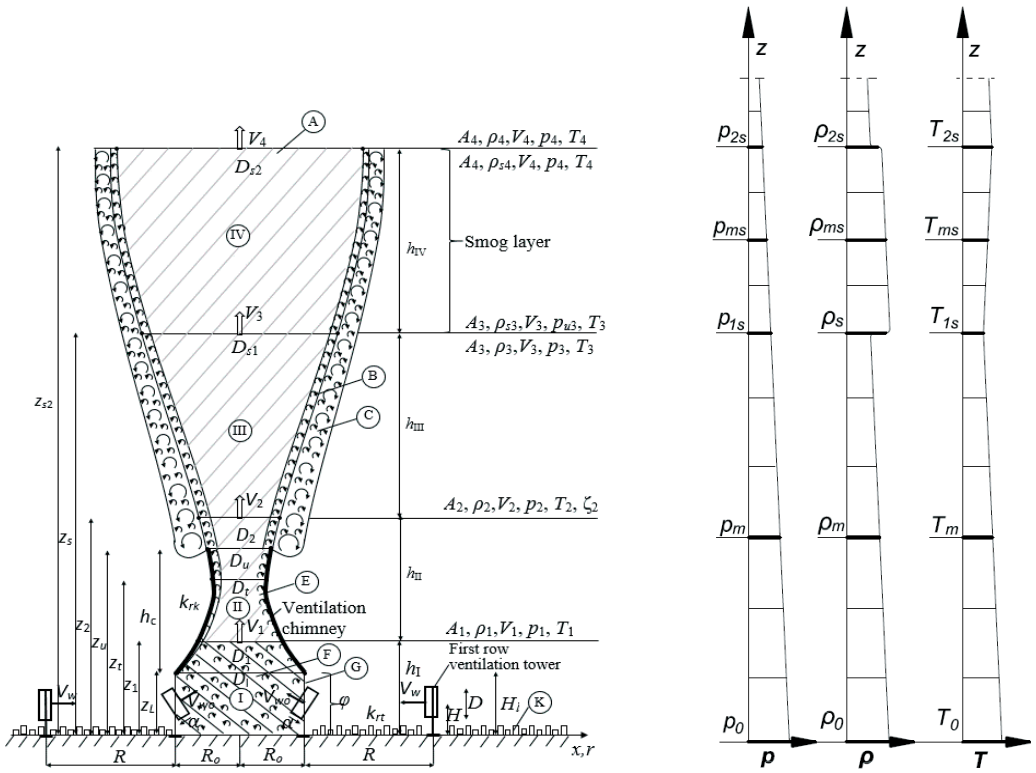

Figure 10. Sketch of a set consisting of a ventilation chimney, substitutive ventilation towers as well as a relevant section of atmospheric boundary layer with marked vertical distribution of static pressure p, mass density ρ and absolute temperature T; A – core of air stream with dominant component V of flow velocity; B – contact boundary/shear layer of stream core (area of turbulent flow with small scale vortexes); C – strongly turbulent mixing area with vortexes of smaller and larger scale; E – ventilation chimney boundary/shear layer of mean height of inner surface roughness k_{rc}; F – strongly turbulent inlet of mixing area with vortexes of smaller and larger scale; G – inlet wall of ventilation chimney with permeability coefficient φ; K – rough terrain with mean height of surface roughness k_{rt}.

Now, taking into account the most important geometric, kinematic and physical quantities of the presented set, let us carry out the analysis of similarity criteria for the particular subsystems I-IV and the whole system V [35].

Subsystem I:

$$V_1 = F_I\left(V_w, V_{w0}, \rho_H, p_H, C_p, T_H, \nu_H; H, D, H_w, z_1, D_1, R, R_0, \alpha, \beta; \varphi, \zeta_2; k_{rt}\right), \tag{10}$$

where: V_1 – mean velocity of air stream in the ventilation chimney on the level z_1 (i.e. near the ventilation chimney inlet); V_w – mean air velocity on the outlet of the each first order ventilators; V_{w0} – mean air velocity on the inlet of each inlet ventilators (i.e. zero row ventilators); ρ_H – air mass density (on the H level) ($\rho_H \cong 1{,}225$ kg/m^3 at $p_H = 1013$ Pa and $T = 289$ K); p_H – atmospheric static pressure; C_p – specific heat at constant pressure; T_H – absolute temperature; ν_H – air kinematic viscosity; H, D, H_w – geometric parameters of the substitutive ventilation towers (respective heights); α – inclination angle of the substitutive inlet ventilators (in radians); $R, R_0, \beta = \frac{2\pi}{n_\beta}$ – geometric parameters of the radial locations of the substitutive ventilation towers (n_β – number of towers in row); φ – permeability of the inlet wall corresponding to the substitutive inlet ventilation towers defined as: $\varphi = \frac{A_{free,inlet}}{A_{total,inlet}}$ (where: $A_{free,inlet}$ and $A_{total,inlet}$ are respective inlet wall areas); k_{rt} – mean irregularities height of the terrain roughness; ζ_2 – coefficient of local losses due to the end of the ventilation chimney.

Assuming the dimensional base for the subsystem I as (V_w, ρ_H, H) and using the Π theorem of the dimensional analysis, the following dimensionless functional relationship can be written:

$$\frac{V_1}{V_w} = F_I\left(\frac{V_{w0}}{V_w}, \pi_{pI}, \pi_{T,I}, Re_I; \frac{D}{H}, \frac{H_w}{H}, \frac{z_1}{H}, \frac{D_1}{H}, \frac{R}{H}, \frac{R_0}{H}, \alpha, \beta; \varphi, \zeta_2; \frac{k_{rt}}{H}\right), \tag{11}$$

where: $\pi_{pI} = \frac{p_H}{\rho_H V_w^2}$; $\pi_{T,I} = \frac{C_p T_H}{V_w^2}$; $Re_I = \frac{V_w H}{\nu_H}$ (Reynolds number). All dimensionless quantities appearing in above relationship are the similarity numbers of the subsystem I. Fulfilment of these similarity criteria in model tests – excluding Reynolds number Re_I – is possible and simple. Reynolds number Re_I influences vortexes dimensions in mixing area F (comp. Fig.7) in subsystem I and hence the size of this area. It indirectly affects D_1 parameter of area I. From the continuity equation of air flow in area I it results that the change in mean velocity V_1 at the outlet of this area depends on the change in D_1 parameter. So, the hypothesis can be assumed, that influence of Reynolds number Re_I on V_1 is a secondary issue. However, validation in this matter is needed on the basis of measurement results which should be conducted in two different model scales differing at least in one order of magnitude.

Subsystem II:

$$V_2 = F_{II}(V_1, \rho_1, p_1, e_1, \Delta e_{II}, \nu_{II}; D_1, D_t, D_u, D_e, z_1, z_t, h_c, z_e; k_{rc}), \tag{12}$$

where: V_2 – mean air stream velocity corresponding to the width D_e at the height z_e; $V_1, \rho_1, p_1, \nu_{II}$ – similarly as before; $D_1, D_t, D_u, D_e, z_1, z_t, h_c, z_e$ – geometric parameters of the ventilation chimney; k_{rc} – mean irregularities height of the

chimney roughness; $e_1, \Delta e_{II}$ – quantities connected with respective pressures, gravitational energies and inner energies (per unit mass of air) defined as follows:

$$e_1 = \frac{p_1}{\rho_1} + gz_1 + C_\Omega T_1 = RT_1 + gz_1 + C_\Omega T_1 = C_p T_1 + gz_1 \cong C_p T_1, \quad (13)$$

$$\Delta e_{II} = e_1 - e_2 = \left(\frac{p_1}{\rho_1} - \frac{p_2}{\rho_2}\right) + g(z_2 - z_1) + C_p(T_1 - T_2) \cong C_p(T_1 - T_2). \quad (14)$$

Assuming in this case the dimensional base as (V_1, ρ_1, h_c), one can write:

$$\frac{V_2}{V_1} = \breve{F}_{II}\left(\pi_{p1}, \pi_{T1}, \pi_{\Delta T,II}, Re_{II}; \frac{D_1}{h_c}, \frac{D_t}{h_c}, \frac{D_u}{h_c}, \frac{D_e}{h_c}, \frac{z_1}{h_c}, \frac{z_t}{h_c}, \frac{z_e}{h_c}; \frac{k_{rc}}{h_c}\right), \quad (15)$$

where: $\pi_{p1} = \frac{p_1}{\rho_1 V_1^2}$; $\pi_{T1} \cong \frac{C_p T_1}{V_1^2}$; $\pi_{\Delta T,II} \cong \frac{C_p(T_1 - T_2)}{V_1^2}$ $Re_{II} = \frac{V_1 h_c}{\nu_{II}}$.

Comparing similarity numbers for model test in smaller scale (subscript M) with these in natural scale (subscript P) and taking into account that atmospheric air is in usual conditions, it is obtained that: $(T_1 - T_2)_P \neq 0 = (T_1 - T_2)_M$; $(h_c)_P \neq (h_c)_M$. Thus, two similarity numbers – $\pi_{\Delta T,II}$ and Re_{II} – will not be fulfilled. It was shown in report [35] that Reynolds number Re_{II} has negligible importance, however it is also necessary to prove it experimentally. Fulfilment of the number $\pi_{\Delta TII}$ (the number of significant importance) is artificially possible with quite good approximation if air layer h_{II} will be divided into smaller layers of thicknesses Δh_i, density ρ and temperature differences ΔT_i and grid with orthogonal wires electrically heated will be added for every layers, according to relationship: $C_p \Delta T_i = \frac{\Delta \dot{q}_i}{\rho \Delta h_i}$, where: $\Delta \dot{q}_i$ – density of heat stream generated by one mesh net. The grids should be placed one above one both inside ventilation chimney and in contact air area outside the chimney.

Subsystem III:

$$V_3 = F_{III}(V_2, \rho_2, p_2, e_2, \Delta e_{III}, \nu_{III}; D_2, h_{III}), \quad (16)$$

Assuming dimensional base as (V_2, ρ_2, h_{III}) the following dimensionless quantities will be obtained:

$$\frac{V_3}{V_2} = \breve{F}_{III}\left(\pi_{p2}, \pi_{T2}, \pi_{\Delta T,III}, Re_{III}; \frac{D_2}{h_{III}}\right) \quad (17)$$

Definitions of criterial numbers and problems with their fulfilment in layer of thickness h_{III} are similar to these in layer of thickness h_{II}. However, it is necessary to validate experimentally the influence of Reynolds number Re_{III} on the velocities ratio $\frac{V_3}{V_2}$. Reynolds number Re_{III} has influence on vortexes dimensions in the mixing area C (comp. Fig.10) and hence, on the size of this area. Then, it has indirect effect on width of stream core, which is characterized by the parameter D_2. On the basis of continuity equation, change in the parameter D_2 influence the value of mean velocity V_3. It is assessed that influence of Reynolds number Re_{III} on velocities ratio $\frac{V_3}{V_2}$ will be of secondary importance.

Subsystem IV:

$$\frac{V_4}{V_3} = \breve{F}_{IV}\left(\pi_{p3}, \pi_{T3}, \pi_{\Delta T,IV}, Re_{IV}; \frac{D_3}{h_{IV}}\right), \quad (18)$$

where: $\pi_{p3} = \frac{p_3}{\rho_{s1} V_3^2}$; $\pi_{T3} \cong \frac{C_{ps} T_3}{V_3^2}$; $\pi_{\Delta T,IV} \cong \frac{C_{ps}(T_3 - T_4)}{V_3^2}$ $Re_{IV} = \frac{V_3 h_{IV}}{\nu_s}$ as well as it is assumed that: $\rho_s \neq \rho$, $\nu_s \neq \nu$ and $C_{ps} \neq C_p$.

Remark concerning unfulfilment of Reynolds number Re_{IV} is similar as before (in case of Re_{III}). In terms of the other criterial numbers, in report [35] it was shown the way of artificial substituting the smog layer by the system of additional multiple grids/ beehive frames placed one above the other. This results in dimensionless pressure losses in model tests in such a way that they are equivalent to dimensionless pressure losses generated by smog layer in nature.

Whole system V:

$$\frac{V_4}{V_w} = \breve{F}_V(\dots, \pi_i, \dots) \quad (19)$$

where: $(\dots, \pi_i, \dots)$ – the set of similarity numbers π_i from all subsystems I-IV.

4. Objectives of the preliminary model tests and summing up conclusions

After all the necessary criteria of similarity had been derived, it was possible to carry out a number of experimental preliminary model tests included three stages mentioned earlier.

Stage I

The objectives of the first stage of the study were: development of practical model of air flow in urban areas along with elaborating similarity criteria for the analysed issue; preparing work station for measurement of air flow velocity field generated by ventilation towers in chosen variants of their parallel configuration; conducting model tests to measure air flow velocity field in the proximity of ventilation towers in parallel configuration with different fan rotation speeds, number and location of the fans; smoke visualisation of the phenomena.

It was decided that the series of model tests would differ in the number of rows and lines in which the fans are arranged. The distances between fan rows resulting in generation of the air stream (i.e. keeping the air flow velocity at a specified level) were specified empirically during preliminary model tests.

a)

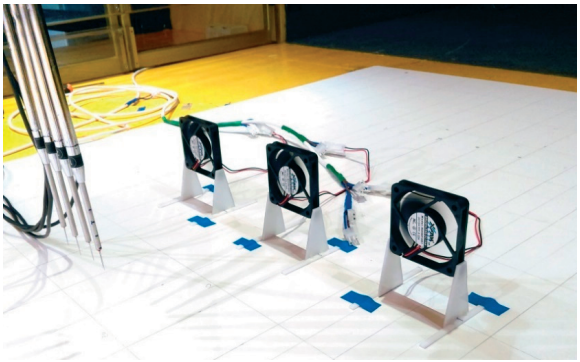

b)

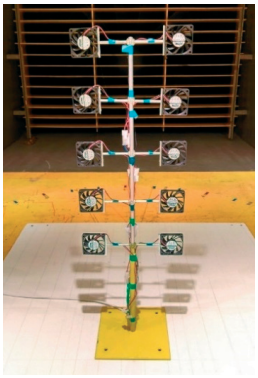

Figure 11. Models of ventilation towers used in model tests: a) set of 3 fans – substitutive ventilation towers, scale 1:833; b) single ventilation tower, scale 1:100.

The fans used in experiments (Fig.11) are CPU cooling fans measuring 60x60x10 mm in size and nominal voltage DC 12 V, 0.22 A. Rotation speed was controlled by adjusting the voltage. The air flows were measured by four hot-wire anemometers spaced by 20 mm located in the central plain of the fan. The case was different in series VI where the complete ventilation tower was modelled in the scale of 1:100. Measurements for this series was conducted on three horizontal plains at different heights.

The results of the stage I study gave the following conclusions:

1. Despite the change of the number of fans from 1 to 8 and the change of scale from 1:833 to 1:100, the flow patterns of the air streams were similar to the previous series. This confirms the thesis that in model tests a group of fans cooperating close to each other can be replaced by a single fan in larger scale (i.e. 1:833) as it was assumed in remaining experiments.

2. Relative wind velocity at a distance of more than 30 cm is kept on a similar level for every tested rotation speeds. It means that the Reynolds number is not a significant factor influencing the results in the small scale experiments;

3. The range of air suction in front of the fan is limited to no more than 10-20 cm. Thus, it is economically reasonable to place the second row of fans at a distance where the air stream is fading away. For the case of study, the distance was x = 280 cm. Placing the rows of fans closer to each other has insignificant influence on increasing the air flow velocity, so there is no reason for it;

4. The spread of fans in a single row was adjusted between 1.5 D (series III) and 3 D (series IV). The air flow velocity at the end of the stream (i.e. at a distance x = 370 cm) reached similar values for both cases, although at the spacing of 3 D the total width of the stream, so also the area of action of the fans, was two times larger than at 1.5 D and the same number of fans. Therefore, it was decided to increase the spread of the fans on the ventilation tower to 3 D and continue the tests with this spacing;

5. The wide stream generated with 3 fans spaced by 3 D can be successfully kept by adding another row of fans at a distance of x = 370 cm. No significant difference of air flow velocity was observed in close ranges ahead of the 2nd row (i.e. 340-360 cm); hence it was concluded that the location of 2nd row was correct. Increasing the distance further could result in decreasing the air flow velocity or even interrupting the continuity of the stream.

Stage II

The purpose of the second stage of model tests was to measure air flow velocity fields in the proximity of system of ventilation towers in concentric configuration with central ventilation chimney and specifying the effective range of the vertical air flow generated by the system of ventilation towers and chimney. The model tests in the scale of 1:833 included 8 series that differ by: shape of ventilation chimney, inclination of the fans that model the ventilation towers (perpendicular to the bottom of the chimney or inclined 47 degree from vertical direction) and permeability of the inlet wall (i.e. different types of closure of the space between ventilation towers: no fence, fences between the base construction of fans, full fences between the ventilation towers). These variants are presented in Fig.12.

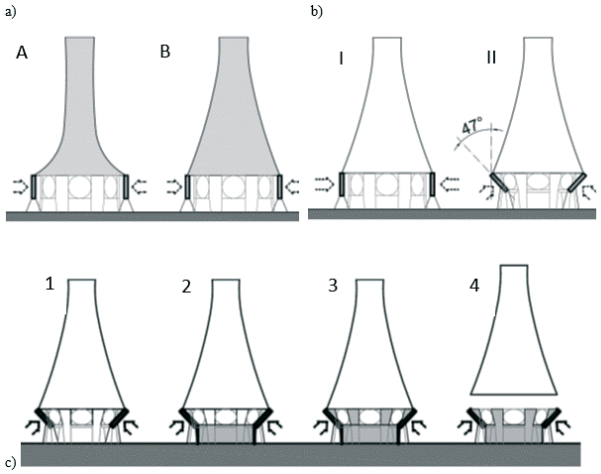

Figure 12. Variants of the system used in tests (stage II): a) shapes of the ventilation chimney, type A and B; b) angle set-up of the fans, type I and II; c) permeability of the system type 1, 2, 3 and 4

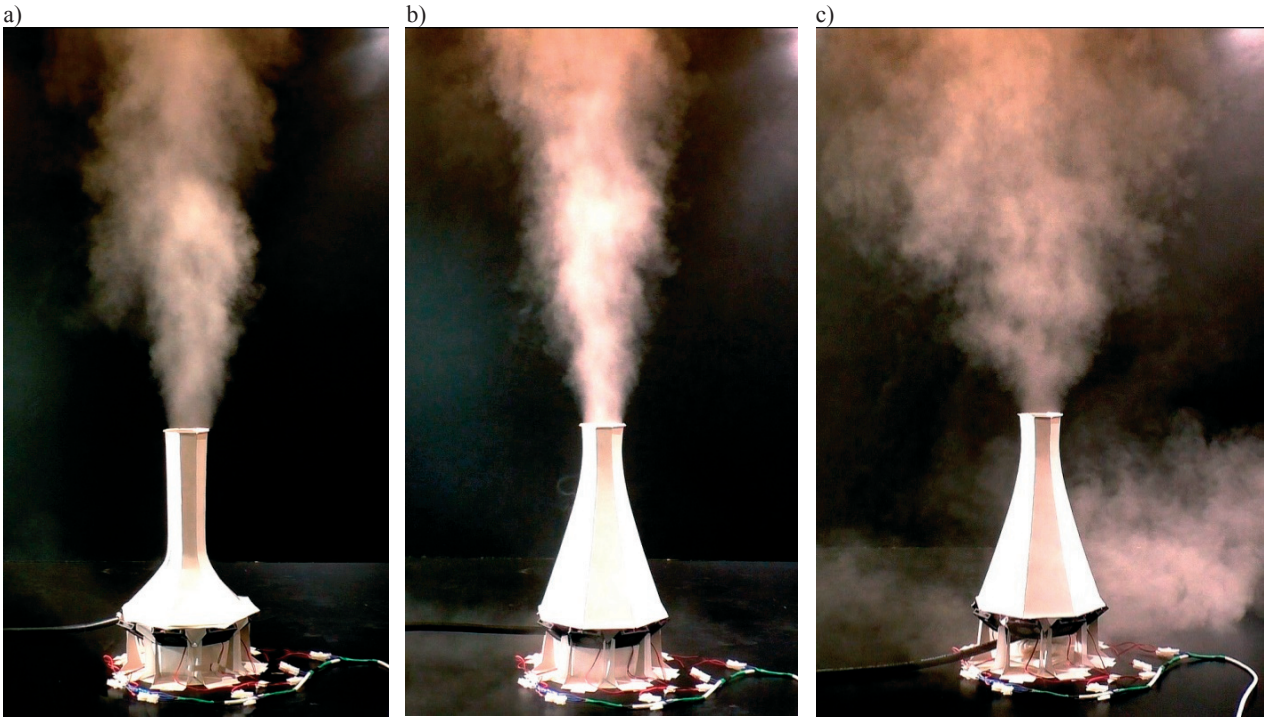

Figure 13. Smoke visualisation of chosen system set-ups used in tests showing the efficiency of the proposed solution: a) chimney shape A, closed space between fans; b) chimney shape B, closed space between fans where the optimal smoke cone is generated above the chimney; c) chimney shape B, open space between fans, large spread of the smoke at the outside of the chimney.

During the model tests it was recognised that:

1. Adding the ventilation chimney vastly increases the efficiency of the generated stream. It is especially observed for outlet velocity of air above the ventilation chimney that is in the range of effect of the system (i.e. over the chimney by 10 times the diameter of the chimney in the widest part). It is important that the kinetic energy of moving air flow is meant to break the resistance of the smog layer and move above it.

2. The chosen configuration of ventilation towers (shape B, inclination II, permeability 3) generates relatively strong and wide stream. Smoke visualisations, showing efficiency of selected solutions are presented in Fig.13. What is important, such an effect of generating a high air stream can be achieved also in nature which confirms the photo shown in Fig.14.

Figure 14. Photo of the flow velocity field above the cooling tower and chimney - power plant in Cracow.

Stage III

The aim of these research works was preliminary recognizing the possibility of dynamic action on the ventilation of urbanized areas by mechanical forcing of additional air streams, reducing the phenomenon of smog.

The most important conclusions that can be drawn from the third stage of the research are summarized below.

1. Surface roughness does not significantly affect the decreasing of stream parameters nor does it interrupt its continuity. This means that there is a possibility effective using of the system in practice over urbanized areas. However, it is necessary to examine in detail the type of turbulence arising in the roughness conditions and their impact on the movement of air masses, e.g. through smoke visualizations of the phenomenon;

2. When using an additional outer ring of ventilation towers in concentric configuration with a central ventilation chimney, continuity of the stream allowing for the supply of polluted air masses to the chimney from the impact area, was obtained; this means the cooperation of the linear system with a ventilation chimney;

3. Measured velocity values at the level corresponding in the model to the altitude of the temperature inversion layer occurrence shows that created vertical stream is able to reach this level, keeping the stream speed at a satisfactory level;

4. Among the chimney shapes tested, the best results were obtained for the B shape (the highest speed at the outlet of the chimney and at the inversion layer) and the shape of D (no chimney - the easiest and most economical solution to use with satisfying effects). Therefore, it is proposed that in further research works and possible implementations of the solutions these types of chimneys should be taken into account;

5. At lower initial air stream speeds, the important similarity criterion is the Reynolds number. Higher speeds, on the other hand, give results that most likely, can be referred to the natural scale and eventual use of the solutions in practice. This conclusion, however, should be verified in model studies on a larger scale;

6. Smoke visualizations using heavy/dense smoke allow to conclude that the solutions will be able to effectively reduce pollution in the area of impact.

5. General conclusion

The obtained results are very encouraging, hence the following general research hypothesis has been set up:

Proposed solutions (S1 and S2) of dynamic action on air boundary layer as a method of improving the ventilation of cities and urban areas are effective, feasible and economically reasonable.

Hence, it was claimed that it is worth continuing this research in wider range: in small model scale in wind tunnel and in large model scale in enclosed space of suitable dimensions, as well as by using numerical simulations.

6. References

[1] http://www.who.int/phe/health_topics/outdoorair/databases/cities/en/ (11.09.2017).

[2] Błażejczyk K. *Air exchange and regeneration system as a factor in the improvement of aerosanitary and bioclimatic conditions.* Eds. Degórska B., Baścik M., Kraków's natural environment: Resources – Protection – Shaping, IGiGP UJ, UMK, WGiK PW, Krakow 2013, 187-190 (in Polish).

[3] Godzik S., Hławiczka S., Poborski P. *Smog – Reasons, Effects, Countermeasures.* PIOŚ, Warszawa 1995 (in Polish).

[4] Shi H., Wang Y., Chen J., Huisingh D. *Preventing smog crises in China and globally.* Journal of Cleaner Production 112 (2016) 1261-1271.

[5] New Directions: *The future of European urban air quality monitoring.* Atmospheric Environment 87 (2014) 258-260.

[6] Ng E. *Policies and technical guidelines for urban planning of high-density cities – air ventilation assessment (AVA) of Hong Kong*. Building and Environment 44 (2009) 1478-1488.

[7] Buccolieri R., Salim S.M., Leo L.S., Di Sabatino S., Chan A., Ielpo P., de Gennaro G., Gromke Ch. *Analysis of local scale tree – atmosphere interaction on pollutant concentration in idealized street canyons and application to a real urban junction*; Atmospheric Environment 45 (2011) 1702-1713.

[8] Błażejczyk K., Degórska B. *Możliwości poprawy jakości powietrza*. Red. Degórska B., Baścik M., Środowisko przyrodnicze Krakowa: Zasoby – Ochrona – Kształtowanie, IGiGP UJ, UMK, WGiK PW, Kraków 2013, 190-192.

[9] US 20090308244 A1. *Method and Equipment for Filtering Air in an Urban Environment*.

[10] WO 2010084385 A1. *Intake and filtering device for fine particulates present in the air*.

[11] CN 101991999 A. *City air purifier*.

[12] CN 203620447 U: *Device for preventing pollution of air suspended particles in urban industrial district*.

[13] Chu A.K.M., Kwok R.C.W., Yu K.N. *Study of pollution dispersion in urban areas using Computational Fluid Dynamics (CFD) and Geographic Information System (GIS)*. Environmental Modelling & Software, 20 (2005) 273-277.

[14] Wingstedt E.M.M., Osnes A.N, Akerwik E., Eriksson D., Pettersson Reif B.A. *Large-eddy simulation of dense gas*

dispersion over a simplified urban area. Atmospheric Environment 152 (2017) 605-616.

[15] Carpentieri M., Robins EnFlo A.G. *Wind tunnel experiments of flow and dispersion in a real urban area*; The 7th International Conference on Urban Climate, 29 June – 3 July 2009, Yokohama, Japan.

[16] Buccolieri R., Sandberg M., Di Sabatino S. *City breathability and its link to pollutant concentration distribution within urban-like geometries*. Atmospheric Environment 44 (2010) 1894-1903.

[17] Ramponi R., Blocken B., de Coo L.B., Janssen W. D. *CFD simulation of outdoor ventilation of generic urban configurations with different urban densities and equal and unequal street widths*. Building and Environment 92 (2015) 152-166.

[18] Oke T.R. *Boundary layer climates*. Methuen, Nowy Jork 1978.

[19] Sorbjan Z. *Turbulence and diffusion in the lower atmosphere*. PWN, Warszawa 1983 (in Polish).

[20] Hang J., Sandberg M., Li Y.: *Effect of urban morphology on wind condition in idealized city models*. Atmospheric Environment 43 (2009) 869-878.

[21] Jiang Y., Alexander D., Jenkins H., Arthur R., Chen Q.: *Natural ventilation in buildings: measurement in a wind tunnel and numerical simulation with large-eddy simulation*. Journal of Wind Engineering and Industrial Aerodynamics 91 (2003) 331-353.

[22] Omrani S., Garcia-Hansen V., Capra B., Drogemuller R. *Natural ventilation in multi-storey buildings: Design process and review of evaluation tools.* Building and Environment 116 (2017) 182-194.

[23] Yang L., Qian F., Song D.X., Zheng K.J. *Research on Urban Heat-island Effect*. Procedia Engineering 169 (2016) 11-18.

[24] Yang L., Li Y. *Thermal conditions and ventilation in an ideal city model of Hong Kong*. Energy and Buildings 43 (2011) 1139-1148.

[25] Lewińska J. *Klimat miasta. Vademecum urbanisty*. Instytut Gospodarki Przestrzennej i Komunalnej, Oddział w Krakowie, 1991, s. 151.

[26] Cao Z., Wang Y., Duan M., Zhu H. *Study of the vortex principle for improving the efficiency of an exhaust ventilation system*. Energy and Buildings 142 (2017) 39-48.

[27] US 4164256 A. *Cooling tower with forced ventilation and natural draft*.

[28] US 5425413 A. *Method to hinder the formation and to break-up overhead atmospheric inversions, enhance ground level air circulation and improve urban air quality*.

[29] Spurr G. *The penetration of atmospheric inversions by hot plumes*. Journal of Meteorology 16 (1959) 30-37.

[30] DE 3503138 A1.: *Process for reducing smog by the chimney inversion/injector effect*.

[31] Blackman K., Perret L., Savory E., Piquet T. *Field and wind tunnel modelling of an idealized street canyon flow*. Atmospheric Environment 106 (2015) 139-153.

[32] Zhai Z.J., Brannon B. *Performance comparison of destratification fans for large spaces*. Procedia Engineering 146 (2016) 40-46.

[33] Flaga A. *Model similarity criteria for a parallel configurations of ventilation towers*. Research Report, Wind Engineering Laboratory, Cracow University of Technology, Cracow 2017 (in Polish).

[34] Flaga A. *Basic relationships of fluid mechanics used for a ventilation chimney*. Research Report, Wind Engineering Laboratory, Cracow University of Technology, Cracow 2017 (in Polish).

[35] Flaga A. *Model similarity criteria for a ventilation chimney with a radial system of substitutive ventilation towers*. Research Report, Wind Engineering Laboratory, Cracow University of Technology, Cracow 2017 (in Polish).

[36] Flaga A., Flaga Ł., Krajewski P., Pistol A. *Preliminary investigations of the possibility of dynamic action on the atmospheric ground level: Stage 1 - Measurements of flow velocity fields and ranges of the air streams generated by the models of fans / ventilation towers in different variants of their parallel configurations*. Research Report, Wind Engineering Laboratory, Cracow University of Technology, Cracow 2017 (in Polish).

[37] Flaga A., Flaga Ł., Krajewski P., Pistol A. *Preliminary investigations of the possibility of dynamic action on the atmospheric ground level: Stage II - Measurements of flow velocity fields and ranges of air streams generated by models of system of fans/ventilation towers in different variants of their concentric configurations with a ventilation chimney located in the centre.* Research Report, Wind Engineering Laboratory, Cracow University of Technology, Cracow 2017 (in Polish).

[38] Flaga A., Flaga Ł., Krajewski P., Pistol A. *Preliminary investigations of the possibility of dynamic action on the atmospheric ground level: Stage III - Measurements of selected issues from stages I and II, taking into account the influence of terrain roughness (urban development).* Research Report, Wind Engineering Laboratory, Cracow University of Technology, Cracow 2017 (in Polish).

Modelling tornadoes from wind engineering perspective

Mark Sterling[1], Chris Baker[1]

[1]*School of Engineering, University of Birmingham, Edgbaston, Birmingham, UK*
e-mail: m.sterling@bham.ac.uk

Abstract: This paper represents a series of personal reflections concerning the modelling of tornadoes and the approaches largely adopted by the wind engineering community. Analytical, physical and numerical modelling of such phenomena are explored and a number of drawbacks have been highlighted which have previously been ignored by many. A framework which potentially outlines how tornadoes could be included in every-day design is briefly presented.

Keywords: Tornadoes, analytical modelling, physical modelling, numerical modelling, transient wind engineering design framework.

1. Background

The development of wind engineering as a separated discipline can be traced back to the late 1950s early 1960s. One of the early developments which has arguably shaped the discipline was the work of van der Hoven (van der Hoven, 1957), where the concept of a spectral gap was noted and provided a justification for the decoupling of the macro-metrological (synoptic) winds from the micro-meteorological winds. van der Hoven provided a number of caveats to his work which, as time has progressed, have tended to be forgotten. Thus, the concept of the spectral gap is now fully embedded in the discipline despite other evidence which suggests that it may not be as apparent as initially envisaged (Richards et al., 2000). Notwithstanding the latter research, the ability to decouple the parent winds from mechanical and convective turbulence, and thus assume a degree of statistical stationarity, has proved reasonably robust and has enabled the discipline to develop. Unfortunately, such an approach is not valid for smaller, non-synoptic weather systems whose transient nature render the assumption of stationarity invalid and require a different approach.

It has come to be appreciated that transient winds such as tornadoes can cause significant damage/disruption and hence warrant more research. For example, in the USA between 1987 and 2016, approximately 60% more fatalities occurred due to tornadoes than Hurricanes (NOAA, 2016). In the UK, where tornadoes are commonly (and mistakenly) thought to not occur, the 2005 Birmingham tornado caused £40m of damage (BBC, 2005). Partially as a result of these events, tornado research (from an engineering perspective) has gained popularity over the last 10-15 years and recently, a conceptual framework has been developed which is perhaps the first step in bringing this work together in a form that could be usefully employed in every day practice (Baker and Sterling, 2018a). This paper outlines the recent tornado related work undertaken by the authors (Section 2), which has led to the development of the framework (Section 3). Concluding remarks are given in Section 4.

2. Modelling Tornado winds

2.1. Analytical modelling

Largely due to their simplicity, analytical models have traditionally been used to describe the flow field within a tornado-like vortex. Such models typically start with the Navier-Stokes and make a number of simplifying assumptions. Gillmeier et al. (2018) recently outlined the derivation of the most popular models and discussed their short comings which (similar to the spectral gap) have traditionally not been acknowledged as they perhaps should have been – which is surprising since analytical models are a simple representation of an extremely complex phenomena.

A recent model by Baker and Sterling (2017) which unlike previous analytical approaches, represents a solution of the high Reynolds number Navier-Stokes has been developed and where possible validated against full-scale data. This model is not without its drawbacks but its ability to represent multi-celled tornado-like flow in a relatively simple way enables the model to be successfully incorporated into every day design (Baker and Sterling, 2018a). This point will be discussed further in section 3.

Figure 1 illustrates some typical velocity distribution distributions which can be generated by the model and are consistent with full-scale and model-data (Baker and Sterling, 2017). The flow field is given by the following equations:

$$\overline{U} = \frac{-4\bar{r}\bar{z}}{(1+\bar{r}^2)(1+\bar{z}^2)} \quad \overline{V} = \frac{2.88S\bar{r}[ln(1+\bar{z}^2)]}{(1+\bar{r}^2)} \quad \overline{W} = \frac{4\delta[ln(1+\bar{z}^2)]}{(1+\bar{r}^2)^2} \qquad (1)$$

where $\overline{U}$, $\overline{V}$ and $\overline{W}$ represent the normalised radial, circumferential and vertical velocities respectively (all velocities have been normalised by the maximum radial velocity, U_m). $\bar{r}$ ($=r / r_m$) and z ($= z/ z_m$) represent the normalised radial (r) and vertical (z) distances respectively both of which have been normalised by their respective values corresponding to the location of U_m. Finally, S is the swirl ratio (a surrogate for the strength of circulation in a tornado to its updraft velocity) and $\delta = z_m/r_m$.

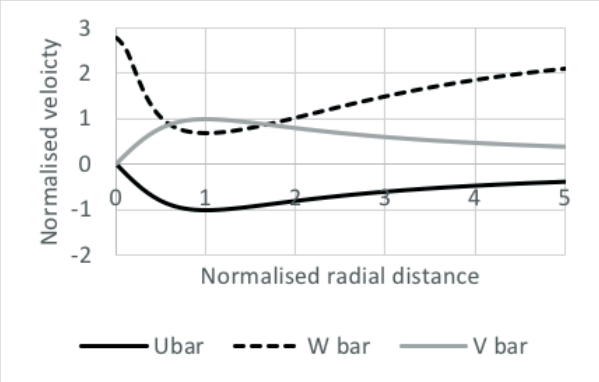

Figure 1. Velocity profiles from the Baker and Sterling (2017) model. ($\bar{\bar{z}} = k = S = \delta = 1$).

2.2. Physical modelling

In keeping with the early development of modelling in boundary layer type flows, extensive physical modelling of tornado-like vortices has been undertaken. Most of the approaches

adopted have built upon the foundations laid by Ward (1972). Ward type simulators typically consist of two chambers – a convection chamber and a convergence chamber. Fans are normally located on top of the convection chamber which are used to generate an updraft. Immediately below the convection chamber, a convergence chamber acts to draw the air in and focus the generated vorticity of the tornado-like vortex. The vorticity is introduced in part by a series of guide vanes at the edge of convergence chamber. These guide vanes can be rotated in order to alter the angular momentum of the incoming flow and thus influence the swirl ratio. Different sizes of chamber exist ranging from the relatively small (D~1m, where D is the diameter of the convergence chamber) to the medium scale (D~3m) and to the large-scale (D>10m). Despite the different size of these chambers, it was until recently assumed that if the swirl ratio and the aspect ratio (a parameter related to the relative dimensions of the updraft hole and height of the convergence chamber) were kept constant, comparable results could be obtained which are independent of the scale of the simulator. However, work undertaken by Gillmeier et al. (2018) has cast doubt on this assumption and provided evidence that the pressure and flow field within a Ward-type simulator may depend on other dimensionless parameters related to the scale of the simulator. On reflection, this finding is perhaps not too surprising since the generated flow field is a function of the boundary conditions, which in turn relate to the design of the simulator. Thus, the general applicability of much of the data obtained from such physical simulators remains at present an unresolved issue.

2.3. Numerical simulations

Despite the issues outlined in section 2.2, it is envisaged that physical simulations are likely to continue to be used. However, due to scale of most of the Ward-type simulators (and thus the size of the generated tornado-like vortices), it is at present not possible to obtain a reliable (and accurate) insight into the complicated flow near the ground, i.e., the tornado boundary layer. Numerical modelling perhaps offers a solution since the size of the grid near the ground can (with sufficient computational resources) be refined as necessary. For example, figure 2 illustrates a large eddy simulation of the flow within the University of Birmingham's simulator corresponding to a swirl ratio of 0.69. From figure 2 it is possible to discern an organized flow structure close to the surface of the generator – such an insight would not have been possible with physical measurements. However, it should be noted that this figure is a numerical simulation of the flow within a Ward-type simulator and as such may not be physically realistic for the reasons outlined above.

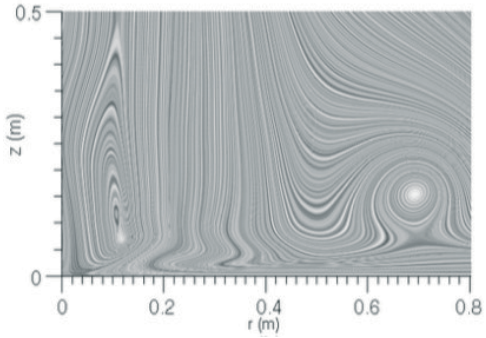

Figure 2. Streamlines of radial and vertical velocity on an axial plane in a Ward-type simulator (S = 0.69).

3. Design framework

As outlined above, the transient nature of tornadoes has hampered their incorporation into every day design. Recently, Baker and Sterling (2018b) have outlined an approach which perhaps resolves this issue. The framework is based on the following form:

- The specification of structural parameters for which the design is being undertaken.
- The specification of probability distribution functions (PDFs) which describe the tornado characteristics.
- The calculation of a large number of random realizations for tornado characteristics (in order to account for the variability inherent between each tornado).
- For each realization, the calculation of the wind velocity and pressure time histories for the structure of interest.
- For each realization, the calculation of the specific load effect of interest.
- The formation of the cumulative distribution function (CDF) for the above load effects.
- The evaluation of the overall risk, i.e., the convolution of these CDFs with the PDFs which describe possibility of tornado occurrence within the geographical area of interest.

Examples of how such a framework could be applied to a variety of scenarios has been presented in Baker and Sterling (2018b).

4. Conclusions

This brief paper has introduced a number of issues concerning tornadoes – in particular their modelling and how they could be included in a design framework. It is acknowledged that there are still a variety of open questions and it is hoped that at the very least, this work will encourage open debate on the subject.

5. References

van der Hoven I. *Power spectrum of horizontal wind speed in the frequency range from 0.0007 to 900 cycles/h*. Journal of Meteorology 14 (1957) 160–164.

Baker C.J., Sterling M. Modelling wind fields and debris flight in tornadoes. *Journal of Wind Engineering and Industrial Aerodynamics* 168 (2017) 312-321.

Baker C.J., Sterling M. *A conceptual model for wind and debris impact loading of structures dues to tornadoes*. Journal of Wind Engineering and Industrial Aerodynamics 175 (2018a) 283-291.

Baker C.J., Sterling M. *A framework for the design of structures loaded by small-scale wind systems*. International Workshop on Wind-Related Disasters and Mitigation, Tohoku University, Sendai, Japan. 11 – 14 March, 2018b.

BBC (2005) http://news.bbc.co.uk/local/birmingham/hi/people_and_places/newsid_8973000/8973381.stm. Last accessed April 2018.

Gillmeier G., Sterling M., Hemida H., Baker C.J. *A reflection on analytical tornado-like vortex flow field models*. Journal of Wind Engineering and Industrial Aerodynamics 174 (2018) 10-27.

NOAA (2016) http://www.nws.noaa.gov/om/hazstats.shtml. Last accessed April 2018.

Richards P.J., Hoxey R.P., Short J.L. *Spectral models for the neutral atmospheric surface layer*, Journal of Wind Engineering and Industrial Aerodynamics 87(2-3) (2000) 167-185.

Ward N.B. The exploration of certain features of tornado dynamics using a laboratory model. J. Atmospheric Science 29 (1972) 1194–1204.

Wind environmental characteristics around super-tall buildings with various configurations

Yukio Tamura[1], Xiaoda Xu[2], Qingshan Yang[3], Akihito Yoshida[4]

[1] *School of Civil Engineering, Chongqing University, Chongqing, China*
e-mail: yukio@arch.t-kougei.ac.jp
[2]*School of Civil Engineering, Beijing Jiaotong University, Beijing, China*
e-mail: 13115279@bjtu.edu.cn
[3] *School of Civil Engineering, Chongqing University, Chongqing, China*
e-mail: qshyang@bjtu.edu.cn
[4]*Tokyo Polytechnic University, Atsugi, Kanagawa, Japan*
e-mail: yoshida@arch.t-kougei.ac.jp

Abstract: Many studies have been carried out on pedestrian-level winds around tall buildings. However, these studies have focused on conventional rectangular-plan buildings up to approximately 200m high. Recently, because of the social demand for more iconic buildings and to achieve excellent aerodynamic performance and/or for architectural aesthetic reasons, super-tall buildings with unconventional configurations have been constructed all over the world. However, the nature of pedestrian-level winds around super-tall buildings with various unconventional configurations have not been studied well. In this study, with reference to researches on aerodynamic characteristics of various super-tall building configurations (Tamura 2010), a series of wind-tunnel tests were carried out to investigate pedestrian-level winds around 40 super-tall building models with various configurations, including basic models, tapered models, corner modified models, opening models, helical models, tilted models, composite models, triangular models, and polygonal models. The results of these tests have led to comprehensive discussions on the pedestrian-level wind characteristics of various super-tall building configurations.

Keywords: various configurations, super-tall building, pedestrian-level wind, speed-up ratio, speed-up area.

1. Introduction

Recently, more and more tall and super-tall buildings with unconventional configurations have been constructed worldwide, such as Turning Torso (2005), Burj Khalifa (2010), and Shanghai Tower (2015). For urban areas with unconventionally shaped tall and super-tall buildings, past studies on pedestrian-level winds may be insufficient to assess the environmental conditions. Therefore, a series of wind tunnel tests were carried out to investigate the characteristics of pedestrian-level winds around 40 super-tall building models with various configurations such as square plan, rectangular plan, elliptical plan, polygonal plan, corner modifications, tilted angle, taper, setbacks, twist angle, openings and so on. This research was aimed at comprehensively investigating pedestrian-level wind characteristics around super-tall building models with various configurations and to examine the effects of some important parameters such as corner modifications, twist angle of helical models, number of sides of building plan, projected width, etc. on speed-up ratio and speed-up area.

2. Wind Tunnel Experiments

2.1. Approaching flow conditions and anemometers

Wind tunnel experiments were performed in a closed-circuit-type boundary-layer wind tunnel whose working section was 1.8m high by 2.0m wide. The approaching turbulent boundary layer flow had a power-law index of 0.27, representing an urban area (Xu et al. 2017).

To make the measurements more accurate, thermistor anemometers were set 5mm above the wind tunnel floor (2.5m above the ground in full-scale), a little bit higher than an average human being's height. Anemometers were distributed over an area of 792mm×792mm, which is almost 8 times the square model's side, and the pitch between two sensors was a minimum of 2cm in the inner area (Xu et al. 2017).

2.2. Models of super-tall building with various configurations

Pedestrian-level wind measurements were conducted on 40 super-tall models with various configurations and 11 square type models with different heights but a constant width (B=50m≡B_0).

The 40 super-tall building models with different configurations were grouped as nine types of models and denoted as Basic, Tapered, Corner Modified, Opening, Helical, Tilted, Composite, Triangular, and Polygonal. These configurations are similar to those of Tamura et al. (2010), Tanaka et al. (2012) and Kim (2015) for investigating aerodynamic characteristics of 400m-high super-tall buildings, and the scale ratio was set to 1/500 in this study to simplify the wind speed measurement near the ground (Xu et al. 2017).

3. Parameters for Describing Pedestrian-level Wind Characteristics

3.1. Speed up ratio R

Speed-up ratio R is the parameter usually applied in evaluating a building's effect on the pedestrian wind environment and is defined as:

$$R = \frac{U_i}{U_{i0}} \tag{1}$$

where U_i and U_{i0} are the mean wind speeds at point i with and without the model (Xu et al. 2017).

3.2. Normalized speed-up area A^*_{R,θ_j}

The normalized speed-up area A^*_{R,θ_j} is defined for each wind direction with angle (θ_j) and denoted as:

$$A^*_{R,\theta_j} = \frac{A_{R,\theta_j}}{B^2} \quad (2)$$

where B^2 is the plan area of model SQU, and A_{R,θ_j} is the speed-up area for speed-up ratio R and wind direction θ_j (Xu et al. 2017).

3.3. Integrated normalized speed-up area $A^*_{R\text{-}int}$

The integrated normalized speed-up area $A^*_{R\text{-}int}$ is defined as the average of the normalized speed-up areas for all directions:

$$A^*_{R-\text{int}} = \frac{\sum_{\theta_j=1}^{N} A^*_{R,\theta_j}}{N} \quad (3)$$

where N is the number of tested wind directions (Xu et al. 2017).

4. Pedestrian-level wind characteristics

4.1. Characteristic of maximum speed-up area R_{max}

The maximum speed-up ratios R_{max} of the models range from 1.9 to 2.3, and the differences among building configurations are not significant. The maximum speed-up ratio R_{max} of Rectangular, Elliptic, Tapered Square, Helical, Tilted, and Triangular models are higher than the value of 2.0 for the Square model. On the other hand, Circular, Octagon and Dodecagon models show lower values. (Xu et al. 2017)

4.2. Integrated normalized speed-up area $A^*_{R\text{-}int}$

Elliptic, Circular, Inversely 4-Tapered, Bulged, Corner Chamfered, Corner Cut, 180° Helical Elliptic, Corner Cut + 360°Helical, and Polygon Models show better results than the Square model, and the Circular model shows the smallest integrated normalized speed-up areas $A^*_{1.3\text{-}int}$. The results demonstrate the efficiency of corner modifications in improving pedestrian-level wind quality.

However, Rectangular, 2-Tapered, 4-Tapered, Setback, 180° Helical, Setback + 45° Rotation, Triangular, Corner Cut Triangular, and 180° Helical Triangular models show worse results than the Square model, and the Triangular model shows the worst. These worse building configurations commonly have larger projected widths near the bottom part of the building. 4-Tapered and Inversely 4-Tapered models are typical contrasts. The latter, with a smaller projected width, shows the better result. (Xu et al. 2017)

4.3. Effects of number of sides of polygon models

The integrated normalized speed-up areas $A^*_{1.3\text{-}int}$, $A^*_{1.5\text{-}int}$, and $A^*_{1.7\text{-}int}$ clearly decrease with the number of sides N_S for Polygon models including Triangular, Square, and Circular models (N_S = ∞). In particular, the integrated normalized speed-up areas significantly decrease from N_S = 3 to 5, keeping almost constant up to N_S = 8, then gradually decease to that of the Circular model. In practice, the number of sides N_S = 5 (Pentagon model) seems to be enough to improve pedestrian-level wind conditions (Xu et al. 2017).

4.4. Speed up ratio and speed up area for square models with different heights and constant width

For square models with different heights (H= 50m~600m) and constant width (B=50m≡B_0) in boundary layer flow, the maximum speed-up ratio R_{max} shows a clear increasing tendency with height H and aspect ratio H/B. However, this increasing tendency becomes less significant for higher height H or the higher aspect ratio H/B range. The integrated normalized speed-up area $A^*_{R\text{-}int}$ presents a geometric logarithmic increase with height H. It is suggested that the effects of height on Pedestrian-level wind for models with relatively low altitude are obvious, while they will become smaller and smaller with constant increase in height.

5. Concluding Remarks

Based on comprehensive experimental studies on pedestrian-level wind characteristics around super-tall buildings, the following results are obtained. (Xu et al. 2017)

- The maximum speed-up ratios R_{max} of pedestrian-level winds are almost 2.1 for 400m-class super-tall buildings, while those of 200m-class tall buildings are 1.5 according to past studies.

- Circular, Corner Chamfered, Corner Cut and Polygon models show better performance for pedestrian-level wind characteristics. However, Rectangular, 2-Tapered and Triangular models are worse for pedestrian-level wind characteristics.

-The normalized integrated speed-up area A^*_R clearly decreases with the number of sides N_S of Polygon models, including Triangular, Square and Circular models. In particular, significant reduction is observed from N_S = 3 to 5, and the Pentagon model with N_S = 5 seems to be enough to improve the pedestrian-level wind environment.

- The effects of height on Pedestrian-level wind for square models (B=50m≡B_0) at relatively low altitude is obvious, while they become smaller and smaller with constant increasing in height.

6. Acknowledgements

This study has been partially supported by the 1000 Foreign Talents Plan, the 111 Project, and the NSFC 51578060 of the Chinese Government and the TPU Wind Engineering Joint Usage/Research Center Project of MEXT, Japanese Government. The authors are grateful for these financial supports.

7. References

Kim Y.C., Bandi E.K., Yoshida A., Tamura Y. *Response characteristics of super-tall buildings–Effects of number of sides and helical angle.* Journal of Wind Engineering and Industrial Aerodynamics 145 (2015) 252-262.

Tamura Y., Tanaka H., Ohtake K., Nakai M., Kim Y. *Aerodynamic characteristics of tall building models with various unconventional configurations.* Structures Congress, 3104-3113, 2010.

Tanaka H., Tamura Y., Ohtake K., Nakai M., Kim Y.C. *Experimental investigation of aerodynamic forces and wind pressures acting on tall buildings with various unconventional configurations.* Journal of Wind Engineering and Industrial Aerodynamics 107 (2012) 179-191.

Xu X., Yang Q., Yoshida A., Tamura Y. *Characteristics of pedestrian-level wind around super-tall buildings with various configurations.* Journal of Wind Engineering and Industrial Aerodynamics 166 (2017) 61-73.

Wind interaction design challenges in solar shading louver systems and porous double skin façades

Alberto Zasso

Department of Mechanical Engineering, Politecnico Milano, Italy,
e-mail: alberto.zasso@polimi.it

Abstract: The energetic and environmental costs and the request of adequate people comfort within modern glass façade buildings is a key issue for sun-shading design.

The Wind-Interaction design challenges and opportunities are discussed with reference to two different strategies of sun-shading. First, the adoption of external vertical Louvers is considered, then the adoption of a double skin porous façade concept is studied. In both cases the Wind-Interaction is a typical multi-scale problem due to the relevant and simultaneous effects of the large scale of the building within the Atmospheric Boundary Layer and to the great relevance of small scale details of the shading components geometry.

With reference to the Louvers case, a multi-scale wind tunnel test methodology is presented, adopting at first a small scale model (1:70) able to deal with the effects of the whole building geometry. A 1:4 model of a building corner is then used, to assess the dependency of the loads on the Louver's shape, on the local flow characteristics and on the porosity of the supporting frame. Two sectional models (1:4, 1:1) of a single Louver are finally considered to account for the Reynolds dependency in full scale.

With reference to the permeable Double Skin Façade case (permeable DSF), an accurate assessment of the wind loads inclusive of the porosity effects is crucial for a correct design and performance evaluation. Measuring and predicting DSF airflow is not a straightforward task due to the interaction between the wind turbulence and the outer porous skin. Moreover, Eurocode and many other National Codes do not supply any prescription about such issue. A comprehensive experimental study of wind loads acting on the porous double skin facade of a new building development under construction in Milano is presented. The methodology is again necessarily considering the multi-scale issues, adopting a sequence of two different scale models. Interesting opportunities of wind loads reduction are shown, due to the porous facade characteristics, compared to what expected on a standard glazed facade.

Keywords: multi-scale approach, wind tunnel test, louvers; wind loads, Pressure Measurements, Double Skin Facade, Porous Double Skin Facade, Porous Facade.

Unsteady method and nonlinear mechanism of galloping of rectangular-type cross sections

Le-Dong Zhu[1], Wan-Lyu Zhuang[2], Bi-Shang Zhang[3], Xiu-Yu Chen[4]

[1] *State Key Laboratory of Disaster Reduction in Civil Engineering / Department of Bridge Engineering, college of Civil Engineering / Key Laboratory for Wind Resistance Technology of Bridges (Ministry of Transport), Tongji University, China, e-mail: Ledong@tongji.edu.cn*

[2] *Zhejiang Provincial Institute of Communications Planning, Design & Research, China, 1329971961@qq.com*

[3] *Department of Bridge Engineering, College of Civil Engineering, Tongji University, China, e-mail: zhangbishang@126.com*

[4] *Department of Bridge Engineering, College of Civil Engineering, Tongji University, China, e-mail: 954746082@qq.com*

Abstract: A direct measurement of galloping self-excited force on a spring-suspended sectional model of a rectangular cross section with a width-to-depth ratio of 3:2 was carried out for various cases of Scruton numbers and wind speeds by using two deliberately-manufactured small dynamic force balance mounted inside the model. On this basis, a refined unsteady and nonlinear mathematical model was proposed to express the galloping self-excited force, and verified through comparing the calculated displacement response with the measure one. This refined model was then simplified by including only the aerodynamic damping force components for predicting the stable amplitude of galloping. The unsteadiness of galloping force was then demonstrated by the variation rules of the identified aeroelatic coefficients of galloping force. The nonlinear behaviours as well as the driving and self-limited mechanisms were discussed from the view angles of aeroelastic coefficients as well as energy evolution rules of different components of nonlinear galloping force by means of hysteresis plots. The evolutions of total damping of the oscillation sectional model system under galloping as well as its different damping components during the whole procedure of the galloping development were also investigated to help to a better understanding on the mechanisms of the driving power source and the inherent factor of self-limited phenomenon of galloping.

Keywords: rectangular cross section, galloping, unsteadiness, nonlinearity, self-excited force, mathematical model

1. Introduction

Rectangular prism often serves as bridge members, such as, stiff hangers or support columns on arch rib of arch bridges, pylons of cable-supported bridges. With the increase of bridge span length, such rectangular prism members become slender and slender, thus the risk of their galloping rises significantly. Galloping of bluff bodies has been widely investigated with quasi-steady theory for so long. However, increasing experimental and analytical evidences suggest that galloping exhibits significant unsteadiness, especially when the reduced wind speed is not sufficiently large (Parkinson, 1989; Païdoussis et al., 2010), as reviewed by Mannini et al. (2014). Although, many efforts have been made by investigators to propose a feasible unsteady galloping force model, but almost none of them completely jumped out of the frame of quasi-steady theory and there is no pure unsteady theory of galloping yet. The universality of these modified quasi-steady galloping approaches are generally not well.

By taking a rectangular section with a 3:2 width-to-depth ratio as an example, a pure unsteady mathematical model of galloping force is presented and discussed in this paper on a direct measurement of galloping force on vibrating sectional model, and used to explore the mechanisms of its nonlinearity, self-limited behaviour and bifurcation phenomenon.

2. Brief introduction of the test

The sectional model test of synchronous measurements of dynamic force and displacement were carried out in the TJ-2 Boundary Layer Wind Tunnel in Tongji University (see Fig. 1). The width (B) and depth (D) of the model were 0.15m and 0.1m respectively. The total length of the model was 1.5m, and the total mass (M_s) is 10.573kg. To reduce the inertial force acting on force balance and thus to enhance the measurement accuracy of the galloping force measurement, an internal-placed force balance method was presented and implemented in cooperation with two small three-component dynamic force balances, which were elaborately design and manufactured specially for this purpose. The model was comprised of an inner aluminium framework, exterior coat made of thin wood plate and inside liner of high-density foam (see Fig. 2). The exterior coat was divided into three parts(see Fig. 1) and only the middle part, which was mounted on the inner framework through tow balances (see Fig. 2), was measure in the test. The length of the middle part was 0.7m and its mass (M_c) is only 0.466kg.

In all, 13 cases as listed in Tab. 1 were tested, where, f_0 and ξ_0 are vertical natural frequency and damping ratio of the sectional model system, $Sc=4\pi M_s\xi_0/\rho D^2 L$ is Scruton number, R_{er} is the Reynolds number corresponding to the onset wind speed of vibration, U_{VIV} is the onset wind speed of vortex-induced vibration determined by the Strouhal number $St=f_sD/U$, which is 0.109 for the 3:2 rectangular cross section determined via force measurement test of rigid model, $U_{g\_quasi}=2S_cf_0D/a_g$ is the onset galloping wind speed calculated according to the linear quasi-steady theory, a_g is the quasi-steady galloping coefficient determined by the drag coefficient and the slope of lift coefficient with respect to wind attack angle, is equal to 3.544 for the 3:2 rectangular cross section. The range of test wind speed is from 0 to 18m/s. The galloping displacements were measured with 4 laser sensors.

Figure 1. Sectional model installed in TJ-2 Wind Tunnel

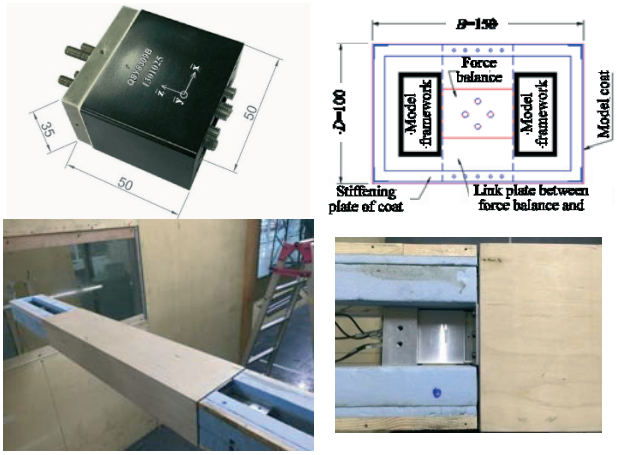

Figure 2. Dynamic force balance and fixing way in model.

Table 1. Test cases for 3:2 rectangular cross section

Test case	M_s(kg)	f_0(Hz)	ξ_0(%)	S_c	U_{VIV} (m/s)	U_{g_quasi} (m/s)	R_{er} (×10³)
A1	10.573	5.029	0.147	10.60	4.61	3.23	30.76
A2		5.029	0.345	24.91	4.61	7.59	30.76
A3		5.028	0.425	30.73	4.61	9.36	30.75
A4		5.032	0.590	42.63	4.61	13.00	30.78
B1	14.582	4.297	0.098	9.74	3.94	2.54	26.28
B2		4.294	0.219	21.88	3.94	5.69	26.26
B3		4.290	0.339	33.79	3.94	8.79	26.24
B4		4.289	0.453	45.15	3.94	11.74	26.23
C1	10.573	3.550	0.111	8.05	3.26	1.73	21.71
C2		3.551	0.258	18.66	3.26	4.02	21.72
C3		3.548	0.364	26.33	3.26	5.66	21.71
C4		3.543	0.453	32.78	3.25	7.04	21.69
C5		3.538	0.561	40.56	3.25	8.71	21.67

3. Displacement responses of galloping

The test results show that for all the test cases, the galloping at every wind speed experienced an onset-developing-stable procedure as shown in Fig. 3, as an example, for Case C1 at the reduced wind speed ($U^*=U/\omega B$) of 2.01 when the stable amplitude is about 0.42D. This indicates that galloping of bluff bodies is a kind of self-excited vibration with strong nonlinear and self-limited behaviours. Fig. 4 gives out the variations of stable galloping amplitudes of different test cases with reduced wind speed. It can be seen that the onset reduced wind speeds of galloping for all the test cases with different Scruton numbers or different frequencies are almost consistent with each other and are very close to the onset reduced wind speed of vortex-induced vibration determined by the Strouhal number, which are generally far away from the quasi-steady ones as shown in Tab. 1. This means that the unsteadiness of galloping of bluff bodies is significant and cannot be ignored. Furthermore, the stable amplitudes of all test cases are closes to each other and increase with the increase of the reduced wind speed almost linearly. Moreover, for some cases, such as A3, A4, B3, B4, C4, and C5, when the reduced wind speed exceeds a certain value, the galloping disappear suddenly if there is no initial excitation or the initial excitation is not sufficiently large. This should be because of the existence of strong nonlinearity of galloping force.

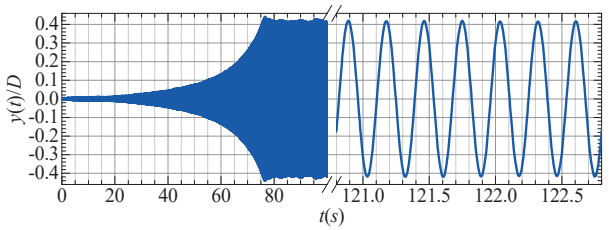

Figure 3. Time history of galloping displacement responses (Case C1, U^*=2.01)

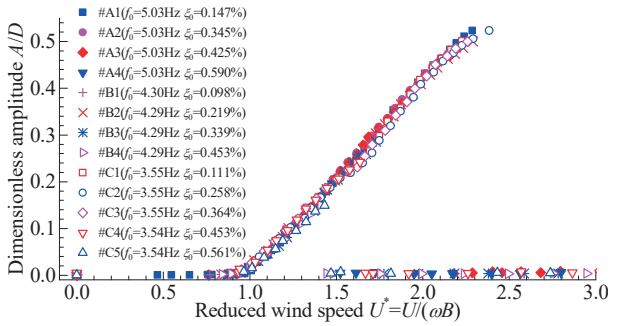

Figure 4. Galloping amplitudes vs. with reduced wind speed

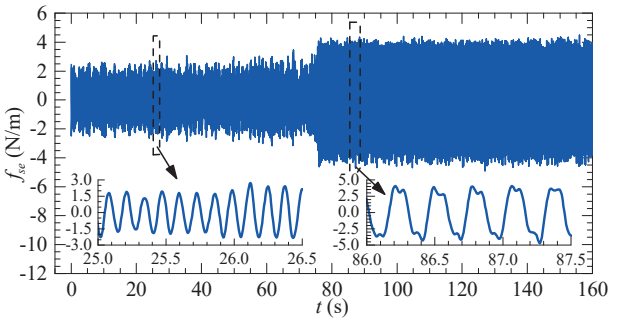

(a) Time history

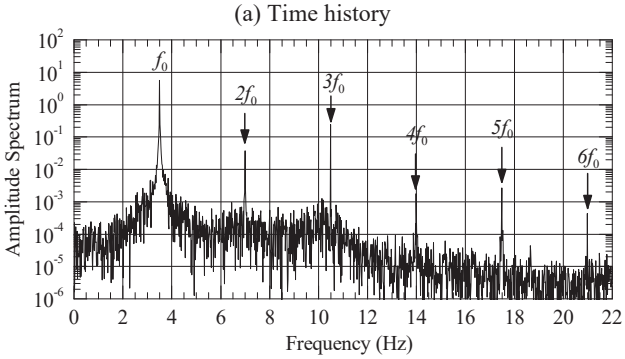

(b) Amplitude spectrum at stable stage

Figure 5. Measured galloping force for Case C1 at U^*=2.19

4. Extraction of galloping force

The per-unit-length self-excited force of galloping on coat of the oscillating model (f_{se}) can be determined as follows:

$$f_{se} = f_m^c + m_c\ddot{y} - f_{se}^0 \tag{1}$$

$$f_{se}^0 = f_{aI}^0 + f_{aD}^0 = -m_a^0(a_t)\ddot{y} - c_a^0(a_t)\dot{y} \tag{2}$$

$$a_t(t) = \sqrt{y(t)^2 + \left[\dot{y}(t)/(2\pi f_0)\right]^2} \tag{3}$$

where, m_c is the mass of the middle measured coat per unit

length; f_m^c is the measured total dynamic force acting on the middle measured coat per unit length; f_{se}^0 is the non-wind-induced additional self-excited force acting on the middle measured coat per unit length; m_a^0 and c_a^0 are the non-wind-induced additional aerodynamic mass and damping coefficients, which are the functions of instantaneous amplitude $a_i(t)$ defined as Eqn.(3), and can be determined via a similar test at zero wind speed; $y(t)$ and $\dot{y}(t)$ are displacement and velocity responses of galloping, respectively (Gao and Zhu, 2016); t is time.

As an example, Fig. 5 gives the time history the measured galloping force f_{se} for Case C1 at U^*=2.19 and the corresponding amplitude spectrum at the stable stage of galloping. The accuracy of the measured f_{se} was verified to be quite well by comparing the calculated displacement responses of the sectional model system by using the measured time history of f_{se} with the measured one.

5. Nonlinear mathematical model of unsteady galloping force

5.1. Refined model

From Fig. 5, it can be seen that the galloping self-excited force has distorted waveform from sinusoidal on in time domain and contains significant multiple-frequency components besides the fundamental one in frequency domain, indicating that its nonlinearity is notable. According to the situation of multiple-frequency components of the galloping self-excited force as shown in Fig. 5(b), an refined unsteady nonlinear mathematical model as follows was then proposed through a trial-error way:

$$f_{se}(y,\dot{y},K) = \underbrace{a_{01}(K)\dot{y} + a_{03}(K)\dot{y}^3 + a_{05}(K)\dot{y}^5}_{\text{damping terms}} + \underbrace{a_{10}(K)y}_{\text{stiffness terms}} + \underbrace{a_{11}(K)y\dot{y} + a_{22}(K)y^2\dot{y}^2 + a_{04}(K)\dot{y}^4 + a_{60}(K)y^6}_{\text{pure force terms}} \quad (4)$$

where, "damping terms" means that they do effective work in every oscillation periods, i.e., provide energy to or dissipate energy of the vibration system, in another word, provide effective (either negative or positive) aerodynamic damping; "stiffness terms" means that they do effective reactive work in every oscillation periods, i.e., provide effective (either positive or negative) aerodynamic stiffness; "pure force terms" means that they do neither effective work nor effective reactive work in every oscillation periods, and thus provide neither effective aerodynamic damping nor effective aerodynamic stiffness to the oscillation system.

The parameters a_{ji}, i.e., aeroelastic coefficients of nonlinear unsteady galloping force, can be identified based on the measured time histories of galloping force and displacement by using a three-step nonlinear least square approach. The first step is to identify the parameters of damping terms (a_{01}, a_{03}, a_{05}) by least square fitting on the time history of the periodical work of the galloping force. The second step is to identify the parameter of the stiffness term (a_{10}) by least square fitting on the time history of the periodical reactive work of the galloping force; the third step is to identify the parameters of the pure force terms (a_{11}, a_{22}, a_{04}, a_{60}) by least square fitting on the time history of galloping force, when the parameters of the damping and stiffness terms are already known. It should be noted that the galloping force parameters (a_{ji}) depend on the reduced wind speed (U^*) or the reduced frequency K ($=\omega B/U=1/U^*$) because of the unsteadiness of the galloping self-excited forces.

As an example, Fig. 6 shows the comparison of the galloping force time history and amplitude spectrum rebuilt by the refined model shown as Eqn.(4) with the measured ones for Case C1 at U^*=2.01. It can be found that the measured galloping force can be fitted rather well by the refined model.

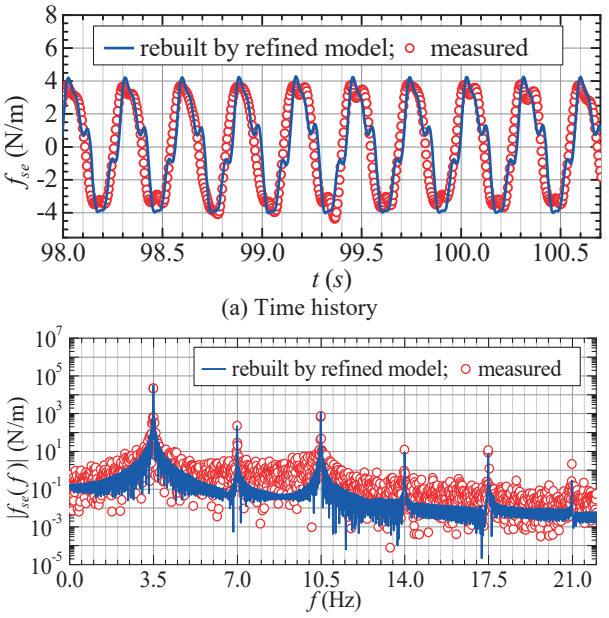

(a) Time history

(b) Amplitude spectrum

Figure 6. Comparison of galloping force rebuilt by refined model with measured one (Case C1 at U^*=2.01)

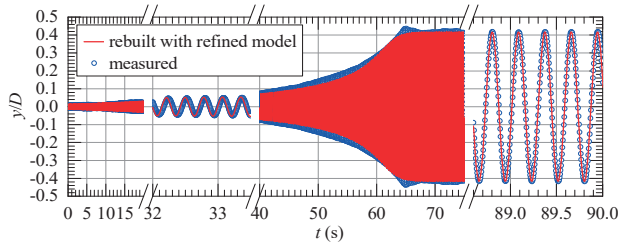

Figure 7. Comparison of galloping displacement reconstructed by refined galloping force model with measured one (Case C1 at U^*=2.01)

The refined model is then verified via comparing the time history of galloping displacement of the sectional model system rebuilt by the refined model with the corresponding measured one. As example, Fig. 7 exhibits such a comparison for Case C1 at U^*=2.01. It can be seen that both the amplitude and phases of the rebuilt response are well consistent with the measured ones.

5.2. Simplified model

Because the stable amplitude of galloping displacement is mainly governed by the components of galloping force providing effective energy to the oscillation system, the Eqn.(4) can be simplified as follows if only the stable amplitude is concerned.

$$\begin{aligned} f_{se} &= a_{01}(K)\dot{y} + a_{03}(K)\dot{y}^3 + a_{05}(K)\dot{y}^5 \\ &= \rho U^2 BKH_1^*(K)\left(1 + \varepsilon_{03}(K)\frac{\dot{y}^2}{U^2} + \varepsilon_{05}(K)\frac{\dot{y}^4}{U^4}\right)\frac{\dot{y}}{U} \end{aligned} \quad (5)$$

where, ρ is air density; U is wind speed; H_1^*, ε_{03} and ε_{05}, as functions of K, are aeroelastic coefficients of damping terms of nonlinear unsteady galloping force.

Taking Case C1 at U^*=2.01 as an example, Fig. 8 shows the comparison of the galloping force time history and amplitude spectrum rebuilt by the simplified model shown as Eqn.(5), which contains only the damping terms, with the measured ones. Fig. 9 gives a comparison of the time history of galloping displacement of the sectional model system rebuilt by the simplified model with the measured one. One can then found that ig-

noring the stiffness and pure force components of the galloping force leads to a significant deviation of the rebuilt time history and amplitude spectrum from the measured ones, however, the amplitude of the rebuilt galloping displacement can still meet the measured one very well within the whole evolution procedure of galloping vibration whilst the phases of the two sets of responses show some difference, especially between the long term responses. This means that the simplified model has enough accurate for predicting the stable amplitude of the unsteady galloping of the rectangular cross sections.

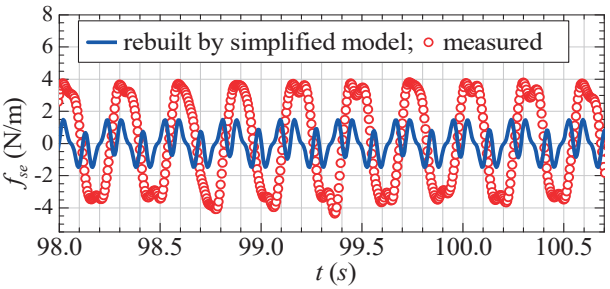

(a) Time history

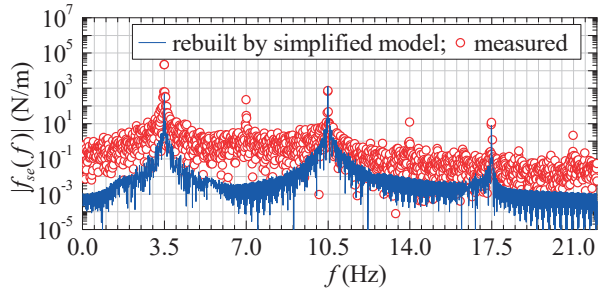

(b) Amplitude spectrum

Figure 8. Comparison of galloping force rebuilt by simplified model with measured one (Case C1 at U*=2.01)

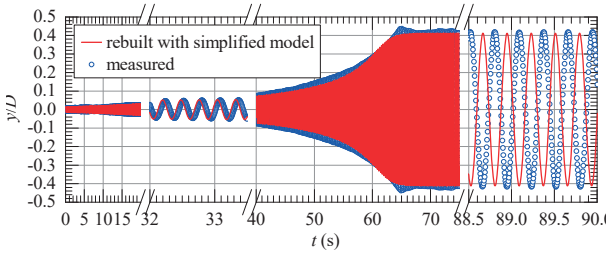

Figure 9. Comparison of galloping displacement rebuilt by simplified galloping force model with measured one (Case C1 at U*=2.01)

5.3. *Aeroelastic coefficients of nonlinear unsteady galloping force identified from different test cases*

Theoretically, the above-mentioned aeroelastic coefficients of the nonlinear unsteady galloping force should only depend on the exterior shape of the bluff body and the reduced frequency (or reduced wind speed). However, there may be some discrepancy among the identified results of the aeroelastic coefficient of a certain cross section identified from different test cases of Scruton number, for one reason being the test error, especially in the case of small vibration, and another reason being the ignorance of the nonlinear terms with the order higher than 6 in the galloping force models as shown in Eqn.(4) or and Eqn.(5).

Fig. 10 shows the three major aeroelastic coefficients (H_1^*, ε_{03}, ε_{05}) identified from six teste cases (A1, A2, B1, B2, C1, C2). It can be seen that the identified results are slightly discrete, and good smooth fitted curves of the aeroelastic coefficients vs. reduced wind speed can be obtained for later use in galloping analyses.

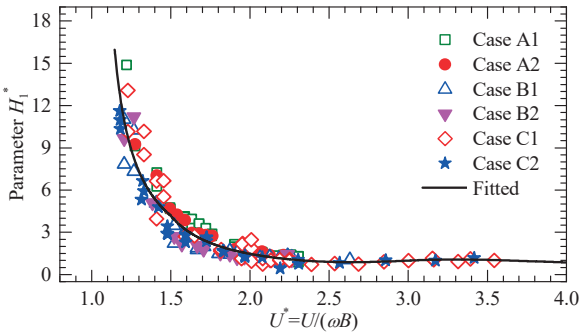

(a) H_1^* vs. U*

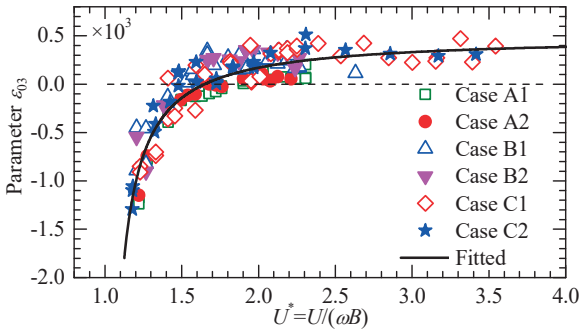

(b) ε_{03} vs. U*

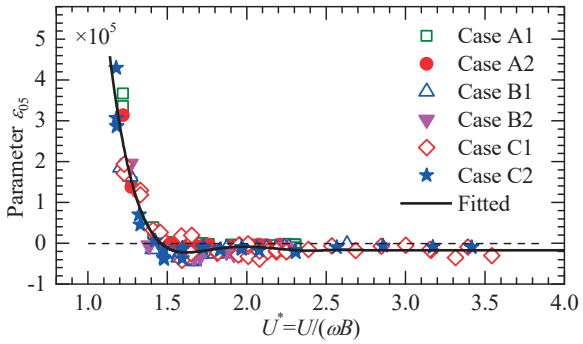

(c) ε_{05} vs. U*

Figure 10. Aeroelastic coefficients of nonlinear unsteady galloping force

From Fig. 10, one can also find that H_1^* and ε_{05} decrease while ε_{03} increases almost monotonously with the rise of U*. The values of the aeroelastic coefficients change rapidly within the lower range of U* and slow within higher range of U*, and approach to constants when U* is sufficiently large. The above behaviours of the aeroelastic coefficients indicate that their unsteadiness is strong when the reduced wind speed is low and then gets weaker and weaker with the increase of the reduced wind speed, and finally become steady.

6. Nonlinear behaviour, driving and self-limited mechanisms of galloping

6.1. *From the view angle of aeroelastic coefficients*

Fig.10a demonstrates that after the onset of galloping (U*≈0.9), H_1^* is always positive, indicating that the linear item of velocity of the galloping force always provides negative aer-

odynamic damping and is one of the major power source driving the galloping growth.

From Figs.10b and 10c, one can fine that when $U^*>1.8$, ε_{03} keeps positive indicating that the cubic item of velocity provide nonlinear negative aerodynamic damping and also is one of the major power source driving the nonlinear development of galloping. Meanwhile ε_{05} is generally negative indicating that the fifth-power item of velocity provide nonlinear positive aerodynamic damping, which increases rapidly with the growing amplitude during the later stage of galloping development, thus is the inherent factor resulting in the galloping getting stable, i.e., is the inherent factor of the self-limited phenomenon.

When $U^*<1.5$, the situations and functions of the two items of ε_{03} and ε_{05} are inversed. However, in this case, the vibration is not significant, and the contribution of the ε_{05} item to the negative damping is quite small compared with that provided by the H_1^* item, and can almost be ignored. Thus, the major power driving the galloping is the negative damping force provided by the linear item of velocity, and the major inherent factor of the self-limited phenomenon is the positive damping force provided by the cubic item of velocity.

When U^* is between 1.5 and 1.8, both the values of ε_{03} and ε_{05} are close to zero, and often switch between positive and negative values, which may be because the test error or the approximation of the galloping force model. However, by inspecting carefully the data, one can find that ε_{03} and ε_{05} always have the opposite signs for every test cases. Also because the vibration amplitude is not significant in this cases of U^*, the major power driving the galloping comes from the linear item of velocity, while the major factor leading to the self-limited phenomenon of galloping is one of the cubic or fifth-power item of velocity.

6.2. From the view angle of hysteresis plots

The Case C1 at U^*=2.01 is taken as an example to discuss the behaviour of the hysteresis plots between the galloping force or its components and displacement. Fig. 11 shows the hysteresis plots of the total galloping force at typical time zones of the whole procedure of galloping (for time history of displacement, please refer to Fig. 7 or 9).

From Fig. 11, it can be seen that in the initial stage of galloping the hysteresis loops had a normal elliptical shape, indicating that the nonlinearity of the galloping force was insignificant. Actually, the vibration amplitude was very small in the initial stage, the nonlinear components of the galloping force can thus be ignored. Furthermore, the hysteresis curve looped in clockwise direction, indicating that the galloping force did positive work, and the galloping grew with time.

With the elapse of time, the galloping developed, the shape of hysteresis loop was distorted more and more remarkable from the normal ellipse. For instance, it became mango-shaped around 58s. From 0s to about 58s, the the area of the hysteresis loop became larger and larger indicating that the contribution of the cubic item of velocity became more and more significant. The loop shape further became peanut-shaped around 62s, and dumbbell-shaped around 63s, and the loop concaved inward more and more notably in its middle zone, leading to the loop area smaller and smaller. This indicates that the positive work done and the energy input by the galloping force dropped, and implying that the nonlinear damping component of the fifth-power item of velocity exerted more man more important role by dissipating more and more energy from the galloping vibration. Since then, the effect of the fifth-power item of velocity became much more significant, causing the loop surfaces in the middle zone to concave to the opposite sides and making the loop look like a fried dough twist with the two side clockwise enclosed zones providing positive work, and the middle anti-clockwise enclosed zone providing the negative work. This led to a further drop of the net energy input by the galloping force. Finally, with the elapse of time, the galloping vibration became more and more violent and the nonlinearity of galloping force got stronger and stronger until that the galloping oscillation reached to a stable stage, often called as limit-circle oscillation (LCO).

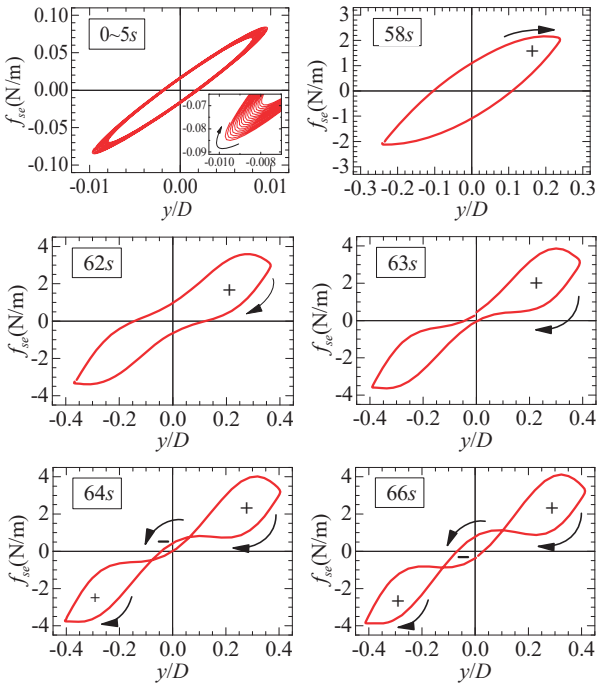

Figure 11. Hysteresis plot between the total galloping force and the displacement (Case C1 at U^*=2.01)

Fig. 12 shows the hysteresis plots of different components of the galloping force at four typical stages (0-5s, around 58s, 63s and 66s) during the galloping for Case C1 at U^*=2.01, where, f_{se} represents the total galloping self-excited force; f_v, f_{v3}, f_{v5} represent, respectively, the components of aerodynamic damping force (see Eqn.(4)) coming from the linear, cubic and fifth-power items of velocity, respectively; f_d represents the component of aerodynamic stiffness force (see Eqn.(4)) coming from the linear item of displacement; f_{dv}, f_{d2v2}, f_{v4} and f_{d6} represent the components of pure aeroelastic force coming from the product item of displacement and velocity, the product item of displacement square and velocity square, the item of velocity biquadrate and the sixth power item of displacement, respectively.

It can be seen from this figure that during the whole procedure of the galloping, the hysteresis loops of f_d and f_{d2v2}, f_{v4}, f_{d6} are of either straight line or curved line without any enclosed area, indicating that these force components don't do any work and have thus little influence on the galloping amplitude. The slop of f_d keeps unchanged however the displacement changes with time, indicating it provide a linear aerodynamic stiffness. On the other hand, the slops of f_{d2v2}, f_{v4} and f_{d6} are very close to zero, providing almost no aerodynamic stiffness. The hysteresis loop of f_{dv} is of very flat a horizontal 8 shape, and its two enclosed sub-loops rotate in opposite directions and have a positive area and a negative area, respectively. Its total area is hence zero, indicating that f_{dv} also does not do any work with every oscillation period. Furthermore, the link line between the two end points of the hysteresis loop of f_{dv} is horizontal, indicating that f_{dv} does not provide any aerodynamic stiffness. As a summary, f_d is a linear stiffness component whilst f_{d2v2}, f_{v4}, f_{d6} as

well as f_{dv} are "pure force components", providing neither aerodynamic damping nor aerodynamic stiffness.

The hysteresis loops of the f_v , f_{v3}, f_{v5} components also lies horizontally, because they are aerodynamic damping forces and don.t provide any aerodynamic stiffness. The loop of f_v component is a normal ellipse as f_v is a linear damping force. However, the loops of f_{v3}, f_{v5}, which are nonlinear, deviate apparently from normal ellipse and are olive nut-shaped.

In the initial stage of galloping (0-5s) the linear damping component, f_{v1} goes along a clockwise loop with the change of displacement, thus provides effective positive energy and a constant negative aerodynamic damping ratio to the oscillation system. However, because the oscillation amplitude is very small in the initial stage, both the loop areas of the nonlinear damping components of f_{v3}, f_{v5} are almost zero, and the wind energy is input mainly by f_{v1}. The absolute value of the constant negative damping ratio provide by f_{v1} must be greater than the structural damping ratio because this is the precondition that the galloping amplitude can grow.

Then, in the middle stage of the galloping development, with the increase of oscillation amplitude, the energy input by f_{v1} increases, but the negative damping ratio provided by f_{v1} keeps constant. Meanwhile, the cubic item of velocity f_{v3} plays more and more significant role, and inputs more and more energy to the oscillating system. It also provides a negative aerodynamic damping ratio, which increases nonlinearly with the oscillating amplitude, and makes the oscillation amplitude grows rapidly. During this rapid growing stage of oscillation amplitude, the influence of the fifth-power item of velocity, f_{v5}, is still not significant because the oscillating amplitude is not large enough.

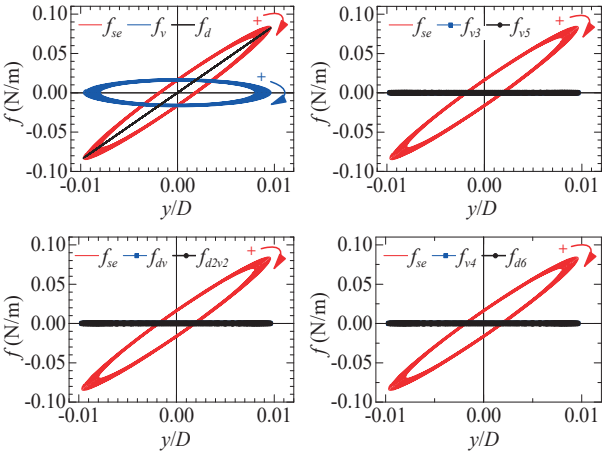

(a) 0-5s

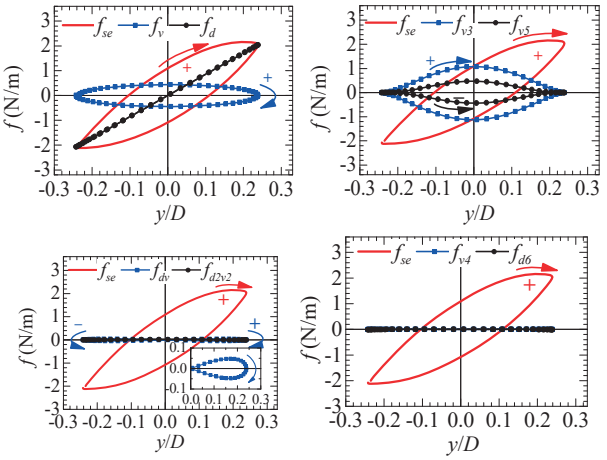

(b) 58s

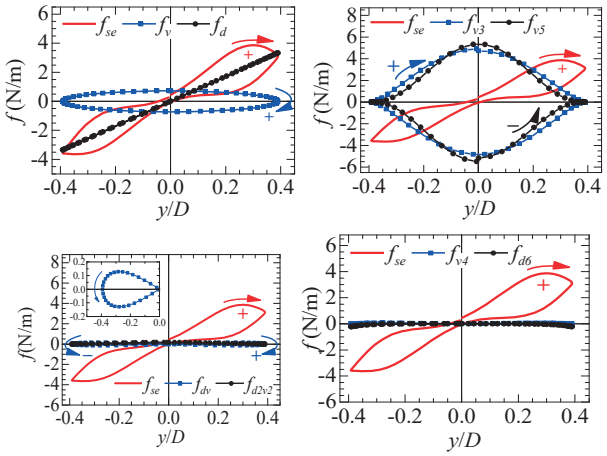

(c) 63s

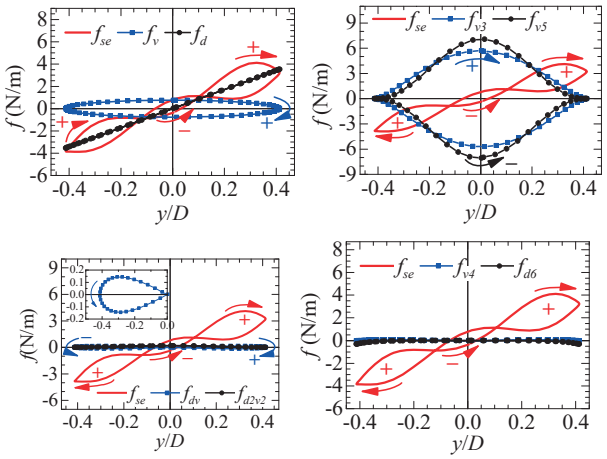

(d) 66s

Figure 12. Hysteresis plots between galloping force components and displacement (Case C1 at U^*=2.01)

In the later stage of the galloping development, when the time is approaching 58s, the loop of f_{v5} bulges gradually indicating that the fifth-power item of velocity begin to exert a notable role. Because the loop of f_{v5} rotates anticlockwise, f_{v5} dissipates energy of the oscillation system, i.e., provides a positive aerodynamic damping ratio which rises nonlinearly with the increase of the galloping amplitude.

At about 63s, the loop area of f_{v5} reaches the same level of that of f_{v3}. The energy input by f_{v3} is approximately counteracted by the energy dissipated by f_{v5}. This results in the increasing rate of the galloping amplitude begins to drop (see Figs.7 and 9).

At about 66s, the loop area of f_{v5} exceeds that of f_{v3}. The energy input by f_{v1} and f_{v3} is dissipated almost completely by the positive damping provided by f_{v5} together with the structural damping. This leads to that the galloping attains a stable LCO state, i.e., self-limited state (see Figs. 7 and 9).

The above analyses demonstrate that for the Case C1 at U^*=2.01, the galloping onset is stimulated by the negative aerodynamic damping provided by the galloping force component of linear velocity item (f_{v1}), and the rapid growth of the amplitude in the middle stage of galloping development is driven by the nonlinear negative damping provided by the galloping force component of the cubic item of velocity (f_{v3}). The drop of the increasing rate of amplitude and the self-limited phenomenon occurred in the later stage of the galloping development is mainly caused by the nonlinear positive aerodynamic damping provided by the galloping force component of the fifth-power item of velocity (f_{v5}).

As mentioned before, for the lower reduced wind speed cas-

es, the situation may be some different because the signs of ε_{03} and ε_{05} are interconverted. In these cases, the stimulation and growth of galloping are mainly due to by the negative aerodynamic damping provided by f_{v1}. And the self-limited phenomenon of galloping is caused by the nonlinear aerodynamic positive damping provided by f_{v3}.

7. Evolution of damping coefficients

According to Eqn.(5), the motion-dependent linearized aerodynamic damping coefficient (c_a) provided by the galloping self-excited force can be expressed as follows:

$$\begin{aligned} c_a(a_t) &= -a_{01} - a_{03}\dot{y}^2 - a_{05}\dot{y}^4 \\ &= -\rho UBKH_1^*(K)\left(1+\varepsilon_{03}(K)\frac{\dot{y}^2}{U^2}+\varepsilon_{05}(K)\frac{\dot{y}^4}{U^4}\right) \\ &= c_{H_1}+c_{\varepsilon_{03}}+c_{\varepsilon_{05}} \end{aligned} \tag{6}$$

The total damping coefficients of the oscillation system (c_{total}) is equal to the superposition of aerodynamic damping coefficient and the structural effective damping coefficient (c_s^e), which includes the non-wind-induced additional aerodynamic damping coefficient and may also nonlinear with respect to the instantaneous amplitude (a_t) of vibration as defined by Eqn.(3).

$$c_{total}(a_t) = c_s^e + c_a = c_s^e + c_{H_1} + c_{\varepsilon_{03}} + c_{\varepsilon_{05}} \tag{7}$$

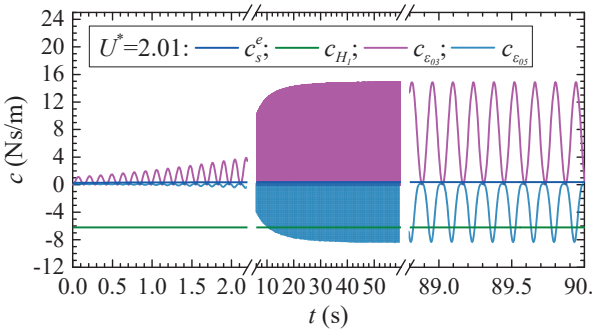

Figure 16 Evolutions of different damping components during galloping development (Case C1, U*=1.33)

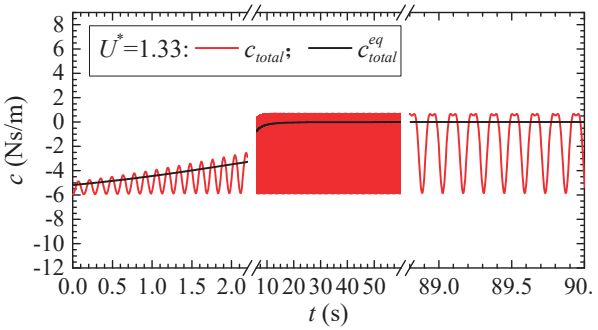

Figure 17 Evolutions of total damping coefficient and energy-equivalent total damping coefficient during galloping development (Case C1, U*=1.33)

Figs. 16 and 17 show the variation rules of c_{H_1}, $c_{\varepsilon_{03}}$, $c_{\varepsilon_{05}}$ and c_{total} with time during the whole procedure of galloping for Case C1 at U*=1.33, and Figs. 18 and 19 show those for the Case C1 at U*=2.01. It can then be seen that c_{H_1} keeps constant with a negative value whilst the values of $c_{\varepsilon_{03}}$ and $c_{\varepsilon_{05}}$ oscillate with time because they are functions of vibration velocity. The oscillation of $c_{\varepsilon_{03}}$ and $c_{\varepsilon_{05}}$ are unstable until the galloping oscillation gets stable. Moreover, the oscillation of $c_{\varepsilon_{03}}$ and $c_{\varepsilon_{05}}$ are not symmetric, and takes zero as an upper or lower bound. For the reduced wind speed lower than 1.5, $c_{\varepsilon_{03}}$ is always positive and takes zero as its lower bound whilst $c_{\varepsilon_{05}}$ is always negative and takes zero as its upper bound.

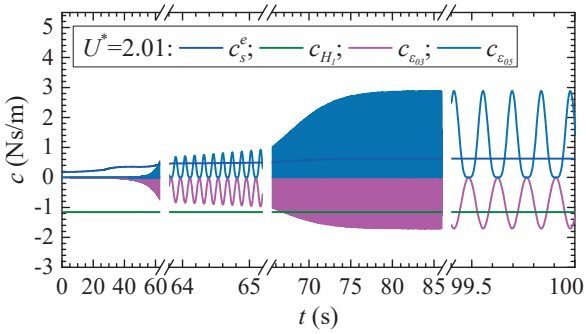

Figure 18 Evolutions of different damping components during galloping development (Case C1, U*=2.01)

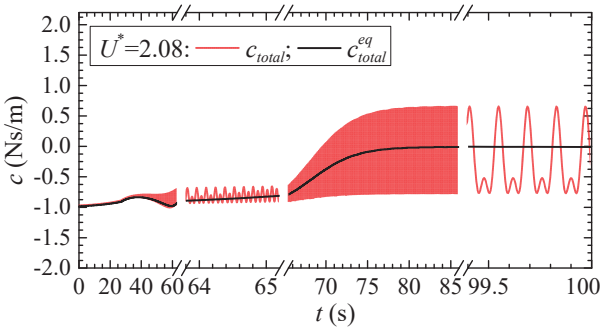

Figure 19 Evolutions of total damping coefficient and energy-equivalent total damping coefficient during galloping development (Case C1, U*=2.01)

For the reduced wind speed larger than 1.8, the situations of $c_{\varepsilon_{03}}$ and $c_{\varepsilon_{05}}$ is just interconverted. The phenomenon about the sign interconversion between $c_{\varepsilon_{03}}$ and $c_{\varepsilon_{05}}$ with the change of the reduced wind speed is consistent with that discussed before on the hysteresis loop behaviours of different components of galloping force.

The structural damping coefficient sometimes varies to some extent with the change of the vibration amplitude during the stage before the stability of galloping vibration, for both the sectional model system and the non-wind additional aerodynamic damping are nonlinear to some extent.

The total damping coefficient c_{total} also oscillates asymmetric with time, and the oscillation also grows until the galloping becomes stable. The arithmetic average of c_{total} is not zero even during the stable stage of galloping because it is nonlinear with respect to the vibration.

Considering that the energy input by the negative aerodynamic damping force and the energy dissipated by the positive aerodynamic damping force in conjunction with the structural damping force are balanced, therefore the following energy-equivalent total damping coefficient is defined for an easy and straightforward understand on the growth mechanism and the self-limited phenomenon of galloping.

$$c_{total}^{eq} = \frac{\int_t^{t+T} c_{total}\dot{y}^2 d\tau}{\int_t^{t+T} \dot{y}^2 d\tau} = \frac{\int_t^{t+T} \left(c_s^e(a_t) - a_{01} - a_{03}\dot{y}^2 - a_{05}\dot{y}^4\right)\cdot \dot{y}^2 d\tau}{\int_t^{t+T} \dot{y}^2 d\tau} \quad (8)$$

Provided that the displacement response of galloping is governed by its fundamental frequency and the higher order multiple frequency components can be ignored. Furthermore, the amplitude, phase and frequency of response can be assumed commonly to vary slowly, then, Eqn.(8) can be simplified as follows:

$$c_{total}^{eq} = c_s^e(a_t) + c_{H_1} + c_{\varepsilon_{03}}^{eq}(a_t) + c_{\varepsilon_{05}}^{eq}(a_t) \approx c_s^e(a_t) - a_{01} - \frac{3}{4}a_{03}\omega_0^2 a_t^2 - \frac{5}{8}a_{05}\omega_0^4 a_t^4 \quad (9)$$

Figs. 20 and 21 show the evolutions of different components of the energy-equivalent total damping coefficient during galloping development for Case C1 at a lower reduced wind speed of 1.33 and at a higher reduced wind speed of 2.01. It can be seen that the oscillation phenomena vanishes in the evolutional curves of the energy-equivalent total damping coefficient as well as its all components.

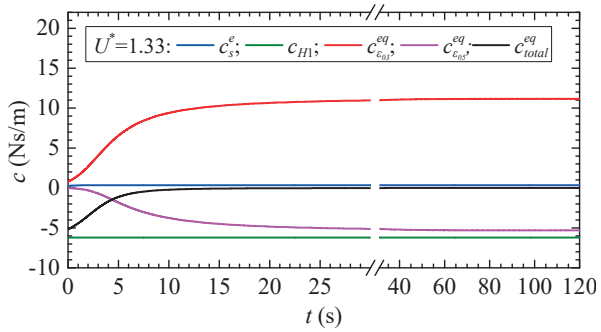

Figure 20 Evolutions of different components of energy-equivalent total damping during galloping development (Case C1, U^*=1.33)

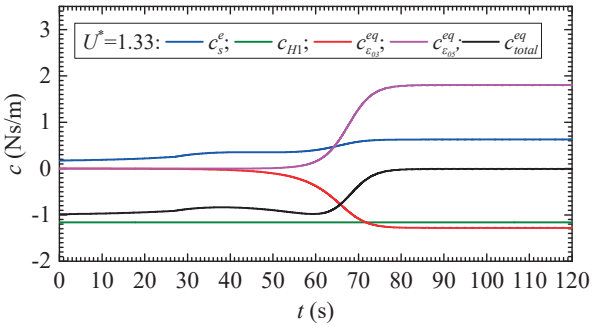

Figure 21 Evolutions of different components of energy-equivalent total damping during galloping development (Case C1, U^*=2.01)

For the case of lower reduced wind speed, the energy-equivalent nonlinear damping coefficient of $c_{\varepsilon_{03}}^{eq}$ provided by f_{v3} is positive and rises with the increasing galloping amplitude and finally attains to a maximal constant value when the galloping reaches to a stable state of LCO. On the contrary, the energy-equivalent nonlinear damping coefficient of $c_{\varepsilon_{05}}^{eq}$ provided by f_{v5} is negative and drops with the increasing galloping amplitude and finally attains to a minimal negative constant value when the galloping gets stable. The energy-equivalent total damping coefficient, c_{total}^{eq}, rises from a certain minus value to zero, which is corresponding to the stable state of galloping LCO,

When the reduced wind speed changes to a higher value of 2.01 from the lower value of 1.33, the evolution rules of $c_{\varepsilon_{03}}^{eq}$ and $c_{\varepsilon_{05}}^{eq}$ are interconverted, however, both of them are almost zero before t=40s. The energy-equivalent total damping coefficient, c_{total}^{eq} waves slightly before t≈60s due to joint influence from variations of the structural effective damping coefficient and the nonlinear aerodynamic damping coefficients $c_{\varepsilon_{03}}^{eq}$ and $c_{\varepsilon_{05}}^{eq}$. Afterwards, c_{total}^{eq} rapidly increases to a constant value of zero, which is corresponding to the stable state of galloping LCO, because of the rapid climb of $c_{\varepsilon_{05}}^{eq}$.

8. Bifurcation of galloping

The bifurcation phenomenon of galloping of the rectangular cross section were also observed in some test cases. The mechanism of this phenomenon can also be well explained and reproduced by using the unsteady and nonlinear mathematical model discussed supra. The details about the bifurcation phenomenon of galloping will not be discussed in this paper because of space limitation.

9. Concluding remarks

Both the presented refined and simplified unsteady and nonlinear mathematical model are adequate for predicting the galloping amplitude of rectangular cross sections.

In the case of lower reduced wind speeds, the linear negative aerodynamic damping force is the major power source driving galloping growth while the nonlinear positive aerodynamic damping force provided by the cubic item of velocity is the inherent factor of the self-limited phenomenon of galloping.

In the case of higher reduced wind speeds, both the linear negative aerodynamic damping force and the nonlinear negative aerodynamic damping force provided by the cubic item of velocity are the major power sources driving galloping growth while the nonlinear positive aerodynamic damping force provided by the fifth-power item of velocity is the inherent factor leading to the self-limited phenomenon of galloping.

10. Acknowledgments

This work was sponsored by the National Natural Science Foundation of China (Grant 51478360) the Fundamental Research Fund for State Key Laboratories from the Ministry of Science and Technology of China (SLDRCE15-A-03).

11. References

Gao G., Zhu L. *Measurement and Verification of Unsteady Galloping Force on a Rectangular 2:1 Cylinder*. Journal of Wind Engineering and Industrial Aerodynamics 157(2016) 76-94.

Mannini, C., Marra, A.M., Bartoli, G. *VIV-galloping instability of rectangular cylinders: review and new experiments*. Journal of Wind Engineering and Industrial Aerodynamics 132 (2014) 109-124.

Parkinson, G.V. *Phenomena and modelling of flow-induced vibrations of bluff bodies*. Progress in Aerospace Sciences 26 (1989) 169-224.

Païdoussis, M.P., Price, S.J., Langre, E. *Fluid-structure interactions: cross-flow-induced instabilities*. Cambridge University Press, Cambridge, 2010.

The work of silo capacities under the influence of the wind load

Sergei Pichugin[1], Anton Makhinko[2], Natalia Makhinko[3]

[1] *Poltava National Technical Yuri Kondratyuk University, Ukraine,*
e-mail: pichugin.sf@gmail.com
[2] *ETUAL LLC, Ukraine,*
e-mail: pasargada1981@gmail.com
[3]*National Aviation University, Ukraine,*
e-mail: pasargada1985@gmail.com

Abstract: This paper deals with the detailed studying of work of cylindrical silo capacity with vertical stiffeners under the influence of asymmetric wind load, which is represented by the completed trigonometric cosines-series. Figures of changing of the internal forces for steel silos with different geometric characteristics (the height, the diameter, the thickness of ribs and the wall of the body) are shown and the detailed analysis of factors, which influence the deflected mode of the framework, is done. The assessment of borders of the use of the capacities' calculation method is given in a table. It is offered convenient representation of the capacities' reactions in the non-dimensional polar frame of axes.

Keywords: cylindrical silos, internal forces, polar coordinates, thin-walled shell, wind loads.

1. Introduction

Cylindrical silo capacity is a shell of rotation, which is reinforced by vertical stiffeners. The main loads of the framework are the pressure of the bulk material, which cause axially symmetric load of the capacity, and the pressure of the wind flow, which belong to the asymmetric loads. The research of the deflected mode of the steel shells under the load, which is defined by the exponential law, was thoroughly examined in this paper (Makhinko and Makhinko 2018). The wind load on the vertical silos affects stiffeners and the body. Uneven distribution of the wind load along the perimeter of cylindrical capacities is described by the function of the aerodynamic coefficient $C_{aer}(\varphi)$. The factorization of the function $C_{aer}(\varphi)$ and the wind load, correspondingly, into the completed trigonometric series allow simplifying the determination of internal forces in the framework's elements. Meanwhile, the problem solving could be separate to the each element. A series of premises are taken in order to avoid complications, which is caused by the secondary factors and considering of which is of no practical value and engineering benefit. In particular, hypothesis about the absence of shifts in the middle of the capacity surface, the absence of extension of the capacity in the annular direction and assumptions about the unknown tensions, efforts of deformation and displacements, are the functions of the one coordinate x, which is plot along the height of the capacity.

2. The main material

In the general case elements of the wind load could be introduced as $W_k = A_k \cos(k\varphi)$, and the equation of equilibrium according to the momentless theory (Lessing, 1970) will be

$$N_{h,k}(\varphi) = W_k D_w / 2, \quad (1)$$

where $N_{h,k}$ are linear longitudinal efforts in radial direction; A_k is an amplitude k value of the element; D_w is the diameter of the shell.

On the fig. 1 there is more detailed information about the work of the cylindrical capacity's body under the influence of asymmetric load according to the harmonic law of cosine. From the given analysis and series of analogous figures (for silos of different height H_w, diameter D_w, thickness of rib t_p, the wall of the body t_w and different number of ribs n_p) we can make a generalizing conclusion. For capacities from the flat sheet of the small elongation $\Delta_w \le 1{,}5$ the increase of the thickness of the body sheets results in decrease of linear efforts in vertical ribs, whereas the increase of ribs' thickness, on the contrary, results in the small growth of efforts. Meanwhile, the harmonica's parameter of the load k (to $k = 6$) practically does not affect monotonous character of the given dependence. Monotony began to disappear when moving to the higher capacities $\Delta_w > 1{,}5$ or to the corrugated plates of the body. In this case, already when $k = 5$, curves of linear longitudinal efforts in meridional (longitudinal) direction $N_{p,k}(x)$ are gradually shifted to the left in the area of the little value of efforts, changing to the negative area. It means that there are zones that appear on a certain height, within which efforts of extension is functioning in vertical stiffeners. The higher capacity is, the longer the given zone.

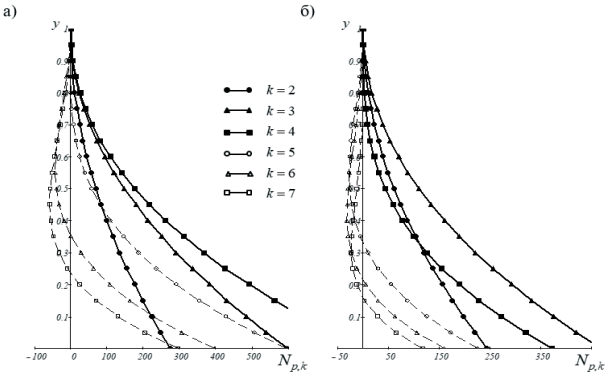

Figure 1. Linear efforts in vertical ribs of the capacity under the load $\cos(k\varphi)$ when $D_w = 10$m, $H_w = 30$m, $n_p = 30$: (a) $t_w = 6$mm, $t_p = 6$mm; (б) $t_w = 6$mm, $t_p = 12$mm

The use of corrugated plates does not eliminate the given zone, but compared to the flat sheets it "presses down" the curve of efforts stronger to the axis of ordinates. This is because the profiling reduces efforts in ribs. With regard to radial displacements, they decrease with the growth of the sheets' thickness or with the use of corrugated plates, and also decrease less with the growth of transverse section of vertical ribs. It means that from the point of view of rigidity it is more effectively to increase the thickness of body than of its ribs.

The analysis shows that one of the main factors, which influence the deflected mode of capacity, is the value of *k* harmonica of the external load. That is why there is a question about the existence of the boundary value *k*, higher of which the offered method will result in a significant mistake. The numeral value of the given mistake could be defined on the basis of the A.L. Goldenveyzer's research (Goldenveyzer, 1976).

$$k_{\ell im} = 1.67\delta_{Dt}^2\sqrt{\left(1+\alpha_{wp}\right)/\Delta J_w} \quad (2)$$

where ΔJ_w is the ratio of inertia moments of corrugated and flat sheets; α_{wp} is the coefficient that shows the ratio of the area of transverse section of stiffeners and sheets of the body; δ_{Dt} is the coefficient of the geometric scale.

Calculations, using the formula (2) for capacity D_w = 10 m, are given in the tab. 1, the data of which shows obvious suitability of the described method.

Table 1. The assessment of borders of using the method of capacities' calculation on the asymmetric load, which is represented by the trigonometric cosine-series.

t_w, mm	Flat sheet			Corrugated plate		
	k_{lim} when n_p = 30 and t_p,			k_{lim} when n_p = 30 and t_p		
	2mm	6mm	12mm	2mm	6mm	12mm
2	9958	12590	15740	1174	1485	1856
6	2969	3319	3784	1051	1174	1340
12	1438	1530	1660	1017	1083	1174

Total deflected mode of the capacity under the influence of the wind load will be consisted of the separate deflected modes of the *k* influence

$$R_D(y,\varphi) = \sum_{k=0}^{m} a_k R_k(y,\varphi) \quad (3)$$

where *R* is a generalized parameter of the reaction; *y* is a non-dimensional height $y = x/H_w$; a_k are coefficients of the factorization, the numerical values of which could be calculated by method of the least quadrates using (DBN V.1.2-2:2006, 2006).

The zero term of series (3) corresponds to the axially symmetric load, that's why it does not cause efforts in ribs. Displacements of the body are also very small, that is why in the next calculations we could ignore them. The second element a_1R_1 is the one unbalanced part of the wind load in each annular section, which causes a usual bend of the capacity. Other terms of series (3), when $k \geq 2$, could be rewritten in the form of a sum of products of some value $r_{D,k}(y)$, which corresponds to the reaction of the capacity in the point (y; φ = 0), on the cosine (sinus) of function of the reaction changing according to φ:

$$R_D(y,\varphi) = \sum_{k=1}^{m} r_{D,k}(y)\cos(k\varphi) \vee R_D(y,\varphi) = \sum_{k=1}^{m} r_{D,k}(y)\sin(k\varphi) \quad (4)$$

We could not say for sure that this conditional separation significantly simplifies calculation, but undoubtedly gives them obviousness. As an example there was made calculation of coefficients $r_{D,k}(y)$ of the linear efforts in vertical ribs and radial displacements of the body points in the table 2. It was selected a capacity with a flat wall for the calculations when D_w = 10 m, H_w = 20 m, n_p = 30: (a) $t_w = t_p$ = 6 mm. The calculated value of the wind load was w_p = 1 kPa, and conditions of fixing near the basis corresponded to the hard closing. The similar tables uniquely determine the deflected mode of capacities and are the basis for acceptance further design solutions.

Table 2. The example of amplitude calculation of trigonometric series of reactions.

y	1φ	2φ	3φ	4φ	…	10φ
Amplitude values for linear efforts in vertical stiffeners						
0.0	0	0	0	0		0
0.1	0.1	0.8	1.2	0.2		0
0.2	0.4	3	4.7	0.7		0
1.0	9.2	75.3	118.9	18.2	-	0.9
Amplitude values for radial displacements of body points						
0.0	0.5	5	17.8	4.8		0.1
0.1	0.4	4.3	15.4	4.2		0.1
0.2	0.4	3.7	13.1	3.5		0.1
1.0	0	0	0	0		0

As a convenient method of analysis of the obtained results, it is recommended to use the only non-dimensional polar frame of axes, in which dependence of the radius-vector ρ_D on angular coordinate φ is expressed as $\rho_D(\varphi) = R_D / \max(R_D)$. With the such content, the area of changing of any capacity's reaction has a diapason [-1;1], and reactions could be plotted on the one plane of references. On the fig. 2 it is shown the given frame of axes as an example of the tab. 3 and are shown figures of reactions for analogous capacity when H_w = 10 m (to the right)

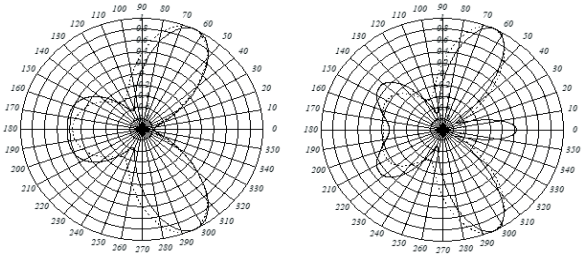

Figure 2. The representation of the capacities' reactions in the non-dimensional polar coordinates.

3. Conclusion

1. One of the main factors, which affect the deflected mode of the silo capacity under the influence of the asymmetric load according to the harmonious law of cosine, is the value of *k* harmonica of the external load.
2. The analysis of quantitative evaluation of the mistake of the border value *k* shows the obvious suitability of the described material.
3. Total deflected mode of the capacity under the influence of the wind load will be consisted of the separate deflected modes of the *k* influence, for representation of which it is convenient to use non-dimensional polar frame of references.

4. References

Goldenveyzer A *Teoriya uprugih tonkih obolochek.* Moscow, Russia, 1976.

DBN V.1.2-2:2006: *Systema zabezpechenniana diinostita bezpeky budivelnykh obiektiv. Navantazhennia i vplyvy. Normy proektuvannia*, Kyiv, Ukraine, 2006.

Lessing E.; Lileev A.б Sokolov A. *Listovyie metallicheskie konstruktsii*. Moscow, Russia, 1970

Makhinko A., Makhinko N. *Analysis of the deflective mode of thin-walled barrell shell* Academic journal. Industrial Machine Building, Civil Engineering, Poltava, Ukraine, 2 (2018) 69-78.

Wind loads for designing the main wind force resisting systems of cylindrical free roofs

Yasushi Uematsu[1], Roma Yamamura[2]

[1]*Department of Architecture and Building Science, Tohoku University, Japan,*
e-mail: yasushi.uematsu.d8@tohoku.ac.jp
[2]*Central Japan Railway Company (formerly Graduate Student, Graduate School of Engineering, Tohoku University)*

Abstract: Wind loads on cylindrical free roofs have been investigated in a wind tunnel. The main objective of the present study is to propose appropriate wind force coefficients for designing the main wind force resisting systems of the roofs considering the dynamic load effects of turbulent winds. The rise-to-span ratio, *f*/*B*, is changed from 0.1 to 0.5. The wind tunnel models were made by using a 3D printer. Overall aerodynamic force and moment coefficients were measured by a six-component force balance. Wind force distributions along two representative arc lines on the roof were measured by differential pressure transducers. Assuming that the roof is rigid and supported by four corner columns, the axial forces induced in the columns are regarded as the most important load effect for discussing the design wind loads. Based on the results, design wind force coefficients are proposed as a function of *f*/*B* for two representative wind directions. The roof is divided into three zones, i.e. windward, central and leeward zones, and constant wind force coefficients are provided to these zones. Two load cases, which correspond to the maximum tension and compression induced in the columns, are considered.

Keywords: cylindrical free roof, wind load, main wind force resisting system, wind tunnel experiment, dynamic load effect.

1. Introduction

Free roofs are widely used for structures providing shade and weather protection in public spaces. The roof is supported by columns and no walls. Being light and flexible, they are vulnerable to dynamic wind actions. Therefore, the wind resistance is one of the most important technological problems, when designing these roofs. Regarding planar free roofs, such as gable and mono-sloped roofs, extensive researches have been made by many researchers, e.g. Uematsu et al. (2007). Wind loads on hyperbolic paraboloid free roofs were studied experimentally by Uematsu et al. (2014) and numerically by Takeda et al. (2014).

Only a few studies have been made of the wind loads on cylindrical free roofs, probably due to the difficulties in model making and pressure measurement. Natalini et al. (2013) investigated the wind loads on cylindrical free roofs in a wind tunnel. They measured only the mean wind pressures acting on the roof. Dynamic load effect of turbulent winds was not discussed.

The present paper investigates the design wind loads for the main wind force resisting systems of cylindrical free roofs, based on the measurements of the overall aerodynamic forces and moments on the roof model as well as of the wind force distributions along two representative lines on the roof.

2. Wind tunnel experiment

Fig.1(a) shows the model buildings under consideration here together with the notation and coordinate system used in the present paper. The span B and the width W are both 15 m. The rise-to-span ratio, f/B, ranges from 0.1 to 0.5. The mean roof height H is 8 m regardless of the f/B ratio.

Two series of wind tunnel experiments are carried out; the lift L and the aerodynamic moments, M_x and M_y, about the x and y axes are measured by a six-component force balance in the first series of experiments, while the wind force distributions along two representative lines, referred to as Lines C and E in Fig. 1(b), are measures by differential pressure transducers in the second series of experiments. The wind tunnel models are made by using a 3D printer with a geometric scale of 1/100. The roof thickness and the diameter of four columns supporting the roof are respectively 1 mm and 5 mm in the first series of experiments and 2 mm and 6.5 mm in the second series of experiments.

The wind tunnel flow is a turbulent boundary layer simulating a suburban exposure. The power law exponent of the mean wind speed profile is approximately 0.2. The wind tunnel speed U_H at the mean roof height H is approximately 9 m/s for f/D = 0.1 and 0.2 and approximately 10 m/s for f/D = 0.3 – 0.5. The turbulence intensity I_{uH} at the mean roof height is approximately 0.16. The wind direction θ is changed from 0° to 90° (Fig.1(a)).

The sampling rate of measurements is 200 Hz in the wind force measurements and 500 Hz in the wind pressure measurements. Each measurement is made for a time period of 10 minutes in full scale. The measurements are repeated 10 times under the same condition. The statistical values of wind force coefficients etc. are evaluated by applying an ensemble average to the results of these 10 runs.

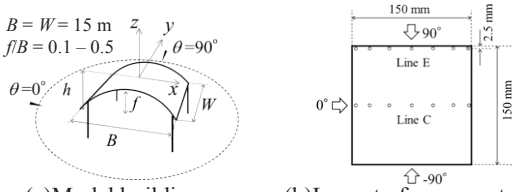

(a)Model building (b)Layout of pressure taps

Figure 1. Notation and coordinate system.

3. Experimental results

3.1 Effect of the Reynolds number on the aerodynamics

The Reynolds number Re is defined in terms of U_H and two times the radius of curvature, R, of the cylindrical roof, corresponding to a circular cylinder. The wind speed U_H at the mean roof height H was varied from 3 to 11 m/s. The distributions of mean wind pressure coefficients $C_{p,\mathrm{mean}}$ along Line C on the top and bottom surfaces of the roof were measured at various Re numbers; the wind pressure coefficient is defined in terms of the velocity pressure q_H at the mean roof height of the approach flow. When f/D = 0.1, the distribution did not change with Re, which implies that the wind flows along the roof surface without separation. On the other hand, when $f/D \geq 0.2$, the distribution on the top surface changes with Re, which implies that the flow separates from the top surface and the separation point shifts with Re. Fig. 2 shows the results for f/B = 0.4. It is found that the distribution is hardly affected by Re when $Re > 1.0\times 10^5$. This feature is consistent with the finding by Macdonald et al. (1988) for cylindrical structures. They showed that the results obtained under such a condition represented the practical situation in full-scale. Therefore, the measurements are made at $Re > 1.0\times 10^5$ in the following sections.

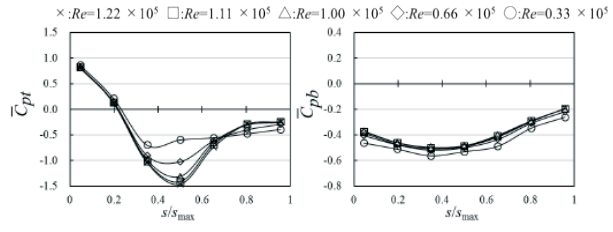

(a) Top surface (b) Bottom surface

Figure 2. Distributions of $C_{p,\mathrm{mean}}$ ($f/B = 0.4$, $\theta = 0°$, Line C)

3.2 Characteristics of wind force coefficients and load effect

Fig. 3 shows the variation of the mean values of lift coefficient C_L and aerodynamic moment coefficient C_{My} with wind angle θ. Note that C_L and C_{My} are defined as follows:

$$C_L = \frac{L}{q_H \cdot B \cdot W} \qquad C_{My} = \frac{M_y}{q_H \cdot R \cdot f \cdot W} \qquad (2), (3)$$

When the f/B ratio is small, e.g. $f/B = 0.1$, the maximum values of $C_{L,\mathrm{mean}}$ and $C_{My,\mathrm{mean}}$ occur at $\theta \approx 0°$. As the f/B ratio increases, the maximum values of $C_{L,\mathrm{mean}}$ and $C_{My,\mathrm{mean}}$ increase and the wind angles providing these maximum values also increase. For example, when $f/B \geq 0.3$, the maximum values occur at $\theta \approx 30°$.

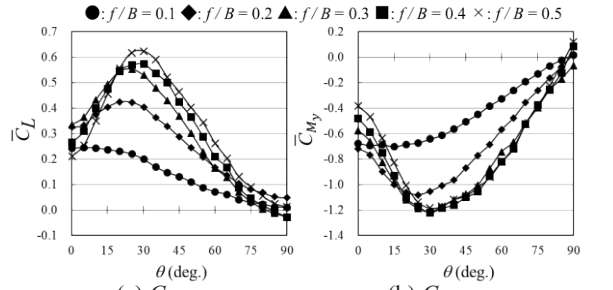

(a) $C_{L,\mathrm{mean}}$ (b) $C_{My,\mathrm{mean}}$

Figure 3. Variation of $C_{L,\mathrm{mean}}$ and $C_{My,\mathrm{mean}}$ with wind angle θ.

Next, focus is on the axial forces induced in the columns by wind loading as the load effect for discussing the design wind loads for the main wind force resisting systems, assuming that the roof is rigid and supported by four corner columns. Fig. 4 shows the variation of the maximum and minimum peak values of the non-dimensional axial forces N^* in the columns with wind angle θ. The axial forces N are computed by using the time history of C_L and C_{My} and reduced by $1/4q_HBW$. It is interesting to note that the behavior of the maximum and minimum values of N^* with θ is similar to that of $C_{L,\mathrm{mean}}$ and $C_{My,\mathrm{mean}}$.

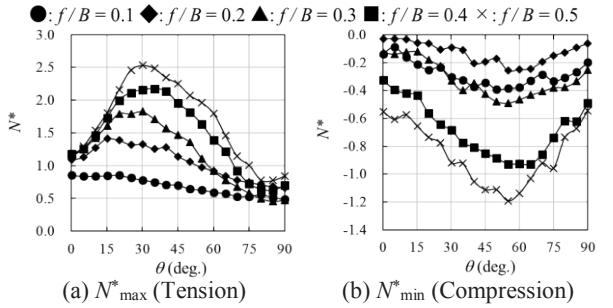

(a) $N^*_{\max}$ (Tension) (b) $N^*_{\min}$ (Compression)

Figure 4. Variation of $N^*_{\max}$ and $N^*_{\min}$ with wind angle θ.

4. Design wind force coefficients

According to the above-mentioned results, we consider two wind directions, i.e. $\theta = 0°$ and 45°, as representative values when discussing the design wind force coefficients. Considering the distribution of wind force coefficients in the arc direction, the roof is divided into three zones, R_1, R_2 and R_3, as shown in Fig. 5. Constant values of wind force coefficients, C^*_{NW}, C^*_{NC} and C^*_{NL}, are provided to these zones so that the column axial forces calculated from these wind force coefficients together with the gust effect factor G_f are equivalent to the maximum and minimum axial forces computed from the time history of C_L and C_{My} for a wind direction range around $\theta = 0°$ or 45° (WD0 or WD45). Two load cases, A and B, corresponding to the maximum tension and compression are considered. The procedure for determining the design wind force coefficients is similar to that we used in our previous studies (Uematsu et al. 2007). The results are summarized in Tab. 1.

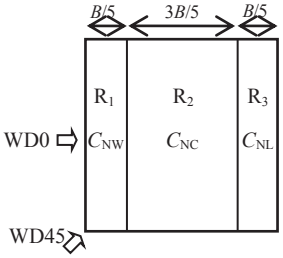

Figure 5. Zoning of the roof

Table 1. Design wind force coefficients

(a) Wind direction WD0

		C_{NW}^*		C_{NC}^*		C_{NL}^*	
Load case		A	B	A	B	A	B
f/B	0.1	1.3	0.6	-0.5	0.0	-0.5	-0.4
	0.2	0.8	0.1	-0.6	0.0	-1.0	-0.3
	0.3	0.8	0.2	-0.7	0.0	-1.0	-0.4
	0.4	0.9	0.3	-0.8	0.0	-0.7	-0.7

(b) Wind direction WD45

		C_{NW}^*		C_{NC}^*		C_{NL}^*	
Load case		A	B	A	B	A	B
f/B	0.1	0.2	0.7	-0.6	0.0	-0.4	-0.4
	0.2	0.8	0.6	-0.7	-0.1	-1.0	-1.3
	0.3	0.8	0.8	-0.8	-0.3	-1.1	-2.1
	0.4	0.7	0.8	-0.8	-0.3	-1.3	-2.7

5. Concluding remarks

The wind force coefficients for designing the main wind force resisting systems of cylindrical free roofs have been proposed as a function of the rise-to-span ratio. Based on the variation of wind forces and the resulting load effect with wind angle, two wind direction ranges are considered, WD0 and WD45.

The present study was financially supported by Nohmura Foundation for Membrane Structure's Technology (2015).

6. References

Macdonald, P.A., Kwok, K.C.S. and Holmes, J.D. *Wind loads on circular storage bins, silos and tanks: I. Point pressure measurements on isolated structures*. Journal of Wind Engineering and Industrial Aerodynamics 31 (1988) 165-188.

Natalini M.B., Morel C., Natalini B. *Mean loads on vaulted canopy roofs*. Journal of Wind Engineering and Industrial Aerodynamics 119 (2013) 102-113.

Takeda F., Yoshino T., Uematsu Y. *Design wind force coefficients for hyperbolic paraboloid free roofs*. Journal of Physical Science and Application 4(1) (2014) 1-19.

Uematsu Y., Iizumu E., Stathopoulos T. *Wind force coefficients for designing free-standing canopy roofs*. Journal of Wind Engineering and Industrial Aerodynamics 95 (2007) 1486-1510.

Uematsu Y., Miyamoto Y., Gavanski E. *Wind loading on a hyperbolic paraboloid free roof*. Journal of Civil Engineering and Architecture 8(10) (2014) 1-19.

A short historical overview of wind characteristics and wind pressure for design in Romania

A. Aldea[1*], S. Demetriu[1], R. Văcăreanu[1], D. Lungu[1], C. Neagu[2], C. Arion[1]

[1]*Technical University of Civil Engineering Bucharest, Romania,*
** Corresponding author, e-mail: alexandru.aldea@utcb.ro*
[2]*Dublin City Council, Ireland,*

Abstract: The paper gives an overview of the wind observations in Romania, with historic data especially after the creation of the national meteorological network in 1884. Data on wind directions and velocities are presented, with a focus on a sample of 14 cities including the capital Bucharest. The historical evolution of the national zonation maps for wind pressure is shown. A statistical description of the maximum annual wind velocity database is also presented.

Keywords: wind characteristics, wind velocity, wind pressure, zonation map.

1. Introduction

Located in the East of Europe, Romania is a country with a transition temperate-continental climate (*National Meteorological Agency*). Its territory spreads between 43.55º and 48.28º North latitude and 20.25º and 29.83º East longitude.

The Meteorological Institute (founded in 1884) started to provide data on July 1st 1884. At the beginning of 1885 there were 5 stations in operation: Bucharest, Sulina, Galati, Giurgiu and Strihareţ. In the same year other 6 stations were installed: Turnu-Severin, Balota, Constanta, Craiova, Păncesci-Dragomiresci and Iaşi. On July 3rd, 1948, Romania joined the Convention of the World Meteorological Organisation (created at Washington on 11th of October 1947).

The meteorological network developed rather quickly: 1887 – 30 stations, 1899 – 50 stations, 1906 – 66 stations (*Romania's climate*, 2008), 2013 – 258 stations. Nowadays the *National Meteorological Administration* (http://www.meteoromania.ro) is officially in charge with the meteorological observations. It operates 160 automated stations: 71% of stations in lowlands, 12% in hilly areas, 4% on the sea shore and 13% in mountains. Some stations are located at high altitudes, like Ceahlău Toaca – 1897 m and Călimani – 2021 m, the highest station being Vârful Omu, located at 2504 m.

The Romanian meteorological network is part of the permanent world survey – Region VI – Europe of the World Meteorological Organization.

2. Wind characteristics in Romania

2.1. Wind directions

Wind directions in Romania are influenced by the regional air movement and by the Carpathian Mountains. On the open mountain heights, the dominant wind direction is from West, which is characteristic for median latitudes (*Romania's climate*, 2008), In the centre and south of Romanian Plain the main wind directions are from West and East. In Western Romania the predominant wind direction is from South.

2.2. Wind velocity

The highest directional mean wind velocities are generally observed on the directions with higher frequencies. The study of the Meteorological Institute (*Climate of Popular Republic of Romania,1962)* indicates maximum wind velocities of 29m/s in South and East of Romania, and of 23-27m/s in West. In Central Romania wind velocity rarely reached 20-25m/s. At Varful Omu wind velocity overpasses 30m/s almost each year, on 9th of December 1955 being recorded a maximum of 43.8m/s.

A more recent study of the National Meteorological Administration (*Romania's climate*, 2008) indicates that the annual maximum wind velocity was ≥40m/s at all mountain stations in open terrain, in most of the Moldavia region, North of Dobrogea and on the Black Sea coast. In few areas in Transylvania plateau and in protected mountain areas, the annual maximum wind velocity was lower than 20m/s. In the rest of the territory the annual maximum wind velocity is 20÷30m/s.

2.3. Wind direction and velocity in Bucharest

Bucharest, the capital city of Romania, is located in the southern part in the Romanian plain; its altitude varies between ~60 m and ~100 m. Maybe the oldest methodical observations on wind directivity in Bucharest are the ones made by Lessmann in 1870.

Wind directivity (NE-E) displays a rather constant pattern.

3. Evolution of wind pressure maps

The first provisions for design for wind action were included in *STAS 946-56* together with those for snow and temperature actions. The wind pressure map has 2 zones with 0.5 and 0.7 kN/m^2. Romanian standards *STAS 10101/20-75* and *STAS 10101/20-78* were devoted to wind action and the wind pressure map have 5 zones: 0.45, 0.55, 0.7, 0.85 kN/m^2 and a special mountain area region. The 1990 edition of the *standard STAS 10101/20-90* included a new zonation map with 5 zones: 0.30, 0.42, 0.55 kN/m^2 and 2 special zones. The map is based of reference wind velocity values with a mean return period of 10 years.

In preparations for joining the European Union in 2007, a new edition of the wind code was issued: *NP-082-2004*, representing a transition toward Eurocodes. The wind pressure map, has 4 zones: 0.4, 0.5, 0.7 kN/m^2 and a special mountain region where wind pressure is ≥ 0.7 kN/m^2. The reference wind velocities are characterised by a 50 year mean return period (Lungu et al., 1995, Lungu et al., 2010).

4. CR-1-1-4/2012 design code

The code *CR-1-1-4/2012* follows the *EN 1991-1-4* provisions, it is mandatory and was enforced by Order 1751/2012 of the Minister of Regional Development and Tourism. As the EN, the code applies to buildings and civil engineering works with heights up to 200 m and to bridges having no span greater than 200 m, provided that they satisfy certain criteria for dynamic response.

The basic (reference) wind velocity and pressure have the same definitions as in the EN. The code provides a national zonation map (Fig. 1) for the reference wind pressure (computed from the fundamental value of basic wind velocity, which is the characteristic wind speed averaged on 10 minutes, at a height of

10 m above flat open country terrain, having 2% annual probability of exceedance) to be used for altitudes lower than 1000m.

Based on the zonation map, the code provides a table with reference wind pressure values for 337 localities.

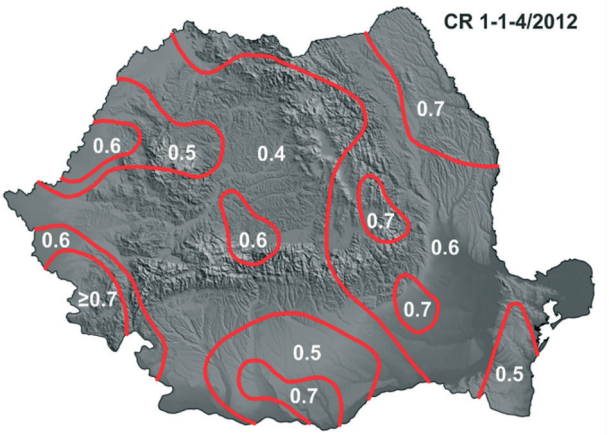

Figure 1. Wind pressure zonation map in CR-1-1-4/2012 (kN/m^2).

For the region is South-West of Romania (where the reference wind pressure is ≥ 0.7 N/m^2) and for the mountain areas at an altitude ≥ 1000m, the use of recent data from the National Meteorological Administration is recommended.

For developing the zonation map, statistical analysis and probabilistic modelling of the maximum annual wind velocities were performed. Data from the National Meteorological Administration was available at 145 stations, with records during 35 to 75 years, up to 2005. The Extreme Value (Gumbel for maxima) probability distribution was used for computing characteristic values of wind velocity with 2% annual probability of exceedance. For the selected sample of stations, the statistical characteristics of maximum annual wind velocities are presented in Tab 1.

A graphical description of the wind velocities database is also presented (for example Fig. 2).

Table 1. Statistical characteristics of maximum annual wind velocities (Lungu et al., 2010)

Location	Years of Records	Obs. Max m/s	Mean, m/s	Coef of var.	Charact, velocity *T*=50yr. m/s
Iaşi	44	33.6	16.6	0.31	29.9
Bacau	44	33.6	14.1	0.32	26.0
Tulcea	44	28.6	16.6	0.31	30.1
Constanta	44	23.5	15.8	0.18	23.3
Calarasi	44	27.7	14.6	0.29	25.8
Ploieşti	44	23.5	14.9	0.22	23.5
Bucureşti Baneasa	42	23.5	14.0	0.26	23.4
Craiova	43	28.6	18.0	0.23	28.9
Timişoara	45	24.4	14.8	0.32	27.1
Oradea	44	21.0	13.4	0.19	20.0
Targu Mureş	44	18.5	12.4	0.18	18.1
Sibiu	44	28.6	17.5	0.23	27.9

The wind pressure for design is established in the Romanian code CR 1-1-4/2012 in the same way as in the Eurocode, with the same approach, coefficients and provisions. However, a supplementary factor is considered: the wind importance-exposure factor γ_w defined for the 4 importance-exposure building categories in the Romanian code *CR-0/2012 „Basis of constructions design*".

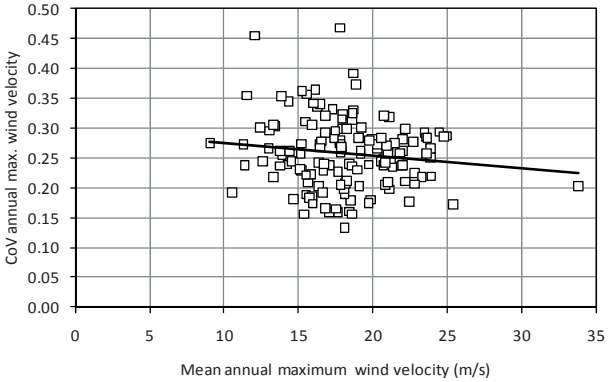

Figure 2. Coefficient of variation vs mean annual maximum wind velocity.

5. Final considerations

The recent wind load code of Romania (*CR 1-1-4/2012*) is harmonised with the *Eurocode EN 1991-1-4*. The characteristic value of the maximum annual wind velocity is obtained using Gumbel for maxima distribution, and a 2% annual probability of exceedance is considered. CR 1-1-4/2012 is accompanied by comments and examples that were published as an informative annex. A wind load application/guide volume was published (Vacareanu et al., 2013).

An update of the zonation map is necessary for considering the observed wind data from the last 13 years. It is also of interest to perform a detailed analysis on the most appropriate probability distribution model.

6. References

Climate of Popular Republic of Romania, Meteorological Institute, 1-2 (1962).

CR 1-1-4/2012, Design code. Evaluation of wind action on Constructions, MDRAP, Romania, 2012.

EN 1-1-4 Eurocode 1: Actions on structures - Part 1-4: General actions - Wind actions, CEN, 2005.

Lungu D., Vacareanu R., Demetriu S., Arion C., Aldea A.,. *Statistics of the Maximum Annual Wind Load in Romania,* 6th International Symposium on Environmental Effects on Buildings and People: Actions, Influences, Interactions, Discomfort, Eds. Flaga, A., Lipecki, T., Cracow, Polish Association for Wind Engineering, 2010.

Lungu D., Demetriu S., Aldea A. *Basic Code parameters for Environmental Actions in Romania harmonised with EC1,* Proc. 7th ICASP-7, Paris, Vol. 2, 881-887,Balkema, 1995.

National Meteorological Agency http://www.meteoromania.ro

NP-082-04, Design code. Basis of design and actions on constructions. Wind action, MTCT, Romania, 2004.

Romania's climate, National Meteorological Administration, Romanian Academy Publishing House, 2008.

STAS 946-56 Climatic Loads, Romanian Standardization Institute, Bucharest, 1956.

STAS 10101/20-75, Actions upon structures. Loads due to wind, Romanian Standardization Institute, Bucharest, 1975

STAS 10101/20-78, Actions upon structures. Loads due to wind, Romanian Standardization Institute, Bucharest, 1978

STAS 10101/20-90, Actions upon structures. Loads due to wind, Romanian Standardization Institute, Bucharest, 1990.

Vacareanu R., Pavel F., Aldea A., *Guide for evaluation of wind action on constructions according to CR 1-1-4/2012*, Ed. Conspress of Technical University of Civil Engineering Bucharest, 2013.

Wind tunnel tests of wind pressure distributions over wall and roof surfaces of the Sienna Towers high-rise building

Grzegorz Bosak[1], **Renata Kłaput**[1], **Agnieszka Kocoń**[1], **Andrzej Flaga**[1]

[1] *Wind Engineering Laboratory, Department of Structural Mechanics, Faculty of Civil Engineering, Cracow University of Technology, e–mail: liwpk@windlab.pl*

Abstract: The article presents results of model tests carried out in an aerodynamic tunnel with a wall layer wind pressure distributions over exterior surfaces of a Sienna Towers building model. The Sienna Towers building complex consists of three high-rise buildings placed near to each other. The nearest surroundings of the complex was modelled. A structure of wind flow in urban terrain was simulated, which corresponds with the destined location of the designed building. Wind tunnel tests were carried out to obtain wind pressure distributions over wall and roof surfaces of the building model. On the basis of the obtained wind pressure distributions the aggregate components of the horizontal aerodynamic forces and the rotation aerodynamic moment were calculated as a result of the integration process for each building.

Keywords: wind pressure measurements, wind tunnel, high-rise building, aerodynamic forces.

1. Introduction

A high-rise building complex, Sienna Towers, consists of three buildings marked A, B and C, which heights are equal to 86.5 m (building A) and 130.5 m (buildings B&C) respectively. The building complex is located in the centre of Warsaw in the quarter limited by Prosta street and Towarowa street. The two different measurement configurations were considered during the wind tunnel tests: first the current state of the surroundings, next the surroundings contained the buildings, which are planned to be constructed in the analysed neighbourhood. The planned structures are marked in Fig. 1 with blue colour. Computer visualization of Sienna Towers building with the nearest surroundings is presented in Fig.1.

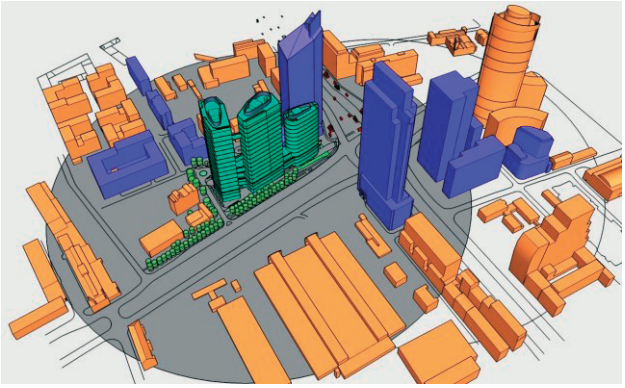

Figure 1. Computer visualization of Sienna Towers building with the nearest surroundings.

A study of the wind action on the structure is the main aim of the paper. Wind pressure distributions using during structure design and extreme values of wind pressure over the external building surfaces were obtained. On the basis of the wind pressure distributions the aggregate components of the horizontal aerodynamic forces and the rotation aerodynamic moment were calculated as a result of the integration process for each building.

2. Characteristics of wind tunnel tests

The wind tunnel tests were conducted on 1:300 scale building model in the wind tunnel of Wind Engineering Laboratory of Cracow University of Technology. The nearest surroundings was modelled. The building model was instrumented with 575 pressure taps. The test model was mounted on a turntable, allowing any wind direction to be simulated by rotating the model to the appropriate angle in the wind tunnel working section. The measurements were taken for 36 wind directions at 10° steps. The mean pressure was obtained at each tap, then the measured data were converted into the form of pressure coefficients based on the measured wind reference pressure at height equivalent to 135 m above ground on full scale. Two different measurement configurations were examined. In the first one, the nearest surroundings of the building model was in the current configuration (configuration A), in the second one planned buildings were taken under consideration (configuration B). A view of the tested model in the second measurement configuration in the wind tunnel working section is presented in Fig. 2.

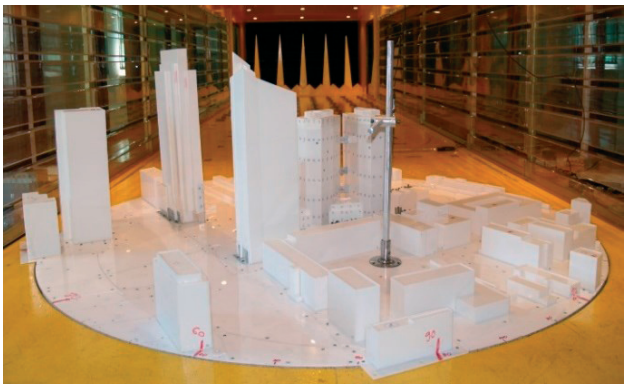

Figure 2. A view of the second measurement configuration in wind tunnel working section.

The experiments were performed at the following conditions: power law exponent of the mean wind velocity profile α=0.32; area-averaged turbulence intensity I_v=16% at the reference level (0.45m in model scale equivalent to 135m on full scale); reference velocity V_{ref}=11.3 m/s.

During the experiments, a profile pressure probe, a pressure electronic scanner, which allows measuring wind pressure in 64 taps simultaneously and a hot–wire anemometer system, were used.

On full scale, the horizontal wind action on the building was obtained by using the external pressure coefficients, taken from the measurements and the peak wind velocity pressure calculated on the reference level in Warsaw terrain. Following, the wind actions on the particular building surfaces were summed up according to Eqn. (1).

$$F_k(dir) = q_p(z_{ref}) \cdot \sum_{p=1}^{32} \sum_{A_p} C_{pe}(x,y,z,dir) \cdot \Delta A_p(x,y,z) \cdot n_k(p) \qquad (1)$$

where: $k = x,y$

3. Exemplary results

Due to set the wind pressure results the external surfaces of the analysed complex buildings were divided into sub-areas. The sub-areas have rectangular shape in most cases. Only on roof surfaces the sub-areas are marked with irregular shapes. For each sub-area a mean value of wind pressure was determined. In Fig. 3 exemplary wind pressure distributions for *dir*=90° over external surfaces of the building complex for two analysed configurations A&B using during structure design are presented. The whole result set for each configuration (A&B) consists of 36 wind pressure distributions corresponding to the analysed wind directions.

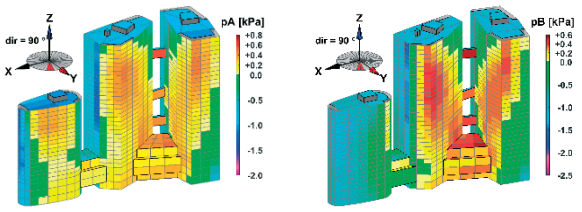

Figure 3. Exemplary wind pressure distributions (*dir*=90°) over external surfaces of the building complex for two analysed configurations A&B using during structure design.

In connection with the elevation design process the extreme positive and negative wind pressure were determined for each sub-area. Distributions of the extreme wind pressure values are presented in Fig. 4 and Fig.5.

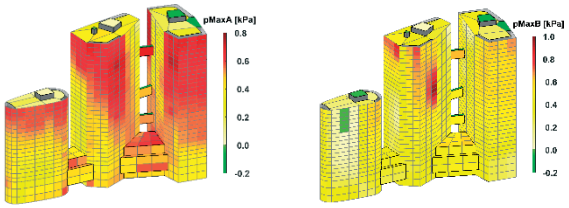

Figure 4. Extreme positive wind pressure distributions over external surfaces of the building complex for two analysed configurations A&B using during elevation design.

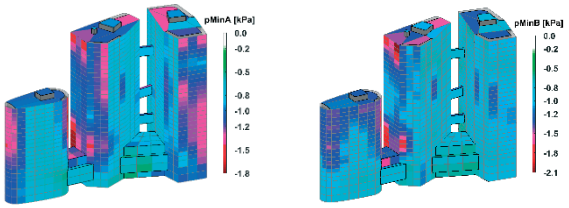

Figure 5. Extreme negative (suction) wind pressure distributions over external surfaces of the building complex for two analysed configurations A&B using during elevation design.

Generally it can be noticed that the distributions are vary in the shape but the extreme values of wind pressure in two analysed configurations A&B are not differ widely.

Wind action on the walls of the building can be reduced to resultant aerodynamic forces in horizontal plane. As a result of this, roof surfaces were not considered in determining global components of wind action. Therefore, pressure distribution on buildings walls was the base to determine horizontal aerodynamic forces acting on the buildings. The components of the horizontal wind action global forces F_x, F_y depending on the direction of air inflow *dir*, were calculated from the relationships (1) and are presented in Fig. 5.

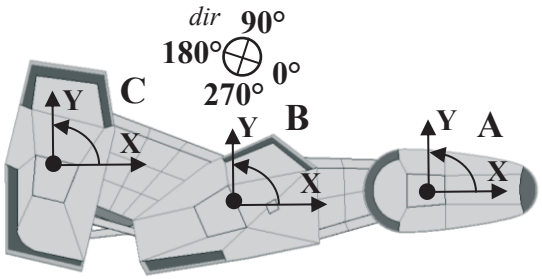

Figure 4. A global coordinate systems of buildings A, B, C in relation to a wind direction *dir*.

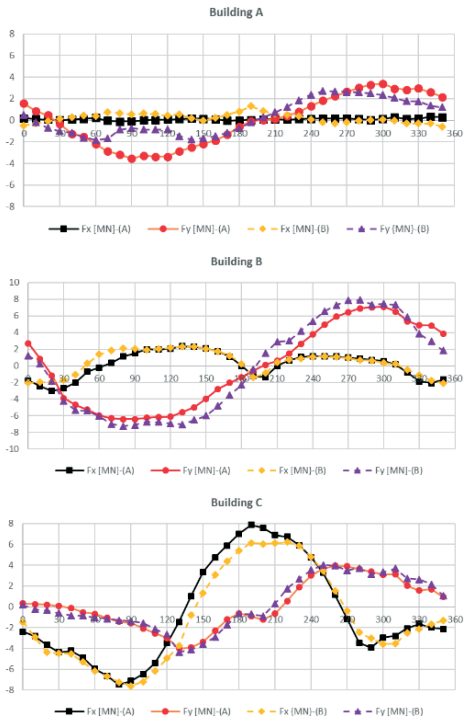

Figure 5. A global force components for building A, B, C as a function of the wind direction *dir* in A&B configurations.

4. General conclusions

As a result of the wind tunnel tests and the calculations following general conclusions are formulated:

- the horizontal global wind force components values are not differ widely compering results obtained from configurations A&B,
- it was not observed the significant difference between extreme wind pressure values occurring in configurations A&B.

5. References

Flaga A., Bosak G., Flaga Ł., Kłaput R., Porowska A., Krajewski P., Augustyn A., Pistol A. Kompleksowe badania modelowe w tunelu aerodynamicznym budynków Sienna Towers w Warszawie, Raport z badań, Politechnika Krakowska, Kraków 2017.

Global stability of lightning protection masts under wind action

Andrzej Flaga[1], Renata Kłaput[2], Agnieszka Kocoń[3]

[1]*Wind Engineering Laboratory, Faculty of Civil Engineering, Cracow University of Technology, Poland, e-mail: liwpk@windlab.pl*
[2]*Wind Engineering Laboratory, Faculty of Civil Engineering, Cracow University of Technology, Poland, e-mail: rklaput@gmail.com*
[3]*Wind Engineering Laboratory, Faculty of Civil Engineering, Cracow University of Technology, Poland, e-mail: agnieszka.kocon89@gmail.com*

Abstract: The paper presents results of wind tunnel experiments concerning wind action on two types of free-standing lighting protection masts: cantilevered and tripod. Two forms of global stability loss of lighting protection masts in strong wind were considered: overturning and shifting of mast. Own similarity criteria concerning analysed phenomena were used in these tests. It was determined whether masts fulfill the requirements of overturning and shift global stability in different wind conditions.

Keywords: wind tunnel tests, lightning protection masts, similarity criteria, global stability.

1. Introduction

Wind action has significant influence on free-standing lightning protection masts and it must be taken into account in their design. Problems concerning aerodynamics of such type of structures were considered in many publications e.g: in the case of free-standing towers (Ahmad et al., 1984, Schafer et al., 1990) or in the case of guyed masts (Gioffrè et al., 2004, Peil and Nölle, 1992). Totally different aerodynamic and stability problems take place in the case of small light free-standing lightning protection towers placed on the building roofs, together with additional supporting ballast.

Two types of lightning protection masts, i.e. cantilevered and tripod masts, have been considered in the paper. Two possible forms of global stability loss of lightning protection masts in strong winds were tested and analysed: overturning and shifting of the masts. The investigations were conducted on prototypes of the masts, so it had mainly practical aspect.

2. Wind tunnel tests

Wind tunnel tests of the cantilevered and tripod free-standing masts of 4.0 m and 6.0 m height (Fig. 1) were carried out in a boundary layer wind tunnel of the Wind Engineering Laboratory at the Cracow University of Technology.

Figure 1. View of cantilevered mast (a) and tripod mast (b).

The models of masts were made in a scale of 1:6. The measurements were realized at the following measuring conditions:

- Two terrain roughness categories: suburban (III) and city (IV) according to (PN-EN 1991-1-4, 2008),
- Specific kind of roof: flat, covered with asphalt, rectangular (2:1), 15 meters height,
- Placement of masts on the roof: in the middle and in the roof corners (a distance between the building edge and mast vertical axis is 0,25 m in model scale),
- Two arrangements of tripod mast on the roof with respect to wind direction,
- Eight angles of wind onflow,
- Range of wind velocities: 22-36.2 m/s (corresponding with 1-3 wind zones according to (PN-EN 1991-1-4, 2008).

A view of the measuring position in the wind tunnel working section is presented in Fig. 2.

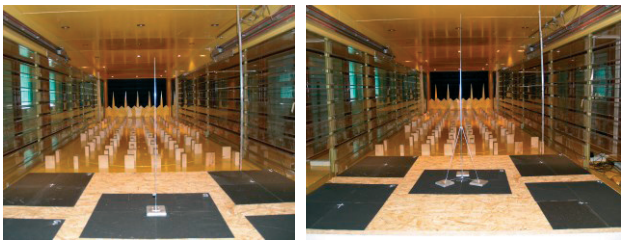

Figure 2. Models of the masts: cantilevered (a) and tripod (b) in the wind tunnel working section.

3. Similarity criteria concerning global stability loss of lighting protection masts in strong wind

Two possible forms of global stability loss of lighting protection masts in strong wind were considered:

- Mast overturning – it appears when aerodynamic rolling moment is equal to restoring moment,
- Mast shifting – it appears when aerodynamic sliding force is equal to drag force.

To determine similarity criteria of these phenomena the sets of variable quantities and parameters influencing the loss of global stability of lighting protection masts were defined. Then, the dimensional base of the issue was assumed and dimensionless quantities were designated. Finally, dimensionless functional relationships characteristic for analysed phenomena were determined. All dimensionless quantities appearing in these functional relationships are the similarity criteria of the analysed issue.

In problem of stability loss of lighting protection masts the structure gravity forces are the most meaningful, so fulfillment of Froude number is essential. The fulfilment of similarity criteria for Froude number gives the relation: $k_V = \sqrt{k_H}$.

However, the criterion of Froude number is inconsistent with criterion of Reynolds number. Nevertheless, the range of wind velocity for both models and prototypes are at a subcritical range of Reynolds number. Hence, unfulfillment of this criterion does not give essential mistakes in the results of tests in model and natural scales.

Moreover, it is impossible to fulfill criteria of Froude and Cauchy numbers simultaneously. Taking into account that vibrations of mast have secondary role in stability loss, unfulfillment of Cauchy number is not significant negligence in practical assessment of investigated phenomena.

Finally, assuming Froude number as a basic similarity criterion, the velocity scale was: $k_V = 0.41$.

4. Results

A set of arrangements for cantilevered and tripod masts for different angles of wind onflow is given in Tab.1 and Tab.2. In further analysis the respective masts arrangements are identified by the prescribed numbers.

Table 1. Set of arrangements for cantilevered and tripod masts with respect to the roof.

1	2	3
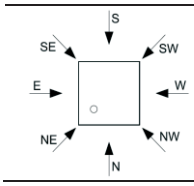	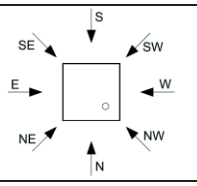	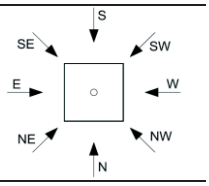

Table 2. Set of arrangements of tripod mast with respect to the windward edge of the roof.

A	B
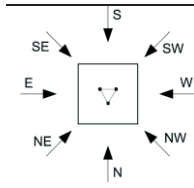	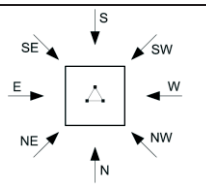

Figs. 3 and 4 show wind velocities at which masts started losing its stability because of foundation one-side-lifting in the case of IVth terrain category. Dash lines mark basic wind velocity for 1 and 3 wind zones according to (PN-EN 1991-1-4). All presented velocities are in model scale.

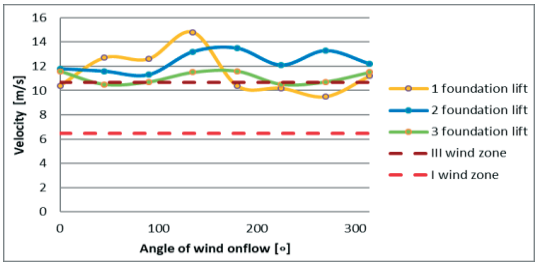

Figure 3. The velocities of the windward foundations lift for cantilevered mast and IV terrain category

The following remarks concerning cantilevered mast can be drown:

- The most unfavorable angles of wind onflow appear in the situations when mast is localized in the middle of the building roof,
- The most favorable angles of wind onflow appear in the situations when mast is localized on the leeward side of the building.

For tripod mast it can be concluded that:

- The most unfavorable angles of wind onflow appear in the situations when one mast leg is on the windward side and two legs are on the leeward side of the mast. The most favorable are the opposite situations.

a)

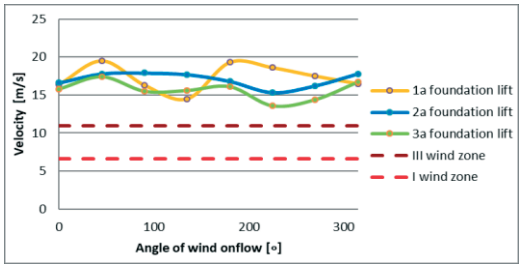

b)

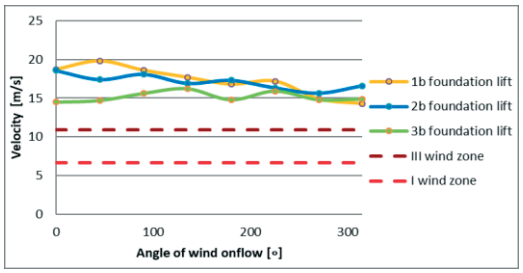

Figure 4. The velocities of the windward foundations lift for tripod mast and IV terrain category for arrangements: A (a), B (b).

5. Conclusions

Basing on the results the following two general conclusions can be drawn:

1. The cantilevered mast is safe with respect to global stability loss in the range of the base wind velocities up to 30 m/s.
2. The tripod mast is safe with respect to global stability loss in the range of the base wind velocities up to 36.2 m/s.

These conclusions concern nature scale. On the basis of them it can be stated that tripod mast can be safely located in all wind zones in Poland while cantilevered mast only in I and II wind zone. The latter should not be located in III zone which is generally area of mountains where terrain height changes rapidly. It should be pointed out that even if free-standing masts are located in appropriate wind zone, there will be still need to check local features of their localization place. Moreover, any circumstances which could increase wind action on masts must be considered and if such situation appears this instance should be examined separately.

6. Acknowledgments

This research work was supported by ZERPOL.

7. References

Ahmad M.B., Pande P.K., Krishna P. *Self-supporting towers under wind loads*. ASCE, J. Struct. Eng 110 (1984) 370-384, 1984.

Gioffrè M., Gusella V., Materazzi A.L., Venanzi I. *Removable guyed mast for mobile phone networks: wind load modeling and structural response*. Journal of Wind Engineering and Industrial Aerodynamics 92 (6) (2004) 463-475.

Peil U., Nölle H. *Guyed masts under wind load*. Journal of Wind Engineering and Industrial Aerodynamics 43 (1–3) (1992) 2129-2140.

Schafer B.L., Banks R.W., Holmes J.D. *Wind-induced oscillations of a free-standing tower*. 8th Conference on the 'In situ Behaviour of Structures', Bacu, Romania, 20-22 September 1990.

PN-EN 1991-1-4 *Eurocode 1: Actions on structures. Part 1-4: General actions. Wind actions*; PKN, November, 2008.

Wind flow around a church – Full scale measurements

Paulina Jamińska-Gadomska[1], Tomasz Lipecki[2], Michał Pieńko[3], Jerzy Podgórski[4]

Department of Structural Mechanics, Lublin University of Technology, Poland,
[1]e-mail: p.jaminska@pollub.pl
[2]e-mail: t.lipecki@pollub.pl
[3]e-mail: m.pienko@pollub.pl
[4]e-mail: j.podgorski@pollub.pl

Abstract: The paper presents results of full-scale measurements of wind flow passing through the bell tower rising over a church roof. Three ultrasonic anemometers were mounted on the roof of the church, along the horizontal centreline of the bell towers. The main goal was to capture the increase and decrease of the wind speed caused by the layout of the bell tower walls. The wind speed ratios where calculated in the three measurement points. The obtained results were used for validation of the CFD simulations.

Keywords: wind engineering, full-scale measurements, CFD, environmental actions, wind speed.

1. Introduction

The changing speed of the wind flow going through a passage is a well-known problem in Wind Engineering, e.g. (Blocken et al., 2007, Blocken et al., 2008). This phenomenon is very important especially from the pedestrian comfort point of view (Li et al., 2015, Stathopoulos and Wu, 1995). All of the cases that the authors found in the literature are based on the theoretical shapes, and the test where performed in wind tunnels or using CFD. The structure of the bell-tower described in this paper is raised above the roof of the church, so it does not influence people. It has very interesting layout and can be used to study the presence of Venturi effect in a full scale in civil engineering. Moreover, the authors had the opportunity to validate CFD simulations by the data obtained from the full-scale measurements.

2. Bell-tower description

The discussed bell tower raises above the roof of the cylindrical church (diameter equals to 44 m, height – 15 m) with a sloping roof (Fig. 1). The bell tower consists of two walls coming from the ground as a broad structures up to 38.5 m of height where they become more slender. The wall thickness is 0.4 m with the increase in the dimension to 0.8 m at the passage end. The horizontal angle between the walls is equal to 100°. The passage between the walls is in west-east direction and its dimension is constant (2.5 m).

Figure 1. Front view of the church, with the anemometers placed along the horizontal centreline of the passage.

The predominant wind direction in Poland is from the west, therefore the authors expected to encounter significant values of wind speed from that direction.

3. Full-scale measurements

Three ultrasonic anemometers were mounted on the higher part of the church roof, along the horizontal centreline of the bell towers, at height of 3.4 m over the roof (Fig. 2). The position of the measurement points was established based on the CFD simulations (Jamińska-Gadomska et al., 2018) which indicated the approximate location of maximum and minimum values of wind speed in the front and at the back of the passage. Two location variants were tested. The first one is shown in Fig. 3, in the second one, anemometers w2 and w1 where shifted 1 m away from the first position, outside the centre of the church bell tower.

Figure 2. View of the anemometers placed in the horizontal centreline of the passage.

The measurements lasted 3 months with short technical breaks. The data was gathered with use of the National Instruments equipment, described by Sumorek (2016), and recorded with the time step of 0.2 s.

For control purposes three cap anemometers were mounted on the same masts as ultrasonic ones, at height of 2 m. They recorded data every 10 s giving mean value in such time duration and 2 s max values.

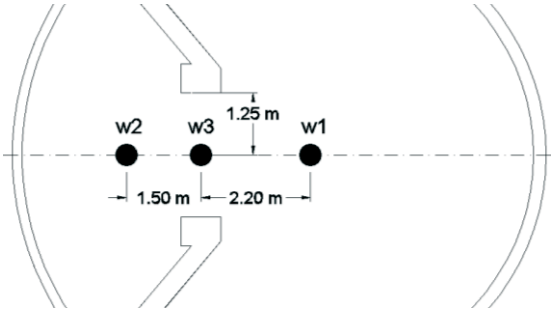

Figure 3. Top view, location of the measurement points.

4. Results

The 3D CFD simulations were performed for different angles of wind attack including diverging and converging arrangements of walls. The influence of the bell tower walls on the flow was calculated as the amplification factor K – defined as the ratio of the local wind speed at a given height (U_H) to the wind speed at the same height in undisturbed conditions (U_{0_H}), (Jamińska-Gadomska et al., 2018):

$$K = \frac{U_H}{U_{0\_H}} \tag{1}$$

The CFD simulations indicated approximate distances from the bell tower centreline where the maximum amplification/reduction of the speed took place. In these places ultrasonic and cup anemometers were mounted. Since it was impossible to measure the wind speed in full-scale in the undisturbed flow at the same height as the sonic anemometers were placed, the amplification factors were calculated as ratios between values obtained in points w2, w3, w1. The results from the full-scale measurements were normalized with the values measured in point w3 and compared with simulation results. Figures 4 and 5 presents amplification factor K obtained from CFD simulation, for converging and diverging arrangement of the bell tower walls with the normalized mean wind speed results based on full-scale measurements.

Full-scale measurements were conducted in 3-4 hours intervals. Only wind speeds corresponding to the west or east wind (converging walls – 0° and diverging walls – 180°, respectively) were taken for further analyses and on this base mean values were calculated.

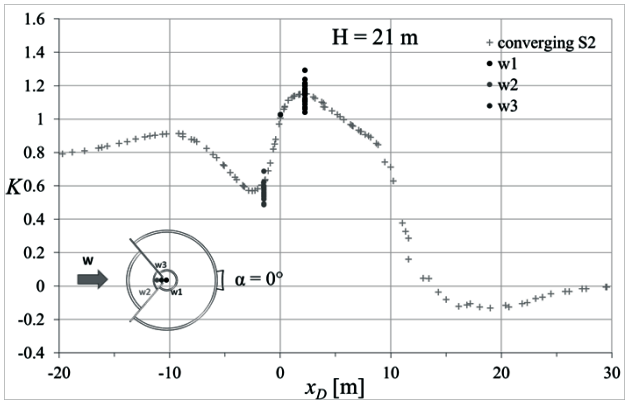

Figure 4. Amplification factor along the horizontal centreline of the bell tower for converging arrangement for the CFD and full-scale results.

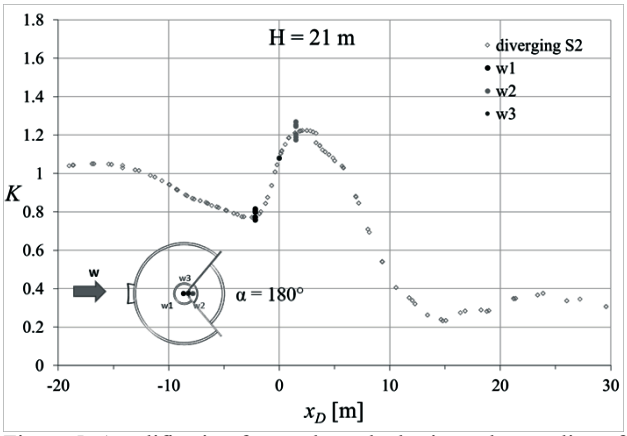

Figure 5. Amplification factor along the horizontal centreline of the bell tower for diverging arrangement for the CFD and full-scale results.

5. Conclusions

Basing on the amplification factor K, it can be noticed that the wind speed decreases in front of the walls and speed up just behind the passage. The amplification of the flow is higher in case of diverging walls. The CFD results and the results obtained from the full-scale measurements are similar.

6. References

Blocken B., Moonen P., Stathopoulos T., Carmeliet J. *Numerical Study on the Existence of the Venturi Effect in Passages between Perpendicular Buildings*. Journal of Engineering Mechanics 134(12) (2008) 1021-1028.

Blocken B., Carmeliet J., Stathopoulos. *CFD evaluation of wind speed conditions in passages between parallel buildings - effect of wall-function roughness modifications for the atmospheric boundary layer flow*. Journal of Wind Engineering and Industrial Aerodynamics 95(9-11) (2007) 941-962.

Jamińska-Gadomska P., Lipecki T., Podgórski J. *Wind Flow around a Church – Case Study*. AIP Conference Proceedings Computer Methods in Mechanics (CMM2017) 1922(110002) (2018) 1-8.

Li B., Luo Z., Sandberg M., Liu J. *Revisiting the 'Venturi Effect' in Passage Ventilation between Two Non-Parallel Buildings*. Building and Environment 94 (2015). 714-722.

Stathopoulos T., Wu H. Generic Models for Pedestrian-Level Winds in Built-up Regions. Journal of Wind Engineering and Industrial Aerodynamics 54-55 (1995): 515-525.

Sumorek A. *System Do Pomiarów Obciążenia Wiatrem Rusztowań Elewacyjnych*. Informatics Control Measurement in Economy and Environment Protection 6(4) (2016) 37-42.

Tornado-induced wind load on structures and its risk assessment

Shuyang Cao[1], Jin Wang[2], Jinxin Cao[3]

[1]*State Key Lab of Disaster Reduction in Civil Engineering, Tongji University, Shanghai 20092, China, e-mail: shuyang@tongji.edu.cn*
[2]*College of Civil Engineering, Tongji University, Shanghai 20092, China, e-mail: shuyang@tongji.edu.cn*
[2]*State Key Lab of Disaster Reduction in Civil Engineering, Tongji University, Shanghai 20092, China, e-mail: jinxin@tongji.edu.cn*

Abstract: Tornadoes are strong vortices with high wind speeds that cause severe damage to structures. This paper presents physical and numerical simulations of tornado-induced wind loads on structures, followed by a risk assessment of roof structure. This study shows that the tornado-induced wind pressures have different characteristics than those caused by boundary layer flows. A fragility framework of wood-frame low-rise building subjected to tornado hazards is established, based on which the equivalent Enhanced Fujita scale of a tornado can be estimated from the damage extent.

Keywords: Fragility analysis, low-rise building, numerical simulation, physical modelling, tornado-induced wind load.

1. Introduction

Tornadoes are strong vortices with high wind speeds that cause severe damage to structures. Researchers have qualitatively studied tornado-induced wind loads on structures and realized that tornado-structure interaction is different from that under a known, steady velocity profile in a planetary turbulent boundary layer. For a structure attacked by a tornado, some important features such as sudden pressure suction on outer building surfaces during the passage of the tornado, dynamic loading from the tornado, additional loading due to peak pressure and flow unsteadiness, and the impact of flying debris have been previously identified (Chang 1971). However, because the probability of a building being hit by a tornado is extremely low, there has been less study on tornado loads than on conventional strong boundary-layer winds, and no tornado-resistant design method for structures has been established. However, in the past two decades, the incidence of tornadoes in non-traditional tornado-prone countries such as China has increased. Although tornadoes in China are not as strong as those in the USA, they do occur in eastern China. Golden and Snow (1991) reported that China experiences 10-100 tornadoes per year. This has had a significant impact on society, and has motivated the present study.

This paper describes recent tornado-related researches conducted at Tongji University, China. The numerical and physical modelling of tornado-like vortices are introduced, followed by a description of tornado-induced wind loads on low-rise building models. Finally a fragility framework of wood-frame low-rise building subjected to tornado hazards is established.

2. Physical and numerical modelling of tornado-like vortices

Physical simulations of tornado-like vortices have been many commencing with Ward (1972), who modelled tornado-like flow by mounting a fan above the test area to provide an updraft, and guide vanes around the test area to generate swirling flow. On the other hand, Haan et al. (2008) constructed a large tornado vortex simulator at Iowa State University, USA for wind engineering applications, which was a modification of the Ward-type tornado vortex simulator. The differences between the wind-load characteristics of buildings of tornado type and conventional boundary-layer type strong winds, as well as the effects of translation velocity of a moving tornado, have been intensively investigated (Mishra et al. 2008, Sengupta et al. 2008, Haan et al. 2010, Sabareesh et al. 2013). In addition, the 25-m diameter WindEEE dome at Western University, Canada offers a novel technique to physically model EF3 (Enhanced Fujita Scale 3) tornado-like flows (Hangan et al. 2015).

The tornado-like vortex simulator built at Tongji University, China adopted the same mechanism as ISU-type simulator to generate tornado-like vortices. As shown in Figure 1(a), the physical simulator has a circular duct, 1.5m in diameter and 1.0m in height, which is suspended over head with a 0.5m diameter updraft holding a controlling fan to generate a strong updraft. A screen and a honeycomb below the fan are mounted at the centre of the duct. In total, 18 guide vanes with adjustable orientation angle are placed at the top of the simulator equally along the inner periphery of the annular duct to generate a rotating downdraft that causes a swirling flow.

The tornado-like vortex simulator is numerically modelled, in which a partial angular duct illustrated in Figure 1(b) is set to introduce the rotating downdraft flow by imposing boundary conditions of velocity instead of physical modelling of guide vanes. An open source solver OpenFOAM is used to solve the governing equations.

Figure 2 compares the horizontal profile of tangential velocity of large eddy simulation with the experimental and field measurement data, which shows that the numerical, laboratory and field data exhibit a similar variation tendency of tangential velocity, i. e, the tangential velocity increases and decreases with distance from the vortex centre inside and outside the vortex core, respectively, with a maximum tangential velocity at the vortex core radius.

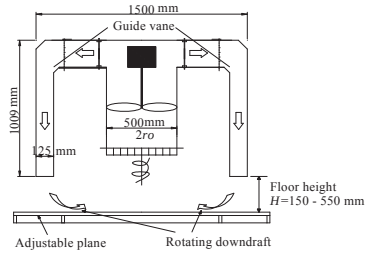

(a) ISU-type simulator at Tongji University

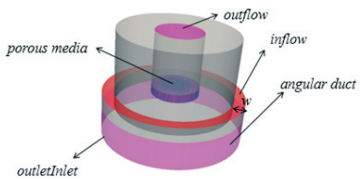

(b) Numerical ISU-type simulator

Figure 1. Schematic diagram of physical and numerical tornado simulators.

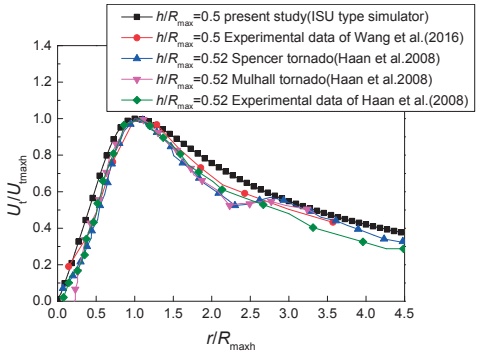

Figure 2. Comparison of horizontal mean velocity profile among numerical, experimental and field data.

3. Physical and numerical investigations of tornado-induced wind loads

The characteristics of wind pressures on a cubic building model exposed to stationary and non-stationary tornado-like vortices are investigated. The wind pressures are measured on both external and internal surfaces of the building model placed at several locations with different distances to the tornado core. Different opening configurations with three opening ratios and two azimuths of large opening are considered for the cubic building model used in the tornado simulator experiments. The effects of opening ratio, single central opening azimuth and radial distance between the building model and tornado-like vortex on external and internal wind pressure distributions are analysed. The difference of wind pressures between the tornado-like flow and the standards of ASCE 7-10 (USA) and GB 50009-2012 (China) are quantified.

Figure 3 illustrates the flow around the cubic model at model height at different radial distance to vortex centre. Figure 4 shows the external wind pressure coefficients at walls and roof when the model is located at tornado centre.

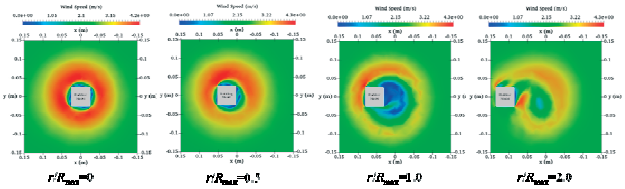

Figure 3. Flow around the cubic model at model height.

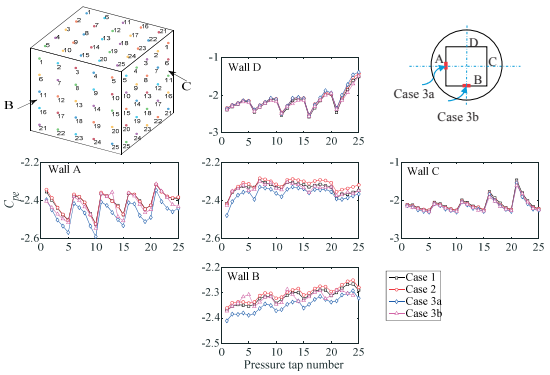

Figure 4. External wind pressure coefficients at walls and roof.

4. Fragility analysis of wood-frame low-rise building roof subjected to tornado hazards

Roof damage is one of the most common failure mode in a high wind event such as tornado. The fragility curves of roof failures for low-rise building are developed with the focus on the roof panels and roof-to-wall connections failures. Two different nail spacing for roof panels and three types of roof-to-wall connections are considered. This study considers different damage levels for roof panels and roof-to-wall connections. In addition, the failure probabilities of roof panels and roof-to-wall connections as a function of the proximity of the tornado to the low-rise building (i.e. radial distance to vortex center) is explicitly studied. The results show that improving the attachment strength of the roof sheathing and roof-to-wall connection have significant effects on reducing the failure probabilities of the roof system. Additionally, the results show that under the same maximum wind speed in a tornado and a straight-line wind event, the tornado would cause more severe damages to roof sheathing panels and roof-to-wall connections when the building is inside or at the core radius of the tornado, which indicates that a direct use of the provisions in ASCE 7-10 code for designing for tornado hazard would underestimate the failure probability of the roof system. Figure 5 displays the failure probability of roof panels with different damage levels.

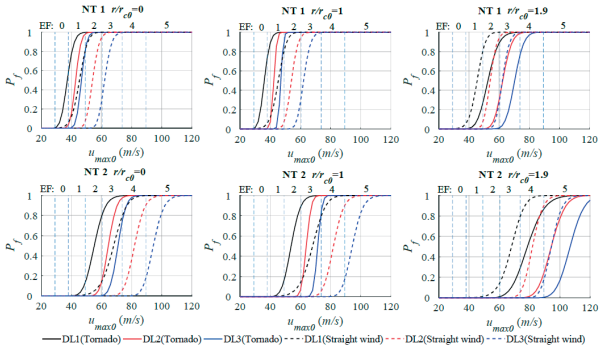

Figure 5. Failure probability with different damage levels.

5. Acknowledgments

This research was funded by Chinese NSFC Grant No. 51720105005 and 51478358, Cooperative Research Program of Tongji University No. TMGFXK-2015-003 and Fundamental Research Funds for the Central Universities.

6. References

Chang C.C. *Tornado wind effects on buildings and structures with laboratory simulation*. Proceedings of the third international conference on wind effects on buildings and structures, Tokyo, Japan, 1971.

Golden J. H., Snow J.T. *Mitigation against extreme wind storms*. Rev. Geophys. 29(1991) 477-504.

Haan F.L., Sarkar P.P., Gallus W.A. *Design, construction and performance of a large tornado simulator for wind engineering applications*. Eng Struct 30 (2008) 1146-1159.

Haan F.L., Balaramudu V.K., Sarkar P.P. *Tornado-induced wind loads on a low-rise building*. Struct Eng 136 (2010) 106-116.

Hangan H. et al. *Novel techniques in wind engineering*. J Wind Eng Ind Aerodyn 171 (2017), 12-33.

Mishra A.R., James D.J., Letchford C.W. *Physical simulation of a single-celled tornado-like vortex, Part B: Wind loading on a cubical model*, J. Wind Eng. Ind. Aerodyn. 96 (2008) 1258-1273.

Sabareesh G.R., Matsui M., Tamura Y. *Characteristics of internal pressures and net local roof wind forces on a building exposed to a tornado-like vortex*. J Wind Eng Ind Aerodyn 112 (2013), 52-57.

Sengupta A., Haan F.L., Sarkar P.P. *Translating loads on buildings in microburst and tornado winds*. J Wind Eng Ind Aerodyn 96 (2008), 2173-2187.

Ward N.B. *The exploration of certain features of tornado dynamics using a laboratory model*. J Atmos. Sci. 29 (1972) 1194-1204.

Sensitivity of simulated tornado-induced tree-fall patterns to choice of vortex model: Application to empirical tornado fragility functions

Maciej Dutkiewicz[1], David B. Roueche[2]

[1]*Faculty of Civil and Environmental Engineering and Architecture, UTP University of Science and Technology, Bydgoszcz, Poland, e-mail: macdut@utp.edu.pl*
[2]*Assistant Professor, Department of Civil Engineering, Auburn University, USA, e-mail: dbr0011@auburn.edu*

Abstract: Direct measurements of near-surface tornado wind fields has proven difficult, leading to a number of indirect estimation methods. One promising method is the analysis of patterns of trees felled by tornadoes, which can be used to condition theoretical vortex models for providing the distribution of peak near-surface winds in a tornado path. To date, tree-fall patterns have been only used to condition theoretical wind fields based on the Rankine vortex model. This paper evaluates to what extent the choice of vortex model affects the ensuing tree-fall patterns, specifically evaluating the Burgers-Rott and the Baker vortex models.

Keywords: tornado, tree-fall pattern, vortex models, wind engineering.

1. Introduction

Direct measurement of near-surface wind fields in tornadoes is difficult to achieve, hindering the advancement of tornado climatology across the world and the advancement of tornado-resilient communities. Due to the lack of direct measurements, peak tornado wind speeds are typically estimated from the assessment of damage to buildings, infrastructure and trees. Holland et al. (2006) demonstrated a methodology for conditioning a theoretical tornado wind field model, based on the Rankine vortex model, to tree-fall patterns. This methodology is particularly useful for estimating tornado intensity for tornado tracks through largely forested areas, or areas with a mixture of trees and buildings, and has been used successfully in recent events (Beck and Dotzek, 2010; Lombardo et al. 2015) to estimate tornado intensity. The method also provides an important independent estimate of tornado wind speeds throughout the tornado path that can be used to empirically assess the fragility of structures impacted by the tornado, as demonstrated in Roueche et al., (2017). However, the models thus far have been based solely on the Rankine vortex model. It is unclear how different vortex models may affect the simulated tree-fall patterns and whether alternative models may provide a better fit to observed tree-fall patterns. The objective of this paper is to specifically evaluate how tree-fall patterns may differ for various vortex models. Specifically, the Burgers-Rott and Baker vortex models are analysed in this paper in comparison to the traditional Rankine vortex model.

2. Models of tornado

2.1. *Fluid flow*

The model of incompressible density-uniform ideal fluid is used for analysis of vortex motion. Viscous liquids are described by Navier – Stokes equations (Alekseenko et al., 2003)

$$\frac{\partial \boldsymbol{u}}{\partial t} + (\boldsymbol{u}\cdot\nabla)\cdot\boldsymbol{u} = \boldsymbol{g} - \frac{\nabla p}{\rho} + \nu \ \ \boldsymbol{u} \tag{1}$$

Where ν is the coefficient of kinemtaic viscosity, ρ is the density of the air, t is the time, p is the static pressure and **g** is the gravity and **u** is the velocity. Equation of mass conservation has the following form:

$$\frac{\partial \rho}{\partial t} + div(\rho \boldsymbol{u}) = 0 \tag{2}$$

2.2. *Burgers-Rott vortex model*

Burgers-Rott model is a one-cell vortex model. The following assumption are introduced to the equations of Navier-Stokes:

$$V = V(r), \qquad W = W(z), \qquad U = U(r), \tag{3}$$

$$p = p(r,z)$$

where $U, V,$ and W are the tangential, radial and vertical velocity components respectively, r is the radial distance from the tornado centre, z is the height above the ground surface, and p is the pressure. The flow field is steady state, the viscosity is constant, and body forces can be neglected. Fluid flow equations after the above arrangements have the form:

$$U\frac{\partial U}{\partial r} - \frac{V^2}{r} = -\frac{1}{\rho}\frac{\partial p}{\partial r} + \nu\left(\frac{\partial^2 \mathrm{U}}{\partial \mathrm{r}^2} + \frac{1}{r}\frac{\partial U}{\partial r} - \frac{U}{r^2}\right), \tag{3}$$

$$U\frac{\partial V}{\partial r} + \frac{UV}{r} = \nu\left(\frac{\partial^2 \mathrm{V}}{\partial \mathrm{r}^2} + \frac{1}{r}\frac{\partial V}{\partial r} - \frac{V}{r^2}\right), \tag{4}$$

$$W\frac{\partial W}{\partial z} = -\frac{1}{\rho}\frac{\partial p}{\partial z} + \nu\frac{\partial^2 \mathrm{W}}{\partial \mathrm{z}^2}, \tag{5}$$

$$\frac{\partial (rU)}{\partial r} + \frac{\partial (rW)}{\partial z} \ = 0. \tag{6}$$

2.3. *Baker vortex model*

Baker and Sterling developed a vortex model also of three velocity components, describing a single and two-celled vortex. In this model the steady state, inviscid flow are analysed and body forces are neglected. The assumptions are made:

$$V = V(r,z), W = W(r,z), \tag{7}$$

$$U = U(r,z), \qquad p = p(r,z)$$

Fluid flow equations have the form:

$$U\frac{\partial U}{\partial r}-\frac{V^2}{r}+W\frac{\partial U}{\partial z}=-\frac{1}{\rho}\frac{\partial p}{\partial r}, \tag{8}$$

$$U\frac{\partial V}{\partial r}+\frac{UV}{r}+W\frac{\partial V}{\partial z}=0, \tag{9}$$

$$U\frac{\partial W}{\partial r}+W\frac{\partial W}{\partial z}=-\frac{1}{\rho}\frac{\partial p}{\partial z}, \tag{10}$$

The resulting horizontal velocity components have the form:

$$U=-\frac{4\bar{r}\bar{z}}{(1+\bar{r}^2)(1+\bar{z})^2}U_m \tag{11}$$

$$V=K\bar{r}\frac{[\ln(1+\bar{z})^2]}{(1+\bar{r}^2)}U_m \tag{12}$$

where $\bar{r}$ is the radial distance from the tornado centre normalized to the radius to maximum winds, K is a constant related to the swirl ratio of the tornado, $\bar{z}$ is the height above ground level normalized to the height at which the maximum radial velocity, U_m occurs.

The distribution of tangential velocity of Rankine, Burgers – Rott and Baker model are presented in Figure 1 for different distance from the centre of tornado. The Baker model assumes K=2.88, and plots V/V_m.

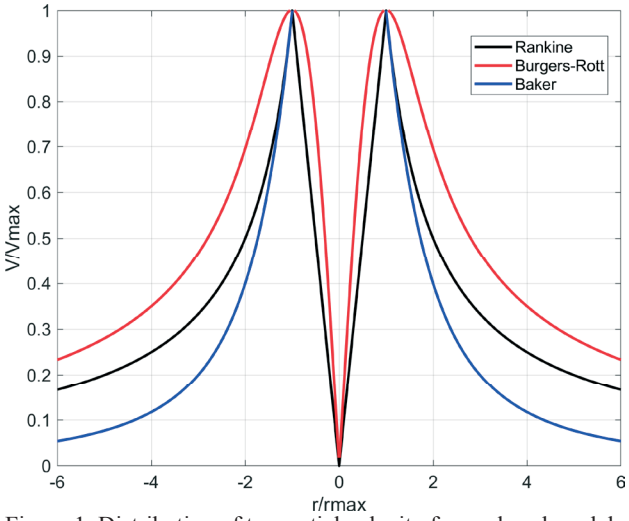

Figure 1. Distribution of tangential velocity for analysed model

3. Conditioning wind field models to tree-fall patterns

Tree-fall patterns are typically captured from the tornado path using high-resolution satellite or aerial imagery. Figure 2Figure 2 shows a close-up view of trees felled by a tornado in Jacksonville, AL on March 19, 2018 that was surveyed by the authors. The wind speed required to fell the tree (either through uprooting or snapping of the trunk) is deemed the critical tree-fall wind speed, V_c, and is a function of the tree height, age, species, canopy size, soil conditions and more (Holland et al., 2006). There is considerable uncertainty in V_c for individual trees, but if sufficient number of trees have been felled, overall patterns become more clear that in essence average out much of the individual uncertainty and can be used to condition theoretical wind field models. The process for conditioning the theoretical models consists of translating the vortex model across a pre-defined Cartesian grid in incremental time steps, and calculating at each time step the total wind speed and direction at each {x,y} grid point, $V_{x,y}(t)$ based on the radial distance from the tornado centre, the assumed translation speed of the vortex and the chosen vortex model. When $V_{x,y}(t) > V_c$, the wind direction at $\{x, y\}$ is recorded. The output is an array of simulated tree-fall directions over the $\{x, y\}$ domain that can be compared to observed tree-fall patterns. Parameters of the vortex models can be modified to optimize the fit of the simulated tree-fall patterns to the observed tree-fall patterns as demonstrated in Lombardo et al. (2015). This paper will simulate tree-fall patterns for the same common tornado parameters – radius to maximum wind speeds, maximum horizontal wind speed, and vortex translation speed – but utilizing different vortex models to estimate the wind speed at each grid point within the domain. Specifically the Rankine, Burgers-Rott and Baker vortex models will be used.

Empirical fragility functions will be simulated for wood-frame residential buildings using the methodology demonstrated by Roueche et al. (2017) to assess sensitivity to vortex model.

Figure 2. Tree-fall caused by a tornado in Jacksonville, AL on March 19, 2018.

4. References

Alekseenko S.V., Kuibin P.A.,·Okulov V.L., *Theory of Concentrated Vortices*, Springer 2003.

Baker, C.J., Sterling, M., *Modelling wind fields and debris flight in tornadoes*. J. Wind Eng. Ind. Aerodyn., 168 (2017) 312–321.

Burgers J.M., *A mathematical model illustrating the theory of turbulence*. Adv. Appl. Mech. 1 (1948) 171–199.

Holland A.P., Riordan A.J., Franklin E.C., *A Simple Model for Simulating Tornado Damage in Forests.*, J. Appl. Meteor. Climatol., 45 (2006) 1597–1611, https://doi.org/10.1175/JAM2413.1

Lombardo F.T., Roueche D.B., Prevatt D.O. *Comparison of two methods of near-surface wind speed estimation in the 22 May, 2011 Joplin, Missouri Tornado*. J. Wind Eng. Ind. Aerodyn., 138 (2015) 87-97.

Rankine W.J.M., *A Manual of Applied Physics*, tenth ed. Charles Griff and Co., p. 663, 1882.

Rott N., *On the viscous core of a line vortex*, Zeitschrift für angewandte Mathematik und Physik ZAMP 9 (1958) 543–553.

Roueche D.B., Lombardo F.T., Prevatt D.O. Empirical Approach to Evaluating the Tornado Fragility of Residential Structures. *Journal of Structural Engineering*, 143(9) (2017) 04017123.

Wind-tunnel modelling of wind flows above a hill in the thermally stratified atmospheric boundary layer

Sergey Kuznetsov[1], Stanislav Pospíšil[1], Hrvoje Kozmar[2], Arsenii Trush[1]

[1] *Institute of Theoretical and Applied Mechanics, Prosecká 76, 190 00 Prague, Czech Republic, e-mail: kuznetsov@itam.cas.cz, pospisil@itam.cas.cz, trush@itam.cas.cz*
[2] *Faculty of Mechanical Engineering and Naval Architecture, University of Zagreb, Ivana Lučića 5, 10000 Zagreb, Croatia, e-mail: hkozmar@fsb.hr*

Abstract: The experimental wind-tunnel modelling of thermal stratification of the atmospheric boundary layer (ABL) developing above a hill is presented. The focus is on stratified, low-turbulent flows above topographic models with the special focus to create nearly the same Richardson number *(Ri)* as it appears in the full scale. This was successfully achieved in the complex terrain.

Keywords: atmospheric boundary layer, atmospheric turbulence, complex terrain, thermal stratification, wind tunnel experiments.

1. Introduction

The stability and the stratification characteristics in the atmosphere exhibit a wide variety of important physical phenomena. The study of the stratification effects on flow in the ABL is important in understanding and analysing the motion patterns in the vicinity of topographic features, which is one of the most important aspects of air pollution, see Bowen and Lindley (1977), Ferreira et al. (1995). It is well known that the thermal stratification plays a major role in diffusion in the atmosphere, and often, the most hazardous environmental conditions are a direct result of those effects.

2. Wind-tunnel experiments

2.1. Heated models

Wind-tunnel experiments were carried out in the closed-circuit Vincenc Strouhal Climatic Wind Tunnel (CWT) of the Centre of Excellence Telč (CET), Czech Republic (http://www.itam.cas.cz/CET/). The method used to produce a downscaled version of the ABL is a variation of the Counihan method, see Michalcová et al. (2014) and Kuznetsov et al. (2017). Conventionally, stable stratification in wind tunnel is simulated using ambient air that is heated using electrical resistors placed on a turntable. The 1 m long and 1 m wide terrain models were made modularly from six heated plates. The hill model has the height H = 200 mm. The lower surfaces of the terrain models were covered with aluminium foil-wrapped insulation to reduce heat loss and thermal inertia. All joints between the plates were taped to smooth the intersections and thus avoid the flow leaking. Each element was individually rated to 3.5 kW for a 400 V potential, and they were connected in various serial and parallel combinations. At the low velocities used (0.5 m/s), a dissipation of about 2 kW occurred. This energy sufficed to heat the 300 mm thick ABL model, which is 5 to 10 times larger than the anticipated model-scale Monin-Obukhov stability length, L_{mo} = 30-60 mm, at the adopted simulation length scale. Once the flow speed and heating elements were turned on, it took about one hour for the flow stratification conditions to become steady.

2.2. PIV measurement set

PIV equipment from Dantec and Litron Lasers was used. A Dantec FlowSense EO camera captured snapshots of the flow-field in resolution of 2048 × 2048 pixels. A pulsed Nd:YAG laser illuminated the flow. The flow was seeded using a fog generator, which was placed in the climatic test section, i.e. upstream of the fan and honeycombs, thus resulting in the homogeneously seeded flow field. A series of 50 double pictures at a rate of 10 Hz was recorded. The Reynolds number during the PIV experiment was $Re = 5.3 \times 10^3$. It was calculated using the mean freestream velocity and the hill-model height. The flow and temperature profiles can be seen in Figs 1 and Figs 2 respectively.

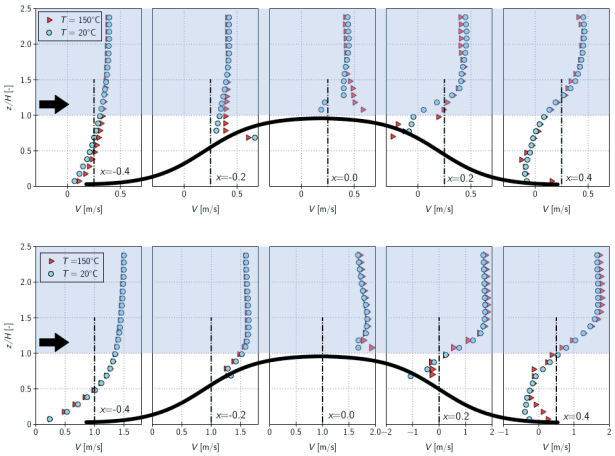

Figure 1. Flow shear profiles in the wind tunnel developed above the heated hill model for the free field wind speed 0,5 m/s (top) and 1,5 m/s (bottom).

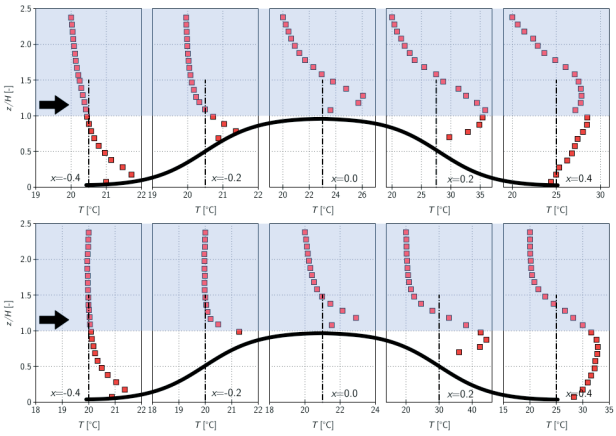

Figure 2. Temperature profiles above the heated hill heated to the temperature 150°C, wind speed 0,5 m/s (top) and 1,5 m/s (bottom)

2.3. CTA settings

The low air velocities and high temperature differences required that special instrumentation and methods were utilized to assure that measurements were not biased by radiation errors.

The method developed by Jonáš (2013), which uses rotating hot-wire (or film) probe with inclined CTA sensors, was used. This method allows for determination of mean velocity vector, complete Reynolds stress tensor and heat fluxes (i.e. velocity-temperature covariances) and temperature variance in a given point in space. The CTA sensor was inclined to the fixed axis of rotation at an angle of 45°, and it operated in the CTA mode. Hot-wire cooling is a function of the effective flow velocity and the fluid state (pressure, temperature) and it can be described by the generalized Collis-Williams (1959) cooling law:

$$Nu\left(\frac{T_m}{T}\right)^M = A + B \cdot \mathrm{Re}^N \tag{1}$$

where T_m is the average temperature of the flow and the sensor; A, B, M, N are empirical constants.

3. Results and discussion

The thermal stability is characterized using the Richardson number that describes the effects of the buoyant and inertial forces. The Richardson number (Ri) is given by the equation:

$$Ri = \frac{g}{\Theta}\frac{\partial\Theta/\partial z}{(\partial V/\partial z)^2} \tag{2}$$

where g is acceleration of gravity, Θ is absolute temperature, V is mean flow velocity, and z is distance in vertical direction. A positive Richardson number denotes a thermally stable flow. In the theory, above the flat terrain, critical Richardson number Ri = 1 separates two regimes of the turbulence production. In case of the model surface heating, which results in an upward heat flux, the mechanical turbulence production is augmented with buoyant turbulence production. Near the surface the mechanical energy production dominates but decreases with height, while on the other hand the buoyant production is almost constant. Away from the surface, the boundary layer undergoes strong vertical mixing due to positive buoyancy forces and the production of large-scale convective turbulence.

This well-mixed layer, which extends to the inversion point that is situated at a lower altitude, is characterized by an almost uniform potential temperature and a constant flow speed and direction. In addition, there is a downward flux of momentum and heat due to entrainment into the boundary layer. Near the surface, the turbulent heat and momentum flux exist as a result of temperature and velocity gradients; however, in the mixed layer the fluxes are maintained by buoyancy effects and entrainment. In this layer, the fluxes become insensitive to existing gradients and away from the surface the interaction of the gradient-produced turbulence and buoyancy-driven turbulence controls the flow.

In the case of the more complex terrain, e.g. a hill, the situation is different. The gradient Richardson number Ri is calculated using Eq. (2). The resulting profiles of Ri are shown in Figs 3 and 4 for several downstream distances. The attention of this work however, is focused on the downstream distance x = 0.4 m as the place of, e.g., potential building site. Ri is negative in the upper part of the profile, however, in the lower (green) part of the profiles Ri increases and becomes positive but lower than 1, a theoretical value where all the turbulence is dissipated as the result of stable thermal stratification (see Fig. 3). In the intermittent (blue) region at $z/H \approx 1.0$, where the temperature gradient is jumping from the positive to the negative values, Ri changes accordingly. Close to the surface, Ri is still positive, as the temperature gradient is positive, but it is smaller due the higher velocity shear $\partial V/\partial z$, see Pospíšil et al. (2017).

At larger wind speed, see Fig. 4, Ri is negative throughout the entire region. The turbulence production is larger as well as the temperature gradient (Fig. 2), which is negative or almost neutral above the hill top (blue zone).

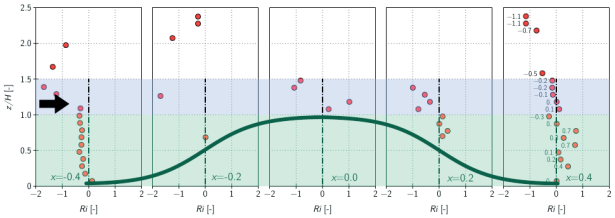

Figure 3. Ri profiles at x = -400 mm, x = - 200 mm, x = 0 mm, x = 200 mm, and x = 400 mm at V_0 = 0.5 m/s; T = 150 °C..

In the wake of the hill at x = 400 mm close to the ground the value of gradient Ri is in the range of estimates of the bulk Ri reported in Zilitinkevich and Baklanov (2002). At $z/H \approx 0{,}5$ the Ri is higher than 1, thus the production of the turbulence is supressed due to the mixing of the thermal convection creating the local stable stratification.

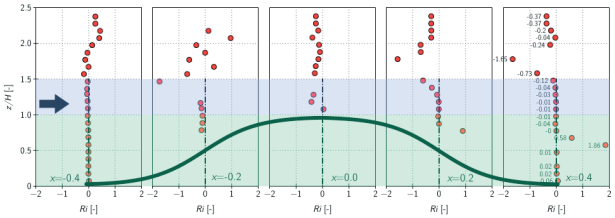

Figure 4. Ri profiles at x = -400 mm, x = - 200 mm, x = 0 mm, x = 200 mm, and x = 400 mm at V_0 = 1.5 m/s; T = 150 °C.

4. Acknowledgments

This study was supported by CET sustainability project LO1219 (SaDeCET) of the Ministry of Education, Youth and Sport of the Czech Republic, Croatian Science Foundation IP-2016-06-2017 (WESLO).

5. References

Bowen A., Lindley D. *A wind-tunnel investigation of the wind speed and turbulence characteristics close to the ground over various escarpment shapes.* Boundary-Layer Meteorology 12 (1977), 259-271.

Collis D.C., Williams M.J. *Two-dimensional convection from heated wires at low Reynolds numbers*. Journal of Fluid Mechanics 6 (1959), 357-389.

Ferreira A.D., Lopes A.M.G., Viegas D.X., Sousa A.C.M. *Experimental and numerical simulation of flow around two-dimensional hills.* Journal of Wind Engineering and Industrial Aerodynamics 54/55 (1995), 173-181.

Jonáš P. *Rotary slanted single wire CTA-a useful tool for 3D flows investigations.* EPJ Web of Conference 45 (2013), http://dx.doi.org/10.1051/epjconf/20134501047.

Kuznetsov S., Ribičić M., Pospíšil S., Plut M., Trush A., Kozmar H. *Flow and turbulence control in a boundary layer wind tunnel using passive hardware devices*. Experimental Techniques 41(6) (2017), 643-661.

Michalcová V., Brožovský J., Kuznetsov S., Pospíšil S. *Numerical and experimental investigations of air flow turbulence characteristics in the wind tunnel contraction*. Applied Mechanics and Materials 617 (2014), 275-279.

Pospíšil S., Kuznetsov S., Kozmar H., Michalcová V. *Wind-tunnel Simulation of Thermally Unstable Atmospheric Flow in Complex Terrain*. Procedia Engineering, vol. 190, 2017.

Zilitinkevich S., Baklanov A. *Calculation of the height of the stable boundary layer in practical applications*. Boundary-Layer Meteorology 105(3) (2002), 389-409.

Numerical and wind-tunnel analysis of convective heat transfer at ground surfaces around complex building models

A. Moediartianto[1], H. Montazeri[1, 2], B. Blocken[1, 2]

[1]Building Physics and Services, Department of the Built Environment, Eindhoven University of Technology, the Netherlands
e-mail: a.moediartianto@tue.nl
[2]Building Physics Section, Department of Civil Engineering, KU Leuven, Belgium

Abstract: Knowledge of convective heat transfer at ground surfaces around buildings is required for urban canyon models and for research on asphalt and road collectors, heat stresses in urban areas, etc. However, while many studies of convective heat transfer around buildings have been performed in the past, the focus of most of these studies was on rather simple building geometries and external surfaces of buildings. This paper, therefore, presents computational fluid dynamics (CFD) simulations and wind-tunnel measurements of convective heat transfer at ground surfaces around complex building models. The 3D Reynolds-averaged Navier-Stokes equations are solved with a combination of the high-Re number realizable k-ε model and the low-Re number Wolfshtein model. The evaluation is based on validation with wind-tunnel measurement of ground surface temperature around a complex building model acquired through infrared thermography.

Keywords: pedestrian level wind, wind comfort, heat transfer, infrared thermography, CFD validation.

1. Introduction

Urban canyon models, which are based on energy balance equations that represent the heat transfer between pavements and building walls, requires the knowledge of convective heat transfer at ground surfaces around buildings (Kusaka et al., 2001). Convective heat transfer at ground surfaces is also essential for research on asphalt and road collectors, heat stresses in urban areas, etc.

However, while many studies of convective heat transfer around buildings have been performed in the past, the focus of most of these studies was on rather simple building geometries (Yamada et al., 1996, Nakamura et.al., 2001), and external surfaces of buildings (Saneinejad et. al., 2001, Montazeri et al., 2015). This paper, therefore, presents CFD simulations of convective heat transfer at ground surfaces around complex building models. The simulations are performed for five different building geometries and for three approaching wind directions. The evaluation is based on validation with high-resolution wind-tunnel measurements of surface temperature around a complex building model acquired through infrared thermography.

2. Description of wind tunnel experiment

The measurements are performed in an open-circuit wind tunnel of the Unit Building Physics and Services (BPS) of the Department of the Built Environment at Eindhoven University of Technology (Fig. 1).

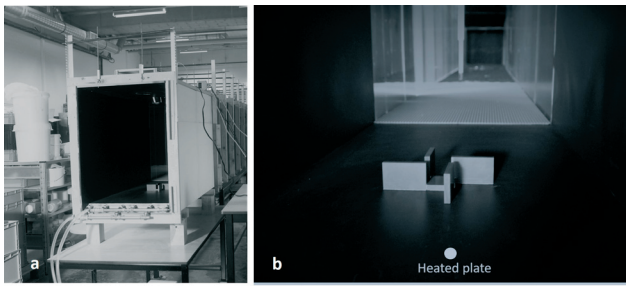

Figure 1. Pictures of the test-section of the wind tunnel with building model. (a) View of the downstream domain with building model and (b) Close-up view of the building model for wind direction 0°.

The test-section of the wind tunnel is 1.3 m long with a cross-section of 0.5 m (width) × 0.64 m (height). The side planes of the test-section are made of glass. Two layers of insulation are added on each plane to minimize heat losses. A layer of Styrofoam with 0.05 m thickness and a layer of M-XPS core with a solid Polyethylene terephthalate (PET) with 0.0022 m thickness are installed on the outer and inner surfaces of the planes, respectively. The physical properties of both materials are provided in Table 1.

The test section floor is composed of a layer of PVC with 0.012 m thickness and two layers of aluminum with 0.0049 m and 0.0019 m thickness. The physical properties of PVC and aluminum are given in Table 1. The outer surface of the PVC plate is coloured in black to enhance emissivity and minimize light reflection during the experiment. The test section bottom surface is heated using a hot water system, which consists of a water reservoir, a thermostat to control the water temperature inside the reservoir, a circulation pump and six U-shaped heat pipes. The water pipes are made of copper (0.001 m thickness) covered by a layer of aluminum (0.0019 m thickness) that are welded to the bottom of the floor (Figs. 2b & c). A layer of spray foam is used below the floor (and between the pipes) to minimize heat loses.

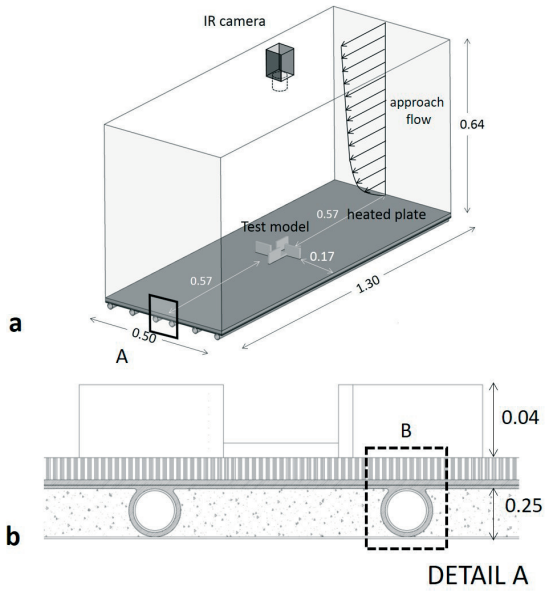

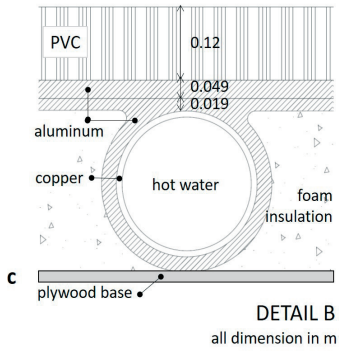

Figure 2. Schematic view of (a) the test section of the wind tunnel with the building model and water pipes. (b, c) Detail of the test section floor.

Table 1. Physical properties of materials used in the wind tunnel setup.

Material	Density (ρ)	Thermal conductivity (k)	Specific heat (C_p)
	Kg. m^{-3}	W. m^{-1}.K^{-1}	J. m^{-3}.K^{-1}
PVC	1.43×10^{3}	1.94×10^{-1}	1.38×10^{3}
Aluminium	2.72×10^{3}	2.02×10^{2}	8.71×10^{2}
Copper	8.98×10^{3}	3.88×10^{2}	3.81×10^{2}
Styrofoam	0.04×10^{3}	3.73×10^{-2}	8.00×10^{6}
XPS + PET	0.05×10^{3}	6.67×10^{-2}	0.08×10^{6}

The measurements are performed for a reduced-scale building model that consists of a rectangular prism with square base (L × W × H = 0.048 × 0.048 × 0.008 m³) surrounded by four rectangular prisms (L × W × H = 0.048 × 0.008 × 0.04 m³) (Fig. 1b), resulted in a blockage ratio of about 1.9%. The measurements are performed for three wind directions (θ = 0°, 45°, 67.5°) and for a range of Reynolds number between 11,000 to 25,000 based on the height of building model (H).

The surface temperature distribution around the building models is acquired through infrared thermography. More detailed information about the measurement procedures will be provided in the full paper.

3. CFD simulations

A computational domain is made of the cross-section of the wind tunnel including the reduced-scale building model, the two layers of aluminum, the PVC layer underneath the wind-tunnel floor and the water pipes. The computational grid is generated using the surface-grid extraction technique (Van Hooff and Blocken, 2010). This results in 17,618,018 hexahedral cells. The minimum and maximum cells volume in the domain are 4.8×10^{-13} m³ and 5.0×10^{-6} m³, respectively. The distance from the centre point of the wall-adjacent cell to the wall is $y_P = 8.0 \times 10^{-4}$ m, corresponding to an average y* value of 0.796 over the ground surface. The maximum y* value is about 8.06.

The inlet boundary conditions are according to the measured data. The thermal boundary conditions are a fixed inlet air temperature of 22.11˚C and fixed temperature at the outer surfaces of the water pipes.

The 3D Reynolds-averaged Navier-Stokes (RANS) equations are solved with a combination of the high-Re number Realizable k-ε model (Shih et al., 1995) and the low-Re number Wolfhstein model (1969).

4. Results

Fig. 3 compares the surface temperature distribution around the building model obtained by the wind tunnel measurements and CFD simulations ($Re_H = 1.1 \times 10^4$, and θ = 0°). A good agreement can be clearly seen in regions with high wind speeds. The maximum and average deviations are 5.92% and 5.39%, respectively. Fig. 3 also shows that the temperature (and convective heat transfer) distribution around the building is very complex because of the complex nature of the 3D flow field around the building with impingement, separation and vortex shedding.

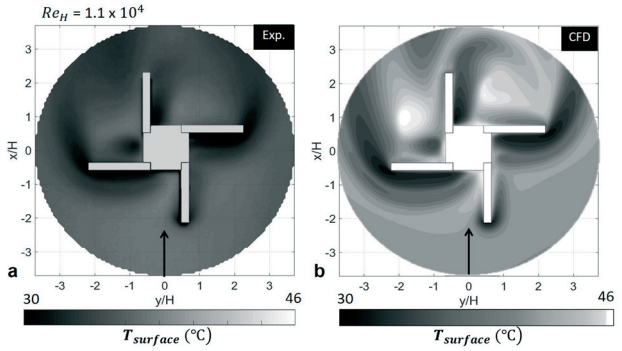

Figure 3. Ground surface temperature distribution obtained by (a) thermography infrared and (b) CFD simulation for wind direction θ = 0°.

5. Acknowledgments

The authors thank Directorate General of Resources for Science, Technology and Higher Education (DGRSTHE) of Indonesia for their financial support. The second author is currently a postdoctoral fellow of the Research Foundation – Flanders (FWO) and is grateful for its financial support (project FWO 12M5316N). The authors gratefully acknowledge the partnership with ANSYS CFD.

6. References

Kusaka H., Kondo H., Kikegawa Y., Kimura F., *A simple single-layer urban canopy model for atmospheric models: Comparison with multi-layer and slab models.* Bound.-Layer Meteorol. 101 (2001) 329–358.

Nakamura H., Igarashi T., Tsutsui T., *Local heat transfer around a wall mounted cube in the turbulent boundary layer*. Int. J. Heat and Mass Transf. 44 (2001) 3385–3395.

Montazeri H., Blocken B., Derome D., Carmeliet J., Hensen J.LM., *CFD analysis of forced convective heat transfer coefficients at windward building facades: influence of building geometry*. Journal of Wind Engineering and Industrial Aerodynamics 146 (2015) 102-116.

Yamada M., Uematsu Y., Sasaki R., *A visual technique for the evaluation of the pedestrian-level wind environment around buildings by using infrared thermography*, J. Wind Engineering and Industrial Aerodynamics 65 (1996) 261-271.

Wolfhstein M., *The velocity and temperature distribution of one-dimensional flow with turbulence augmentation and pressure gradient.* International Journal of Heat and Mass Transfer 12 (1969) 301-318.

Saneinejad S., Moonen P., Defraeye T., Carmeliet J., *Analysis of convective heat and mass transfer at the vertical walls of a street canyon,* J. Wind Engineering and Industrial Aerodynamics 99 (2011) 424-433.

Shih T. H., Liou W.W., Shabbir A., Yang Z., Zhu J., *A new k-ε eddy viscosity model for high Reynolds number turbulent flows*. Computers Fluids, 24(3) (1995) 227-238.

Van Hooff T., Blocken B., *Coupled urban wind flow and indoor natural ventilation modeling on a high-resolution grid: a case study for the Amsterdam Arena Stadium.* Environ. Model. Softw. 25 (2010) 51-65.

Proposed classification of stationary and nonstationary winds in Poland

Tadeusz Chmielewski

Department of Structural Mechanics, Opole University of Technology, Katowicka 48, 45-061 Opole, Poland, e-mail: t.chmielewski@po.opole.pl

Abstract: An overview of international scales describing the intensity of tornadoes and reports from the Polish Government Security Centre on strong winds and tornadoes, downbursts, the incidence of tornadoes, downbursts and microbursts in Poland, and the proposed classification in 2012 by Lorenc, for the maximum wind speed in Poland and effects of their actions are presented. This information was analysed and on the basis of available statistical data, two separate intensity scales of strong winds and tornadoes, downbursts, and microbursts in Poland are proposed. The proposed P scale is the adoption of the existing scale (EF) combined with wind speed modification.

Keywords: tornadoes, downbursts, microbursts, intensity scales in Poland.

1. Introduction

Severe thunder storms, tornadoes, hurricanes, downbursts, and microbursts are among the most destructive natural hazards on Earth. Tornadoes occur on every continent except Antarctica. Hurricanes occur over the tropical oceans. But strong winds, on the other hand, occur on all continents. High wind speeds associated with these meteorological events have caused in the past and will continue to cause destruction of buildings, civil infrastructure, and vegetation. They also constitute a threat to human health and life.

The purpose of this paper is to present an overview of international approaches to tornado damage and intensity classification, and to identify similarities and differences in current scales. Then the newest Polish proposals to classify strong winds, called as stationary winds, and tornadoes, downbursts and microbursts, called nonstationary winds, are discussed. Based on the published statistics of strong winds and tornadoes, downbursts, and microbursts in Poland, two separate intensity scales for their classification are proposed.

2. Strong winds, tornadoes, and downbursts in Poland

2.1. The Report of the Polish Government Security Centre about winds, tornadoes, and downbursts

Strong winds, tornadoes, downbursts, and microbursts are the leading causes of economic loss in Poland. Each year windstorms lead to significant structural damage and even loss of life. The report of the Polish Government Security Centre (PGSC) (2012) shows that the greatest potential natural threat each year are floods, while strong winds, tornadoes, and downbursts, are second.

2.2. An overview of tornadoes, downbursts, and strong winds occurrences in Poland

In Poland there is no institution which collects data about the occurrence of tornadoes and downbursts. The first researcher who collected, the data on the tornado occurrence in the years 1979-1988 and 1998- 2010 in Poland was Lorenc and she published them in 1996, 2012. The total number of tornadoes in the years 1979-1988 was 42, which gave the average number of 4 tornadoes per year, but the total number of tornadoes in the years 1998-2010 was 80, which gave the average number of 6 tornadoes per year. The third estimation of the occurrence of tornadoes in Poland in the years 2011-2016 was made by the author of this paper and it is presented in Table 1. The total number of tornadoes was 31, which gives an average of 5 tornadoes per year.

Table 1. The occurrence of tornadoes in Poland in the years 2011 – 2016.

Year	Month						Together
	III	IV	V	VI	VII	VIII	
2011			1	2	1	3	7
2012			1	1	2	1	5
2013			2	1	1		4
2014			2		1	1	4
2015	1			3			4
2016	1			4	2		7
Total	2		6	11	7	5	31

Based on the data given in the above overview, the author came to the conclusion that it is very likely that some tornadoes might appear in Poland each year. This statement is also very likely as far as strong winds, with downbursts, and microbursts are concerned, i.e. about ten strong winds with downbursts, and microbursts might also appear each year. This is the conclusion which is drawn from Table 2 which was prepared by the author. The author collected data about damage description, victims and sometimes measured wind speed after each event during the last six years. One example: on August 11, 2017 a severe downburst caused damage in two provinces of Poland – Bydgoszcz and Gdańsk. Along the 150 km path, 3000 buildings and 38000 hectares of forests were damaged, 6 people were killed, 51 were injured. The wind speed of 41 m/s was measured.

Table 2. The occurrence of strong winds, tornadoes, and downbursts in the years 2012 – 2017, together 60.

2012	2013	2014	2015	2016	2017
13	8	8	9	9	16
4F	6 F	1 F	2 F	13 F	10 F
+ 11 In	+ 11 In	+ 3 In	+ 41 In	+ 14 In	+86 In

where: F – number of fatalities, In – number of injured people

2.3. Classification of maximum wind speeds in Poland and their effects - according to Lorenc (2012)

The latest publication addressing maximum wind speeds in Poland is the monograph of Lorenc (2012), who developed the classification of these speeds for our country.

3. Analysis of measured and estimated wind speeds in Poland and the degrees of their hazards

The monograph by Lorenc (2012) gives a set of maximum wind speeds in gusts measured at 39 synoptic stations from 1971 to 2005, a period of 35 years. From this dataset the maximum gust wind speeds range from 21 m/s to 40 m/s. Also, this

publication gives information on the records of the measured maximum wind speeds, also in the last 35 years. These are the following: Zakopane – 47 m/s on December 1, 1976, Warsaw – 40 m/s on June 14, 1979, Bielsko-Biala 48 m/s on November 6, 1985, Kalisz – 46 m/s on October 21, 1986, Łeba – 44 m/s on February 8, 1990, Hel – 41 m/s on December 4, 1999.

In the second case, a published paper by Chmielewski et al. (2013) can be used, which contains numerical data on human injury and damage after a severe tornado on August 15, 2008. In this paper two approaches were used to estimate the wind speeds of the tornado. The first one was based on the comparison of observed damage caused by the tornado with the TORRO scale. The second approach was based on the structural static analysis of destroyed free standing structures, in this case – three road signs, each mounted on the cantilevered post which were bent to the ground at the bottom of the post, where plastic hinges developed. In the first case, the wind speed range of 52 to 72 m/s (187 to 259.2 km/hr) was estimated, and in the second case, the wind speed of the tornado was greater than 71 m/s (256 km/h). Good estimation was obtained.

4. Proposed scale of intensity of strong winds, tornadoes downbursts, and microbursts in Poland

According to the author, there is no need for cumulative ratings of the maximum wind speeds and descriptions of effects of their actions for different types of wind storms. For synoptic and mountain winds (in the Tatra and Karkonosze regions) whose wind velocity is measured by meteorological stations and this applies for gust speeds ranging from 17 m/s to 40 m/s or from 20 m/s to over 35 m/s the wind can be described by one concept as the strong stationary wind divided into 3 degrees of danger. It is relatively simple and often used in social media. It is also used in everyday life. The author has reviewed descriptions of the damage, economic loss and threats to the population caused by storms in last six years. On this basis, he proposed a relatively detailed description of the effects of strong winds which is an adaptation of the classification of the three high-wind strength hazards proposed by the Institute of Meteorology and Water Management (IMWM) and published by the PGSC (2012).

The second issue in Poland is to categorize tornadoes, downbursts, microbursts (nonstationary winds) by damage and associate the damage with different ranges of wind speeds. Because these meteorological events in Poland average ten occurrences a year, and damage and destruction observations have not been systematically and reliably described, we do not have the reliable statistical material to develop a classification of them in Poland. In this case, it is appropriate to adapt an existing intensity scale of tornadoes. Preferably one which is applied internationally. In this case, the author have considered the Fujita Enhanced Scale (EF), (Mehta, 2013) or the TORRO Scale (Meaden, 1972). Because the EF Scale is relatively new (2007), and an improvement of the F Scale, e.g. increased variety of construction, quality of workmanship, type of materials used, and introduced 28 Failure Indicators, the author therefore recommends using the EF Scale with some wind speed modifications for each grade, which is denoted by the symbol P (for Poland). The proposed wind speed of tornadoes, downbursts, and microbursts according to the degree of the P Scale is shown in Table 3.

Table 3. Wind speed of tornadoes on the EF scale and proposed the scale P for tornadoes, downbursts, and microbursts (Mehta (2013) for the EF scale and the author of the scale P).

EF0	EF1	EF2	EF3	EF4	EF5	Unit of wind speed
105-137	138-178	179-218	219-266	267-322	>322	km/h
29.2-38.1	38.6-49.4	49.7-60.6	60.8-73.9	74.2-89.4	>89.4	m/s
P0	**P1**	**P2**	**P3**	**P4**	**P5**	
<120	**121-170**	**171-220**	**221-270**	**270-324**	**>320**	**km/h**
<33.3	**33.6-47.2**	**47.5-61.1**	**61.4-75**	**75-90**	**>90**	**m/s**

5. Conclusions

Based on the international approaches to tornado intensity classification, the statistical data of strong winds, tornadoes, downbursts, and microbursts in Poland and approaches to their classification, the following conclusions are drawn:

1. There is neither need nor substantive justification for combining the classification of maximum wind speeds for strong synoptic and mountain winds and nonstationary winds, such tornadoes, downbursts, and microburst in Poland (two different types of winds). The statistical data of the IMWM meteorological stations in the period 1971 - 2005 confirm that synoptic and mountain winds (in the Tatra and Karkonosze regions) reach maximum gust speeds from 17 m/s to 35 m/s, only several cases exceeded 40 m/s. Wind speeds of strong nonstationary winds vary from about 35 m/s to over 70 m/s,
2. The author's proposal for two intensity scales to categorize and describe the strong winds with mountain winds and the nonstationary winds in Poland seems entirely justifiable and it is easier than the one put forward by Lorenc (2012). This proposal presented in the paper is only applicable for Poland. Other countries may check if it is applicable for them.
3. The wind speed around 120 km/h (33.3m/s) is the border between the weak and strong tornadoes. Therefore the next degrees above this wind speed for the P scale is proposed to increase equally for 50km/h. The proposed P scale is the adoption of the existing scale (EF) combined with wind speed modification.

6. References

Polish Government Security Centre, *Threats periodically occurring in Poland,* Analysis Division, Warsaw, Poland, 2012.

Lorenc H. *Structure and energy resources in Poland* , Institute of Meteorology and Water Management, Warsaw, Poland, 1996.

Lorenc H. *Maximum wind speeds in Poland*, Institute of Meteorology and Water Management, Warsaw, Poland, 2012.

Chmielewski T., Nowak H., Walkowiak K. *Tornado in Poland of August 15, 2008: Results of post-disaster investigation.* J. Wind Eng. Ind. Aerodyn., 118 (2013) 54-60.

Mehta K. *Development of the EF-scale for tornado intensity*. J. Disaster Research, 8(6) (2013) 1034-1041.

Meaden, G.T. *Tornadoes in Britain: Their intensities and distribution in space and time*. J. Meteor., 1 (1976) 242-251.

Criterion for wind environment assessment considering the effect of turbulence

Akinori Akahoshi[1], Yasushi Uematsu[2]

[1]*Wind Engineering Institute Co., Ltd., Japan,*
e-mail: akahoshi@wei.co.jp
[2] *Department of Architecture and Building Science, Tohoku University, Japan,*
e-mail: yasushi.uematsu.d8@tohoku.ac.jp

Abstract: Turbulence affects the human sensation of wind, the wind-induced damage to buildings, the values of wind speeds measured by 3-cup anemometers, etc. The wind environment assessment criterion proposed by Wind Engineering Institute Co., Ltd. is based on the relation between the mean wind speeds measured by 3-cup anemometers and the surrounding terrain condition. This criterion does not consider the influence of turbulence. Considering the significant urbanization of large cities and the change in anemometers, a new criterion of wind environment assessment that includes the effect of turbulence is required. The present study investigates such a criterion based on a wind tunnel experiment, the field measurements of wind speeds at various locations, and a questionnaire survey on wind environment that was carried out for the residents and pedestrians in Tokyo.

Keywords: wind environment assessment, turbulence intensity, questionnaire survey, wind observation, wind tunnel experiment.

1. Introduction

The criterion for wind environment assessment proposed by Wind Engineering Institute Co., Ltd. (WEI), as shown in Tab. 1, has been used for several decades in Japan. This criterion is based on the relation between the mean wind speeds measured by 3-cup anemometers and the surrounding terrain condition as shown in the study of Nakamura et al. (1986). However, the criterion does not consider the effects of turbulence on the human sensation of wind. Wind turbulence significantly affects the human sensation of wind and the values measured by 3-cup anemometers. Therefore, the present study investigates the effects of turbulence on WEI's criterion.

In recent years, the urbanization of cities has progressed significantly, particularly in large cities such as Tokyo. This has resulted in a major change in public opinion concerning wind environment. In addition, ultrasonic anemometers with lower cost and higher performance, which can measure turbulence precisely, have become popular and replaced 3-cup anemometers. Based on these circumstances, the present study proposes a new criterion for wind environment assessment considering the effect of turbulence based on the result of wind observation in the field, a wind tunnel experiment, and a questionnaire survey on wind environment in Kamiosaki, Shinagawa-ku, Tokyo.

Table 1. WEI's wind environment assessment criterion.

Area	Mean wind speeds at cumulative frequencies of 55 % and 95 %	
	55 %	95 %
A	≤ 1.2 m/s	≤ 2.9 m/s
B	≤ 1.8 m/s	≤ 4.3 m/s
C	≤ 2.3 m/s	≤ 5.6 m/s
D	> 2.3 m/s	> 5.6 m/s

2. Outline of wind observation

The field observation of wind was performed at six points (MG1–MG6) close to the ground (3–5 m high) and at four points (MGO–MGR) on the rooftop of a high-rise building (115 m high) in Kamiosaki. Ultrasonic anemometers were installed at MG1-MG3, and 3-cup anemometers were installed at MG4-MG6. A thermometer was installed at MG6.

3. Outline of wind tunnel experiment

In the wind tunnel experiment, wind speed ratio, gust factor, and turbulence intensity were measured at many points in Kamiosaki using hot-wire anemometers. The values compared with those obtained through the field observation. Good agreement was observed between the results for the mean wind speed ratio. However, gust factor and turbulence intensity were generally underestimated by approximately 20 % in the experiment.

4. Outline of questionnaire survey on wind environment

The questionnaire survey on wind environment carried out for the pedestrians and residents in Kamiosaki consisted of 3 question referring to Murakami et al. (1983). The details of the questions are provided in Tab. 2. The respondents were required to answer in the same area on as many days as possible. 3664 answers were obtained from May 2016 to October 2017.

Table 2. Details of the questions.

Question 1: "How did you feel the wind strength today?"
Answer 1: windless
Answer 2: moderate wind
Answer 3: slightly strong wind
Answer 4: strong and uncomfortable wind
Answer 5: rather strong wind
Answer 6: dangerous wind
Question 2: "How did you feel the temperature of wind today?"
Answer A: unpleasantly hot
Answer B: slightly hot
Answer C: comfortable
Answer D: neither hot nor cold
Answer E: cold
Answer F: so cold as to feel pain
Question 3: "What kind of wind-induced damage did you experience or see today?"
Matter 1: dishevelment of hair and/or cloth
Matter 2: difficulty in walking or falling down
Matter 3: difficulty in using umbrella or breakage of umbrella
Matter 4: falling down of bicycles or motorcycles
Matter 5: blowing up or drift of dust
Matter 6: too strong wind to go out

5. Relation between the results of field observation, wind tunnel experiment, and questionnaire survey

The dependence of the human sensation of wind on the statistics of wind speed is discussed using the results of the field observation and wind tunnel experiment mentioned above. Fig. 1 shows the relation between the effective wind speed, U_e (with

k = 3), defined by Eqn. (1) and the relative frequency, $f_i(U,I_u)$, of the sensation of wind strength defined by Eqn. (2).

$$U_e = U + k\sigma_u = U(1+kI_u) \tag{1}$$

where U is the mean wind speed, k is the weight coefficient, σ_u is the standard deviation of fluctuating wind speed, and I_u is the turbulence intensity. The value of k is assumed to be 3 or 0 in the present study. The averaging time of U_e is 1 hour.

$$f_i(U,I_u) = \frac{N_i(U,I_u)}{\sum_{i=1}^{6} N_i(U,I_u)} \tag{2}$$

where N is the number of answers to each question.

The relation between the sensation of wind strength and the effective wind speed is proposed based on the results shown in Fig. 1 and those provided in Hunt et al. (1976), as shown in Tab. 3. Similarly, the relation between the sensation of the temperature of wind and the mean wind speed and temperature is proposed as shown in Tab. 4.

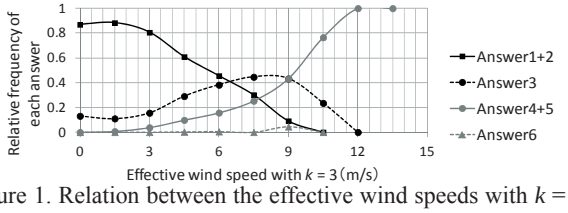

Figure 1. Relation between the effective wind speeds with k = 3 and the relative frequencies of answers 1–6.

Table 3. Relation between the sensation of wind strength and the effective wind speed.

Effective wind speed	Sensation of wind strength
$U_e \leq 6.5$ m/s	I : "calm"
6.5 m/s < $U_e \leq 9$ m/s	II : "slightly strong"
9 m/s < $U_e \leq 15$ m/s	III: "strong and uncomfortable"
U_e > 15 m/s	IV: "dangerous"

Table 4. Relation between the sensation of the temperature of wind and the mean wind speed and temperature.

Mean wind speed and temperature T	Sensation of temperature of wind
$U \leq 1$ m/s ($T \geq 25$ °C)	a : "unpleasantly hot"
$U > 0.5$ m/s ($T < 10$ °C)	b : "it gets cold by the wind"

6. Proposed criterion for wind environment assessment considering the effect of turbulence

6.1. Relation between WEI's criterion and the sensations

Fig. 2 shows the relation between the mean wind speed at a cumulative frequency of 95 % and the cumulative frequency of the effective wind speed corresponding to sensations I–III.

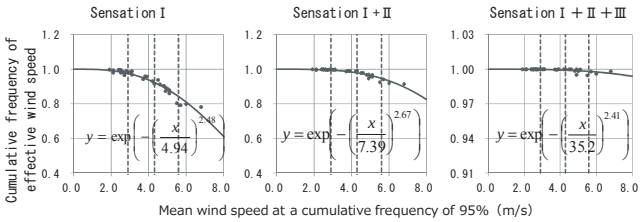

Figure 2. Relation between the mean wind speed at a cumulative frequency of 95 % and the cumulative frequency of effective wind speed corresponding to sensations I–III.

In each figure, the solid line represents an empirical formula approximated by the Weiblle distribution and the vertical broken lines represent the boundary values in WEI's criterion.

Fig. 3 shows the relation between the mean wind speed at a cumulative frequency of 55 % and the relative frequency of the mean wind speed corresponding to "sensation a", when $T \geq$ 25 °C. The solid line represents an empirical formula approximated by the Weiblle distribution.

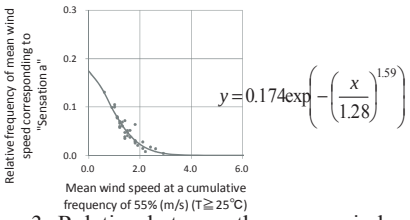

Figure 3. Relation between the mean wind speed at a cumulative frequency of 55 % and the relative frequency of effective wind speed corresponding to "sensation a" ($T \geq$ 25 °C).

6.2. New criterion

The effective wind speeds at a cumulative frequency of 95 % corresponding to the boundary values of WEI's criterion are calculated based on the results shown in Fig. 2. Furthermore, based on the results shown in Fig. 3, we obtained the mean wind speed at a cumulative frequency of 55 % that makes 10 % of people feel "unpleasantly hot" when $T \geq$ 25 °C. The results are given by Eqn. (3). V is defined as the threshold for "discomfort". Based on these results, the relation shown in Tab. 5 is proposed as the new criterion for wind environment assessment considering the effect of turbulence.

$$V = 1.28\left\{-\ln\left(\frac{0.1}{P_{T25}}\right)\right\}^{0.63} \tag{3}$$

where P_{T25} is the ratio of the people that feel "unpleasantly hot".

Table 5. Proposed criterion for wind environment assessment considering the effect of turbulence.

U_e with k = 0 at 55% cumulative frequency ($T \geq 25$ °C)		U_e with k = 3 at 95% cumulative frequency	
discomfort	$\leq V$	Area A	≤ 5.2 m/s
		Area B	≤ 7.4 m/s
		Area C	≤ 9.1 m/s
		Area D	> 9.1 m/s

7. Conclusion

A criterion for wind environment assessment including the effect of turbulence has been proposed as a function of the effective wind speed based on the results of field observation, a wind tunnel experiment, and a questionnaire survey.

8. References

Hunt, J.C.R., Poulton E.C., Mumford, J.C., *The effects of wind on people; New criteria based on wind tunnel experiments.* Building and Environment 11(1) (1976) 15-28

Murakami S., Iwasa Y., Morikawa Y. *Investigation of statistical characteristic of wind at ground level and criteria for assessing wind-induced discomfort: Part III Criteria for assessing wind-induced discomfort*. Transactions of the Architectural Institute of Japan 325 (1983) 74-84

Nakamura O., Yoshida M., Yokotani K., Katagiri J. *Characteristics of wind at ground level in Tokyo*. Proceedings of the 9th National Symposium on Wind Engineering, Tokyo, Japan, 1986.

Understanding urban environments for sustainable urban design

Holger Hundborg Koss[1]

[1]*Department of Civil Engineering, Technical University of Denmark, Denmark,*
e-mail: hko@byg.dtu.dk

Abstract: The open and accessible urban space is that place where people experience a city with respect to its functionality, structure, appearance and its possibilities for work, visit and leisure. Architects, urban planner and developers as well as for urban administration and city councils, strive for creating a good environment to strengthen economic value and life quality at the same time. This effort may be as old as settlements in human history, but the challenges to achieve high standards for urban living and prosperity have increased with the size of the cities we live in. The research in urban environments is in this connection concerned with the urban design and microclimate, biometeorology and their combined impact on human well-being in urban areas. Understanding the interaction between facts and perception is of vital importance for valuable and sustainable urban design.

Keywords: urban environment, microclimate, comfort, architecture, assessment, guidelines.

1. Introduction

Established from religious, economical or simply practical motivation, settlements, towns and cities have evolved and decayed over time due to changing economic, social, political, strategical, but also due to natural, e.g. climatological, boundary conditions. The physical and geometrical design of cities followed in the beginning concepts of reflecting divine order providing the frame setting for early civilisations, their structure and organisation, wealth and growth. Lynch (1981) points out that in spite of external influences and circumstances, the actual layout of cities and their modification over time is primarily 'a human act, however complex, accomplished for human motives, however obscure or ineffective'.

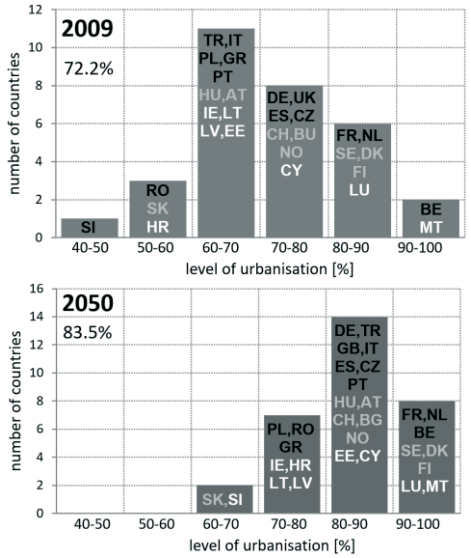

Figure 1. Distribution of urbanisation levels amongst 31 European countries according to statistical census in 2009 and prognosis for 2050 (based on data from 2010 UN report). Country indication after ISO 3166 and colour-coded according to population (published in Koss, 2015).

Today, a large part of the world's population lives in cities. The economic and cultural attraction of cities continues influencing the demographic distribution of country and urbanised population. According to a study on the world urbanisation prospects (UN 2010), in 2050 global urbanisation will reach 69%. In Europe, the level of urbanisation was in 2009 already about 72.2% with a prognosis for 2050 of 83.5%. Figure 1 shows the distribution of urbanisation amongst 31 European countries (OECD and EU members) for 2009 (actual census data) and as a prognosis for 2050. The size of the countries is indicated by colour-code based on population data from 2015: black (above 10Mio), grey (between 5 and 10Mio), and white (below 5Mio). In light of this development, the design of cities is one of the most challenging tasks for modern societies. The organisation of traffic and housing, water and energy supply, and waste management are vital but not the only criteria for urban design. The sheer scale of cities and growing population puts focus on resource conscious designs and life quality as well. It is understood that such high-aiming endeavour needs a profound understanding of the complex relations between all factors and components behind the mechanism of a city and its environment and a suitable evaluation code or guide for planning. 'Decisions about urban policy, or the allocation of resources, or where to move, or how to build something, must use norms about good and bad. […] Without some sense of better, any action is wrong. When values lie unexamined, they are dangerous.' (Lynch, 1981)

Everybody has a natural understanding on what constitutes a good urban environment and a sense for its quality. Even though this understanding may originate individually, there are certain concepts that seem to be more universal and appeal to larger groups of people across regional and cultural boundaries.

2. Analysing Aspects of Urban Environment

2.1. Microclimate

One of the most prominent concepts is the study of local ground-near wind conditions and their evaluation with respect to pedestrian comfort. First assessment methods appeared in the early 70ies (e.g. *Canada*: Davenport 1972; *UK*: Penwarden 1973, Hunt et al. 1976; *France*: Gandemer 1975; *Australia*: Melbourne 1978), and have since been copied, varied and adapted for practical application. More recent review on wind comfort criteria is given by Blocken and Carmeliet (2004) and a comparison of criteria collected in COST Action C14 is published by Koss (2006) to name just a few. [The full paper will discuss present effort to establish official guidelines for wind comfort assessment in urban areas.]

The urban environment is more than just the question of wind affecting human activities in open areas between buildings. Other parameters of the microclimate such as air temperature and sun radiation are important factors for human well-being. Heat stress and chill factor are common descriptors of temperature-related comfort assessment. One of the currently most advanced models considering several parameters of the urban microclimate is the Universal Climate Thermal Index – UTCI (McGregor ed., 2012).

2.2. Life between buildings

A very different approach to assess the quality of urban space was developed by Jan Gehl in the early 70ies and have since been reviewed and refined through application in practice (Gehl and Svarre, 2013). The rating of quality is based on a profound knowledge about human senses and needs and a vast experience from studying urban spaces throughout the world. The all-in-all 12 criteria are grouped into three main categories: safety, comfort, and enjoyment (figure 2). Each criterion is evaluated on a three-point scale by direct observation of the urban space in question. Sometimes several visits are necessary to see and understand how and why humans appreciate the particular urban space and under which conditions.

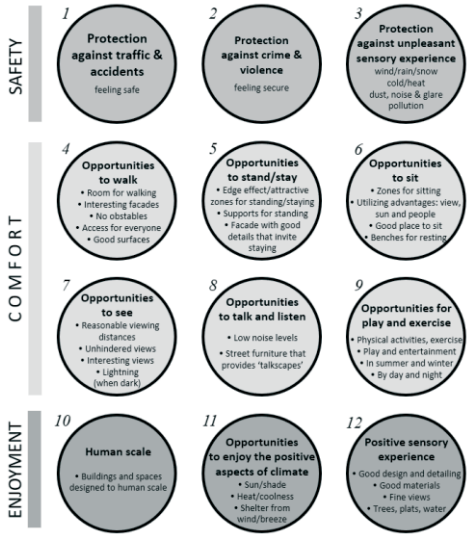

Figure 2. The 12 key quality criteria (Gehl et al., 2006) to ensure safe, comfortable and enjoyable city space for residents.

For working on city development projects where the quality of present and future urban space shall be assessed the understanding of the context of relevant parameters is of vital importance. The approach of the 12 quality criteria has proven to be a valuable and applicable tool in the conversion of parts or even entire cities to a higher level of liveability. For this reason, it could serve as an inspiration for knitting calculable parameters closer together with human perception in a broader context.

3. Elements of Urban Environment

When architects, urban planners or the local municipality commission a study on urban space the question they seek an answer to is how good the space will be. Quite likely 'good' in the sense of the Gehl criteria. However, a classical type of investigation in this connection is the study of pedestrian wind comfort, which, according to figure 2, constitutes only a part of the overall *Genius Loci*. With ever faster advancing technology to calculate and simulate local climate in all its details the need grows for an appropriate interpretation of the results and their influence on urban space quality.

With the 12 quality criteria in mind, a comprehensive description of the urban environment (UE) consists of seven main elements as illustrated in figure 3. Microclimate, materials, space and function constitute the climatic, physical and functional boundary conditions (*parametric elements*), whereas comfort, safety and beauty relate to human perception and reaction to the physical surrounding (*response elements*). Health is in this sense not a direct part of the urban environment but a central aspect when assessing the environmental impact on humans and their well-being.

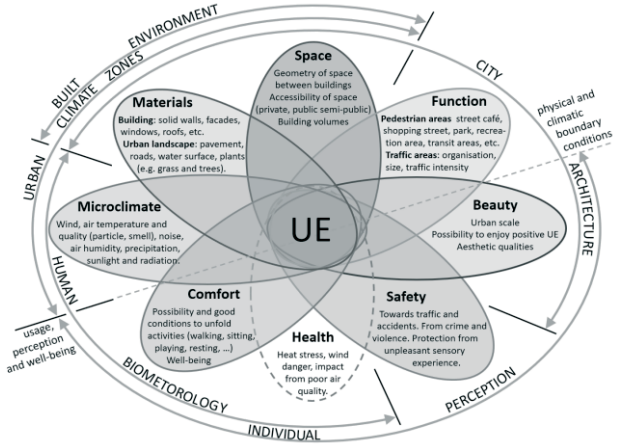

Figure 3. Main elements of the urban environment (UE) with additionally indication of common areas and disciplines in urban planning and urban climatology.

4. Outlook

The full paper will use the parametric and response elements of the urban environment to sketch the current development of UE assessment. Here, the formulation of guidelines plays a central role to make assessment results comparable and accessible for non-experts within the disciplines required for proper simulation (uniformity of assessment method and result presentation). For a better understanding of the combined action of the UE elements, a survey campaign will presented, linking parametric description and response observation through a reference case collection.

5. References

Blocken B., Carmeliet J., *Pedestrian Wind Environment around Buildings: Literature Review and Practical Examples*. Journal of Building Physics, 28(2) (2004) 107-159.

Davenport A.G., *An approach to human comfort criteria for environmental wind conditions*, Colloq. on Building Climatology, 1972.

Gandemer J., *Wind environment around buildings: aerodynamic concept*, 4th Int. Colloq. on Wind Effects on Buildings and Structures, Heathrow, 1975.

Gehl J., Gemsøe L., Kirknæs S., and Søndergaard B.S., *New City Life*. The Danish Architectural Press, Copenhagen, 2006.

Gehl J., Svarre B., *How to study public life*. [Bylivsstudier. English], Island Press, 2013.

Hunt J.C.R., Poulton E.C., Mumfort J.C., *The effects of wind on people; new criteria based on wind tunnel experiments*, Building and Environment, 11(1) (1976) 15-28.

Koss H.H., *On differences and similarities of applied wind comfort criteria*. Journal of Wind Engineering and Industrial Aerodynamics, 94(11) (2006) 781-797.

Koss H.H., *Considerations for the development of a wind comfort guideline* (Überlegungen zur Entwicklung einer Windkomfortrichtlinie), German language, Proc. of 14. D-A-CH Colloquium, 2015

Lynch K., *Good City Form*. MIT Press, Cambridge, Massachusetts, 1981.

McGregor G.R. ed., *Universal Thermal Climate Index* (UTCI), special issue of Int. Journal of Biometeorology, 56 (2012) 419.

Melbourne W.H., *Criteria for environmental wind conditions*, Journal of Wind Engineering and Industrial Aerodynamics, 3 (1978) 241-249.

Penwarden A.D., *Acceptable wind speeds in towns*, Building Science, Vol.8, 1973.

UN, *World Urbanization Prospects – The 2009 Revision Highlights*. United Nations, Department of Economics and Social Affairs, Population Division, New York, 2010.

An ANN-based surrogate model for predicting pedestrian-level wind environment

Asiri U. Weerasuriya[1], Xuelin Zhang[1], Tim K.T. Tse[1]

[1]*Department of Civil and Environmental Engineering, The Hong Kong University of Science and Technology, Hong Kong, China*
e-mail: asiriuw@ust.hk
e-mail: xuelin.zhang@connect.ust.hk
e-mail: timkttse@ust.hk

Abstract: This study proposes an ANN-based surrogated model as an alternative test technique to wind tunnel test and computational fluid dynamic (CFD) simulations to assess pedestrian-level wind (PLW) environments. The surrogate model was developed using wind speed data obtained from CFD simulations of 150 lift-up buildings. The proposed surrogate model successfully replicated both magnitude and direction of wind speed at the pedestrian level by using the minimum computational resource. The analysis suggested adopting a regression-based bias correction method for further improvements of the surrogate model.

Keywords: artificial neural network, pedestrian-level wind environment, lift-up building.

1. Introduction

The assessment of pedestrian-level wind (PLW) environment is currently mandatory for large-scale construction projects in many major cities worldwide. Two main assessment techniques of PLW environment; wind tunnel tests, and Computational Fluid Dynamic (CFD) simulations are costly, time-consuming, and require expert knowledge. The cost of conducting wind tunnel tests or CFD simulations are difficult to be justified in the case of testing a large number of designs with minor changes or the required accuracy of test results is low. In such circumstances, engineers prefer to use a tool that can speedily evaluate many alternative designs with an engineering accuracy. The surrogate modelling, which replicates results based on its prior training data rather than implicitly solving governing mechanisms of the model, would be a fitting tool to evaluate many models with reasonable accuracy.

The surrogate modelling uses different techniques in machine learning to make predictions based on its prior training data sets. This study employs the Artificial Neural Network (ANN) technique to train a surrogate model to predict the PLW environment near lift-up buildings. The ANN, whose structure is inspired by the biological neural system can establish complex non-linear relationships between predictors and dependent variables (Schalkoff, 1997). The predictors are control factors of dependent variables, whose relationships are established by using inter-connecting links, commonly known as neurons, passing through one or more hidden layers. Several previous studies employed ANN to estimate wind pressure on building surfaces (Chen et al., 2003), wind speed-up over hills (Bitsuamlak et al., 2007), interference effect of buildings (Khanduri et al., 1997), but no study adopted ANN to predict wind speeds at the pedestrian level. Therefore, this study aims to investigate the potential of an ANN-based surrogated model to predict PLW environments near 'lift-up' buildings. The proposed surrogate model predicts both the magnitude and direction of wind speed by estimating longitudinal (u) and lateral (v) wind speeds. To explore the full potential of the surrogate model, this study selects an unorthodox building form, the lift-up design, as the test case. The buildings with lift-up designs, hereafter referred to as lift-up buildings, are known to create more complex flow fields than buildings those without lift-up designs (Tse et al., 2017; Zhang et al., 2018(a), (b)).

2. The development of the surrogate model

2.1. Lift-up building model

The surrogated model was constructed using wind speed data of u and v obtained from CFD simulations of 150 lift-up buildings models. The lift-up buildings have a central core with different sizes and shapes as shown in Fig. 1. Each building model was unique as defined by eight design parameters: building height (H), building width (W), height, width, and depth of the lift-up core (h, w, d), the shape of the lift-up core, and orientation (or wind direction θ). Tab. 1 shows the ranges of each parameter used for the 150 building models.

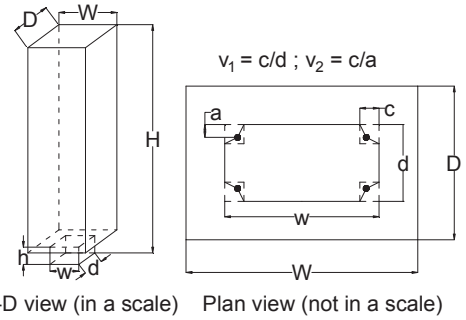

Figure 1. Schematic diagram of a lift-up building

Table 1. Dimensions of the 150 lift-up building models.

Main building	Lift-up core	Orientation
[m]	[m]	[degree]
$45 \le H \le 120$	$3 \le h \le 9$	$0 \le \theta \le 45$
$30 \le W \le 90$	$9 \le w \le$ W	
Depth (D) = 20	$6 \le d \le$ D	
	$0 \le v_1 = c/d \le 1/3$	
	$-1 \le v_2 = c/a \le 0$	

2.2. CFD simulation

A fully automated process was used for CFD simulation. The automated process started with constructing geometries of buildings, then followed by grid discretization, assigning boundary conditions, selecting numerical methods, and finally extracting wind speeds from the simulations. All cases were modelled as the steady state, Reynolds-Averaged-Navier-Stokes (RANS) simulations using standard k- ε turbulence model and approaching profiles of mean wind speed (U) and turbulence intensity (I) as defined in Eqs. 1(a) and (b).

$$U(z) = U_{ref}\left(z/z_{ref}\right)^{0.11} \tag{1a}$$

$$I(z) = I_{ref}\left(z/z_{ref}\right)^{-1/4.3} \tag{1b}$$

where, U_{ref} and I_{ref} were taken as 7.6 m/s and 5.6%, respectively at a reference height, z_{ref} of 120 m.

2.3. The ANN model

The ANN model was constructed using wind speed data extracted at 194 points at the pedestrian level (2 m above ground) near the 150 lift-up buildings. The dataset was divided into three subsets such as 70% of the data for training, 15% for validation, and the rest of 15% for testing the ANN model. Different combinations of hidden layers, neurons and training schemes were tested before selecting one hidden layer with 15 neurons for the ANN model that was trained using the Bayesian Framework. The trained ANN model predicted the magnitudes of u and v wind speeds with zero error at more than 58% and 75% of test points, respectively.

3. The evaluation of the surrogated model

The accuracy of the surrogated model was estimated comparing the results of CFD simulations and predictions of several lift-up buildings with various dimensions and orientations. Here, the results are presented for a lift-up building, which has dimensions of H = 78.51 m, W =90 m, D = 20 m, h = 7.42 m, w = 33.16 m, d = 13.29 m, v_1 = 0.22, v_2 = 0.38, θ = 2.27°.

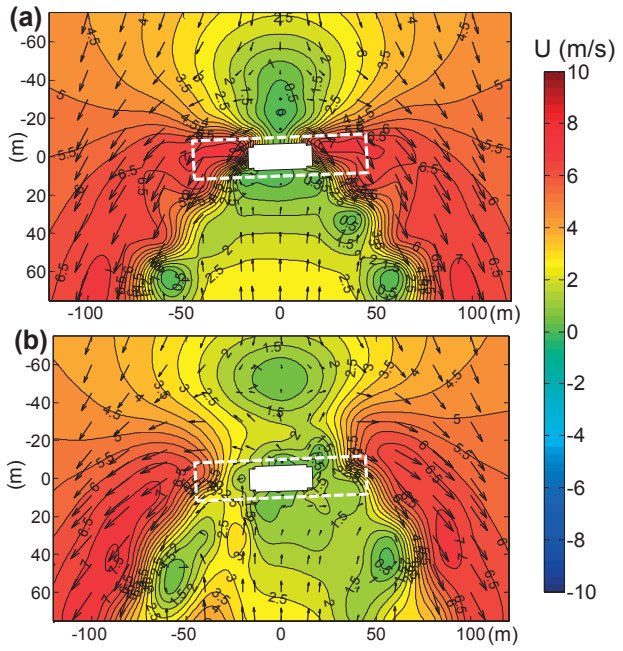

Figure 2. Distribution of resultant wind speed (U) and wind direction from (a) CFD simulation and (b) surrogate model.

Fig. 2 shows the distribution of resultant wind speed (U) at the pedestrian level, which is calculated as $U = \sqrt{u^2 + v^2}$ and wind direction as simulated by CFD and predicted by the surrogate model. The CFD simulation required more than 5 CPU hours on an Intel® Xenon(R)-3.1 GHz (32 GB RAM) workstation to produce these results while the surrogated model spent less than 1 minute on a desktop computer. Notwithstanding its lesser computational cost, the surrogate model produced comparable distributions of wind speed and direction to the CFD simulation. However, few noticeable differences between the two set of results can be identified including the absence of high-speed wind streams in the void underneath of lift-up building and the detachment of the area of low wind speed zone in front of the building in surrogate model's results.

Fig. 3 further discerns the simulated and predicted wind speed by the CFD simulation and the surrogate model. Fig. 3(a) shows noticeable deviations in the magnitude of u between the CFD simulation and the surrogate model while the estimation of v by the surrogated model slightly deviates from those of the CFD simulation. The gradients of regression lines of u and v are close to 1, thus indicative of good similarity between the results of the surrogate model and CFD simulation. Furthermore, high correlations between the two sets of results suggest that the linear regression method can be used as a bias correction method for the proposed surrogate model.

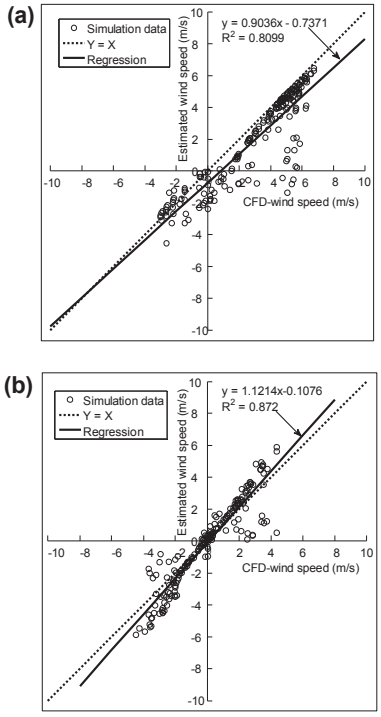

Figure 3. Comparison of the CFD simulation and surrogated model of (a) u, and (b) v.

4. References

Bitsuamlak G.T., Bédard C., Stathopoulos T. *Modeling the effect of topography on wind flow using a combined numerical–neural network approach*. Journal of Computing in Civil Engineering 21(6) (2007) 384-392.

Chen Y., Kopp G.A., Surry D. *Prediction of pressure coefficients on roofs of low buildings using artificial neural networks*. Journal of Wind Engineering and Industrial Aerodynamics 91(3) (2003) 423-441.

Khanduri A.C., Bédard C., Stathopoulos T. *Modelling wind-induced interference effects using backpropagation neural networks*. Journal of Wind Engineering and Industrial Aerodynamics 72 (1997) 71-79.

Schalkoff R.J. *Artificial neural networks*. Vol. 1. New York: McGraw-Hill, 1997.

Tse K.T., Zhang X., Weerasuriya A.U., Li S.W., Kwok K.C.S., Mak C.M., Niu J. *Adopting 'lift-up' building design to improve the surrounding pedestrian-level wind environment*. Building and Environment 117 (2017) 154-165.

Zhang X., Tse K.T., Weerasuriya A.U., Li S.W., Kwok K.C.S., Mak C.M., Niu J., Lin Z. *Evaluation of pedestrian wind comfort near 'lift-up' buildings with different aspect ratios and central core modifications*. Building and Environment 124 (2017) 245-257.

Zhang X., Tse K.T., Weerasuriya A.U., Kwok K.C.S., Niu J., Lin Z., Mak C.M. *Pedestrian-level wind conditions in the space underneath lift-up buildings*. Journal of Wind Engineering and Industrial Aerodynamics 179 (2018) 58-69.

Pedestrian wind comfort around high buildings in Warsaw

Agnieszka Kocoń [1], Magdalena Grzybek[2], Renata Kłaput[3] Andrzej Flaga[4]

[1]*Wind Engineering Laboratory, Faculty of Civil Engineering, Cracow University of Technology, Poland, e-mail: agnieszka.kocon89@gmail.com*
[2]*Faculty of Civil Engineering, Cracow University of Technology, Poland, e-mail: magda.grzybek@o2.pl*
[3]*Wind Engineering Laboratory, Faculty of Civil Engineering, Cracow University of Technology, Poland, e-mail: rklaput@gmail.com*
[4]*Wind Engineering Laboratory, Faculty of Civil Engineering, Cracow University of Technology, Poland, e-mail: liwpk@windlab.pl*

Abstract: The paper presents results of pedestrian wind comfort measurements. Analysis of this problem was conducted in two phases. First stage included measurements of velocities at the pedestrian level in the area around high buildings in Warsaw. Basing on these results probability of threshold wind velocity exceedance was calculated and pedestrian wind comfort was determined. Then the arrangement of wind protection elements in areas of the worst wind conditions was proposed. In the next stage of tests the same model equipped with wind protection shields was used. This solution appeared to be effective in improvement of wind comfort at pedestrian level.

Keywords: wind tunnel tests, pedestrian wind comfort, urbanized area, high-rise buildings.

1. Introduction

Growing density of high buildings in urbanized areas causes the change of wind environment. Effect of this situation are high wind velocities at the pedestrian level which can be uncomfortable and even dangerous for people. Complex wind flow in the building surroundings is the result of man parameters, such as building shape, size, orientation with respect to the wind directions or interaction with the surroundings. This issue was under thorough investigations through past years: Isyumov and Davenport (1978) Stathopoulos et al. (1999).

The pedestrian wind comfort in specific cases was investigated in many research works: Williams and Wardlaw (1992), Blocken et al. (2003). This paper presents an example of new complex of high-rise buildings influence on pedestrian wind comfort in their vicinity. Uniqueness of the structure and the surroundings arrangement caused the necessity to undertake tests in the wind tunnel. Additionally, arrangement of wind protection elements was proposed to improve wind comfort in some areas.

2. Wind tunnel tests

Wind tunnel tests were carried out in the boundary layer wind tunnel of the Wind Engineering Laboratory at the Cracow University of Technology (Research Report, 2018). Measurements were conducted on model in a scale of 1:300. The nearest area of high-rise buildings which will be erected in the city center of Warsaw in Poland was analysed during the tests. In the first stage, pedestrian wind comfort was tested in 93 points localized in this region for twelve angles of wind onflow, with 30° angle increment (fig.1a). Hot-wire anemometer system was used to obtain instantaneous wind velocity at the height 0.55 cm which corresponds with pedestrian level in the nature (1.75 m). The measuring position is presented in fig. 1b.

As a result of these measurements, mean wind velocity at the pedestrian level was obtained. Hence, one can calculate wind velocity amplification coefficient with respect to the angle of wind onflow (θ_i):

$$\gamma(\theta_i) = \frac{\overline{V}_P(\theta_i)}{\overline{V}_{ref}(\theta_i)} \tag{1}$$

where: $\overline{V}_P(\theta_i)$ – mean wind velocity at the pedestrian level, $\overline{V}_{ref}(\theta_i)$ – mean wind velocity at the reference height.

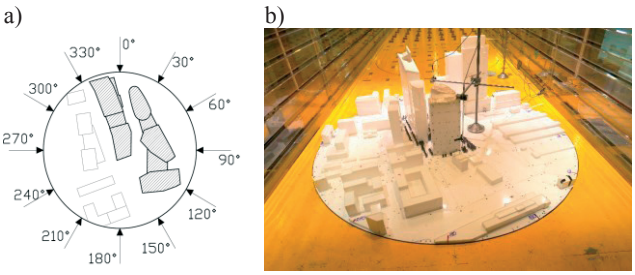

Figure 1. Investigated buildings: wind directions with respect to the model (a), measuring position in the wind tunnel (b).

The velocity amplification coefficient was used to calculate probability of threshold wind velocity exceedance which enabled the assessment of pedestrian wind comfort in the measurement points. Basing on these results and considering the activity of pedestrians in respective places around the buildings, the areas of adverse wind conditions were determined.

To obtain improvement of pedestrian wind comfort it was necessary to use relevant wind protection elements, such as e.g. wind protection shields or green belt. These elements were arranged properly with respect to the wind directions which cause the highest probability of threshold wind velocity exceedence (i.e. the worst pedestrian wind comfort).

The second phase of the measurements was conducted on the previous model equipped with the protection shields which were modelled by the plexiglass shields of dimensions 3 m per 3 m (in vertical plane, in natural scale). In the second stage, the investigations of pedestrian wind comfort were carried out only in the areas of adverse wind conditions.

3. Elaboration of results

To analyse pedestrian wind comfort threshold wind velocity (V_{TRH}) and the probability of exceedance of the threshold wind velocity (P_{exc}) must be defined.

Probability of exceedance of threshold wind velocity for respective wind direction (θ_i) is calculated according to the formula:

$$P_{exc}(\theta_i) = 100 \cdot P(\theta_i) \cdot \exp[-(\frac{V_{TRH}}{\eta(\theta_i) \cdot \gamma(\theta_i) \cdot \beta(\theta_i) \cdot c(\theta_i)})^{k(\theta_i)}] \quad (2)$$

where: $P(\theta_i)$ – probability of wind direction, $c(\theta_i)$, $k(\theta_i)$ – parameters of Weibull distribution function, $\eta(\theta_i)$ – time averaging coefficient, $\gamma(\theta_i)$ – wind velocity amplification coefficient (obtained from wind tunnel tests), $\beta(\theta_i)$ – transition coefficient.

To define the probability of exceedance of threshold wind velocity in one point, one must determine a sum of probabilities $P(\theta_i)$ for each wind direction. This value is needed to assess the fulfilment of pedestrian wind comfort concerning respective pedestrian activity.

The criteria of pedestrian wind comfort adopted in this paper were proposed in Flaga (2008) and they take into account criteria applied in other European countries as well as wind conditions characteristic for Poland. Value of threshold wind velocity adopted in this paper was $V_{TRH} = 5\frac{m}{s}$ (a year-round).

4. Results

Fig.2 presents results of the first phase of wind tunnel tests. The areas where people cannot stay long in steady position were marked as places of adverse pedestrian wind comfort. This is the most rigorous comfort criterion and in most of distinguisged areas people can stay shortly in steady position.

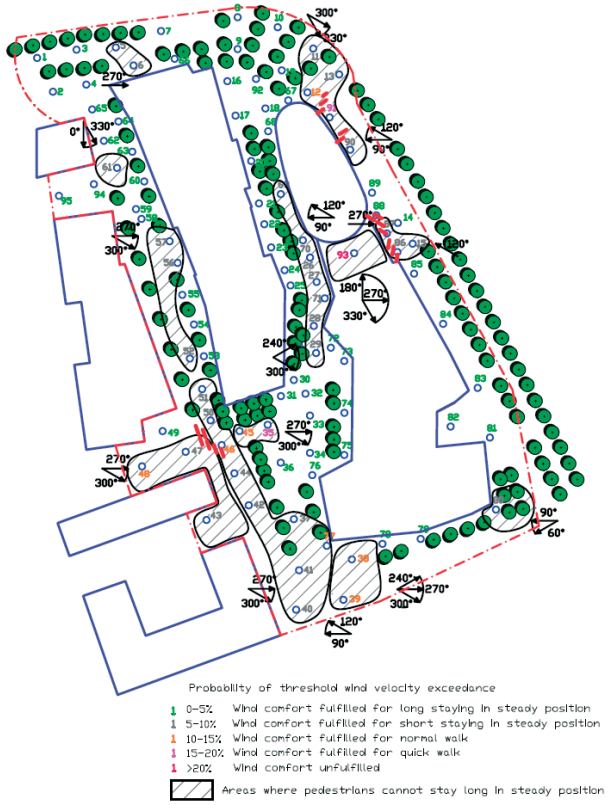

Figure 2. Results of pedestrian wind comfort in first phase of wind tunnel tests and the arrangement of wind protection shields.

For each of the region the wind directions which cause the highest probability of wind velocity exceedance were determined. It is worth to point out that places where is a lot of trees or planting are charaterized by better wind conditions.

The wind protection shields were applied in the arrangement presented in fig.2 (marked red). According to the results of both phases of the measurements wind protection shields caused improvement in pedestrian wind comfort in the analysed areas. The significant change appeared in transition between two buildings (point 93).

5. Conclusions

The results of both phases of measurements lead to the following conclusions:

- Areas sheltered by trees are sufficiently protected from wind action and owing to that pedestrian wind comfort for long or short staying in steady position is fulfilled there,
- Wind protection shields provided the fulfilment of wind comfort at the pedestrian level in most cases. They are effective solution in improvement of pedestrian wind comfort in urbanized area. Alternatively, trees can be used in the same way in the places where planting is possible,
- The arrangement of wind protection elements must take into account wind directions which have predominant impact on deterioration of wind comfort.

6. Acknowledgments

This research work was supported by: Spektrum Real Sp. z o.o.

7. References

Blocken B., Roels S., Carmeliet J. *Pedestrian wind conditions in passages through buildings – Part 2. Case study: the Sillvertop Towers project.* Building Physics Research Report, Laboratory of Building Physics KULeuven, 2003.

Flaga A. *Wind engineering. Fundamentals and applications*. Arkady, Warsaw, Poland, 2008.

Isyumov N., Davenport A.G. *Evaluation of the effects of tall buildings on pedestrian level wind environment*. ASCE Annual Convention, 1978.

Stathopoulos Th., Wu H., Zacharias J. *Field survey on outdoor human comfort in urban climate.* In: Larose, et al (Eds.), Wind Engineering into the 21st Century, Balkema, 1999.

Williams C. D., Wardlaw R.L. *Determination of the pedestrian wind environment in the city of Ottawa using wind tunnel and field measurements*. J. Wind Eng. Ind. Aerodyn. 41 (1992), 255-266.

Badania modelowe w tunelu aerodynamicznym Politechniki Krakowskiej komfortu wiatrowego w poziomie przechodniów wokół wieżowca Skyliner przy ul. Towarowej/Prostej w Warszawie. Research Report, Wind Engineering Laboratory at the Cracow University of Technology, Cracow, Poland 2018.

Identification and analysis of urban solar reflections on the example of The Warsaw Hub buildings

Łukasz Flaga[1]

[1]*Wind Engineering Laboratory, Cracow University of Technology, Poland,*
e-mail: lukasz.flaga@interia.pl

Abstract: This paper presents identification and analysis of urban solar reflections on high-rise buildings of The Warsaw Hub. The study was conducted at Wind Engineering Laboratory of Cracow University of Technology as part of a larger study work containing also investigations of wind action on the buildings, wind comfort on pedestrian level, snow load simulations and vibration comfort analysis of the subject buildings. The aim of this study was to determine areas of solar reflections accumulation as well as to indicate the places and objects potentially exposed to excessive effect of the reflection phenomenon. The evaluation criteria of comfort were elaborated separately for the buildings, communication infrastructure, and for public places. The results obtained during study were supplemented by the shading analysis.

Keywords: reflections, environmental actions, solar analysis, high-rise buildings, simulation.

1. Introduction

The subject of this study was *The Hub* project - three high-rise buildings located in Warsaw (see Fig. 1.). Building A is 86,5 m tall, buildings B and C are 130,5 m tall. Between buildings A & B and B & C there are lower buildings respectively AB and BC that are 26,5 m high. The AB building contains a small passage at the ground level, allowing for communication.

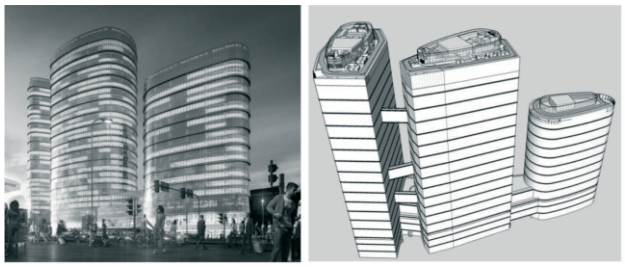

Figure 1. Computer visualization and model of The Hub buildings considered in investigations.

The main scientific aim of the study was to determine the areas of solar reflections accumulation on ground level around the buildings. Identification was aimed at highlighting possible critical zones of public space where sunlight accumulation exceeds adopted criteria of comfort. The results were also intended to indicate the places and objects potentially exposed to excessive effect of the reflection phenomenon. For this cases recommendations possible to apply at the design stage were developed.

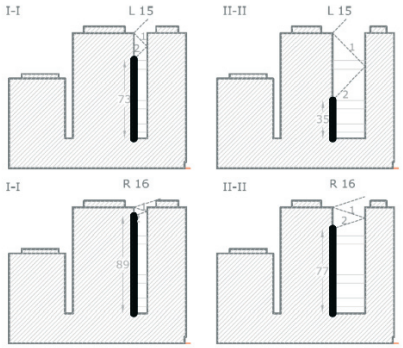

Figure 2. Cross sections presenting the highest number of reflections occurring between the designed buildings B and C for the period March-September between 15:00 and 16:00.

2. Study method

The first stage of the study included determination of: exposure conditions for the site (coordinates of the location are 52°13'42.9" N; 20°59'06.9" E) according to [6, 1], azimuth [7, 9] and the number of hours of solar radiation for Warsaw [10]. The theoretical range of reflected rays incidence was also developed. On this basis, a preliminary analysis was carried out to determine the possibility of multiple sun reflections occurring within the same facades of *The Hub* buildings (see Fig. 2).

In the next stage, based on geometric data, a CAD spatial model of the urban layout was made, according to [3]. Then, using the sun location data [9, 7], 12 maps of potential solar reflections were performed for the 15th of each month of the year (see Fig. 3). On their basis, another 12 maps were elaborated. Each consisted of frequency analysis of potential solar reflections occurrence within a radius of 300 m neighbourhood (see Fig. 4).

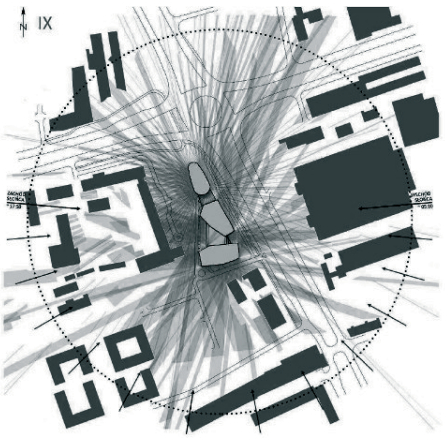

Figure 3. The potential solar reflections analysis for the 15th of September.

The third stage concerned analysis and identification of sites and facilities located in the nearest neighbourhood, which *The Hub* may affect. Three different groups of users were determined, each with different criteria for the evaluation of solar reflections comfort.

In the last stage, the daily and monthly frequency of discomfort caused by solar reflections for each of the three groups of users was developed. In addition, specific areas have been identified where the phenomenon of accumulation (overlap) of reflections from different façades occurs at the same time. The entire

analysis was elaborated in a form schemes (maps) and tables easy to use at the design stage.

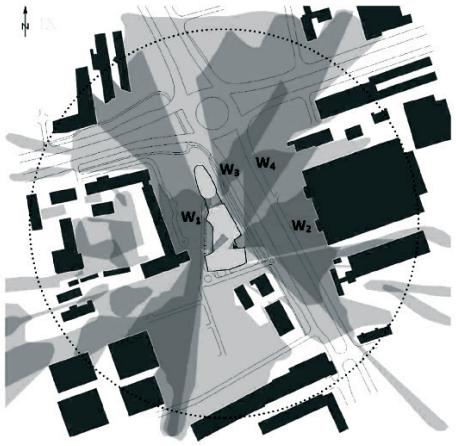

Figure 4. The accumulation of solar reflections from the Hub buildings for the 15th of September. W1 - W4 – areas of overlapping solar reflections.

3. Evaluation of solar reflections comfort criteria

The basic elements of surrounding urban layout included in the analysis were: façades (of both existing and planned buildings) facing front *The Hub*, public places (public transport stops, pedestrian crossings and entrances to the buildings) and sections of communication structure (straight sections of the road system and a circular intersection).

The analysis of communication system took into account only directions of road axis converging with directions of the reflected sunrays, according to [2, 4, 8]. The length of the road segments exposed to the reflection phenomenon was also analysed. Following angular ranges of reflected sunlight which cause discomfort were taken into account in evaluation criterion for users of communication system:

- Winter season in full hourly range (angular range of the sun height is 0^0-$15{,}1^0$);
- Spring and Autumn seasons in hourly range 6:00-8:00 & 16:00-18:00 (angular range of the sun height is 0^0-$18{,}2^0$);
- Summer season in hourly range 4:00-6:00 & 18:00-20:30 (angular range of the sun height is also 0^0-$18{,}2^0$).

The criterion for evaluation of comfort of public space users mainly concerns glare phenomenon – the exceeding of the permissible fields of brightness & contrast in the cone of good vision [2, 7]. It results from a mutual configuration of the subject (e.g. information boards, traffic lights, images seen while using vertical communication elements, e.g. elevators, stairs, etc.) and the observer with respect to sunrays reflected from *The Hub* facade.

Another issue of this criterion is reflections accumulation occurrence. At certain times the inward-curving (concave) curtain wall focuses reflected sunlight to an intense spot that traces across pedestrian areas in front of the building (as in the case of e.g. *Walkie Talkie London* & *Vdara Hotel Las Vegas*) [2, 3].

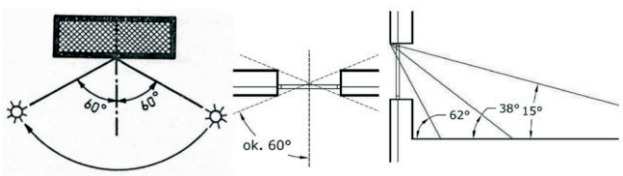

Figure 5. Schematic drawings of: angular limits of façade front lighting and the range of interior penetration with sunrays for characteristic seasons: summer, spring and autumn, winter.

The key issue in evaluation criterion of comfort of nearest building users is configuration of façades with respect to direction of reflected sunrays. According to [5, 6], the frontal exposure was indicated as the most affecting one for users (see Fig. 5). In this comfort criterion, particular attention was paid to sunrays reflected at relatively small angles (angles $<38^0$ – significant influence).

4. Results analysis, conclusions and final remarks

The analysis of accumulation phenomenon of sunrays reflections from *The Hub* showed that the maximum number of coincident reflections in particular areas is 3. The areas of such accumulation overlap widely with zones remaining in the shade for a significant part of the day (about 50-70% of total daylight lighting time). Due to that fact the probability of exceeding the comfort of public space users is very small.

Issues of human comfort due to reflections of solar radiation (especially sunrays) from glazed-façades of buildings are not yet standardized. The results of analyses carried out in this study show that sunrays reflected directly from *The Hub* façade will affect the nearest neighbourhood. However there is no fear of excessive discomfort of users of public space. For areas located further than 300 m from the planned buildings, this influence is negligible.

5. Acknowledgments

This study was conducted in collaboration with KWADRA Architekci. It was done as a commissioned work funded by AMC – Andrzej M. Chołdzyński Sp. z o.o.

6. References

[1] Byrdy Cz. *Designing of lightweight walls and roofs structures made of corrugated sheets* Budownictwo Lądowe 2(65), Politechnika Krakowska 1987, [in Polish].

[2] Danks R. *Urban solar reflection identification, simulation, analysis and mitigation: learning from case studies*, RWDI Inc., Proceedings of the eSim 2016 Building Performance Simulation Conference, p. 309-318, 2016.

[3] Danks R., Good J. *Urban scale simulations of solar reflections in the built environment: Methodology & Validation*, RWDI Inc. Proceedings of the Symposium on Simulation for Architecture and Urban Design. London, 2016.

[4] Flaga Ł., Dubik M. *Method of evaluation of selected parameters of landscape route composition elements on the example of the Częstochowa road system section*, Budownictwo i architektura Częstochowy, Politechnika Częstochowska 2016; [in Polish].

[5] Flaga Ł. *Identification of landscape bridge crossings in terms of a location identity*, Politechnika Lubelska; Lublin 2014; [in Polish].

[6] Mieszkowski Z. *Elements of architectural design,* Arkady Warszawa 1975; [in Polish].

[7] Twarowski M. *Sun in architecture*. Wydanie 4. Arkady. Warszawa 1996; [in Polish].

[8] Windtech Consultants Pty Ltd: *Solar light reflectivity analysis Eastwood Centre*, Yuhu Property (Australia) Pty Ltd, Sydney, 2016.

[9] http://blog.kubiczek.eu/2008/11/kalkulator-polozenia-slonca (12.2016).

[10] https://www.miir.gov.pl/strony/zadania/budownictwo/charakterystyka-energetyczna-budynkow/dane-do-obliczen-energetycznych-budynkow-1/ (06.2018).

Wind study for ventilation corridors in the City of Warsaw

Mariusz Rutkowski[1], Michał Remer[1]

[1]*Institute of Aeronautics and Applied Mechanics, Warsaw University of Technology, Poland,*
e-mail: mrutkowski@meil.pw.edu.pl

Abstract: Presented work describes a CFD simulation of the air flow over two large parts of the city of Warsaw. Finite Volume Method discretization and calculations were carried out in ANSYS environment. Calculation of pedestrian-level wind (PLW) speed for wind comfort for selected areas was the main goal of presented work according to European wind norms in 1:1 scale for unique area of 32 km2. Several improvements of the urban space development were proposed, as a result of carried simulations.
Keywords: CFD, urban flow, turbulence

1. Introduction

Three-dimensional steady Reynolds-averaged Navier–Stokes (RANS) Computational Fluid Dynamics (CFD) simulations are used in presented work to evaluate the pedestrian-level wind conditions for a large area of one of the major cities in the central Europe. Two large parts of the city of Warsaw (2 km x 10 km and 2 km x 6 km) are considered.

To better understand the influence of the urban development as well as the urban flow phenomenon itself, the areas were compared with a several-year interval (2008 and 2015). The simulations were carried out for six wind directions for each geometry. In comparison to the other European cities, City of Warsaw gives an opportunity to examine the issue of the air exchange in rather unique way. The development of the urban space was carried out in such a way, that the next to densely built-up areas, there exists nine so called "ventilation corridors" (Fig. 1), whose main role is to force air movement in their vicinity, as well as to improve the air quality in the city centre. Preparation of the demanding CFD simulations adjusted according to European wind norms in 1:1 was rather unique taking into account area covered which was around 32km2.

2. Problem description

Finite Volume Method discretization and calculations were carried out in ANSYS environment. Calculations were carried out in Finite Volume Method solver – ANSYS Fluent. The solver was used to calculate incompressible steady-state Navier-Stokes equations with SIMPLE algorithm to resolve pressure-velocity coupling.

To obtain reasonable and realistic distributions of the turbulence intensity and velocity profiles, strictly described by the norms (5), the kinetic turbulence energy and the rate of dissipation of turbulence energy were modelled accordingly to several works e.g. Kose (2011) or Topalar (2015).

Information on the pedestrian-level wind (PLW) speed for wind comfort assessment (Fig. 2), for two geometries – year to year (2008 – 2015) was the main goal of presented work. All data were prepared with accordance to all assumptions described in papers e.g. of Blocken (2016). The simulations were carried out for six wind directions for each geometry. To maintain the physical nature of the flow, constant divisions were made on buildings (0.5 meters). Furthermore, a constant division of 4 elements is made between the ground and the measuring surface (1.75 m) (Tominaga 2008). Finally, the size of the grid for the smaller domain was 96 million elements, while for a larger domain, the number of items reached 120 million elements.

Figure 1. One of the ventilation corridors (2km x 6 km).

3. Conclusions

The authors successfully conducted a series of calculations of the presented geometries. The analyses carried out show that the further evolution of the city has a large impact on the air supply and the restoration of the urban boundary layer. Analysis inside the corridors has shown a beneficial effect on regeneration of the higher air velocities near the ground. Unfortunately, the densely built-up areas at boundaries of these corridors limit greatly their functionality. Despite the conclusions obtained from these analyses, attention should be paid to other beneficial functions of ventilation corridors, not addressed in the presented work. Due to numerous parks (full of vegetation) located inside, additional analyses should be taken into account in terms of air filtration and heat exchange.

Figure 2. Pedestrian level wind for the selected region with increased wind speed (4m/s).

Finally, several improvements of the urban space development were proposed, as a result of the presented simulations. All collected knowledge will serve as a prelude to more complex analyses in terms of the modelling of the city space as well as path to improvement of the large-scale analyses.

4. Acknowledgments

The calculations were made in Interdisciplinary Centre for Mathematical and Computational modelling, grant number GB69-23/2017.

Part of the results was prepared for the document "Potencjał do kształtowania warunków klimatycznych –w tym wymiany i regeneracji powietrza w Warszawie"- UM Warszawa, 2017.

5. References

Kose D A, Fauconnier D, Dick E, *ILES of flow over low-rise buildings:Influence of inflow conditions on the quality of the mean pressure distribution prediction*, Journal of Wind Engineering and Industrial Aerodynamics, Volume 99, Pages 1056–1068, 2011

Toparlar Y, Blocken B, Vos P, van Heijst G J F, Janssen W D, van Hooff T, Montazeri H, Timmermans H J P, *CFD simulation and validation of urban microclimate: A case study for Bergpolder Zuid, Rotterdam*, Building and Environment, Volume 83, Pages 79-90, 2015

Blocken B, Stathopoulos T, van Beeck J P A J*, Pedestrian-level wind conditions around buildings: Review of wind-tunnel and CFD techniques and their accuracy for wind comfort assessment*, Building and Environment, Volume 100, Pages 50-81, 2016

Tominaga, Y., Mochida, A., Yoshie, R., Kataoka, H., Nozu, T., Yoshikawa, M., Shirasawa, T., *AIJ guidelines for practical applications of CFD to pedestrian wind environment around buildings,* Journal of Wind Engineering and Industrial Aerodynamics, Volume 96 p 1749-1761, 2008

PN-EN 1991-1-4:2008 with attachment

Model tests of dynamic action on the atmospheric boundary layer – linear configuration of ventilation towers on a rough terrain

Łukasz Flaga[1], Aleksander Pistol[2], Piotr Krajewski[2], Andrzej Flaga[2]

[1]*Wind Engineering Laboratory, Cracow University of Technology, Poland,*
e-mail: lukasz.flaga@interia.pl
[2]*Institute of Structural Mechanics, Cracow University of Technology, Poland,*
e-mail: aleksander.pistol@gmail.com
e-mail: piotrekrajewski@gmail.com
e-mail: liwpk@windlab.pl

Abstract: This paper describes the model tests conducted at the Wind Engineering Laboratory of Cracow University of Technology as the first stage of studies on dynamic action on the atmospheric boundary layer in order to reduce effects of air pollution and smog. It focuses on the cooperation between subsequent ventilation towers placed one by one (or row after row) in order to generate a continuous airstream with sufficient velocity as to aid the natural ventilation of urban areas. The tests were conducted for three different terrain categories with varying roughness. Also, different wind speeds supplied by the fans, different distances between the towers and different configurations of the towers in each row were tested. As a preliminary set of tests, these allowed to verify the feasibility of the solution and its effectiveness on a rough terrain that simulates urban areas.

Keywords: wind engineering, smog reduction, environmental engineering, urban ventilation, terrain roughness.

1. Introduction

The problem of smog and excessive air pollution is faced by many modern cities. So far the countermeasures for this problem are limited to restrictions of car traffic, modernisation of coal-fuelled heating systems or active air purifiers with very local range of impact. The idea of these studies is to apply large ventilation towers (shown in Fig. 1) for creating artificial airstreams in natural ventilation arteries of the cities, effectively improving the urban air quality. They would be put to use during windless periods when the pollution is accumulated in the air. If proven to be working (as in: creating a continuous airstream of desirable wind speed) in the model scale and on the rough terrain, the solution should be tested in a larger scale before implementation in real life. Furthermore, subsequent stages of the preliminary tests will focus on a way of disposing the polluted air from the atmospheric boundary layer and cooperation between the ventilation towers – used to supply the polluted air – and the exhaust system.

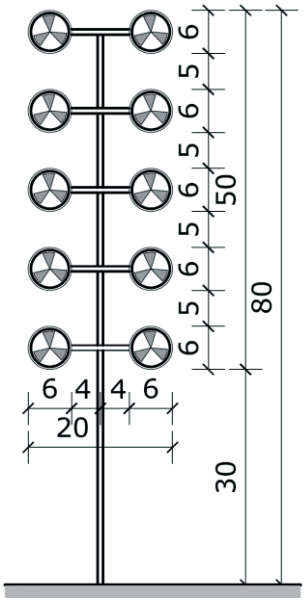

Figure 1. Scheme of the proposed ventilation tower with 10 large fans (all dimensions in [m]).

2. Tests method

2.1. Similarity criteria

Dimension base for the tests is (ρ, V, D) (see Fig. 2) where: ρ – air density, V – fan outlet air velocity, D – fan diameter. Velocity V_x at a distance x from the fan outlet is determined by a number of parameters, shown in Eqn. (1):

$$V_x = F\left(\rho, \mu, V, H, x, D, (\check{G})\right), \tag{1}$$

where: μ – air dynamic viscosity, H – height of fan centre above the ground level, x – distance from the fan, $\check{G}$ – set of dimensionless geometric parameters. The following dimensionless values have been defined (Eqn. (2) – Eqn. (7)):

$$\frac{V_x}{V} = \Pi_V = \check{V} \tag{2}$$

$$\frac{VD}{\nu} = \Pi_\nu = Re \tag{3}$$

$$\frac{H}{D} = \Pi_H \tag{4}$$

$$\frac{x}{H} = \Pi_x = \check{x} \tag{5}$$

$$\frac{V_x}{V} = \check{F}\left(\frac{Va}{\nu}, \frac{H}{D}, \frac{x}{H}, (\check{G})\right) = \check{V} \tag{6}$$

hence:

$$V_x = V \cdot F(Re, \frac{H}{D}, \frac{x}{H}(\check{G})) \tag{7}$$

where: ν – air dynamic viscosity, Re – Reynolds number.

Based on this, it can be observed that the air velocity in the elaborated problem is related to Reynolds number and distance from the fans. Other geometric parameters are constant.

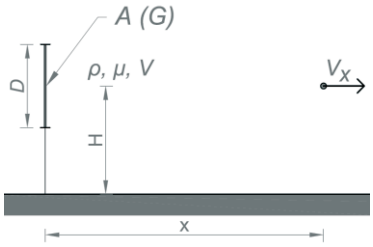

Figure 2. Geometric and physical parameters of the problem.

2.2. Test models

Ventilation towers were modelled with CPU fans of 60 x 60 mm in size. This resulted in the model scale of 1:833. Due to different proportions between height and width of fans and ventilation towers (80 x 20 m), only the vertical size was correctly projected in the scale.

For the 6th series of the tests, a model of ventilation tower in the scale of 1:100 was created, projecting correctly both height and width.

The models were tested in aerodynamic tunnel of WEL CUT. The base for the models was made with a smooth wooden board. For the 7th and 8th series of the tests, terrain roughness was recreated in the model scale for categories III (forests and suburban areas) and IV (downtown urban areas) according to [PN-EN 1991-1-4]. This was performed by using rigid Styrofoam blocks glued to the board in a pattern that would correspond with the guidelines of the standard and based on literature study (Flaga, 2008, Ramponi et al., 2015, Blackman et al., 2015).

2.3. Tests and measuring devices

The tests were conducted by measuring the wind speed generated by the fans in front of them at a distance of every 10 cm in their nearest vicinity, then every 30 cm further from the fans. Each measurement was done on 4 probes. For series III, IV and V, multiple tests were done at each distance in order to cover all the desired points (as shown in Fig. 3).

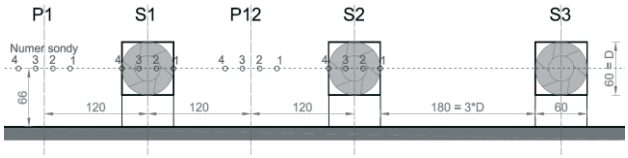

Figure 3. Scheme of fans configuration and measurement points for series IV and V (all dimensions in [mm]).

The airstream continuity was investigated by testing the interference of two subsequent fans (or rows of fans). Between the subsequent fans, there could be no point at which the wind speed dropped to the level of background fluctuations or below.

The velocity of generated air stream was measured using ATU 2001 monofilament hot-wire anemometers. Air stream was generated with CPU fans produced by Xfan, model: RDH6010S1 with nominal voltage of 12 V, 0.22 A. They were supplied by a stabilized power supply of direct current. The level of generated wind speed was controlled by adjusting the voltage provided to the fans.

3. Experiment implementation and model tests results

The air stream velocity and continuity investigations were conducted in six different series, presented in Table 1. Additional two series were conducted to check the influence of terrain roughness categories III and IV.

Table 1. Details of model test series.

Series No.	Description
Series I	Single fan at varying wind speed generated with nominal voltages of 5.6 V, 7.7 V, 9.5 V, 11.4 V, 13.6 V.
Series II	Two fans placed one by one at a distance of 250 cm and 280 cm, nominal voltage of 13.6 V.
Series III	A row of 3 fans spaced by 90 mm, nominal voltage of 13.6 V.
Series IV	A row of 3 fans spaced by 180 mm, nominal voltage of 13.6 V.
Series V	Two rows of 3 fans spaced by 180 mm, distance between rows: 370 cm, nominal voltage of 13.6 V.
Series VI	Single ventilation tower at a scale of 1:100, nominal voltage of 13.6 V.
Series VII	Single fan on category III and IV terrain roughness at varying wind speed generated with nominal voltages of 4.0 V, 5.6 V, 9.5 V, 13.6 V.
Series VIII	Two fans placed one by one at a distance of 250 cm on category III and IV terrain roughness, nominal voltage of 13.6 V.

4. Results analysis and conclusions

By comparing relative velocity of airstream at a distance further than 30 cm from the fan outlet (which is where the influence of turbulence resulting from fan rotation decreases) for different voltage supplied to the fans, it can be observed that there are no significant differences between them. This means that the influence of the Reynolds number on the phenomenon is negligible, thus the model scale tests might be related to natural scale.

The suction of air behind the fan starts only 10-20 cm from it. This means that it is economically reasonable to place another fan in the place where the stream from antecedent fan fades away. This distance was established at 280 cm for the case of one row of fans.

Placing 3 fans in a row increased the distance at which the generated airstream maintained its continuity to 370 cm. Comparing the spacing between fans of 90 mm and 180 mm, the latter produced similar wind speeds, but covered a larger area. Thus the spacing of 180 mm between fans in each row was established as default for further tests.

Adding terrain roughness to the tests only slightly diminished the wind speed of the airstream. It was determined that they kept the same continuity as with the smooth surface, which means they might be used in urban areas in nature, where the generated airstream will be affected by the buildings (Hang et al., 2009).

5. Acknowledgments

This work was founded from internal grant of Faculty of Civil Engineering of Cracow University of Technology.

6. References

Blackman K., Perret L., Savory E., Piquet T. *Field and wind tunnel modelling of an idealized street canyon flow*. Atmospheric Environment 106 (2015) 139-153.

Flaga A. *Wind Engineering. Fundamentals and Applications*. Arkady, Warsaw, 2008 [in Polish].

Hang J., Sandberg M., Li Y. *Effect of urban morphology on wind condition in idealized city models*. Atmospheric Environment 43 (2009) 869-878.

PN-EN 1991-1-4: Eurocode 1: *Actions on structures – Part 1-4: General actions – Wind actions.*

Ramponi R., Blocken B., de Coo L.B., Janssen W.D. *CFD simulation of outdoor ventilation of generic urban configurations with different urban densities and equal and unequal street widths*. Building and Environment 92 (2015) 152-166.

Model tests of dynamic action on the atmospheric boundary layer – vertical ventilation towers of urban areas

Piotr Krajewski[1], Aleksander Pistol[1], Łukasz Flaga[2], Andrzej Flaga[1]

[1]*Institute of Structural Mechanics, Cracow University of Technology, Poland,*
e-mail: piotrekrajewski@gmail.com
e-mail: aleksander.pistol@gmail.com
e-mail: liwpk@windlab.pl
[2]*Wind Engineering Laboratory, Cracow University of Technology, Poland,*
e-mail: lukasz.flaga@interia.pl

Abstract: This paper describes the model tests conducted at the Wind Engineering Laboratory of Cracow University of Technology as the second stage of studies on dynamic action on the atmospheric boundary layer in order to reduce effects of air pollution and smog. It focuses on vertical exhaust (ventilation chimney). The tests were conducted for different shapes and height of the ventilation chimneys and wind speeds provided by the ventilation towers. This led to a comparison of efficiency of different solutions and gave elaborate conclusions on the influence of the Reynolds number on the phenomenon and the possibility of application as the vertical exhaust in the urban area ventilation system.

Keywords: ventilation chimney, smog reduction, wind engineering, environmental engineering, urban ventilation.

1. Introduction

The second stage of studies on dynamic actions on the atmospheric boundary layer focused on vertical exhaust that would be used for elevating the polluted air supplied by the towers above the atmospheric inversion layer. The stage 1 determined the ability to create and maintain an air stream by ventilation towers placed one by one (or in a couple of parallel lines) even with large distances between the towers and with relatively low wind speed produced by each tower. It proved to be effective also on the rough terrain which simulated an urban area.

However, a longitudinal ventilation has its own limits due to deterioration of the air condition as the stream length increases. A vertical ventilation could provide a fresh air from the higher layer of the air and break a smog layer which cover the urban area and blocks natural air circulations. A number of chimney shapes were tested in Wind Engineering Laboratory of Cracow University of Technology with varying lean angles of inlet ventilation towers and permeability of the lower part of the chimney structure.

2. Models, measuring devices and tests method

2.1. Models

The ventilation towers were modelled with CPU fans of 60 x 60 mm in size. This resulted in the model scale of 1:833. Due to different proportions between height and width of fans and ventilation towers (80 x 20 m), only the vertical size was correctly projected in the scale.

Four different shapes of ventilation chimneys were tested, shown in Fig. 1. The base of each chimney has a diameter of 240 mm. There are eight inlet ventilation towers placed under the chimney, with lean angle of 0° and 47°.

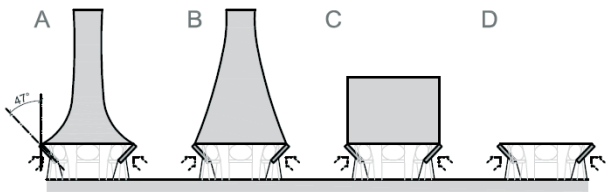

Figure 1. Tested shapes of the chimneys with inlet fans.

The system, consisting of ventilation chimney and ventilation towers, was planned on an octagon with eight ventilation towers located around the central chimney at a distance of 150 cm and 120 cm in different series of tests. Each ventilation tower was placed on different path and directed towards the chimney.

During the subsequent series of the tests, shapes A and B of the chimneys were tested in three different variants, example shown in Fig. 2. Such variants were tested as they may be vastly more economic and technically feasible to create in natural scale.

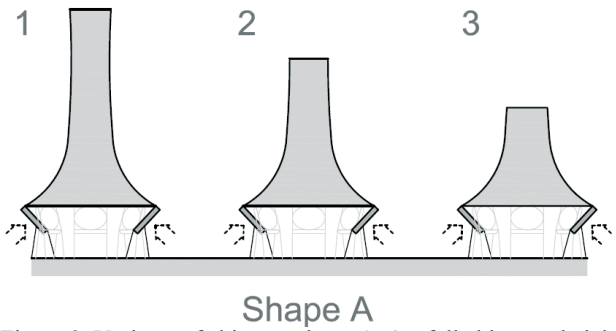

Figure 2. Variants of chimney shape A: 1 – full chimney, height of 360 mm; 2 – chimney trimmed to ¾ height, 240 mm; 3 – half size chimney, height of 180 mm.

2.2. Test method and measuring devices

The main scientific aim of this stage was to evaluate the most efficient, practical and economical solution for the ventilation chimney. This was done by measuring the wind speed at four different points along the path of the stream. The first measuring point of the horizontal wind speed was placed 400 mm from the outer edge of the chimney structure, along the path of one of the ventilation towers. Three other ones were measuring the vertical wind speed at heights of 460 mm above the ground level (right above the chimney outlet), 860 mm above the ground level (start of the temperature inversion layer which has to be penetrated by the generated stream (Spurr, 1959) and 1200 mm (1 km above the ground in natural scale). Also a qualitative research was conducted using heavy smoke generator.

The velocity of generated air stream was measured using ATU 2001 monofilament hot-wire anemometers. Air stream was generated with CPU fans produced by Xfan, model: RDH6010S1 with nominal voltage of 12 V, 0.22 A. They were supplied by a stabilized power supply of direct current. The level of generated wind speed was controlled by adjusting the voltage provided to the fans.

3. Tests and their results

The air stream velocity and continuity investigations were conducted in different series, presented in Table 1.

Table 1. Details of model test series.

Series No.	Shapes of chimney	Variants of shapes
Series I	A, B, C, D	1
Series II	A, B, C, D	1
Series III	A, B	1, 2, 3

Each series was realized for three different wind speeds generated by the fans, resulting from supplied voltages of:

- wind speed 1 – supplied voltage of 4.0 V,
- wind speed 2 – supplied voltage of 9.5 V,
- wind speed 3 – supplied voltage of 13.6 V.

In order to compare the results between different series, the wind speed was shown in dimensionless form Flaga (2008). This was done by dividing the velocity at each measuring point by V^*, where V^* is the reference velocity.

Different types of comparisons have been made in the form of graphs, comparing, respectively, different shapes of chimneys at fixed voltage supplied to the fans, results at different fan speeds for each shape of the chimney (for investigating the influence of the Reynolds number. For series III, also different variants of the same shape of chimney have been compared at fixed voltage supplied to the fans and same variants of shapes A and B. Exemplary graphs showing the results are presented in Figs. 3-5.

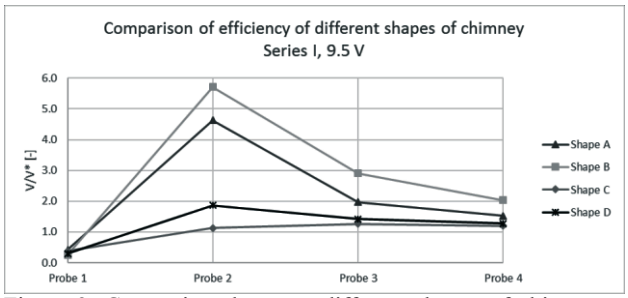

Figure 3. Comparison between different shapes of chimney – series I, supplied voltage 9.5 V.

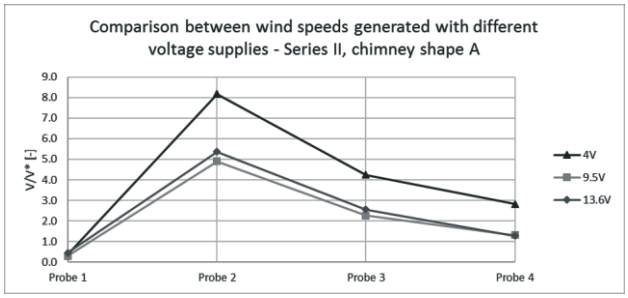

Figure 4. Comparison between different fan speeds – series II, chimney shape A.

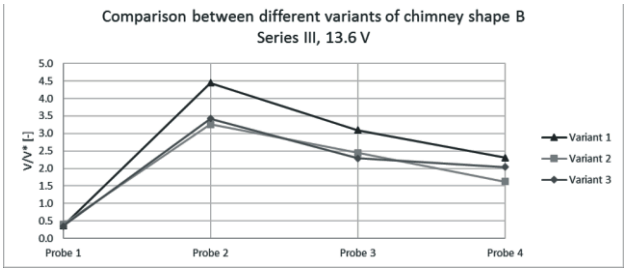

Figure 5. Comparison between different variants of chimney shape B – series III, supplied voltage 13.6 V.

4. Results analysis and conclusions

Probe no. 1 was located at a place where the stream generated by ventilation tower of outer ring weakens, yet there is no remarkable suction from chimney inlet fans. Achieving a noticeable wind speed at this point means that there is interference between outer ring of ventilation towers and the inlet fans of chimney. In practice this would mean the ventilation towers are able to supply the polluted air into the central vertical exhaust.

On probes no. 2 and 3, the highest wind speeds were achieved for chimney shapes A and B, which perhaps results from their forms resembling confusors. However, similar wind speed on probe no. 4 was also achieved for shape D, that is no physical chimney at all. If verified in larger scale, this solution would be the most advantageous for practical implementation. However, it may result in the vertical stream having too much turbulence and no longer being able to penetrate through the inversion layer. Shape C produced the most disappointing results on each measuring point in terms of wind speed, in most cases slightly below the level of shape D.

The influence of the Reynolds number can be observed for the wind speed resulting from the lowest power supplied to the fans. It provides relatively the highest wind speeds above the chimney, however it would not be feasible to accomplish in natural scale as this wind speed level would be too low.

Investigations of different variants of chimney shapes A and B showed that shape A produces lower wind speeds with each modification, while shape B might be trimmed up to half of its size with no significant deterioration of its efficiency.

Generally, chimney shapes B (highest wind speeds) and D (technically feasible, economic and producing relatively satisfying results) were proved to be the most effective. The investigations showed that on the level of temperature inversion (probe no. 3) the vertical stream achieves satisfying values of wind speed that should be able to penetrate through that layer.

5. Acknowledgments

This work was founded from internal grant of Faculty of Civil Engineering of Cracow University of Technology.

6. References

Błażejczyk K. *Air exchange and regeneration system as a factor in the improvement of aerosanitary and bioclimatic conditions*; ed. Degórska B., Baścik M., Środowisko przyrodnicze Krakowa: Zasoby – Ochrona – Kształtowanie, IGiGP UJ, UMK, WGiK PW, Kraków (2013), 187-190 (in Polish).

Buccolieri R., Salim S., Leo L.S., Di Sabatino S., Chan A., Ielpo P., de Gennaro G., Gromke Ch. *Analysis of local scale tree – atmosphere interaction on pollutant concentration in idealized street canyons and application to a real urban junction*; Atmospheric Environment 45 (2011) 1702-1713.

Flaga A. *Wind Engineering. Fundamentals and Applications*. Arkady, Warsaw, 2008 [in Polish].

Spurr G. *The penetration of atmospheric inversions by hot plumes*. Journal of Meteorology 16 (1959) 30-37.

Model tests of dynamic action on the atmospheric boundary layer – concentric configuration of ventilation towers with central ventilation chimney

Aleksander Pistol[1], Piotr Krajewski[1], Łukasz Flaga[2], Andrzej Flaga[1]

[1]*Institute of Structural Mechanics, Cracow University of Technology, Poland,*
e-mail: aleksander.pistol@gmail.com
e-mail: piotrekrajewski@gmail.com
e-mail: liwpk@windlab.pl
[2]*Wind Engineering Laboratory, Cracow University of Technology, Poland,*
e-mail: lukasz.flaga@interia.pl

Abstract: This paper describes the third stage of model tests conducted at the Wind Engineering Laboratory of Cracow University of Technology on dynamic action on atmospheric boundary layer in order to reduce effects of air pollution and smog in urban areas. It focuses on the cooperation between concentric system of ventilation towers and vertical exhaust (ventilation chimney). The tests were conducted for different diameter of the concentric system and wind speeds provided by ventilation towers. A heavy smoke visualisation was carried out to evaluate the efficiency of different solutions and gave elaborate conclusions on the idea. The performed tests confirmed a sufficient efficiency to clean an area where the circular system is placed.

Keywords: wind engineering, smog reduction, environmental engineering, urban chimney ventilation, concentric airstreams.

1. Introduction

Deterioration of air quality is caused by the growth of industry, communication or population, but also by blocking of natural ventilation channels (Buccolieri et al., 2011). To improve the conditions of urban areas an idea of ventilation by forcing dynamically the movement of air mass in urban areas was developed. However, it is crucial to examine the phenomenon of dynamic action on atmospheric boundary layer as well as to determine whether such action is feasible and effective. The most effective and economically reasonable places are natural ventilation ducts and their ends. Giving an example of Cracow city in Poland, possible locations of mentioned systems are show in Fig. 1 (Błażejczyk, 2013).

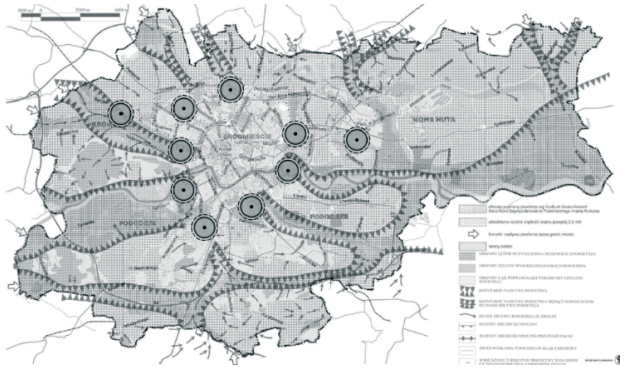

Figure 1 Concept sketch for locating the areas for horizontal radial air streams generation and the central ventilation vertical exhaust systems – on the example of air exchange and regeneration system for Cracow.

The third stage of research on dynamic actions on atmospheric boundary layer was a direct continuation of previous two stages. Stage 1 determined the ability to create and maintain an air stream by ventilation towers placed one by one (or in a couple of parallel lines) even with large distances between the towers and with relatively low wind speed produced by each tower. It proved to be effective also on the rough terrain, which simulated an urban area. The second stage focused on vertical exhaust that would be used for elevating the polluted air supplied by the towers above the atmospheric inversion layer. Hitherto, each tested solution was verified positively on its own, but in order to allow the results to be put into practical use, the efficiency of cooperation between the two parts of the system had to be examined.

2. Models, measuring devices and tests method

2.1. Models

During this stage, the models created for the previous stages were reused. The ventilation towers were modelled with CPU fans of 60 x 60 mm in size. This resulted in the model scale of 1:833. Due to different proportions between height and width of fans and ventilation towers (80 x 20 m), only the vertical size was correctly projected in the scale.

The system, consisting of ventilation chimney and ventilation towers, was planned on an octagon with eight ventilation towers located around the central chimney at a distance of 150 cm and 120 cm in different series of tests. Each ventilation tower was placed on different path and directed towards the chimney (comp. Fig. 2a).

In previous stage of the experiments four different shapes of ventilation chimneys were tested, one of them is shown in Fig. 2b. The base of each chimney has a diameter of 240 mm. There are eight inlet ventilation towers placed under the chimney, with lean angle of 47° an a fan inside.

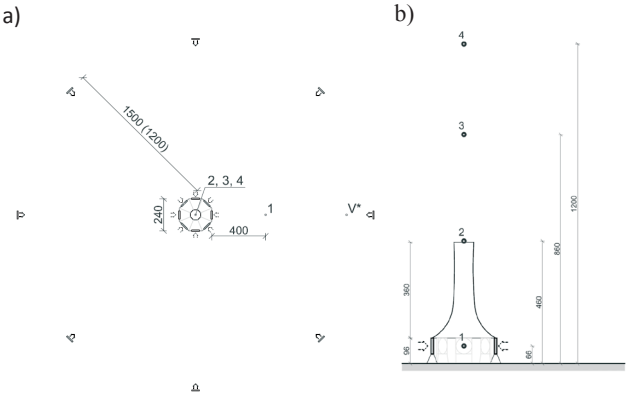

Figure 2.Location of hot-wire probes on the model of concentric system: a) top view, b) side view.

2.2. Tests method and measuring devices

The main scientific aim of this stage was to determine the continuity of air streams generated by ventilation towers and the possible upward exhaust resulting from combining the towers with the chimney. This was done by measuring the wind speed at four different points along the path of the stream. The first measuring point of the horizontal wind speed was placed 400 mm from the outer edge of the chimney structure, along the path of one of the ventilation towers. Three other ones were measuring the vertical wind speed at heights of 460 mm above the ground level (right above the chimney outlet), 860 mm above the ground level (start of the temperature inversion layer which has to be penetrated by the generated stream (Spurr, 1959) and 1200 mm (1 km above the ground in natural scale).

The velocity of generated air stream was measured using ATU 2001 monofilament hot-wire anemometers. Air stream was generated with CPU fans produced by Xfan, model: RDH6010S1 with nominal voltage of 12 V, 0.22 A. They were supplied by a stabilized power supply of direct current. The level of generated wind speed was controlled by adjusting the voltage provided to the fans.

2.3. Smoke visualisation

A qualitative studies were conducted using heavy smoke generator. The ground of workspace was clouded in heavy smoke, mimicking the urban air pollution (Fig. 3). Subsequently, the stream generation system was turned on (Fig. 4.) to observe the efficiency and thoroughness at which the area would be cleared of smoke (Fig. 5).

The smoke was made of vapour and dry ice in order to simulate a dense layer of smog and disperse uniformly in accordance with natural scale urban conditions (Carpentieri and Robins, 2009).

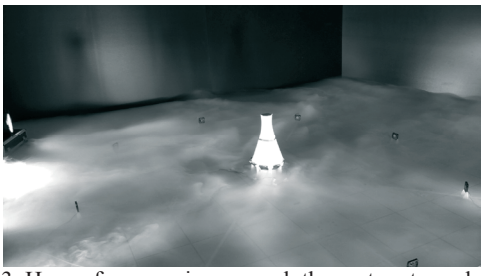

Figure 3. Heavy fog covering ground, the system turned off.

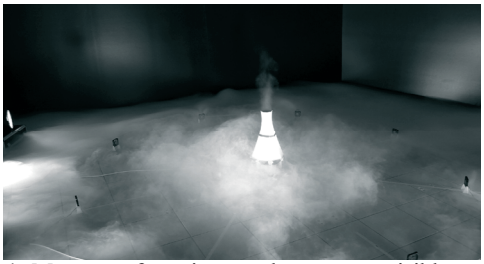

Figure 4. Moment of turning on the system, visible a circular gap in the fog, forming due to the air movement.

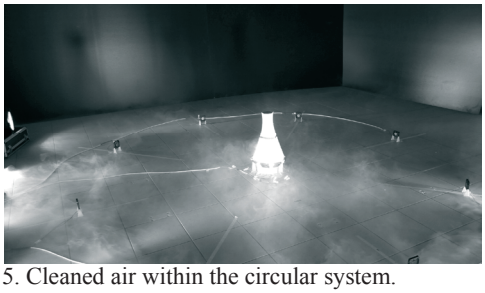

Figure 5. Cleaned air within the circular system.

3. Model tests and their results

The air stream velocity and continuity investigations were conducted in three different series, presented in Table 1.

Table 1. Details of model test series

Series No.	Distance of 1st row towers	Shapes of chimney	Variants of shapes
Series I	1 500 mm	A, B, C, D	1
Series II	1 200 mm	A, B, C, D	1
Series III	1 200 mm	A, B	1, 2, 3

Each series was realized for three different wind speeds generated by the fans, resulting from supplied voltages (comp. Fig. 6.).

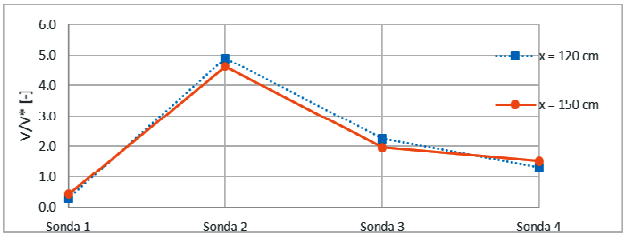

Figure 6. A comparison of efficiency depending on the distance of the outer ring of fans, chimney shape – A, voltage 9.5V.

4. Results analysis and conclusions

The influence of distance between the chimney and first row of outer ventilation towers on maintaining the continuity of generated air stream is negligible. The continuity was achieved with both tested distances.

The investigations showed that on the level of temperature inversion (probe no. 3) the vertical stream achieves satisfying values of wind speed that should be able to penetrate through that layer. In addition, the visualisations provides a quantitative view on a large scale and efficiency of the system. The results prove a compatibility with a theory being developed by A. Flaga in the Wind Engineering Laboratory.

5. Acknowledgments

This work was founded from internal grant of Faculty of Civil Engineering of Cracow University of Technology.

6. References

Błażejczyk K. *Air exchange and regeneration system as a factor in the improvement of aerosanitary and bioclimatic conditions*; ed. Degórska B., Baścik M., Środowisko przyrodnicze Krakowa: Zasoby – Ochrona – Kształtowanie, IGiGP UJ, UMK, WGiK PW, Kraków (2013), 187-190 (in Polish).

Buccolieri R., Salim S.M., Leo L.S., Di Sabatino S., Chan A., Ielpo P., de Gennaro G., Gromke Ch. *Analysis of local scale tree – atmosphere interaction on pollutant concentration in idealized street canyons and application to a real urban junction*. Atmospheric Environment 45 (2011) 1702-1713.

Carpentieri M., Robins A.G. *Wind tunnel experiments of flow and dispersion in a real urban area*. 7th International Conference on Urban Climate, 29 June – 3 July 2009, Yokohama, Japan.

Flaga A. *Wind Engineering. Fundamentals and Applications*. Arkady, Warsaw, 2008 [in Polish].

Spurr G. *The penetration of atmospheric inversions by hot plumes*. Journal of Meteorology 16 (1959) 30-37.

A study on the temperature during the strong wind in Japan

Daisuke Somekawa[1], Satoru Goto[2], Kiyotoshi Otsuka[3]

[1]*Technical Research Institute, Obayashi Corporation, Japan,*
e-mail: somekawa.daisuke@obayashi.co.jp
[2]*Technical Research Institute, Obayashi Corporation, Japan,*
e-mail: goto.satoru@obayashi.co.jp
[3]*Technical Research Institute, Obayashi Corporation, Japan,*
e-mail: otsuka.kiyotoshi@obayashi.co.jp

Abstract: The maximum temperatures during the strong wind are investigated and the design temperature for viscoelastic dampers are proposed. The observed daily maximum wind speeds and temperatures at the Japan Meteorological Agency (JMA) stations are used in the analysis. The differences between the daily maximum temperatures and the temperatures at the time of the occurrences of the daily maximum wind speeds are shown not small. From the results of the analysis, it is found that, in designing a viscoelastic damper applied to wind induced vibration, the annual maximum temperatures will not necessarily be used. The temperature at the time of the occurrence of the half a year recurrence wind speed with the exceedance probability of 10% is proposed to be a candidate of reasonable design temperature for the viscoelastic damper.

Keywords: wind resistance design, temperature, the habitability to building vibration, viscoelastic damper.

1. Introduction

Recent developments of isolation devices and seismic control devices are remarkable in building constructions. As to winds, these devices work to reduce building vibration and, consequently, improve the habitability during strong wind blows. A viscoelastic damper has higher vibration control performances than those of a hysteresis damper. However, performances of a viscoelastic damper are strongly dependent on its temperature. So, the damper is usually designed so that it works well under high ambient temperatures like the yearly maximum atmospheric temperature at the construction site, whereas the above-mentioned temperatures can be of an over specification as will be shown later.

In this paper, the maximum atmospheric temperatures during strong wind are investigated and design temperatures will be proposed based on the investigation. It is noted that the primary concern here is to propose reasonable design temperatures for the viscoelastic damper.

2. Correction of observation data

2.1. Wind speed

The observed daily maximum wind speeds and temperatures for the period from January 1, 2009 to December 31, 2017 are used in this study. Wind speeds are generally rather strongly affected by the anemometer heights and the nearby surface roughness conditions. For the sake of homogeneity of the analysis of wind data, wind speed is converted into the values at the height of 10m above the ground using the vertical profile function written as,

$$V_{10} = V_Z \times \left(\frac{Z_G}{Z}\right)^{\alpha} \times \left(\frac{10}{350}\right)^{0.15} \quad (1)$$

Where V_z is the observed value of wind speed, Z_G is the gradient height (=550m), and α is the exponent (=0.27) of the power law profile function.

In this study, all the observation points (JMA stations) are treated as those for urban areas for simplicity. So that, the wind speeds can be overrated for many of the stations located in the open countries and the suburban areas. This is not a severe problem, however, for the evaluation of the temperatures, because the temperature tends to take lower values as the wind speed increases.

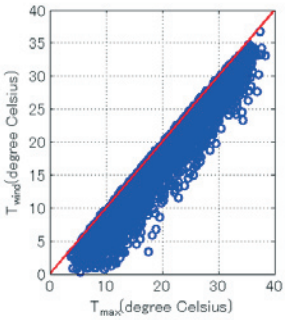

Fig. 1 Comparison between T_{max} and T_{wind} in Tokyo

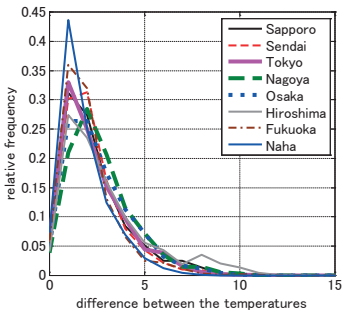

Fig. 2 Histogram of the difference between T_{max} and T_{wind}

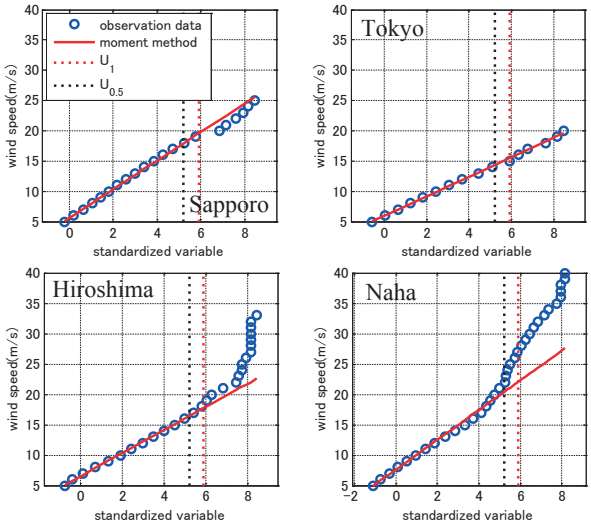

Fig. 3. Standardized variable vs wind speed

2.2. Temperature

The daily maximum temperature T_{max} is not generally the same as the temperature when the daily maximum wind speed occurs (T_{wind}). A comparison of these temperatures is given in Fig. 1. Temperatures are not corrected by observation heights. The difference between these temperatures are not always small, and the magnitudes of the differences of up to larger than 10 degrees Celsius are found for some data.

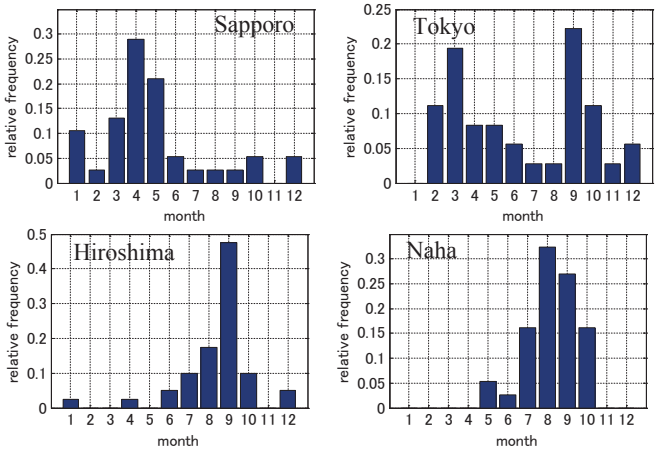

Fig. 4. Frequency of one year recurrence wind speed

Fig. 2 shows the histogram of the T_{max}-T_{wind} calculated for some cities. Slight differences in the frequency distributions among the cities are seen, where the temperature differences of 1-2 degrees Celsius are prevailing. However, there are some data of the differences of 5 degrees Celsius or more. This implies that T_{max} may be too large to be used in designing a damper, and T_{wind} will be concerned hereinafter of this study.

3. Estimation of one year recurrence of 10-min mean wind speed

Fig. 3 shows the one year and the half a year recurrence wind speeds (U_1 and $U_{0.5}$) calculated using observational data. Since Sapporo is located in Hokkaido, the northern of Japan islands, it is rarely affected by typhoons. So, the relationships between the wind speed and the standardized variable is almost linear. On the other hands, Hiroshima and Naha are situated in the locations frequently affected by typhoons, so the relations are not linear for these cities. Tokyo is also occasionally affected by typhoon, but the standardized variable is almost linearly proportional to wind speed.

Seasonal variations of the frequency of one year recurrence wind speed are shown in Fig. 4. In Sapporo, strong wind favours to occur in spring, especially in April. While Hiroshima and Naha suffer from strong wind caused by typhoons in August and September. Tokyo is located on the middle of these cities, where strong wind can blow in both months.

4. Exceedance probability of temperature

Comparison of the daily maximum wind speed and T_{wind} is shown in Fig. 5. It is found that most of T_{wind} are mainly distributed in the range of wind speed below 10 m/s at all cities. Since the surface atmospheric temperatures tend to decrease as the wind speed increase as noted before, in designing a viscoelastic damper for the application to wind induced vibration, the annual maximum temperature is not necessarily to be used.

There are two periods favourable of strong wind occurrence in a year as shown in Fig. 4. So that the temperature at the time of the occurrence of the half a year recurrence wind speed $T_{wind,\,0.5}$ will be discussed. Fig. 6 shows exceedance probability of $T_{wind,\,0.5}$. As the location of the city go to south, the temperature with an exceedance probability of 10% get higher. In the area significantly affected by typhoon, the temperatures are ranging from 25 to 28 degrees Celsius. In Okinawa, $T_{wind,\,0.5}$ with an exceedance probability of 50% is higher than 25 degrees Celsius, but $T_{wind,\,0.5}$ does not change even if the exceedance probability becomes smaller.

A contour map of $T_{wind,\,0.5}$ with an exceedance probability of 10% is shown in Fig. 7. The observation data of the JMA's weather stations and AMeDAS at 859 points are used in making the map. In Hokkaido (Sapporo) and Tohoku (Sendai), strong wind often blows in winter, where $T_{wind,\,0.5}$ is less than 10 degrees Celsius in some points. On the other hand, in the urban areas to the west of Tokyo and in the most areas of Kyushu, $T_{wind,\,0.5}$ is exceed 25 degrees Celsius.

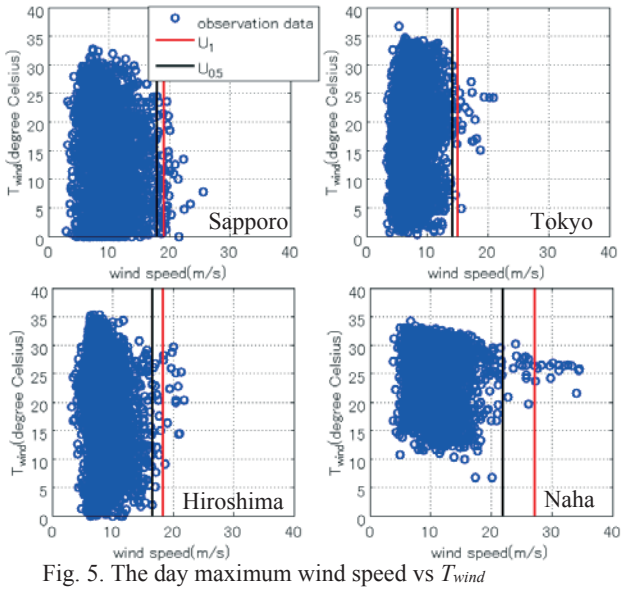

Fig. 5. The day maximum wind speed vs T_{wind}

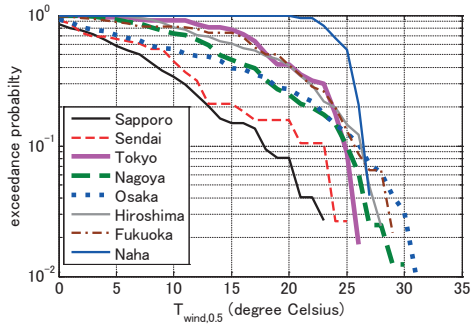

Fig. 6. Exceedance probability of $T_{wind,\,0.5}$

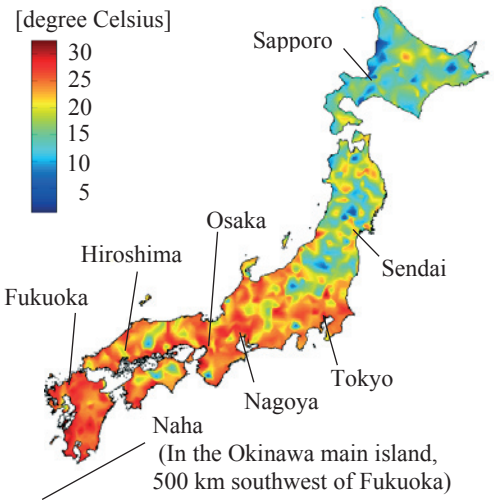

Fig. 7. Contour map of $T_{wind,\,0.5}$ with an exceedance probability of 10%

5. References

Japan Meteorological Agency Home Page, http://www.jma.go.jp/jma/index.html

New Polish Guidelines of human exposure to vibrations in buildings

Alicja Kowalska-Koczwara[1], Krzysztof Stypuła[2]

[1]*Institute of Structural Mechanics, Cracow University of Technology, Poland,*
e-mail: akowalska@pk.edu.pl
[2]*Institute of Structural Mechanics, Cracow University of Technology, Poland,*
e-mail: kstypula@pk.edu.pl

Abstract: Humans in buildings located in the city centres are exposed to vibrations coming from different types of sources. There are internal sources of vibrations like working machines, ventilation and human induced vibrations and external sources of vibrations like tramways, railways, roads etc. Analysing standards of different countries on the subject of human exposure to vibrations in buildings similar trends are noticeable. After 2003 there have been changes in standards in this area in many countries. There are some trends to connect the regulations for passive and active perception of vibration in standards approach. Seemingly similar regulations specified in standards can be interpreted differently in various countries. Following world trends Polish regulations on that subject have been changed last year, new Polish guidelines appeared in June 2017 year. According to international trends two methods of assessment have been introduced to the regulations: basic RMS method and additional VDV method. Basic RMS method concerning not only whether or not the comfort level is exceeded, but also within which frequency band any exceedance has occurred. This information can be obtained by comparing the frequency structure of the measured frequency curve with the corresponding frequency providing the necessary comfort of vibration to people in the building. Comfort level should not be exceeded. Sometimes, in the experts opinion, it tends to not exceed the so called perception threshold of vibration. The perception threshold of vibration in both horizontal and vertical directions is shown in Fig. 1.

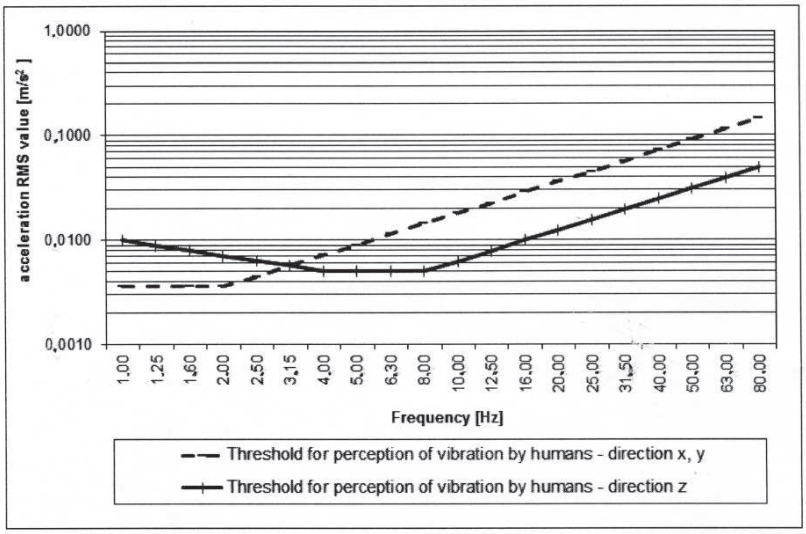

Figure 1. Basic lines corresponding to the perception threshold of vibration (according to ISO 2631-2 or Polish standard PN-B-02171:2017-06).

For comfort level threshold lines shown in Fig. 1 should be multiplying by factor "n" which depends on the purpose of the room in the building (*e.g.* operating theatres, precision laboratories, hospitals, apartments, residential rooms, offices, classrooms, workshops, factories etc.); the time of the occurrence of the vibration (daytime or night-time); the nature of vibrations and the frequency of their occurrence (continues or sporadic vibrations). For more visibility of this method the human vibration perceptivity ratio – HVPR was introduced to new Polish regulations. This ratio was proposed by K. Stypula and it is the measure of vibration perception by people. It is the maximum ratio of the acceleration RMS value obtained from the analysis to the acceleration RMS value equivalent to the threshold for the perception of vibration by humans (in the same 1/3 octave band) chosen from each 1/3 octave band. In the article some examples of usage of that ratio have been shown.

In appendix to the Polish standard vibration dose value (VDV) method occurred. Vibrations in this method of evaluation are considered during the entire period of human exposure. The fourth power vibration dose method is more sensitive to peaks than the RMS method and this is why VDV is mostly used in shock analysis. The VDV method is defined as an additional method in cases when the crest factor is higher than 9 and it is focused on probability of adverse comments. In the article criteria for assessing human exposure to vibrations according to VDV method are proposed and compared with those available in selected national standards.

The third important change in new version of Polish standard is measurement equipment that should be used for human perception evaluation. New regulation strictly described what kind of equipment should be used for low-frequency recording and new measurement disc for human perception of vibration on the floor was introduced to the Polish standard.

All changes in the Polish regulations has been compared with selected international standard like ISO 2631-2, British BS 6472, Australian AS 2670, Japanese AIJ-GEH-2004

Keywords: human exposure to vibration, standard regulations, RMS method, VDV, measurement equipment.

Vibrational environment at scaffoldings

Jarosław Bęc[1], Ewa Błazik-Borowa[2], Paulina Jamińska-Gadomska[3], Tomasz Lipecki[4]

Department of Structural Mechanics, Lublin University of Technology, Poland,
[1]*e-mail: j.bec@pollub.pl*
[2]*e-mail: e.blazik@pollub.pl*
[3]*e-mail: p.jaminska@pollub.pl*
[4]*e-mail: t.lipecki@pollub.pl*

Abstract: The paper presents analysis of the vibrational environment at scaffoldings. It is based on the results of project considering safety on façade scaffoldings. The total number of 120 scaffoldings of this type were analyzed during last two years. One of the issues analyzed in this project was the vibrations influence on the scaffolding and workers safety. Measurements of free vibrations in-situ allowed obtaining the values of natural frequencies of structures. The results of these tests made possible verification of the built numerical models. Measurements of forced vibrations were also made with various sources of vibrations active at scaffoldings. The detailed numerical dynamic analysis followed. The obtained results were compared with allowable values according to the appropriate Polish standards. In the conclusions, most influential sources of vibrations were indicated.

Keywords: scaffoldings, vibrations, comfort, in-situ measurements, numerical analysis.

1. Introduction

Scaffoldings are temporary structures built-up near main buildings during the erection stage and for the finishing works. They are subjected to various kinds of dynamic loads generated by:

- Nearby traffic;
- Human motion;
- Machinery and equipment;
- Wind action.

The effects of dynamic actions on scaffolding were measured during the project lasting for two years. The total number of 120 façade scaffoldings all around Poland were considered. Free vibrations of the structures were measured. In case of the existing excitement of the selected type at the scaffolding, the vibrations of the structure subjected to the dynamic loading were also measured. The tests were followed by the detailed numerical analysis.

2. Measurements in-situ

Two kinds of scaffolding vibrations were measured. First, free vibrations were induced and saved. Each of scaffoldings was excited with human induced oscillations. The structure vibration accelerations were measured at minimum three points located beneath the last level of decks. Three points of vibrations excitation were also introduced. The frequency analysis of the obtained time series allowed identification of natural frequencies and verification of the numerical model.

Figure 1. Free vibrations excitation.

The measured values of the first natural frequencies ranged from 2 Hz to 4 Hz. These values depended highly on the size of the scaffolding but most of all on the solidity of the anchorage. It has been found, that during the scaffolding operation these values may be lowered even of 0.5 Hz as the result of ease in anchorage.

The next phase of in-situ research was focused on forced vibrations of the scaffolding structure. Depending on the situation observed at the building site, the time series of accelerations were measured during the active nearby road traffic, workers in motion, machinery working near the scaffolding or at the scaffolding.

The effect of nearby traffic was usually small, and no large scaffoldings vibrations produced by cars, and even trams or trains passing by, were observed. The reason of such an effect was probably due to the location of the scaffolding usually in some distance from the road edge. The vibrations were damped in the surrounding ground, but even more by the foundation of the scaffolding at the ground. The levels of accelerations observed at the scaffoldings never reached the values allowable for the workplaces.

Figure 2. Traffic induced vibrations measurements.

Workers motion, horizontal (walking along the deck) or vertical (climbing the ladders) was observed to be very influential to the scaffolding. Especially the vibrations generated by workers walking along the scaffolding decks gave disturbances in the horizontal direction in the plane of the scaffolding with low frequencies strongly transmitted to the whole structure.

The workers active at the scaffolding were usually equipped with heavy drillers or hammers. These accessories in hands of workers produced usually temporary disturbances at scaffoldings. The frequencies of the drillers are in the range of 7 to 8 Hz and the vibrations produced by them are highly filtered and damped by human bodies.

The next group of machines often present at the scaffolding are rope cranes, lifts and chutes. The cranes may be man-powered or with an engine, which in both cases are usually attached to the scaffolding structure. This fact makes them highly affecting the vibrational environment at scaffoldings. They produce vibrations that can be felt at large parts of the structure, but since they are used for transportation of the grout in buckets or other building materials, they are in use only for several seconds. Though producing some discomfort for workers at scaffolding, they do not affect the whole work day strongly. The machine lifts used at high buildings to transport workers and materials are usually separated from the scaffolding and attached to the building structure, and therefore do not affect the vibrations of scaffoldings. The chutes are used to transport debris in vertical direction (downwards). They give large amount of temporary vibrations which can be a strong disturbance for workers comfort at the scaffolding, especially when the debris transportation is repeated frequently.

Figure 3. Lifts and chutes.

The last group of machines often presents at and building sites and affecting scaffoldings are shotcrete machines used for pumping grout. They generate low frequency vibrations around 1-2 Hz, the pipes transporting the grout are usually attached to the scaffolding elements and they are active for the prolonged time. This makes them the most dangerous equipment for the scaffolding vibrational environment.

Figure 4. Shotcrete machines.

Wind action does not significantly affect the scaffoldings. The forces generated by wind are usually small, unless the cladding of the structure is applied. When the scaffolding is cladded, the forces can increase significantly and if there are errors in anchorage then wind action can even lead to the structure collapse. This is not directly affecting the vibrational environment at scaffoldings since in case of strong winds all works at scaffoldings are usually suspended. Detailed analysis of the wind action on scaffolding and on building-scaffolding system was presented in previous papers (Jamińska-Gadomska 2013, Lipecki et al., 2018).

3. Numerical analysis

The numerical model was built for each of scaffoldings. Modal analysis allowed calculation of natural frequencies and mode shapes. These results served in verification of the numerical model accuracy and consistency with the measurements. The process of the numerical model creation and verification of the model based on free vibrations measurements was presented in detail in the paper (Jamińska-Gadomska et al., 2018).

In the second part of the numerical analysis, forced vibrations of the structures were calculated. The obtained results were compared with the ones coming from in-situ measurements. In case of the lack of the information on the source of measurements, the excitation values were adjusted according to the data obtained from measurements.

The results from numerical analysis not only confirmed the results obtained from measurements but gave a wider image of scaffolding vibrations generated by different sources of excitement. Readout of the accelerations in many points of scaffolding was made possible. The obtained results were compared with appropriate Polish standards for estimation of the vibrations effect on buildings structures (PN-B-02170:2016–12) and people inside the buildings (PN-B-02171:2017-06). The analyzed maximum values in most cases were not exceeding the allowable limits for heavy industry workshops (highest of the limits).

4. Conclusions

The nearby traffic, machines working near scaffolding or workers using drillers at scaffoldings are not affecting strongly the scaffoldings vibrations. Wind action is not producing strong vibrations, however can be potentially a source of structural disaster.

Most significant vibrations of scaffoldings are produced by horizontal motion of workers, rope cranes and chutes operation, and most of all by shotcretes pumping the grout. These vibrations can strongly affect the vibrational environment at scaffoldings, make working at scaffolding difficult and they are usually lasting for a long time. Even more these significant actions are affecting large parts of scaffolding structures. However, these actions are in almost all cases harmless to the structure of the scaffolding. If any failures occur, they are always associated with errors in the design or in anchorage.

5. Acknowledgments

This paper has been prepared as a part of the project supported by the National Centre for Research and Development within the Applied Research Programme (agreement No. PBS3/A2/19/2015 “Modelling of Risk Assessment of Construction Disasters, Accidents, and Dangerous Incidents at Workplaces Using Scaffoldings”).

6. References

Jamińska-Gadomska P. *Analiza działania wiatru na układ budynek z rusztowaniem*. Budownictwo i Architektura 2 (12) (2013) 111-118.

Lipecki T., Jamińska-Gadomska P., Błazik-Borowa E. *Dynamic wind action on façade scaffoldings.* AIP Conference Proceedings 1922 (2018) 110001-1-110001-8.

Jamińska-Gadomska P., Bęc J., Lipecki T., Robak A. *Verification of the façade scaffolding computer model*. Archives of Civil Engineering 64(1) (2018) 41-53.

PN-B-02170:2016–12. *Ocena szkodliwości drgań przekazywanych przez podłoże na budynki.*

PN-B-02171:2017-06. *Ocena wpływu drgań na ludzi w budynkach.*

Determination of the probability density function for static service loads of scaffoldings

Ewa Błazik-Borowa[1]

[1]*Department of Structural Mechanics, Lublin University of Technology, Poland,*
e-mail: e.blazik@pollub.pl

Abstract: The paper deals with the selection of probability density functions for description of the maximum service load of a platform and the sum of maximum service loads in a vertical module of scaffolding between adjacent frames. The analysis is performed on the basis of the inventory of the service loads obtained for 110 scaffoldings in Poland in 2016 and 2017. The results are parameters of two functions: Gumbel's and Weibull's distributions which can be used in analysis of structures reliability and for calibration of partial safety coefficients.

Keywords: scaffolding, service loads, histograms, probability density functions.

1. Introduction

The main loads of scaffoldings are dead weight, wind action and service loads. The rules for determination of the above mentioned loads are described in the standards EN 12810-1, EN 12811-1 and EN 1991-1-4. However, both wind and service loads still require more research. The study of the wind action on scaffoldings can be found in such papers as Jamińska-Gadomska (2013), Lipecki et al. (2018), whereas there are no studies concerning scaffolding service loads available in the literature. The description of this type of load is necessary in analysis of reliability of structures, and particularly for calibration of partial safety coefficients. Therefore this paper deals with the selection of probability density functions for the maximum service loads of platforms and the sum of maximum service loads in a vertical module of scaffolding between adjacent frames. The analysis is performed on the basis of the inventory of the service load for 110 scaffoldings in Poland made in 2016 and 2017.

2. Research description

The inventory of the static service load was made in order to evaluate the real service loads of scaffoldings at the construction site. The weight of workers, equipment and building materials is considered to generate the service loads.

Inventory of these loads consisted in location of the maximum load values on the scaffolding scheme for the following periods of the working day: the first round of the research from 8am till 10am, the second round of the research from 11am till 1pm and the third round of the research from 2pm till 4pm. Each scaffolding was observed for five consecutive working days. Next, on the basis of the obtained data, for the *i*-th day the following values were determined:

- maximum uniformly distributed load of the platform in the *j*-th module, calculated from the formula:

$$q_{e,ij} = \frac{Q_{e,ij}}{l_j}, \tag{1}$$

- the sum of maximum uniformly distributed loads of platforms in the *j*-th vertical module of scaffolding between adjacent frames, calculated from the formula:

$$p_{e,ij} = \frac{P_{e,ij}}{l_j}, \tag{2}$$

where: $Q_{e,ij}$ – the highest value of the load which acts on platforms in the *j*-th vertical module of scaffolding between adjacent frames on *i*-th day, $P_{e,ij}$ – the highest sum of loads which act on platforms of the *j*-th vertical module of scaffolding between adjacent frames on *i*-th day, l_j – the length of *j*-th platform.

The tests are biased because scaffolding was often made available for measurements only when the contractor of the construction works decided that the scaffolding would not be fully used. In order to eliminate this error, the days of measurements in which there were no workers on scaffolding had been omitted. On the other hand, if the employee was present at the workplace, then he had to move from the communication section to the place where he worked. Therefore for platforms ranging from the communication section to the workplace the load equals 1.0 kN and it is calculated as the sum of the weight of employee, his tools and materials which can be carried by him. Finally 3350 maximum values of the loads of the platforms and of the vertical modules of scaffolding between frames were obtained. The histograms of these values are shown in Fig. 1. Average values of loads are equal to $\overline{q}_e = 0.31$ kN/m and $\overline{p}_e = 0.35$ kN/m. Their standard deviations are equal to $s_q = 0.32$ kN/m and $s_p = 0.37$ kN/m.

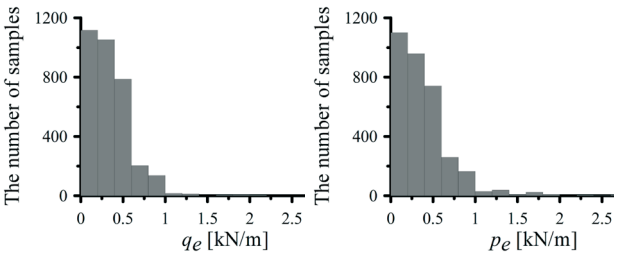

Figure 1. The histograms for the service loads of platforms q_e and vertical modules of scaffolding p_e.

3. The selection of the probability density function

The next stage of the analysis is selection of the probability density function of the service load. The analysis is performed for distribution functions which are applied for maximum values of random variables (comp. Kończak, 2013, Kotowski et al., 2010), it is:

- Gumbel's distribution (Fisher-Tippett's type I) for maximum of random variables which is described by the formula:

$$f(x) = \frac{1}{\hat{\delta}} e^{\frac{x-\hat{\lambda}}{\hat{\delta}} - e^{\frac{x-\hat{\lambda}}{\hat{\delta}}}}, \tag{3}$$

and the cumulative distribution which is described by the formula:

$$F_G(x) = e^{-e^{-\frac{x-\hat{\lambda}}{\hat{\delta}}}}, \tag{4}$$

where: $\hat{\delta}^2 = \frac{6s_x^2}{\pi^2}$ and $\hat{\lambda} = \bar{x} - 0.5772156649\hat{\delta}$.

- Weibull's distribution (Fisher-Tippett' type III)) for maximum of random variables which is described by the formula:

$$f(x) = \frac{\beta}{\tilde{\delta}}\left(\frac{x-\tilde{\lambda}}{\tilde{\delta}}\right)^{\beta-1} e^{-\left(\frac{x-\tilde{\lambda}}{\tilde{\delta}}\right)^{\beta}}, \quad (6)$$

and the cumulative distribution which is described by the formula:

$$F_W(x) = 1 - e^{-\left(\frac{x-\tilde{\lambda}}{\tilde{\delta}}\right)^{\beta}}, \quad (7)$$

where: $\tilde{\delta}^2 = \frac{s_x^2}{\Gamma\left(1+\frac{2}{\beta}\right) - \left[\Gamma\left(1+\frac{1}{\beta}\right)\right]^2}$, $\tilde{\lambda} = \bar{x} - \tilde{\delta}\Gamma\left(1+\frac{2}{\beta}\right)$,

$\Gamma(y) = \int_0^{\infty} t^{y-1}e^{-t}dt$, s_x – standard deviation of the random variable x, $\bar{x}$ – average value of the random variable x.

The distribution functions are adjusted to the test results with use of the least-squares method as it is shown in Fig. 2.

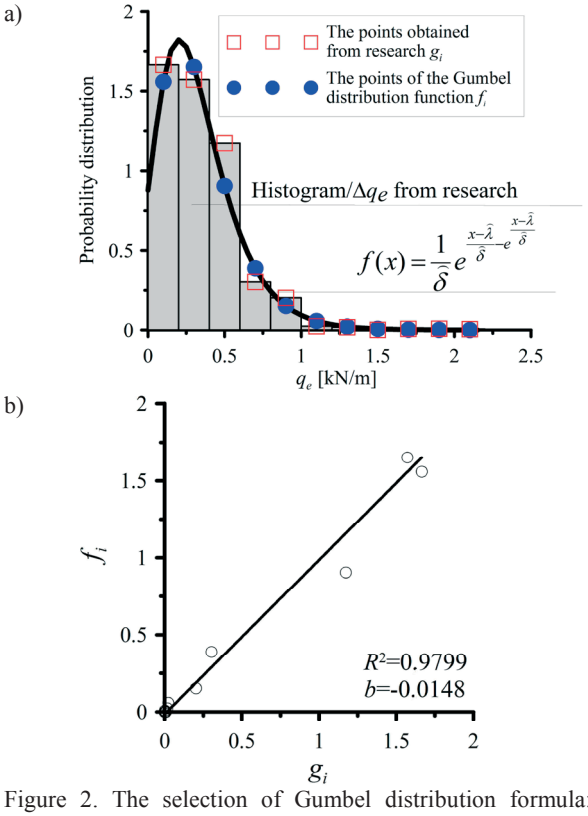

Figure 2. The selection of Gumbel distribution formula: a) probability density function, b) the location of points with coordinates (g_i,f_i) with relation to straight-line formula y=x+b.

It comes from Table 1 that both functions can be used in statistical description of service loads of scaffolding. For both distribution functions the coefficients R^2 reach the values close to 1.0. The average value obtained on the basis of the Weibull distribution is closer to the value from the tests than the average value obtained on the basis of Gumbel distribution.

Table 1. The parameters of probability density functions.

Gumbel's distribution			Weibull's distribution		
	q_e	p_e		q_e	p_e
$\hat{\lambda}$ [kN/m]	0.2033	0.1929	$\tilde{\lambda}$ [kN/m]	-0.0844	-0.0875
$\hat{\delta}$ [kN/m]	0.2019	0.2178	$\tilde{\delta}$ [kN/m]	0.4472	0.4974
			β	1.8780	2.0150
$\bar{x}_d$ [kN/m]	0.3198	0.3187	$\bar{x}_d$ [kN/m]	0.3130	0.3536
R^2	0.9799	0.9829	R^2	0.9866	0.9533

4. Conclusion

On the basis of the adjustment of the distribution functions to the histograms of the maximum service loads of scaffoldings, it is found that both functions describe the probability distribution of the service load with high accuracy. Additional analyses should be performed to determine which probability density distributions are more reliable. For the selected distribution functions, the probability of not exceeding the standard class 3 load in accordance with EN 12811-1 was determined:

- for one platform:

F_G(1.4 kN/m)=0.99734; F_W(1.4 kN/m)=0.99993,

- for all platforms in one vertical module of scaffolding between adjacent frames:

F_G(1,4 kN/m)=0.99609; F_W(1,4 kN/m)=0.99989.

The determined probability density functions can be used to calibrate partial safety factors in ultimate limiting states.

5. Acknowledgments

This paper has been prepared as a part of the project supported by the National Centre for Research and Development within the Applied Research Programme (agreement No. PBS3/A2/19/2015 "Modelling of Risk Assessment of Construction Disasters, Accidents, and Dangerous Incidents at Workplaces Using Scaffoldings").

6. References

EN 12810-1:2010. *Façade scaffolds made of prefabricated components. Part 1: Product specifications.*

EN 12811-1:2007: *Temporary works equipment – Part 1: Scaffolds – Performance requirements and general design.*

EN 1991-1-4:2008: *Eurocode 1: Actions on structures – General actions – Part 1-4: Wind actions.*

Jamińska-Gadomska P. *Analiza działania wiatru na układ budynek z rusztowaniem.* Budownictwo i Architektura 2(12) (2013) 111-118.

Kończak, G. *The use of extreme value distributions in checking the quality shapeless materials homogeneity*. Studia Ekonomiczne, Zeszyty Naukowe Uniwersytetu Ekonomicznego w Katowicach 152 (2013) 82-94.

Kotowski A., Kaźmierczak B., Dancewicz A. *Precipitation modeling for sewerage measuring*, Studies in Engineering, Committee for Civil Engineering Polish Academy Of Sciences, Warsaw, 2010.

Lipecki T., Jamińska-Gadomska P., Błazik-Borowa E. *Dynamic wind action on façade scaffoldings.* AIP Conference Proceedings 1922 (2018) 110001-1-110001-8.

Model investigations of aerodynamic coefficients of iced cable of cable-stayed bridges

Piotr Górski[1], Marcin Tatara[2], Stanislav Pospíšil[3], Sergej Kuznetsov[4]

[1]*Department of Roads and Bridges, Opole University of Technology, Poland,*
e–mail: p.gorski@po.opole.pl
[2]*Department of Roads and Bridges, Opole University of Technology, Poland,*
e–mail: m.tatara@po.opole.pl
[3]*Institute of Theoretical and Applied Mechanics, Academy of Sciences of the Czech Republic, Czech Republic,*
e–mail: pospisil@itam.cas.cz
[4]*Institute of Theoretical and Applied Mechanics, Academy of Sciences of the Czech Republic, Czech Republic,*
e–mail: kuznetsov@itam.cas.cz

Abstract: This paper is concerned with the wind tunnel investigations of static aerodynamic coefficients of stationary iced cable model of cable-stayed bridges. The investigations were performed in a Climatic Wind Tunnel Laboratory of the Czech Academy of Sciences in Telč. The experimental icing of the inclined cable model in the climatic chamber of the laboratory was made. The shape of the iced model was registered by a numerical photogrammetry method. For the aerodynamic investigations the new iced cable model was made by 3D printing method. The drag, lift and moment aerodynamic coefficients were determined using aerodynamic balance with respect to three principal angles of wind attack within the range of the *Reynolds* number (*Re*) between $2.5 \cdot 10^4$ and $13.6 \cdot 10^4$ at the mean turbulence intensity of about 5 %. It was found that the drag coefficient values of the iced cable model are higher than for a circular smooth cylinder in the *Re* range that was studied. The obtained results could constitute the basis to formulate the mathematical description of the wind load acting on the iced cables of cable-supported bridges.

Keywords: bridge cable, ice accretion, angle of wind attack, aerodynamic coefficient.

1. Introduction

The change of the cross-section of bridge cable due to the ice accretion has a significant influence on the flow field around the cable as well as its aerodynamics, and can cause a greater wind load acting on the cable. In the case of an asymmetric airflow around the iced cable an asymmetric distribution of the wind pressure on its surface may exist. For this reason, three aerodynamic coefficients, i.e. drag, lift and moment coefficients should be considered under icing conditions. The values of these coefficients depend on the icing shape, wind velocity, turbulence intensity of the airflow, angle of the wind attack, and character of the flow field in the wake behind the cable. The knowledge of the aerodynamic coefficients could be the basis to formulate the mathematical description of the wind load acting on the iced cables of cable-supported bridges in order to predict the cable response due to the wind.

The literature concerning the icing influence on aerodynamics of cables of cable-stayed bridges is relatively poor and, currently, it is very advisable and valuable to conduct further studies in this field. Some contemporary achievements are presented by Demartino et al. (2015), Trush et al. (2017), and Górski et al. (2016).

The paper presents the method and results of wind tunnel investigations of static aerodynamic coefficients, i.e. drag, lift and moment coefficients of iced cable model of cable-stayed bridges with respect to the angle of wind attack. The tests were performed within the range of the *Reynolds* number (*Re*) between $2.5 \cdot 10^4$ and $13.6 \cdot 10^4$ at the mean turbulence intensity of 5 %. The experiments were carried out in the Climatic Wind Tunnel Laboratory of the Czech Academy of Sciences in Telč.

2. The icing process and preparation of iced cable model for aerodynamic investigations

The experimental icing process of a cable section model was conducted in the climatic chamber of the closed-return wind tunnel of CET ITAM (Kuznetsov et al., 2015). The cable model was made of polyvinylchloride (PVC), which surface is similar to the surface of a cable cover made of high-density polyethylene (HDPE). The 2.5 m long model as a pipe with a circular cross-section and 0.160 m diameter was inclined at an angle of 30° in the vertical plane, and at an angle of 60° in the horizontal plane with respect to the wind direction. The fixation way of the cable model in the climatic section is shown in Fig. 1a. The icing process was performed at the average temperature slightly below 0°C, the mean free stream velocity 2.8 m/s, the rainy conditions using rain sprinklers with the diameter heads 2.8 mm, and during a 40 min time period.

The final ice shape on the bottom side of the cable model was obtained as the characteristic irregularly ice ribs with rounded edges and a relative surface roughness of 18% (see Fig. 1b). On the upper part of the model the ice shape was similar to the circular shape with a surface roughness of 0.73%. The cross-section of the cable with ice became strongly nonsymmetrical with the dimensions of 0.192 m height and 0.181 m width.

Immediately after the icing process the shape of the iced cable model was registered by a photogrammetry method. Using a numerical image analysis a three-dimensional (3D) numerical model of the iced cable was obtained (see Fig. 1c). For aerodynamic investigations the new iced cable model, shown in Fig. 1d, was made of polylactide plastic at a scale of 1:1.6 using a 3D printing procedure. The outer dimensions of the model cross-section were 0.120 m in height and 0.113 m in width while the model length was 0.43 m. The detailed descriptions of the icing process, the final icing effect and preparation of the new iced cable model for the wind tunnel investigations are presented by Górski et al. (2016).

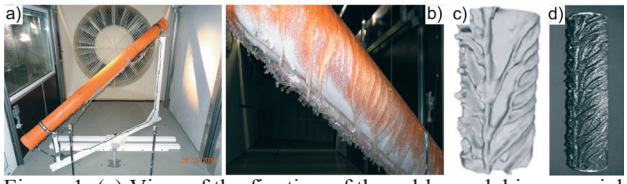

Figure 1. (a) View of the fixation of the cable model in a special frame in the climatic section, (b) final icing effect of the cable model, (c) 3D numerical model in a scale 1:1, and (d) iced cable model for the aerodynamic investigations.

3. Experimental set-up of aerodynamic investigations

The tests were conducted in the aerodynamic section of the wind tunnel. The section has a rectangular cross-section with

the height of 1.8 m, width of 1.9 m, and 11.0 m long. The aerodynamic investigations of the iced cable model were performed with respect to determination of three static aerodynamic coefficients, i.e. drag, lift and moment coefficients as functions of *Re*. The tests were conducted for three principal configurations of the ice cable model in relation to the flow direction which are presented in Fig. 2. In this figure the reference dimension *d* of each model configuration perpendicular to the airflow direction is shown.

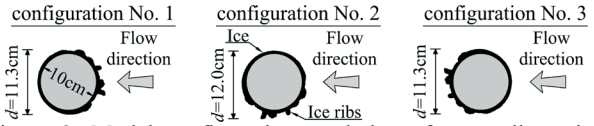

Figure 2. Model configurations and the reference dimension perpendicular to the airflow direction considered for the aerodynamic investigations.

Measurements of aerodynamic forces were made using three-component aerodynamic balance based on the electric resistance wire strain gauges which are able to measure drag, lift and moment forces, simultaneously. Six strain gauges type Megatron KM102 were used with operative range from 0 to 100 N at the temperature range from -10°C to 40°C, and with declared nonlinearity of the sensors of 0.04%. Strain gauges were connected to the Dewetron acquisition system type DEWE-801-TR.

The sectional model was fastened motionlessly in the aerodynamic balance in a horizontal position at a level 69.3 cm above the floor of the aerodynamic section, crosswise to the airflow. Two sides of the balance frame were equipped with the plexi-glass end-plates to ensure two-dimensional flow around the model. The sketch of the experimental set-up in the aerodynamic chamber is shown in Fig. 3.

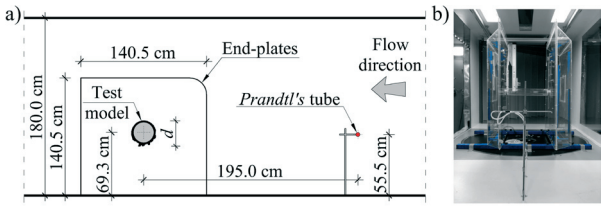

Figure 3. (a) Sketch of the experimental set-up in the aerodynamic section (view along the section), (b) view of the aerodynamic balance with the test model.

During the tests, the airflow was modelled as laminar with a turbulence intensity of the order of 5 %. The mean air temperature was about 27°C. The tests were carried out at twelve sequential free stream velocities in the range between 3.6 m/s and 18.9 m/s. This corresponded to the twelve *Re* regimes in the interval $Re=2.5\cdot10^4$ to $13.6\cdot10^4$.

The aerodynamic coefficients were investigated according to the following methodology. During the tests the free stream velocity was measured by the *Prandtl's* tube placed upstream of the model centreline at a distance of 195 cm. Simultaneously, three radial forces acting on the iced model, i.e. drag, lift and moment forces were measured on both ends of the model by the three-component aerodynamic balance. For each model configurations, three time series of measurements at each mean free stream velocity $\bar{u}$ were made during the 60 s interval with the sampling rate of 100 Hz.

Due to the reduction of the flow area in the aerodynamic chamber by the presence of the force balance the increase of the air flow velocity acting on the model was recognized as the blockage effect. Correction between the *Prandtl's* tube and mean flow velocities averaged along the longitudinal axis of the model was ascertained experimentally. It was found that within the entire $\bar{u}$ range that was studied the increase of the span-averaged flow velocity acting on the model was 6%. The effect of this phenomenon was taken into account for the estimation of the reference wind velocity $\bar{u}_{ref}$, which was used for the calculation of the mean values of aerodynamic coefficients.

4. Experimental results

In order to validate a performance of the aerodynamic investigations, experiment on the smooth cylinder were conducted and compared with the results available in the literature. The drag coefficient was measured around 1.2, which is in good agreement with the value reported by Schewe (1983).

Fig. 4 depicts the variation of the mean aerodynamic forces, i.e. drag $\bar{F}_D$, lift $\bar{F}_L$, and moment $\bar{F}_M$ forces with $\bar{u}_{ref}$ and the variation of the static aerodynamic coefficients, i.e. drag C_D, lift C_L and moment C_M coefficients with *Re* for configuration No. 2. The results for configurations No. 1 and 3 are presented in the full paper.

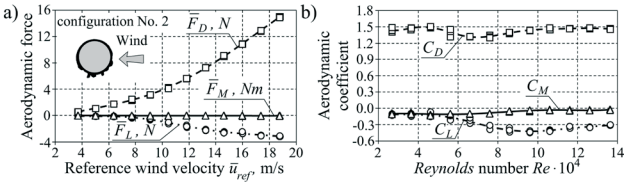

Figure 4. (a) Variation of the mean aerodynamic forces with the reference wind velocity, and (b) variation of the static aerodynamic coefficients with *Re* for configuration No. 2.

5. Conclusions

It was clearly proved that ice accretion on the cable model has a significant influence of the aerodynamic forces acting on the model. The C_D values determined for configuration No. 2 of the iced cable model varies in the range from 1.3 to 1.5 and seems to be slightly depends on *Re*. All obtained the C_D values are 8% to 25% higher than C_D=1.2 obtained for the smooth circular cylinder, and used as a reference. The C_L values were changing in the range of 0.1 to 0.5, while the C_M values were changing from 0.02 to 0.14 for the entire range of *Re* that was studied.

6. Acknowledgments

This research was financially supported by the CET sustainability project LO1219 (SaDeCET) of the Ministry of Education Youth and Sport of the Czech Republic.

7. References

Demartino C., Koss H.H., Georgakis C.T., Ricciardelli F. *Effects of ice accretion on the aerodynamics of bridge cables*. Journal of Wind Engineering and Industrial Aerodynamics 138 (2015) 98-119.

Górski P., Pospíšil S., Kuznetsov S., Tatara M., Marušić A. *Strouhal number of bridge cables with ice accretion at low flow turbulence*. Wind and Structures 22(2) (2016) 253-272.

Kuznetsov S., Pospíšil S., Král R. *Climatic wind tunnel for wind engineering tasks*. Technical Transactions 12(2-B) (2015) 303-316.

Schewe G. *On the force fluctuations acting on a circular cylinder in crossflow from subcritical up to transcritical Reynolds numbers*. Journal of Fluid Mechanics 133 (1983) 265-285.

Trush A., Pospíšil S., Kuznetsov S., Kozmar H. *Wind-tunnel experiments on vortex-induced vibration of rough bridge cables*. Journal of Bridge Engineering 22(10) (2017) 06017001.

Snow accretion prediction on an inclined cable

Krzysztof Szilder

Aerospace Research Centre, National Research Council, Canada,
e-mail: Krzysztof.Szilder@nrc-cnrc.gc.ca

Abstract: We have developed a novel analytical model to predict snow accretions. Our analysis of snow and freezing rain accretions forming on vertical, inclined and horizontal cables revealed that the two most influential parameters are the ratio of windspeed to particle terminal velocity, and cylinder inclination angle. We have also adapted our existing morphogenetic icing model to simulate snow accretions on arbitrarily oriented cylinders/cables. The adapted morphogenetic model can be used to predict complex details of the snow accretion shape, including surface roughness and embedded voids. Detailed accretion structures predicted by the morphogenetic model can be 3D-printed and used to examine the relationship between the amount of snow precipitation and the resulting changes in the aerodynamic characteristics of cables.

Keywords: snow accretion prediction, cable aerodynamics.

1. Introduction

During a snowstorm, snow may accrete on the stay cables of a bridge. Over time, snow metamorphosis may occur, allowing the accretion to settle and consolidate. Partial melting and refreezing may also occur. Snow/ice formation on bridge cables can result in ice falling onto pedestrians and traffic, leading to personal injuries and property damage. In severe cases, the snow/ice accretions may lead to bridge closures due to induced cable vibrations (Roldsgaard et al., 2013).

The objective of this research is to extend the ice accretion models developed for freezing rain applications (Szilder, 2018) to wet and dry snow conditions. The new numerical models we have developed have enabled the prediction of ice accretion details that could not have been anticipated using existing models of snow accretion on cables. These details are crucial for determining the aerodynamic behaviour of bridge cables and other non-rotating cylindrical objects during snowfalls. Using our new numerical model, ice accretion shapes can be predicted for any desired environmental conditions and 3D-printed to make physical models. These physical models can then be tested in a wind tunnel to investigate the aerodynamic characteristics of the ice-covered cables.

In this paper, two types of snow accretion models will be developed: 1. Analytical models that allow a quick estimate of snow accretion size and 2. Numerical models that predict details of snow accretion shapes.

2. Analytical models of snow accretion on a cylinder

As an example of simple snow accretion models, we will discuss snow accretion on bridge safety fences.

2.1. Influence of snow precipitation on fence porosity

Snow and ice accretion forming on safety fences installed on bridge decks can have a significant effect on the aerodynamic stability of the bridge. The low porosity of snow-covered fences influences the flow around the bridge and in the bridge wake. The assumed relationship between precipitation conditions and decreasing fence porosity in a recent state-of-the art paper (Taylor at al., 2017) is rather simplistic. Using the results developed in the present paper, we can now propose a more accurate approach.

Two typical fence designs will be considered: vertical rod and chain link. The porosity of a fence is defined as $\phi=1-A_B/A_T$, where A_B is the blocked area and A_T is the total area. The fence porosity for both designs is shown as a function of vertical precipitation and windspeed and terminal velocity ratio in Figure 1.

The horizontal black line at 30% porosity depicts the condition when flow stagnates and no longer passes through the fence. The critical vertical precipitation that results in 30% fence porosity can be readily estimated from Figure 1. A higher velocity ratio (stronger winds or smaller precipitation particles) produces critical stagnation conditions with less total precipitation, illustrating the important effect of wind in producing blockage. The total precipitation that leads to critical stagnation conditions is approximately three times less for chain link fences than for vertical rod fences.

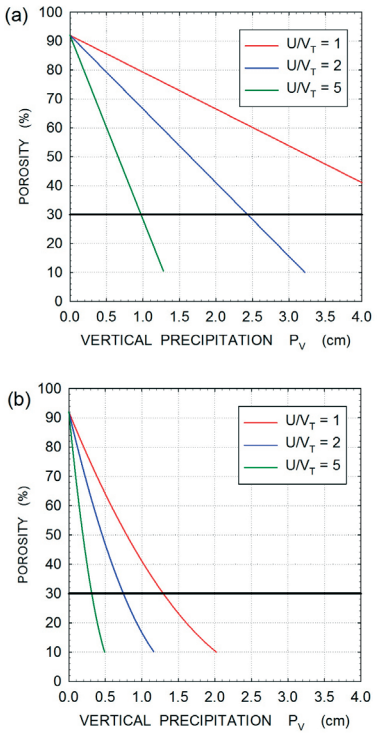

Figure 1. Decrease of fence porosity due to snow/ice accretion as a function of vertical precipitation for three velocity ratio values. (a) vertical rod design (b) chain link design.

3. The morphogenetic snow accretion model

Morphogenetic modelling was originally developed for aerospace in-flight icing applications (Szilder and Lozowski, 2004

and 2017). Recently, the model has been modified to predict ice accretion shapes due to freezing rain precipitation (Szilder, 2018). In this contribution, the morphogenetic model will be further extended for snow accretion applications.

A morphogenetic model is a discrete element, random walk model that emulates the motion of individual elements arriving at the accretion surface. For snow accretion, individual model elements may be imagined to be a single snowflake or to consist of an ensemble of snowflakes that undergo identical histories. Each element has a different history because of the stochastic nature of the model. Element impingement on a cylinder is determined by the distribution of collection efficiency calculated using tools described in the analytical model section. The element impingement locations are determined randomly according to a deterministic distribution. Once an element impinges on the surface, it moves to the closet "cradle" location (Szilder and Lozowski, 2004). The model is sequential, so that as soon as the final location of a particular element is determined, the behaviour of the next element is considered.

3.1. Model result for wind-driven snow

We have looked at snow accretion on a cylinder of 0.2 m diameter. In all cases, the total vertical precipitation was 5 cm. This is the depth of the snow layer that would have accumulated on a horizontal surface. We began by examining wet snow accretion under calm conditions. When the snow accretes on a horizontal cylinder, the surface is relatively smooth, Figure 2a. Maximum snow thickness is almost 5 cm at the top of the cable. Due to shadowing effects, the snow surface becomes rough on its edges. When the cylinder is inclined by 45°, the entire snow surface becomes rough for a similar reason, Figure 2b. The cylinder inclination leads to a smaller impinging flux, and so the maximum snow layer thickness is approximately 3 cm.

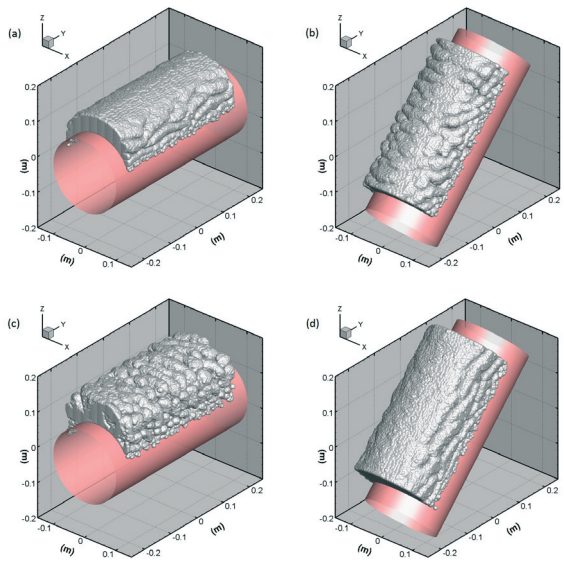

Figure 2. Wet snow accretion on a cylinder of 0.2 diameters for a total vertical precipitation of 5 cm.
(a) Windspeed 0 m/s, inclination angle 0°
(b) Windspeed 0 m/s, inclination angle 45°
(c) Windspeed 2 m/s, inclination angle 0°, yaw angle 0°
(d) Windspeed 2 m/s, inclination angle 45°, yaw angle 0

Wet snow accretions were also examined for a windspeed of 2 m/s. Because the terminal velocity of wet snow particles of 1mm diameter is 1.4 m/s, the particles approach the cylinder at a velocity of 2.4 m/s and the precipitation trajectory angle is 55° from the vertical. When the yaw angle is 0° (the wind blows parallel to the projection of the cylinder axis on a horizontal surface), the snow accretion on a horizontal cylinder has a porous structure, Figure 2c. This porous structure arises because of strong shadowing effects due to a low particle approach angle of 35°. The horizontal wind enhances the approaching snow mass flux and this leads to an increase in the snow layer thickness. When the cylinder is inclined at 45°, the snow structure is compact (approach angle of 80°) and the maximum thickness is approximately 8 cm, which is 60% greater than the snow thickness that would have formed on a horizontal surface.

4. Conclusions

We have developed a novel analytical model to predict snow accretions on cables. This simple model allows a quick analysis of snow accretion size as a function of precipitation type and amount, cable inclination angle, and wind speed and direction. We have demonstrated that the porosity of a chain fence decreases approximately three times faster than the porosity of a vertical rod fence when exposed to the same environmental conditions. Our model allows examination of other possible geometries for safety fences.

We have also adapted our existing morphogenetic icing model to simulate snow accretions on arbitrarily oriented cylinders/cables. The adapted morphogenetic model can be used to predict complex details of the snow accretion shape, including surface roughness and embedded voids.

It should be noted that some model assumptions, such as a constant non-fluctuating windspeed and no snow shedding or sliding, may compromise the model predictions. Consequently, some of the present results should be treated with caution, especially when snow impinges on the cylinder sides. Because there is no shedding, the models tend to overpredict the accreted snow mass, which is unrealistic but adds an engineering safety factor.

In the future, we plan to perform a model validation exercise using experimental data. It is anticipated that this will lead to the development of a snow shedding module that will improve the accuracy of the snow accretion predictions.

5. References

Roldsgaard J.H., Kiremidjian A., Georgakis C.T., and Faber M.H. *Preliminary probabilistic prediction of ice/snow accretion on stay cables based on meteorological variables.* Safety, Reliability, Risk and Life-Cycle Performance of Structures and Infrastructures, ISBN 978-1-138-00086-5, 2013.

Szilder K., Lozowski E.P. *Novel two-dimensional modeling approach for aircraft icing*. Journal of Aircraft 41, 4, 854-861, 2004.

Szilder K., Lozowski E.P. *Three-Dimensional numerical simulation of ice accretion using a discrete morphogenetic approach*. AIAA 2017-3418, 9th AIAA Atmospheric and Space Environments Conference, 2017.

Szilder K. *Theoretical and experimental study of ice accretion due to freezing rain on an inclined cylinder.* Cold Regions Science and Technology, (in press), 2018.

Taylor Z., Stoyanoff S., Dallaire P.O., Kelly D., Irwin P. *Aerodynamics of long-span bridges: susceptibility to snow and ice accretion*, ASCE, Journal of Structural Engineering, 143(7): 04017039, 2017.

A feasibility study of snow load reduction on flat roofs using a photovoltaic system in heating mode

Iver Frimannslund[1], Thomas K. Thiis[2]

[1]*Department of Mathematical Sciences and Technology, Norwegian University of Life Sciences, Norway, e-mail: i.frimannslund@gmail.com*
[2]*Department of Mathematical Sciences and Technology, Norwegian University of Life Sciences, Norway, e-mail: thomas.thiis@nmbu.no*

Abstract: A new PV system combining electrical power production with snow removal intends to reduce the snow load on flat roofs. Applying power to PV cells cause heat production at the module surface, allowing for the ablation of snow. Such a PV-system serves as an alternative to reinforcing the structural bearings of the building or to being dependent of manual removal of snow in a case of heavy snow load. It also aims to compensate for the added weight of the PV-modules by reducing the snow load when needed, allowing even under-designed roofs to have PV-systems. This study combines measurements and theoretical analysis to investigate the PV-heating system feasibility for reducing snow loads on roofs. Several experiments were performed, including a case study with single modules and the test of a full scale PV-power plant/heating system with 720 modules.The results show that melting snow is unproblematic, but refreezing of liquid water and water saturation of snow can result in insufficient load reduction. Heated gutters are recommended to ensure transportation of meltwater off the roof. Sublimation serves as an alternative to melting, conducive under cold and windy conditions. Tests of load reduction by sublimation resulted in an average load reduction of 0,86 kg/m^2 per day. However, load reduction by sublimation can prove to be difficult over longer periods of time due to the metamorphism of the snow. The design snow load can be reduced for buildings having a melting system according to Annex F in ISO 4355. For the PV-heating system further documentation guarantying the load reduction capabilities is needed to reduce the design snow load for new buildings. The results uncovered in the study indicate that reducing snow loads with a PV-heating system is feasible. An adaptation in terms of design and control is recommended to optimize load reduction.

Keywords: PV, snow, load reduction, under-designed structures, heating-mode, melting, sublimation, enhanced solar gains, wintertime power production, drones, thermography, photogrammetry.

1. Introduction

A large portion of the existing building stock in Norway is under-designed with respect to snow load. The growing knowledge and information of snow loads has resulted in the snow load developing from a general load with little variations, to a load varying with local topography and local climate (Meløysund et al. 2008). Since the first snow load standard was introduced in Norway, the characteristic snow load has shown a general trend of increasing. The increase of the characteristic snow load value has placed many older, existing buildings in the under-designed category compared to the existing design regulations. It is estimated that 4,5% of the Norwegian building stock may have lower capacity than what is required in current design regulations (Meløysund 2010).

A study of the vulnerability of the Norwegian building stock with regards to future climate predicts an increase of wet-winter precipitation, contributing to heavy snow loads on roofs (Kvande et al. 2011). A further increase of the snow load will result in additional buildings to be placed in the under-designed category.

Few solutions are available for reducing heavy snow loads occurring on roofs to this date, making building owners dependent on manually shoveling snow off the roof during heavy snowfall.

The PV-heating system combines electrical power production with snow removal. If PV-cells are subjected to forward bias, heat is produced at the surface due to the electric resistance in the cells. Rectifiers are needed to convert AC current from the grid to DC before it is applied to the modules. The heat development at the module surface allows for the ablation of snow and opens for a new application of the system. If the system proves a sufficient load reducer, it can serve as an alternative to reinforcing the structural bearings of the building or to being dependent of manual removal of snow in a case of heavy snow fall. The system can also potentially compensate for its own weight, enabling under-designed roofs to have PV-systems, opening up a previously indisposed marked.

2. Purpose of the work and methology

The study combines measurements and theoretical analysis to investigate the PV-heating system feasibility for reducing snow loads on roofs. The study was performed with the specific intent to document the load reducing capabilities of a PV-heating system, operating under varying climatic conditions. Different strategies for snow load reduction are investigated. Melting the snow is the obvious way of reducing the load. *Sublimation,* the instant transition from solid to vapor, serves as an alternative to melting. Sublimation is conducive under cold temperatures and windy conditions. This makes sublimation an alternative for load reduction in harsh conditions when melting is disadvantageous due to the refreezing of liquid water. Several experiments were performed, including a case study with single modules and the test of a full scale PV-power plant/heating system with 720 modules. An infrared map of the PV-system running in heating mode was made, using an infrared camera attached to a drone. Single photos of the PV-system was merged to a larger map using a photogrammetric software, revealing the achieved temperatures of the cells. The intent was to document the heat emitted from the modules and to evaluate the condition of the system (heat distribution, hot spots etc.)

In addition to investigating the system's snow load reduction performance, it was of interest to examine if the design snow load from the international snow load standard, ISO 4355, could be reduced for new buildings implementing the PV-heating system. The system's potential for enhanced solar gains during winter is also examined. If snow can be melted in order to harvest solar radiation during the typical seasonal snowpack, the net power production can potentially increase. The analysis in this study compare the energy balance of snow metamorphism with wintertime power production.

3. Scientific innovation and relevance

The PV-heating system in this study has a secondary function compared to a normal PV-system. Building owners often experience design limitations due to the preordained disposition of the buildings capabilities. If the system is able to sufficiently reduce the snow load and it is documented accordingly, the system can allow for being installed on flat roofs previously unable to withstand the added weight of the modules, opening up a previously indisposed marked. It can also serves as a strict load reducer for buildings vulnerable to roof collapse due to heavy snow loads.

The system can also potentially result in higher net power production during winter. It is well known that snow decreases power production due to the full or partial covering of modules. If a small snowpack can be melted and the module surface is cleared, solar radiation can be harvested during the typical seasonal snowpack, potentially increasing the yield of the PV-system.

Intentional sublimation of snow from roof surfaces is previously never reported. For the PV-heating system, load reduction by sublimation can be implemented to reduce the load when melting proves difficult and resourceful. Cold and windy conditions, which impedes melting, enhance the potential for sublimation. Cooperating with the climatic conditions can thus make load reduction more effective. The conditions conducive for sublimation are present in the coldest regions experiencing the most long lasting snow covers. Intentional sublimation of snow can also be of interest for other academic fields and entrepreneurs not yet known.

4. Preliminary results and conclusion

The results indicate that the potential of reducing snow loads with a PV-heating system is existent. Melting snow on the module surface is unproblematic, but the transportation of water from the roof surface can be challenging. The snow's capability for water-saturation and freezing of water at the roof can result in insufficient load reduction. A drainage system with heated gutters is recommended to ensure proper load reduction. Tests of sublimating the snow also showed potential. An average amount of 0.86 kg/m^2 snow was sublimated per day during a case study in Nordmarka, Oslo at an average cost of 29,8 W/m^2. However, load reduction by sublimation can prove to be difficult over longer periods of time due to the metamorphism of the snow. To truly uncover the potential of load reduction by sublimation, further research is recommended. An automation of the system, implementing weather forecast and live data measured on site, is considered advantageous to optimize ablation and save energy.

Melting snow on the module surface allows for enhancing solar gains during the winter season. The study weighs the energy used to melt the snow against the potential of producing energy during winter and the results of analysis and theoretical calculation are indicative of an existing potential of enhanced solar gains and a possible new application of the system.

The relation to the law and design regulations is also investigated to consider how the system can be implemented in existing and new buildings. The thesis concludes that further documentation of the system's load reduction capabilities is needed to integrate the system into the design regulations and to establish of a legal precedent for the system.

5. Acknowledgements

Thanks to INNOS for allowing us to research their system and for providing equipment for the case study.

6. References

Kvande, T., Almås, A. J., McInnes, H. & Hygen, H. O. *Klima- og sårbarhetsanalyse for bygninger i Norge. Videreføring av rapport 3B0325. Versjon 01*. Statens bygningstekniske etat: SINTEF Byggforsk. 44 pp. 2011

Meløysund, V., Karl, V. H., Bernt, L. & Lisø, K. R.. *Economical effects of differentiated roof snow loads*. Proc. Of the 6th International Conference on Snow Engineering. New York, USA, 2008.

Meløysund, V. *Prediction of local snow loads on roofs*. Phd. Trondheim: Norges tekniske og naturvitenskapelige universitet, Fakultetet for ingeniørvitenskap og teknologi, Institutt for konstruksjonsteknikk, 42 pp, 2010

Wind tunnel model tests of snow precipitation and redistribution on rooftops, terraces and vicinity of high-rise buildings

Andrzej Flaga[1], Grzegorz Bosak[1], Aleksander Pistol[1], Łukasz Flaga[2]

[1]*Institute of Structural Mechanics, Cracow University of Technology, Poland,*
e-mail: liwpk@windlab.pl
e-mail: gbosak@interia.pl
e-mail: aleksander.pistol@gmail.com
[2]*Wind Engineering Laboratory, Cracow University of Technology, Poland,*
e-mail: lukasz.flaga@interia.pl

Abstract: This paper describes the model tests conducted at Wind Engineering Laboratory of Cracow University of Technology aimed at determining the shape coefficients of snow load on high-rise buildings of The Warsaw Hub. It was conducted as part of a larger research work containing also investigations of wind action on the buildings, wind comfort on pedestrian level, sunlight reflection analysis and vibration comfort analysis of the subject buildings. The shape coefficient was measured at two different situations: snow precipitation and its subsequent redistribution. The model tests were conducted independently for rooftops and terraces in the scale of 1:120 and for the neighbouring area of the buildings in the scale of 1:300. The results allowed for creation of shape coefficient maps on the investigated areas both for snow precipitation and redistribution that can be basis for identifying the possible icings spots, snow erosion and accumulation zones, as well as areas of dust and pollution accretion.

Keywords: snow load, environmental actions, wind engineering, high-rise buildings, snow redistribution.

1. Introduction

The subject of the research work is a planned complex of three high-rise buildings located in Warsaw. Building A is designed to be 86,5 m tall, whilst buildings B and C are intended to be 130,5 m tall. Between buildings A & B and B & C there are lower buildings that are 26,5 m high. The part between buildings A & B contains a small passage at the ground level, allowing for communication. The subject buildings and their surroundings are shown in Fig. 1.

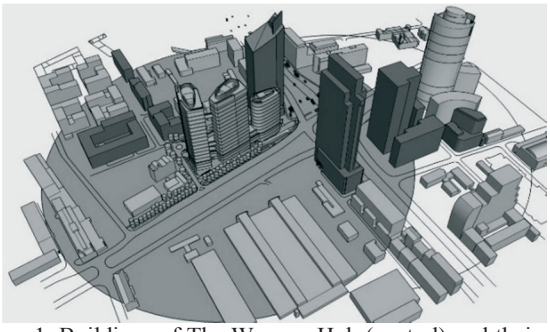

Figure 1. Buildings of The Warsaw Hub (central) and their surroundings as modelled for the tests.

The main scientific aim of the research was to determine the snow load on rooftops, terraces and elevation details of the subject buildings. The results were also intended for use in predicting possible pollution accretion in parts designated for penthouse cafes and restaurants located on the rooftops. The investigation of snow distribution on ground level around the buildings was aimed at identifying possible critical zones of accumulation and erosion and possible dangerous spots where large chunks of snow could be dropped from the rooftops.

2. Similarity criteria

2.1. Snow precipitation

Similarity criterion for model tests of snow precipitation is linked with snow terminal velocity and is defined in Eqn. (1):

$$\Pi_t = \frac{v_{ref}}{v_t} \tag{1}$$

Terminal velocity of snow in nature was established at $v_t^{nature} = 1.5\ m/s$ (Mellor, 1965). The results for the scale of 1:300 situations are presented in Table 1. The criterion was satisfied for both investigated model scales.

Table 1. Similarity criteria for snow precipitation.

Characteristic	Buildings A, B & C – scale 1:300	
	Nature	Model
Exponent α	0.32	0.35
Snow terminal velocity v_t	1.5 [m/s]	0.3 [m/s]
z_{ref}	30 [m]	0.1 [m]
v_{ref}	4.0 [m/s]	0.8 [m/s]
Turbulence intensity I_u	29%	11%
Π_t	2.67	2.67

2.2. Snow redistribution

For redistribution, the criterion of snow terminal velocity (Eqn. (1)) is less important. The main criterion for this situation is linked with lifting the snow particles accumulated on the model. It is defined as in Eqn. (2) (Flaga and Kimbar, 2008):

$$\Pi_g = \frac{(\rho_c - \rho_f) - d \cdot g}{v_{ref}^2 \cdot \rho_f} \tag{2}$$

Air density was established as $\rho_f = 1.23\ kg/m^3$ and standard gravity as $g = 9.81\ m/s^2$. The criteria were satisfied for the values summarized in Table 2.

Table 2. Similarity criteria for snow redistribution.

Characteristic	Buildings A, B & C – scale 1:300	
	Nature	Model
Snow density ρ_c	250 [kg/m^3]	20.53 [kg/m^3]
Particle diameter d	500 [μm]	430 [μm]
z_{ref}	30 [m]	0.1 [m]
v_{ref}	10.0 [m/s]	2.6 [m/s]
Π_t	6.67	8.61
Π_g	0.0099	0.0099

3. Research method

Model tests were conducted at boundary layer aerodynamic tunnel of WEL CUT. Turbulence of inflowing air was created using spires and blocks located in the working section in front of the model. The exponential formula for wind profile exponent was calculated as $\alpha = 0.35$, whilst the turbulence on model reference height was $I_u^{model} = 11\%$. Graph of vertical wind profile is shown in Fig. 2.

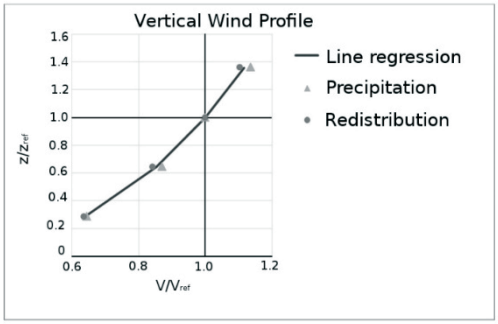

Figure 2. Graph of vertical wind profile used for the model tests of snow precipitation and redistribution.

For the tests, artificial snow was created with Styrofoam grinded on sandpaper until fine, loose consistence was achieved. Prepared like this, the material shows some cohesion, perhaps resulting from electrostatic loads generated in the grinding process, effectively simulating the structure of snow.

After precipitation and redistribution phase was over for each wind direction, the model was scanned using precise optical 3D scanner *GOM ATOS II*. Subsequently, the 3D scans were compared with standard model scan without the snow effects, which allowed for exact determination of the thickness of accumulated artificial snow cover and its distribution on the models.

4. Experiment implementation

The experiment in the scale of 1:300 was conducted for eight different wind directions, ranging from 0° to 315° with an increment of 45°. For the scale of 1:120, only 3 most neuralgic directions were chosen for each building, based on the research staff experience and literature (Flaga, 2008). For building A, the tests were conducted for wind direction angles 0°, 170° and 225°. For buildings B & C, the angles were 0°, 120° and 240°. Snow precipitation was executed by stabilizing the airflow in the working section of the tunnel, then activating a system of double sieves, distributing the artificial snow in a uniform pattern. After snow cover of sufficient thickness was accreted on the models, they were scanned using 3D optical scanner. Subsequently, without removing the artificial snow cover, the redistribution was tested for the same wind direction. The airflow in wind tunnel was put on again, but with higher wind speed according to Tab. 2. This lasted for 10-15 minutes until no more lifting of the particles was observed and the models were scanned once again.

5. Model tests results

The results obtained from the tests were gathered in dimensionless form as shape coefficients μ as defined in (PN-EN 1991-1-3). For model scale 1:120, snow precipitation and snow redistribution coefficients have been calculated, defined in Eqn. (3) and (4):

$$\mu_o = \frac{S_o}{\bar{S}_o} \tag{3}$$

where: μ_o – precipitation shape coefficient, s_o – snow cover thickness at analysed point after precipitation, $\bar{s}_o$ – mean snow cover thickness on the ground level after precipitation.

$$\mu_r = \frac{S_r}{\bar{S}_o} \tag{4}$$

where: μ_r – redistribution shape coefficient, s_r – snow cover thickness at analysed point after redistribution.

For model scale 1:300, also erosion/accumulation coefficient was defined, presented in Eqn. (5):

$$\mu_{ro} = \mu_r - \mu_o \tag{5}$$

The obtained values of these parameters ranged from 0 to 2.0 in case of precipitation and redistribution shape coefficients, and between -0.3 to 0.3 in case of erosion/accumulation coefficient.

6. Results analysis, conclusions and final remarks

6.1. Model scale 1:300

Observing the snow precipitation on the ground level, aerodynamic trails of the buildings (or the whole complex) can be clearly noticed. Another characteristic aspect of the maps is accumulation at windward walls of the buildings. For a number of wind directions, small snowdrifts can be observed near the curved edge of building A, perhaps resulting from vortex creation at that place. Redistribution can lead to large chunks of snow falling from the roofs, but also erosion of pre-accumulated snow on the ground level.

On the rooftops/terraces of lower buildings between the skyscrapers, large accumulation zones adjacent to the windward walls of the tall buildings can be observed. In most cases, subsequent erosion leads to blowing them away or significantly decreasing their height.

6.2. Model scale 1:120

For the rooftops of buildings A, B & C, large accumulations of snow can be observed adjacent to the obstacles like railings or installation elements located on the roofs. These zones may be object to subsequent erosion caused by snow redistribution. However, what may be more interesting, from practical point of view, are the large snowdrifts accreting on the terraces, especially highlighted on building C for wind directions 240°. This can produce significant problems for locating service premises there.

7. Acknowledgments

This research was done as a commissioned work funded by AMC – Andrzej M. Chołdzyński Sp. z o.o.

8. References

Flaga A. *Wind Engineering. Fundamentals and Applications*. Arkady, Warsaw, 2008 [in Polish].

Kimbar G., Flaga A. *A new approach to similarity criteria for predicting a snow load in wind-tunnel experiments*. Snow Engineering VI, Whistler, Canada, 2008.

Mellor M. *Cold regions Science and Engineering Part III, Section A3c: Blowing Snow*. Cold Regions Research & Engineering Laboratory, Hanover New Hampshire, 1965.

PN-EN 1991-1-3: Eurocode 1: *Actions on structures – Part 1-3: General actions – Snow loads.*

Study on noise originating from selected bridge expansion joints

Janusz Bohatkiewicz[1], Michał Jukowski[2], Marcin Dębiński[3], Maciej Hałucha[4]

[1]*Department of Roads and Bridges, Lublin University of Technology, Poland,*
e-mail j.bohatkiewicz@pollub.pl
[2]*Department of Roads and Bridges, Lublin University of Technology, Poland,*
e-mail:m.jukowski@pollub.pl
[3]*Department of Roads and Bridges, Lublin University of Technology, Poland,*
e-mail: m.debinski@pollub.pl
[4]EKKOM Sp. z o.o., *Poland,*
e-mail: maciej.halucha@ek-kom.com

Abstract: Road noise constitutes one of the most adverse impacts of road traffic on the environment. Noise particularly annoying for the inhabitants is recorded in the vicinity of engineering structures, where various types of expansion joints are used (Foglar et al., 2013). There are currently many road connections built in Poland, including a total of almost ten thousand expansion joints. The authors of the article attempted to determine noise differences for several most commonly used expansion joints – single- and double-module, block and one described as one of the most advantageous from the acoustic point of view – finger expansion joint. The study also attempted to determine the impact of expansion joint types on the noise level in comparison to the road section not equipped with these devices, which was adopted as the base noise level. The article also describes the adopted, individual research method, and refers to the regulations in force in the field of noise protection, which currently do not directly regulate this type of problems in Polish conditions.

Keywords: impulse noise, bridge expansion joints, equivalent sound level.

1. Introduction

Poland is one of the countries which, following its accession to the European Union, observed dynamic development of the road infrastructure, manifesting itself in the construction of many kilometers of highways, expressways, and directly related engineering and engineering sites. Each connection of the road with a bridge or viaduct is made using the so-called expansion joint gap, enabling free movement of arches resulting, e.g. from the difference in air temperatures, which may cause expansion or contraction of the material from which the load-bearing structure is made. From an acoustic point of view, it is the contact between the road and the engineering object that is the most important place where the so-called impulsive noise phenomenon occurs, which is the subject of many social disputes (Beczek et al., 2013).

2. Location and purpose of measurements ground

In order to determine the noise level generated during vehicle passage through the object (expansion joint), measurements of traffic parameters and noise on selected test areas were made. The test areas were located in Lublin Voivodeship in two cities, in Puławy and Dęblin, and in Silesian Voivodeship in Knurów. Four types of expansion joints were measured: two single-module expansion joints, one double-module expansion joint, one finger expansion joint, and one block expansion joint. Four test areas were selected, the first one located along the DK12 national road in Puławy, the second one along Marszałka Piłsudskiego Street in Puławy, the third along 15 Pułku Piechoty Street in Dęblin, and the fourth along the A1 Highway in Knurów. The main aim of the study was to identify the noise level during passages of car wheels through these devices, make an attempt to very the sound (impulsive) level and to perform an acoustic comparison analysis of the tested types of expansion joints. With regard to the standard approach concerning road noise, there is no available detailed information on testing and admissible values for the phenomenon of impulse road noise. The admissible values for noise levels in the environment originating from traffic were presented in the Regulation of the Minister of Environment of 8 October, Dz. U. - Journal of Laws, item 1109). It contains a table listing the admissible levels of environmental noise caused by each group of noise sources. For roads or railways, these values depend on the type of terrain and range from 65 dB for daytime to 56 dB for nighttime. They do not take include the sound pressure level of impulse sources. The impulse correction to the results of impulse parameter measurements can be found in the Regulation of the Minister of the Environment of 30th October 2014, Dz. U. - Journal of Laws, item 1542, Appendix no. 8. For the measurement of the equivalent sound level, this correction depends on the type of sound, i.e. whether the sound is highly impulsive, whether the impulse sound has high energy or whether it is a typical impulse sound. These values range from 3 dB to 12 dB, demonstrating that this correction has significant impact on the final value of the measurement, taking into account the value of the equivalent sound level given in the Dz. U. - item 1109.

3. In situ measurements

After a detailed analysis of the tested sections, ten measurement points, marked PPH-(1-10), were selected:

- PPH-1, PPH-2 and PPH-3 - DK 12 Puławy-Zwoleń,
- PPH-4, PPH-5, PPH-6 – Marszałka Piłsudskiego Street in Puławy,
- PPH-7 and PPH-8 – 15 Pułku Piechoty Street in Dęblin,
- PPH-9 and PPH10 – Knurów Highway A1.

An example of the measurement point location is shown in Fig. 1.

Figure 1. Location of measurement points PPH-(1-3).

In order to carry out noise tests on bridge expansion joints, firstly there was a study program developed, which included information on the method of their execution, a list of the measurement equipment used and the organization of the measurement area (Bohatkiewicz et al., 2008). At each measurement point, it was assumed that the microphone of the sound level meter would be mounted 30 cm above the surface of the expansion joint along its axis. In addition, one measurement point, called the "baseline", was added in each test. The baseline was located between two expansion joints (at their mid-span). This approach allowed to compare the sound level from the same source, i.e. a vehicle moving at the same speed, in the same cross-section, but without expansion joint. Over the course of the study, the speeds of passing vehicles were measured, as well as their intensity, along with the division into their type structure. This allowed to read the noise generated by a single vehicle passing by and to conduct a comparative analysis of the expansion joints. All conducted tests were preceded by a field inspection and pilot measurements. Measurement equipment comprising class 1 sound level meters was used in the tests.

4. Results

Due to the limited volume of this text, the complete results of the study were presented in the full text of the research paper. First of all, the results were analyzed in frequency bands divided into 15-minute intervals. The value of L_{Aeq} equivalent sound level was measured over the course of the tests. When analyzing the waveforms of the sound levels

in the different frequency bands, it was noticed that in the 500–1250 Hz band, possible influence of impulsive noise on the equivalent sound level value could be noticed. Example results of measured noise values are shown in Table 1. Over the course of the sound level tests, the intensity of vehicles with a breakdown into their type structure and the vehicle speeds were measured simultaneously. Fig. 2 shows exemplary results of the traffic intensity measurements.

Table 1. One text column table example.

Measuring point No	PPH-7 (block expansion joint)	PPH-8 (baseline)
Measuring equipment type	SVAN 958	SVAN 971
L_{Aeq} value [dB]	79.6 80.7	74.3 75.8

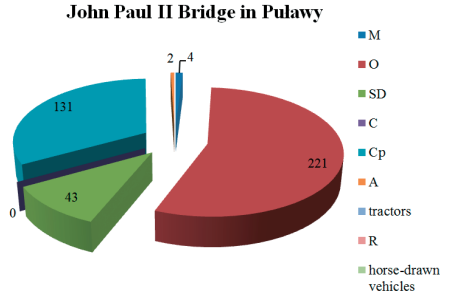

Figure 2. Results of traffic volume on the John Paul II Bridge in Puławy.

5. Conclusion

When analyzing the results of the expansion joint tests, it was concluded that in each case a difference can be observed in the noise level generated by the expansion joint in the frequency band of 500 – 1250 Hz. The noise generated by expansion joint increases the sound level in the foregoing band, which is within the range of the band that can be heard by humans, and can cause adverse effects on humans and the environment. Examples of results indicating this effect are shown in Fig. 3.

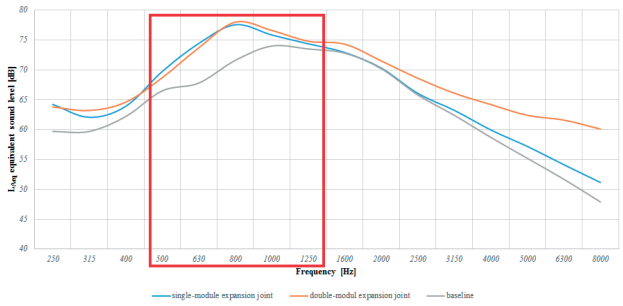

Figure 3. Analysis in frequency band for single- and double-module expansion joints compared to baseline on the John Paul II Bridge in Puławy.

Differences in sound levels with regard to the measured values of the equivalent sound level, depending on the baselines for each analyzed case, are presented in Fig. 4. The PPH-1 (single-module expansion joint at John Paul II Bridge), which was located on the acceleration lane, was not included, because the measured values of the equivalent sound level are lower than the reference point at the road surface.

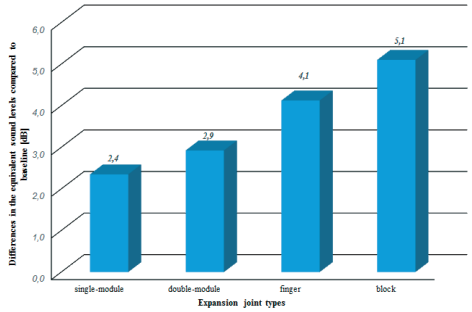

Figure 4. Differences in the equivalent sound levels for each analyzed expansion joint compared to corresponding baselines.

Based on the foregoing graph, it can be concluded that single-module and double-module expansion joints are the quietest, however, when analyzing the obtained values of sound generated when crossing an expansion joint, one should also note the technical condition of the expansion joint and its width. Both parameters significantly affect the obtained results. The width of the finger expansion joint is more than 6 times greater than the width of the double-module expansion joint, and the difference in sound level is only 1.2 dB, therefore it can be concluded that the finger expansion joint demonstrates good acoustic parameters. On the basis of the performed tests, it can be concluded that block expansion joint is the noisiest.

6. Acknowledgments

The tests were carried out as part of the RID I/76 "Protection against road noise" research project.

7. References

Beczek P., Maciejczyk J., Rymsza B. *Pomiar poziomu hałasu generowanego przez urządzenia dylatacyjne*. Materiały Budowlane 8 (2013) 34-36.

Bohatkiewicz J., Adamczyk J., Tracz M., Kokowski A. et al. *Podręcznik dobrych praktyk wykonywania opracowań środowiskowych dla dróg krajowych*. Kraków 2008.

Foglar M., Goringer J., *Influence of the Structural arrangement of Bridges on the noise induced by traffic*. Engineering Structures 56 (2013) 642-655.

Dimensional analysis and similarity criteria for the acoustic model tests

Andrzej Flaga[1], Agata Szeląg[2]

[1]*Institute of Structural Mechanics, Cracow University of Technology, Poland,*
e-mail: aflaga@pk.edu.pl
[2]*Institute of Structural Mechanics, Cracow University of Technology, Poland,*
e-mail: aszelag@pk.edu.pl

Abstract: In the field of acoustics, model tests are performed to a very limited extent due to the lack of strictly defined similarity criteria between the real system and the scale model. The aim of this work is to conduct a dimensional analysis and to determine the similarity criteria for the use in acoustic tests of sound propagation in open and closed spaces. Moreover, the authors present a system of wave equations describing the phenomenon of sound propagation in an elastic medium together with boundary conditions in a dimensionless form. Based on the presented theoretical analyses, it will be possible to plan and conduct acoustic experiments on small-scale models that will significantly reduce the cost and availability of this type of research.

Keywords: acoustic model tests, wave equation, theoretical analysis, scale model, criterion numbers.

1. Introduction

Scale model tests are often the only method of analysing a studied phenomenon or some properties of a considered system; however, the results of such tests frequently give false results since changing the scale, one can unconsciously eliminate or introduce some additional phenomena that have a significant impact on the final result. In order to compare the results of tests carried out on scale models with the results for objects in a real scale, it is necessary to know the similarity criteria determining the conditions which enable the transition of the observation results from the model to reality (Chesters, 1975; Monin, Yaglom, 2007; Flaga, 2008). In the field of acoustics, model tests are performed to a very limited extent due to the lack of strictly defined similarity criteria between the real system and the scale model (Flaga, Szeląg, 2016).

In the paper, the authors present a complete dimensional analysis and similarity criteria for the use in acoustic studies of propagation of sound in open and closed spaces. The starting point was the presentation of a system of wave equations describing the phenomenon of sound propagation in an elastic medium together with boundary conditions in a dimensionless form.

2. Dimensionless form of acoustic equations and the resulting similarity criteria

To write acoustic equations: motion, physical, continuity and boundary conditions in dimensionless form, the following reference (characteristic) values were assumed:

l_o– reference linear dimension (length);
t_o – reference time;
$\rho_o^{\bullet}$ – reference mass density;
$p_o^* = p_o^{\bullet}$ – reference pressure;
K_o – reference compressibility module;
$v_{no}^* = l_0/t_0$ – reference normal speed at the edge (contact surface of the liquid medium and solid medium);
p_o^* – reference pressure at the edge;
$a_{no}^* = l_0/t_0^2$ – reference acceleration at the edge.

Then, the following dimensionless equations can be obtained:

a). the equation of motion in the sourceless field:

$$\frac{\rho_o^{\bullet} l_o^2}{p_o^{\bullet} t_o^2} \cdot \breve{\rho}_o \frac{\partial^2 \breve{\mathbf{u}}}{\partial \breve{t}^2} = -\mathrm{grad}\breve{p}, \tag{1}$$

b). physical equation:

$$\frac{p_o^{\bullet}}{K_o}\breve{p} = -\breve{K}\widetilde{\mathrm{div}}\breve{\mathbf{u}}, \tag{2}$$

c). equation of continuity:

$$\frac{\breve{\rho}-\breve{\rho}_o}{\breve{\rho}_o} = -\widetilde{\mathrm{div}}\breve{\mathbf{u}}, \tag{3}$$

d). boundary conditions:

$$\breve{v}_n^* = \frac{v_n^*}{v_{no}^*} = \frac{\frac{\partial u_n^*}{\partial t}}{\frac{l_o}{t_o}} = \frac{\frac{l_o}{t_o}}{\frac{l_o}{t_o}}\frac{\partial \breve{u}_n^*}{\partial \breve{t}} = \frac{\partial \breve{u}_n^*}{\partial \breve{t}}, \tag{4}$$

$$\breve{p}^* = \frac{p^*}{p_o^*} = \frac{p^*}{p_o^{\bullet}}, \tag{5}$$

$$\frac{\rho_o^{\bullet} l_o^2}{p_o^{\bullet} t_o^2}\breve{\rho}_o \breve{a}_n^* = \pi_1 \breve{\rho}_o \breve{a}_n^* = -\frac{\partial \breve{p}^*}{\partial \breve{n}}. \tag{6}$$

3. Dimensional analysis and similarity criteria of selected issues of environmental and interior acoustics

The following considerations will concern two issues: sound propagation from a point source located near the surface in the open space and sound propagation in a closed room. The first of these issues relates to environmental acoustics, the second – to room acoustics. Generalised functional relations describing these phenomena will be presented, taking into account additional facts determined experimentally. The dimensionless form of these dependencies was obtained in accordance with the principles of dimensional analysis and the similarity theory of physical phenomena. Relevant criteria of similarity result from these dependencies.

3.1. Point source located near the surface generating a quasi-spherical wave in the open space

The dimensionless form of the equation describing the intensity of sound I_r in the place of observation r for the point source located in the open space near the surface is as follows:

$$\breve{I}_r = \frac{\breve{N}G}{4\pi\breve{r}^2}\mathrm{e}^{-(\breve{m}_a+\breve{m}_t)\breve{r}}, \tag{7}$$

where:

$$\breve{I}_r = \frac{I_r}{I_{ref}}, \tag{8}$$

$$\check{N} = \frac{N}{I_{ref} S_{ref}}, \tag{9}$$

$$\check{r} = \frac{r}{\sqrt{S_{ref}}}, \tag{10}$$

$$\check{m}_a = m_a \sqrt{S_{ref}}, \tag{11}$$

$$\check{m}_t = m_t \sqrt{S_{ref}}. \tag{12}$$

Other variables are:

I_{ref} – reference sound intensity (10^{-12} W/m^2),
N – sound power of the source,
G – source directivity factor,
S_{ref} – reference area,
m_a – sound attenuation by the air,
m_t – sound attenuation by the ground.

3.2. Point source generating a quasispherical wave in a closed room

The dimensionless form of the function describing the intensity of sound I_r in the place of observation r for the point source located in a closed room is as follows:

$$\check{I}_r = \mathcal{F}_1\left(\check{N}, G, \check{x}_z, \check{y}_z, \check{z}_z, \check{r}, (\alpha_i), \check{F}_i, \check{V}, \check{m}_a\right), \tag{13}$$

where:

$$\check{I}_r = \frac{I_r}{I_{ref}}, \tag{14}$$

$$\check{N} = \frac{N}{I_{ref} S_{ref}}, \tag{15}$$

$$\check{r} = \frac{r}{\sqrt{S_{ref}}}, \tag{16}$$

$$\check{x_z} = \frac{x_z}{\sqrt{S_{ref}}}, \quad \check{y_z} = \frac{y_z}{\sqrt{S_{ref}}}, \quad \check{z_z} = \frac{z_z}{\sqrt{S_{ref}}}, \tag{17-19}$$

$$\check{F}_i = \frac{F_i}{S_{ref}}, \tag{20}$$

$$\check{V} = \frac{V}{S_{ref}^{3/2}}, \tag{21}$$

$$\check{m}_a = m_a \sqrt{S_{ref}}. \tag{22}$$

Other variables are:

I_{ref} – reference sound intensity (10^{-12} W/m^2),
N – sound power of the source,
G – source directivity factor,
S_{ref} – reference area,
m_a – sound attenuation by the air,
V – volume of the room,
x_z, y_z, z_z – the location coordinates of the sound source,
(α_i) – a set of sound absorption coefficients of the corresponding surfaces that make up the entire surface of the room, the equations of these surfaces are marked as F_i.

4. References

Flaga A., Szeląg A. *Dimensional analysis and similarity criteria for the model tests of sound transmission through simple partitions*. Wydawnictwo Politechniki Krakowskiej, Kraków 2016, 295-303.

Chesters A. *The applicability of dynamic-similarity criteria to isothermal, liquid-gas, two-phase flows without mass transfer*, International Journal of Multiphase Flow, 2(2) (1975) 191-212.

Flaga A. *Inżynieria wiatrowa. Podstawy i zastosowanie*, Wydawnictwo Arkady, Warszawa, 2008.

Monin A., Yaglom A. *Statistical Fluid Mechanics. Mechanics of Turbulance*, Dover Publications Inc., New York, 2007.

Engineering method to measure structure borne sounds transmitted through the building partitions

Katarzyna Baruch[1], Agata Szeląg[2], Aleksandra Majchrzak[1], Tadeusz Kamisiński[1]

[1]*Department of Mechanics and Vibroacoustics, AGH University of Science and Technology, Poland,*
e-mail: kbaruch@agh.edu.pl
[2]*Institute of Structural Mechanics, Cracow University of Technology, Poland,*
e-mail: aszelag@pk.edu.pl

Abstract: In the paper the authors presented an engineering method to measure the structure borne sound transmission paths using a standardised sound source. The clear advantage of this method is that it gives repeatable results; moreover, it allows the isolation of the structure borne sounds from the air borne sounds so that the latter ones do not disrupt the measurement in the case of untight connections or elements of lower acoustic insulation, such as windows, doors or ventilation grates. The research on the verification of the method was carried out on the façade of the Cracow Philharmonics building; the main structure borne sound transmission paths were determined. It was indicated that the main transmission path is the way through the ground – the acoustic waves come through the pavement and radiate from the whole area of the floor. The dominant frequency for this transmission path is about 360 Hz and it can also be observed as dominant frequency in the spectrum of the noise measured inside the room. The knowledge on the sound transmission paths allows the design of efficient vibroacoustic protection.

Keywords: impact sound, vibrations, sound radiation.

1. Introduction

The transmission of structure borne sounds is very difficult to predict (Cremer, Heckl, 1988; Szeląg et al., 2014). It is a significant problem in all types of buildings, especially where the background noise must be kept low, for example – in concert halls. The procedure of the measurement of structure borne sound transmission has not been standardised yet. The main problem which is encountered during this type of measurements is the simultaneous emission of air borne sounds during the excitation of the partitions with an impact sound source (Hassan, 2009). The building partitions are very often equipped with numerous elements of relatively low acoustic insulation – the radiation of sound from these elements do not dominate if it comes to structure borne sounds because of their relatively small area. Yet, the significance of these elements increases when the air borne sound insulation of the whole partitions is to be considered. This phenomenon is very unfavourable for the measurement of structure borne sound transmission paths.

The paper describes the measurement of structure borne sound transmission paths aimed at finding the dominant way which the vibrations are transmitted from the pavement along the Cracow Philharmonics building to the inside of the concert hall. A multichannel simultaneous measurements of vibrations accelerations were performed on the both sides of the investigated façade. The recommendations for lowering the vibroacoustic energy levels transmitted from the outside of the concert hall were formulated as well.

2. Measurement methodology

The partition under study was the façade of the Cracow Philharmonics building; the total area of the wall is 327 m^2. The tested parts of the façade consist of:

- brick wall – 270 m^2;
- window openings walled up with bricks – 47 m^2;
- wooden doors - 10 m^2.

The receiving room was the concert hall of the Philharmonics:

- outer wall: brick wall, window openings walled up with brick;
- inside walls: brick walls;
- floor: concrete;
- ceiling: suspended, drywall.

A standardised tapping machine was used ① as a sound source. It was covered with a mobile insulation case ② in order to insulate the generated air borne sounds (Fig. 1).

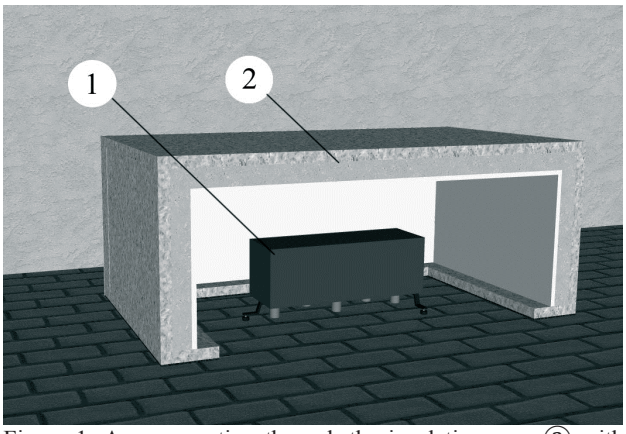

Figure 1. A cross-section through the insulation case ② with a standardised tapping machine inside ①.

The calculations of impact sound transmission were based on the results of vibration acceleration measurements carried out in four individual measurement points inside the room and four points outside the room (Figs. 2&3). The measurement points were distributed in a way which allowed obtaining the information on the values and character of the vibrations of the floor in all the three axes as well as on the wall – in the perpendicular direction (Fig. 3). The used sensors were characterised by the following parameters: sensitivity 1000 mV/g; measurement range 0.4 Hz – 6 kHz (±10% amplitude), 2 Hz – 5 kHz (±5˚ phase).

The measurements were taken with the tapping machine turned on and off. The tapping machine was placed 1.5 m from the façade of the building. Each time the impact sound source was insulated using the mobile insulation case which was a barrier for the air borne sounds generated by the mechanism.

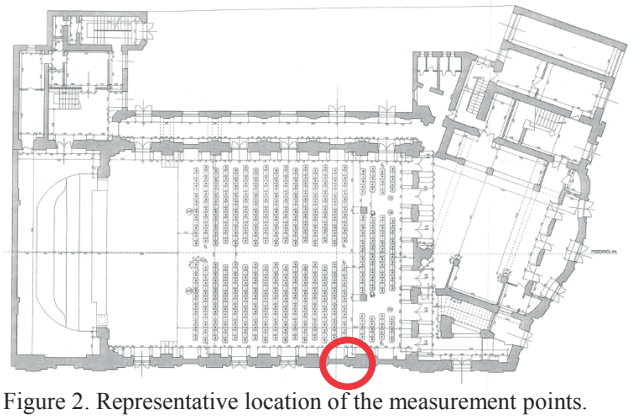

Figure 2. Representative location of the measurement points.

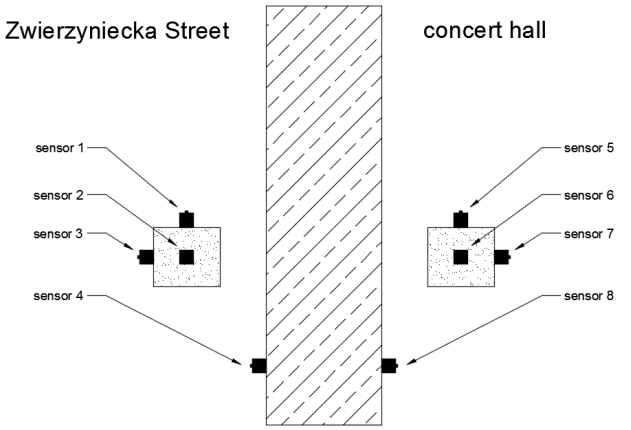

Figure 3. A scheme of the placement of the sensors.

3. Results and conclusions

The main conclusion from the performed analysis was the determination of the dominant structure borne sounds transmission path. It was indicated that the vibrations propagate mainly through the ground – the acoustic wave is transmitted through the pavement and then it radiates from the whole area of the floor in the horizontal direction. The comparison of vibration spectra from the sensors 7 and 8 is shown in Fig. 4. The dominant frequency for this transmission path was about 360 Hz, which is also the dominant frequency in the spectrum of the noise measured inside the concert hall (Fig. 5).

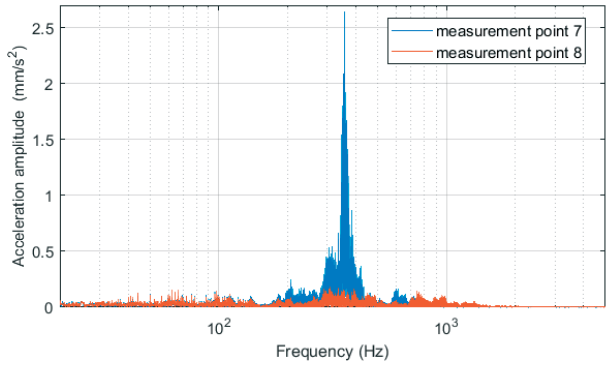

Figure 4. The comparison of the vibration spectra in the measurement points 7 and 8 for the tapping machine turned on.

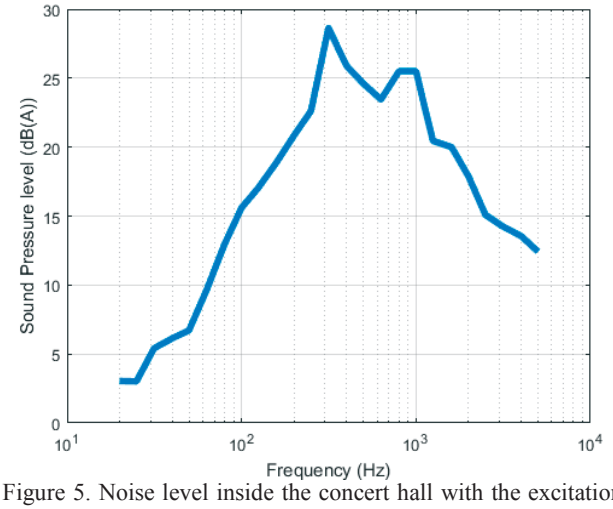

Figure 5. Noise level inside the concert hall with the excitation generated by the standardised impact sound source.

Because of the fact that the main structure borne sound transmission path is the way through the ground and the possibilities of interfering with the construction are strictly limited, the vibroacoustic protection is recommended for the pavement along the Philharmonics building at the Zwierzyniecka Street. Two proposed solutions are:

1) Using the rubber paving for the pavement along the building façade. This solution would guarantee the impact sounds attenuation; it will also reduce the air borne sounds which might be transmitted through the wall and doors to the inside of the concert hall.

2) Using traditional paving along the building façade but on the insulation layer made of material of a proper dynamic stiffness, together with a low anti-vibration partition (about 0.5 m high) in the soil in order to ensure a dilatation of the pavement from the building façade. Such a solution will efficiently reduce the structure borne sounds but it will not affect the air borne sounds.

4. References

Cremer L., Heckl M., *Structure-borne sound. Structural vibrations and sound radiation at audio frequencies*. Springer-Verlag, Berlin, 1988.

Hassan O.A.B., *Building acoustics and vibration. Theory and practice*. World Scientific, Singapore, 2009.

Szeląg A., Stypuła K., Kamisiński T. *Sound radiation by vibrating building partitions in terms of acceptable vibration values*. Acta Physica Polonica A 125 (2014) 122-126.

Probability distribution of the long-term noise indicators on the example of continuous monitoring of the city of Gdańsk

Bartosz Przysucha[1], Pawlik Paweł[2], Jerzy Maciejczyk[3], Tadeusz Wszołek[2], Agata Szeląg[4]

[1]*Department of Quantitative Methods in Management, Lublin University of Technology, Poland,*
e-mail: b.przysucha@pollub.pl
[2]*Department of Mechanics and Vibroacoustics, AGH University of Science and Technology, Poland,*
e-mail: pawlik@agh.edu.pl
[3] *Liga Walki z Hałasem, Poland*
e-mail:jm_jerzy_maciejczyk@tlen.pl
[4]*Institute of Structural Mechanics, Cracow University of Technology, Poland,*
e-mail: aszelag@pk.edu.pl

Abstract: The paper discusses the problem of identifying the probability distribution of long-term noise indicators. This issue is an important aspect of calculating the uncertainty of the noise indicators based on a small measurement sample. The type of the probability distribution determines the choice of the uncertainty calculation model. In the classical methods, noise indicators or corresponding energy levels are determined by normal distributions; however, in the case of a large measurement sample, the arithmetic mean of energy levels can be determined by normal distribution. If these assumptions are not fulfilled, the calculation of the measurement uncertainty may be flawed. In the following study, the authors identified the type of the probability distribution of the noise indicators for a large and varied measurement sample - 56 measurement points from the monitoring of the city of Gdańsk from the period of three years. Based on the performed analyses, it was found that irrespective of the measured noise sources and road types, the distributions of noise indicators can be described by the density function being a mixture of normal distributions.

Keywords: acoustic measurements, statistical analysis, noise protection.

1. Introduction

In the process of assessing traffic noise (road, tram, rail, air) or industrial noise, long-term noise indicators L_n, L_{den} are calculated. Based on these indicators, acoustic maps are constructed. These maps are used while designing environment noise protection, and according to the Directive 2002/49/EC of the European Parliament of 25 June 2002, Member States of the European Union are obliged to create noise maps for the cities of a population exceeding 100,000. On the basis of the constructed maps, the priorities in the selection of places particularly exposed to exceeded noise levels are determined and the strategies for environmental noise protection are constructed.

For economic reasons, the estimation of the values of long-term noise indicators is made on the basis of a small measurement sample. This implicates the need to calculate the uncertainty of the measurement together with the determined indicators. In the models of uncertainty calculation, it is assumed that the probability distribution of the long-term indicators or energy levels corresponding to these indicators is normal (JCGM 100, 2008; ISO 1996-2, 2007). In the previous works (Przysucha, 2015; Przysucha et al., 2015; Batko et al., 2015) it has been shown that such an assumption may lead to errors in calculating the uncertainty and may influence the accuracy of the estimation process of the long-term noise indicators.

In the study, the authors analyse the results of the acoustic monitoring of the city of Gdańsk in terms of the probabilistic properties of the long-term noise indicators obtained from the three years of measurements from May 2013 to May 2016 in 56 measurement points. The probability distributions for all the measurement points were found and the forms of these distributions were determined.

2. Research data

The research data comes from the acoustic monitoring of the city of Gdańsk. The acoustic monitoring was installed in 2009 and the A-weighted equivalent sound levels L_{Aeq} were recorded. The monitoring consists of 71 measurement points, in which road, tram, rail, air and industrial noise are measured. The measurement stations are located in various spots in the city and at various types of roads, so as to monitor the noise from the sources as diverse as possible.

A single station is built of an aluminium plate of a thickness of 25 mm and dimensions 50 x 70 cm (height x width) in which a ¼" microphone has been mounted together with a weatherproof cover. The plate and the windscreen are designed to reduce the effect of the angle of incidence of a sound wave and to minimise the effect of the comb filter. The plate is mounted directly on a building wall. The stations were designed by Sonopan company; they meet the requirements of the Ordinance of the Minister of Economy, Labour and Social Policy from 20 April 2004 on metrological requirements for sound meters. Due to the construction and installation of the stations, the obtained measurement results require a 6 dB reduction, which was included in the analyses.

The research conducted in the work concerned statistical analysis and the identification of the probability distributions of the long-term noise indicators L_d, L_e, L_n and L_{den} for the period from May 2013 to May 2016. The analyses were carried out in three annual time intervals: I - from May 2013 to April 2014, II - from May 2014 to April 2015, III - from May 2015 to April 2016. Due to the lack of measurement data related to technical faults and the temporary lack of operation of measurement stations, 56 points from the total of 71 were taken for the analysis.

3. Determination of the probability distribution of the noise indicators

The sound level indicators are determined by the logarithmic mean of the equivalent sound levels $L_{A,eq,i}$:

$$\bar{L}_{log} = 10\log\left(\frac{1}{n}\sum_{i=1}^{n} 10^{0,1L_{A,eq,i}}\right). \quad (1)$$

Daily noise indicators were calculated:

- day indicator $L_{d,i}$ – calculated as the logarithmic mean of sound levels for a day (hours: 6am-6pm);
- evening indicator $L_{e,i}$ – calculated as the logarithmic mean of sound levels for evening (hours: 6pm-10pm);
- night indicator $L_{n,i}$ – calculated as the logarithmic mean of sound levels at night (hours: 10pm-6am);
- and in the case of a complete measurement day, the day-evening-night indicator:

$$L_{dwn,i} = 10\log\left(\frac{12}{24}10^{0.1L_{d,i}} + \frac{4}{24}10^{0.1(L_{w,i}+5)} + \frac{8}{24}10^{0.1(L_{n,i}+10)}\right), \quad (2)$$

where i is the number of a measurement day.

After conducting the analysis of the probability distribution in all considered measurement points, it turned out that normal distributions could be assigned to a few samples only, whereas in the most cases the distributions could be described with a mixture of normal distributions, just like in the example from the station 159.

Station 159 is located on the two-way one-street road at Budowlanych Street 29, with some industrial complexes and the airport nearby. Table 1 lists the characteristics of the mixture of the normal distributions for the data from the measurement point 159.

Table 1. The characteristics of the mixture of normal distributions for the data from the measurement point 159: p – percentage share of the distribution in the mixture, m_1 – the average of the first variable, s_1 – deviation of the first variable, m_2 – the average of the second variable, s_2 – deviation of the second variable.

	p	m_1	s_1	$1-p$	m_2	s_2
L_d I	0.44	67.41	4.78	0.59	72.14	0.73
L_w I	0.60	65.26	3.17	0.39	67.58	0.92
L_n I	0.43	61.43	4.23	0.57	63.97	0.95
L_{dwn} I	0.54	70.73	3.13	0.45	72.99	0.71
L_d II	0.57	70.73	5.86	0.43	72.31	1.15
L_w II	0.93	65.94	2.60	0.07	77.33	3.93
L_n II	0.93	65.94	2.60	0.07	77.33	3.93
L_{dwn} II	0.34	63.60	0.71	0.66	64.60	5.92
L_d III	0.45	72.86	0.95	0.55	73.48	5.55
L_w III	0.47	68.84	4.89	0.53	71.34	0.62
L_n III	0.47	68.84	4.89	0.53	71.33	0.62
L_{dwn} III	0.61	73.21	1.39	0.38	72.08	3.97

For all measurement periods and all indicators except L_{den} III, the normal distribution could not be assigned (Shapiro-Wilk test). The probability distribution, being a mixture of normal distributions, could be attributed to all indicators except L_e II and L_n II (Anderson-Darling test) – it could be described using a function that is a mixture of normal distributions (Everitt, Hand, 1981):

$$f(x) = pf_1(x) + (1-p)f_2(x), \quad (3)$$

where $f_1(x)$ and $f_2(x)$ are normal density functions with parameters m_1, s_1 and m_2, s_2, respectively.

4. Summary

The paper presents the probability distributions of the long-term noise indicators L_d, L_e, L_n, L_{den} in the acoustic monitoring of the city of Gdańsk. It has been shown that regardless of the measured noise sources (road, rail, air, industrial, tram noise) and regardless of the type of a road, the distributions of the noise indicators can be described by a density function being a mixture of normal distributions.

5. Acknowledgments

The authors thank the Wojewódzki Wydział Ochrony Środowiska in Gdańsk for providing the measurement data.

6. References

Batko W., Pawlik P., Stępień B. *Nieklasyczne metody statystyczne w ocenie niepewności w badaniach i modelowaniu akustycznym*. Wydawnictwo Naukowe Instytutu Technologii Eksploatacji – PIB, Radom, 2015.

Everitt B.S., Hand D.J. *Finite Mixture Distribution*. Chapman and Hall, New York, 1981.

ISO 1996-2:2007. *Acoustics. Description. measurement and assessment of environmental noise. Part 2: Determination of environmental noise levels*.

JCGM 100:2008. *Evaluation of measurement data* - Guide to the expression of uncertainty in measurement. JCGM member organizations (BIPM, IEC, IFCC, ILAC, ISO, IUPAC, IUPAP and OIML).

Przysucha B. *Statystyczne modele w procesach zarządzania ochroną środowiska przed hałasem*. Doctoral dissertation, AGH University of Science and Technology, 2015.

Przysucha B., Batko W., Szeląg A. *Analysis of the Accuracy of the Uncertainty Noise Measurement*. Archives of Acoustic 40(2) (2015) 183-189.

Ordinance of the Minister of Economy, Labour and Social Policy of 20 April 2004 *on metrological requirements for sound meters*.

Forecast of a fire spreading in a large-area shopping hall

Mariusz Maślak[1], Michał Pazdanowski[2], Piotr Woźniczka[3]

[1]*Institute of Building Materials and Structures, Cracow University of Technology, Poland,*
e-mail: mmaslak@pk.edu.pl
[2]*Institute for Computational Civil Engineering, Cracow University of Technology, Poland,*
e-mail: michal@l5.pk.edu.pl
[3]*Institute of Building Materials and Structures, Cracow University of Technology, Cracow, Poland,*
e-mail: pwozniczka@pk.edu.pl

Abstract: The specifics of a forecast fire development in a single fire compartment consisting of a shopping hall characterized by large area and relatively low height are analysed in this paper. The fire initiated locally, and after initiation, depending on the ventilation conditions in the zone, more or less intensively spread to the neighbouring areas with or without full development. The propagation of hot exhaust plume was simulated within the environment of FDS computer code. Three formal models differing in zone size and stacking height have been subjected to analysis. The influence of automatically activated smoke vents has been accounted for.

Keywords: shopping hall, spread of a fire, numerical simulation, fire compartment, ventilation conditions, stacking height.

1. Introduction

Large area shopping halls, usually constituting separate fire zones, belong to the peculiar group of enclosed compartments having relatively low height and a limited number of access openings. Geometries of this type, even when the smoke vents required by law are present and sufficiently numerous, are characterized by difficulties in the efficient ventilation of the considered zone, and this results in a high uncertainty level in forecasting the fire development scenario. Determination, whether in such a case during the fire exposure the developing conditions would allow for creation of a fully developed fire, or for the whole duration the fire would remain localized with limited intensity and affected area, seems to be the key. Credible reply to the question stated above may be different, depending on the size and geometry of fire compartment, the fire load accumulated in the compartment, availability of oxygen in exchange with immediate surroundings and the stacking height of merchandise present – Maślak et al. (2017a). Three mutually corresponding numerical models are analyzed in detail here. For each of these models the fire development is simulated. Each of these models results in a different scenario, i.e. in a different estimate of the warranted safety level.

2. Description of considered numerical models

Numerical simulation of fire development in a large area shopping hall is performed in each case within the environment of FDS (*Fire Dynamic Simulator*) computer program, developed by Mc Grattan et al. (2013). It is assumed, that the fire load is created by the merchandise stacked on racks. It is also assumed, that the merchandise has the parameters of cellulose – Wang et al. (2014). For comparative purposes two alternative scenarios are considered in each case, i.e. when there are automatically activated smoke vents installed, and when there are no such vents. In the first example a small hall is considered (Fig. 1a), while in the second and third example a substantially larger hall is considered (Fig. 1b) – Maślak et al. (2017b). The difference between the second and third example is in the merchandise stacking height. The simulation performed yields the temperature of gases in the fire plume specified in the selected cross sections of the hall after various fire exposure periods (Fig. 2a and 2b, as well as Fig. 3a and 3b). The spatial area affected by fire as well as the temporal fire development are compared (Fig. 4). The obtained results allow for observation how, at the given height above the floor and at the selected cross section, the temperature of exhaust gases evolves (Fig. 5a and 5b). Knowledge of this type allows for drawing more rational conclusions pertaining to fire scenario, and thus allows for better selection of necessary active and/or passive fire protection measures – Fan et al. (2014).

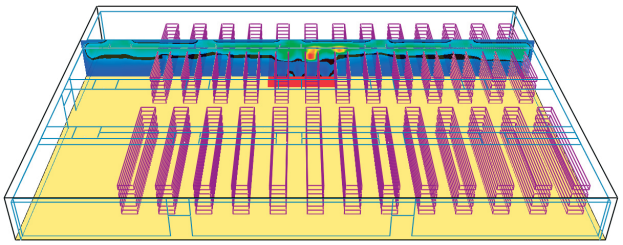

a)

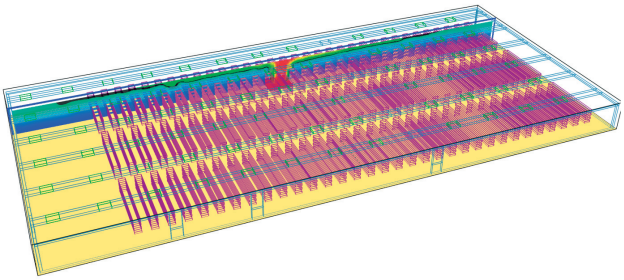

b)

Figure 1. Shopping halls considered in the examples, including: a) smaller hall – first example, b) bigger hall – examples 2 and 3.

a)

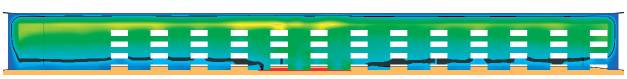

b)

Figure 2. Exhaust plume gas temperature maps obtained after 10 minutes of fire exposure in the case of smaller hall considered in the example 1, including: a) results for the hall equipped with smoke vents, b) results for the hall not equipped with smoke vents – Maślak et al. (2017e).

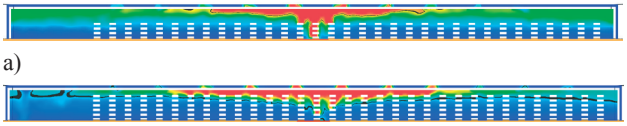

a)

b)

Figure 3. Exhaust plume gas temperature maps obtained after 60 minutes of fire exposure in the case of larger hall equipped with smoke vents, considered in the examples 2 and 3, including: a) results for the hall with lower stacking height – example 2, b) results for the hall with higher stacking height – example 3.

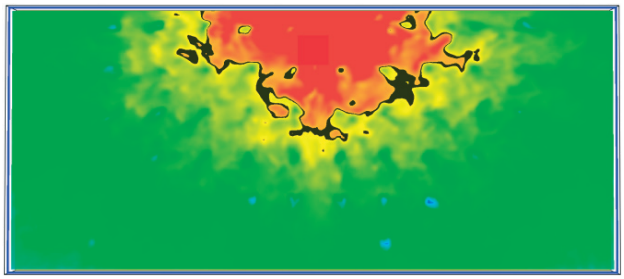

Figure 4. Exhaust plume gas temperature maps obtained after 60 minutes of fire exposure in the horizontal cross section of the larger hall at the height of 6.00 m above floor level – Maślak et al. (2017c).

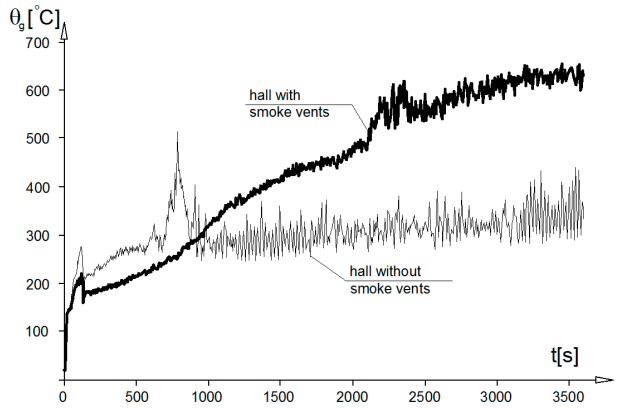

a)

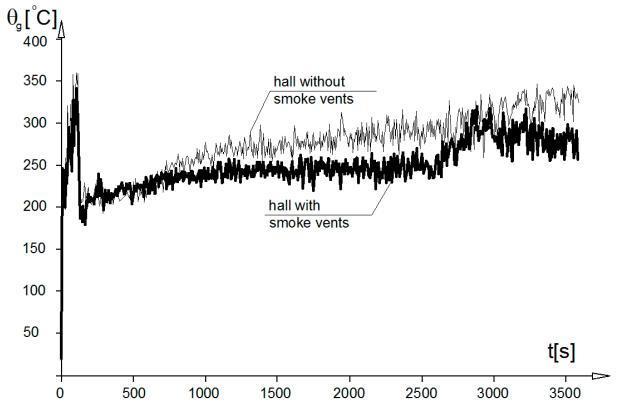

b)

Figure 5. Changes in the exhaust plume gas temperature inside the considered hall in a location at the distance of 3.00 m from the initial fire axis, including: a) result for the smaller hall, at the height of 4.00 m above floor level – example 1, b) result for the bigger hall at the height of 6.00 m above floor level – example 2 – Maślak et al. (2017d).

3. Concluding remarks

The conducted analyses unequivocally indicate, that in the case of large area shopping halls the fully developed fire commonly assumed as the authoritative for evaluation and verification of fire safety level warranted to the users may not be so. In many practically important situations a localized fire with limited intensity and affected zone may be better justified. Parameters of the model are usually determined by the hall geometry, known a'priori, but also real hall ventilation capabilities in the case of fire initiation, as well as quality and quantity of the accumulated merchandise representing potential fuel and constituting the fire load. In the authors' opinion the numerical simulation of fire development performed within the framework of FDS computer code presents an efficient computational tool allowing for reliable prediction of the most unfavourable, but at the same time probable scenario, which may be realized in the given design situation.

4. References

Fan S.G., Shu G.P., She G.J., Liew Richard J.Y. *Computational method and numerical simulation of temperature field for large-space steel structures in fire*, Advanced Steel Construction, 10(2) (2014) 151-178.

Maślak M., Pazdanowski M., Woźniczka P. *Impact of the limited oxygen availability on the localized fire development in a large-area building compartment*, Proceedings of the International Scientific Conference „Fire Protection, Safety and Security 2017", Zvolen, Slovakia, May 3-5, 2017a, 99-109.

Maślak M., Pazdanowski M., Woźniczka P. *Temperature distribution in a large-area shopping hall in the case of a localized fire*, in: Nigro E., Bilotta A. (Eds.) – Proceedings of 2nd International Fire Safety Symposium (IFireSS 2017), Naples, Italy, June 7-9, 2017b, 853-860.

Maślak M., Woźniczka P. *Scenariusze rozwoju pożaru w wielkopowierzchniowej hali handlowej – część 1*, Nowoczesne Hale, 1 (2017) 27-31.

Maślak M., Woźniczka P. *Scenariusze rozwoju pożaru w wielkopowierzchniowej hali handlowej – część 2*, Nowoczesne Hale, 3 (2017d) 64-67.

Maślak M., Woźniczka P. *Wpływ lokalizacji źródła ognia na rozwój pożaru w wielkopowierzchniowym halowym obiekcie handlowym*, Bezpieczeństwo i Technika Pożarnicza, 45(1) (2017e) 154-169.

McGrattan K., Hostikka S., McDermott R., Floyd J., Weinschenk C., Overholt K. *Fire Dynamics Simulator user's guide*, NIST, Gaithersburg, Maryland, USA, 2013.

Wang Y., Burgess I., Wald F., Gillie M. *Performance-based fire engineering of structures*, CRC Press, London, 2014.

The dataware of building structures reliability calculations under temperature effects

S.F. Pichugin[1], V.A. Pashynskyi[2], A.M. Kariuk[3]

[1]*Poltava National Technical Yuri Kondratyuk University, Poltava, e-mail: pichugin.sf@gmail.com*
[2]*Central Ukrainian National Technical University, Kropyvnytskyi, e-mail: pva.kntu@gmail.com*
[3]*Poltava National Technical Yuri Kondratyuk University, Poltava, e-mail: kariuk15@ukr.net*

Abstract: The statistical characteristics of random process of atmosphere air changes, needed for building structures reliability calculations, were generalized. The effects of additional geographical factors, influencing the temperature regime of the locality were analyzed: geographical altitude, proximity to the sea, long-term interannual temperature changes. Recommendations were given as to calculation of atmosphere air statistical characteristics, needed for estimated values normalization and for assessment of building structures reliability indicators.

Keywords: statistical characteristics of temperature, quasi-stationary random process, reliability of building structures.

1. Introduction

Atmosphere air temperature changes significantly influence building structures, in particular, induce forces and shifts in load-bearing structures, lead to damages due to freeze resistance loss of building materials, cause thermal failures of frame fillings, and also affect the processes of erection of buildings and structures. Energy saving issues occupy one of the central places among scientific problems of modern building industry. Taking into account stochastic variations of atmosphere air temperature and their study play the leading role in solving of the above mentioned problems. That is why it is essential to take into account temperature effects both in construction design, in planning construction processes, and during probabilistic calculations of building structures reliability.

Probabilistic calculations require temperature effects representation in the form of random variables or random processes, as well as the creation of representative database of statistical characteristics of random variables and processes of atmosphere air temperature changes. Despite the existence of developed methodology of research, probabilistic representation and normalization of climatic loads and effects [3, 4], as well as the considerable volume of meteorological air temperature monitoring results [1, 2], the creation of representative database of statistical characteristics of temperature effects, needed for reliability calculations, is not complete for Ukraine's territory. Besides, the effects of additional geographical factors (rugged terrain, seaside territory, long-term interannual variability trends etc.) must be analyzed and taken into consideration.

This work was aimed at generalized representation of statistical characteristics of random process of atmosphere air temperature changes, allowing for the above mentioned additional geographical factors.

2. Main body of the abstract

The results of measurements of average daily temperature of air at 485 monitoring stations of Ukraine, which were published in specialized meteorological editions, were used *as basic data*. The results of these observations were mainly analyzed in monograph [2]. The considerable volume of used data ensures the validity of the results, and allocation of monitoring stations in different regions and geographical conditions (flat country and rugged terrain, continental and seaside territories) allow analyzing and taking into account the effect of geographical conditions on atmosphere air temperature regime.

Seasonal and interdiurnal air temperature variability is described with the probabilistic model of quasi-stationary random process. Its possibility of usage in representation of climatic loads and effects was substantiated in [2]. For such a description we need to define the annual functions of mathematical expectation M (t), standard S (t) and asymmetry parameter A (t). Effective frequency value ω = 0,6 1/24hrs is fixed in time and invariable for the whole territory of Ukraine.

The territorial variability of air temperature statistical characteristics is represented on zoning maps of average temperatures of the coldest (January) M_1 and the warmest (July) M_7 months of the year. The obtained from the maps values of average January and July temperatures in the specified geographical point set the annual fluctuation amplitude of air temperature, and enable to calculate the average annual temperature value,

$$M_P = \frac{M_1 + M_7}{2} \tag{1}$$

and set the mathematical expectation function of air temperature M(t) according to sinusoidal law

$$M(t) = \frac{M_1 + M_7}{2} - \frac{M_7 + M_1}{2}\cos\left(\frac{t-15}{57.3}\right) \tag{2}$$

where M_1 and M_7 are the average July and January temperatures from the zoning maps; t is time counted off in days starting from the 1st of January.

The analysis has shown that such an approach ensures satisfactory accuracy, as for 90% of monitoring stations the difference between the factual data and the results, obtained from the maps and formulas (1), (2), is no more than 1°C.

The functions of standard $S(t)$ and asymmetry parameter $A(t)$ are approximately estimated through the mathematical expectation function $M(t)$ and using the formulas:

$$S(t) = 5{,}5\, e^{-0{,}026\, M(t)} \tag{3}$$

$$A(t) = -0{,}3\, e^{-0{,}1\, M(t)} \tag{4}$$

Expressions (3), (4) are satisfactory accurate and have absolutely predictable asymptotic behavior, which allows them to be used in reliability calculations.

Distribution law of the ordinate of the random average daily air temperature process at any moment of time during the year is described by the mixed Gumbel-Gauss law with probability density

$$f(x)=\frac{C}{0.78S}\exp\left[y-\exp(y)\right]+\frac{1-C}{S\sqrt{2\pi}}\exp\left[-\frac{(x-M)^2}{2S^2}\right] \qquad (5)$$

where *M, S, A* are mathematical expectation, standard and asymmetry parameter of ordinate distribution at a particular moment of time according to formulas (2), (3), (4);

$C=-0{,}8775\,A$ – weighting factor;

$y=\frac{\mathrm{x}-M}{0.78\ S}-0.577$ – Gumbel distribution argument.

Probability density expression (5) allows for asymmetry parameter $A\leq 0$ practically in all cases. This is ensured by the formula (4).

Ordinate distribution may also be approximately described by the Gaussian normal distribution law.

Geographical altitude effect was analyzed using the data from 43 monitoring stations, located in the region of the Crimean Mountains, and 74 monitoring stations in the Carpathian Mountains. The length of the observation series varies from 8 to 100 years. 87 monitoring stations are located at altitudes of up to 500 meters above sea level and therefore can be considered flat. 30 monitoring stations are located at altitudes of up to 1500 meters above sea level.

The average January temperature decreases by 4 ... 5°C, and the average July temperature decreases by 6 ... 7°C per every 1 km increase of altitude. Correction for altitude for estimated values of temperatures of the warmest and the coldest days, with different recurrence periods, also fluctuate between 4 ... 7°C per 1 km of altitude above sea level.

The conducted research also confirmed the possibility of using the correction known from the literature for altitude above sea level (-6°C per 1 km of altitude) both for average and for estimated values of atmosphere air temperature.

Seaside territories are characterized by milder temperature conditions, due to heat-accumulating influence of significant masses of sea water.

For 74 monitoring stations, located on the territory of the Crimean peninsula and in the coastal zone of the Black and Azov seas, with a width of up to 100 km, the distance from the nearest seashore and the parameters of the air temperature were determined:

M_1 – the average temperature in January (the coldest month of the year); M_7 – the average temperature in July (the warmest month of the year); M_p – the average annual air temperature; n_p – the average annual quantity of average daily air temperature transitions through 0 ºC.

An analysis of dependency of these parameters on the distance to sea shore enabled to discover the following regularities:

The average temperatures of July M_7, January M_1, and the average annual air temperature M_p tend to decrease with moving from the seashore. With increase of distance L to 100 kilometers they generally decrease by 0,5…2 ºC. In addition, in the charts of dependencies of M_1 and M_p on L, there is also a sharp increase in temperatures in the zone 5 ... 10 km from the seashore. The value of M_1 increases approximately by 3…4°C, and the value of M_p – by 2°C.

The number n_p of transitions of average daily air temperature through 0ºC on average on the continental territory amounts to 12…14 transitions per year, but in 10-kilometers coastal zone decreases to 6…10 transitions per year. The reduction of freezing-thaw cycles positively affects the freeze resistance of building materials.

According to the results of the conducted research, it is recommended, when determining the parameters of the temperature regime for areas located up to 10 km from the seashore, to use the data of the nearest meteorological stations, which are also located in the 10-kilometer coastal zone. When using the zoning maps the average January temperatures in 10-kilometer coastal zone may be increased by 3...4°C (towards warmer temperatures).

Long-term air temperature changes are generally consistent with the known trend of global warming. According to the results of recent 20-year observations at 25 weather stations of Ukraine, the changes in time of average annual air temperature values have been analyzed, as well as the minimum and maximum values, recorded during each of the years of observation. These data characterize the changes in average temperatures, as well as the minimum (winter) and maximum (summer) estimated values of temperature. By approximating the obtained sequences with linear functions, it has been established that the values of annual increments of temperature in general are negligible and vary in different meteorological stations within the interval –0,13°C ... +0,20°C.

State building codes and standards are reviewed every 5-10 years. Thus, during the 10-year period between the regular revisions of norms, the average and estimated values of the air temperature change by no more than 2,0 °C, Such changes will not have any significant influence on the work of frame filling, heating and air conditioning systems. In order to increase reliability, it is recommended to increase the estimated maximum summer air temperature values by 1,0°C, and accordingly reduce the minimum estimated air temperature values by 1,0°C, based on available meteorological data at the time of norms development or revision.

3. Conclusion

1. Changes of average daily atmosphere air temperature are represented in the form of quasi-stationary random process, statistical characteristics of which may be calculated using the developed zoning maps of average January and July temperatures with the help of the above stated formulas.

2. The obtained statistical characteristics of quasi-stationary random process of average daily air temperature changes are close to real results of statistical data analysis of monitoring stations, and may be used for solving of building structures reliability problems.

3. The small annual increments of temperatures allow us to take into account the phenomenon of global warming by adjusting the estimated values of air temperature at regular revisions of the norms of loads and influences, with allowance for the results of observations during the recent years.

4. References

Kariuk A, Mishchenko R. *Metodika statistichnogo analizu meteorologichnih danih z temperaturi povitrya ta rruntu.* Suchasni tekhnologiï v mashinobuduvanni ta transporti 55 (2016) 191-195.

Pashynskyi V., Pushkar N., Kariuk A. *Temperaturni vplyvy na ohorodzhuvalni konstruktsii budivel* (monograph). Odesa, 2012.

Perelmuter A., Gordeev V., Lantuh-Lashchenk A., Mahinko V., Pashynskyi V., Pichugin S. *Nagruzki i vozdejstviya na zdaniya i sooruzheniya.* Yzdatelstvo DShchMK Press. Moscow, 2014.

Pichugin S. *Reliability of industrial building steel structures (monograph)*. Moscow: Izdatelstvo ASV. 2011.

Optimisation of natural smoke control system in isolated industrial building using CWE approach

Wojciech Węgrzyński[1], Grzegorz Krajewski[2]

[1]*Fire Research Department, Building Research Institute, Poland,*
e-mail: w.wegrzynski@itb.pl
[2]*Fire Research Department, Building Research Institute, Poland,*
e-mail: g.krajewski@itb.pl

Abstract: This paper presents a case-study of the design of a smoke control system in an industrial building, following common design standards and performance-based analysis, employing Computational Wind Engineering approach (CWE). The building in question had two tenants, first was an archive storage facility, with additional complexity due to two levels of cat-walks within the building. The second tenant was a high-rack storage of plastic commodities. The standardized approaches employed PN-B 02877-4 and NFPA 204 approach, while the computational analyses were performed as an iterative process until optimisation goal was reached. The analyses shown a significant decrease of total ventilator area required for the system, when calculations were based on CWE approach. Also, additional factors related to occupant safety were pinpointed with the CWE study, which have been missed by the standardized approach.

Keywords: wind engineering, fire, fire safety engineering, smoke control, industrial fire safety.

1. Introduction

Fire safety of industrial buildings is an important design factor, both for occupant safety and protection of property. The major fires in industrial buildings usually lead to large financial losses, and have significant impact on local communities due to the discontinuity of business, leading to local spikes in unemployment. Such events have consequences far greater, than just the loss in goods destroyed by the fire.

To protect the building and its occupants, and to improve the fire-fighting operations in the building, smoke control systems are a golden standard. Their first use may be traced to catastrophic fires in German car-manufacturing plants in 1950's. Some first considerations regarding design of such systems were coined by Thomas et al. (1963), and this work is still considered as a landmark study often referred in the design of modern systems.

However, despite over 70 years of practical use, natural smoke ventilation systems used for smoke control have not changed significantly, which was thoroughly reviewed by Węgrzyński and Lipecki (2018). The use of Computational Wind Engineering (CWE) approach, may allow significant improvements in the design, by improving the spatial distribution of vents and their scenario of operation (Węgrzyński and Krajewski, 2017, Węgrzyński, Lipecki and Krajewski, 2018). These improvements also have significant economic effect (cheaper cost of the system, lower fire loss) and effect on safety (longer available safe evacuation time, lower smoke temperature during firefighting operations).

2. Case study

2.1. General assumptions

The case-study was performed for an isolated building, sized 100 x 50 x 12 m³, which could have been used by two different tenants. The buildings had flat roof, on which the natural vents could be installed. The possible tenant 1 was a document archive, with fuel load density of 500 MJ/m², and challenging two levels of cat-walks placed around the storage at heights of 4 m and 8 m. Tenant 2 was a storage of plastic commodities, with fuel load density exceeding 4000 MJ/m², ESFR-type sprinkler system. The building was a hypothetical development, created for the purpose of comparing design requirements of fire safety features in different countries (Poland, Japan, Australia, USA and Finland). The in-depth characterization of the fire safety features of the buildings was shown in Węgrzyński et al. (2016).

2.2. Hand calculations of smoke-control systems

The calculation methodology in PN-B 02877 standard (PKN, 2001) requires an estimation of the risk of fire in the building by assigning materials stored therein to the corresponding groups from tables, and then matching it with required area of smoke ventilators. The required area itself is presented as a percentage of horizontal projection of the surface area of a single smoke zone. The calculated aerodynamic area of ventilators, as the % of smoke zone area was 1.5 % for tenant 1, that corresponds to 39 m² of required aerodynamic area of ventilators, and for tenant 2 respectively 0.8% and 20.8 m². The building should be sub-divided into two smoke control compartments.

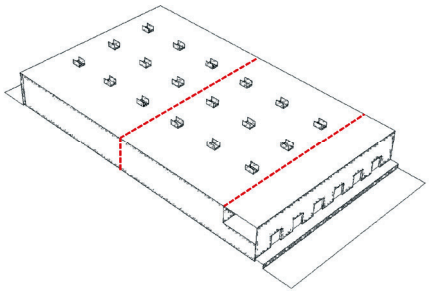

Figure 1. Natural smoke control system based on PN-B 02877.

The same design, following the NFPA 204 standard (NFPA, 2015) allows for optimisation of the size and shape of smoke compartment (one smoke compartment in lieu of two). In this case the total area of ventilators required is 39.6 m² for tenant 1, and less than 10 m² for tenant 2.

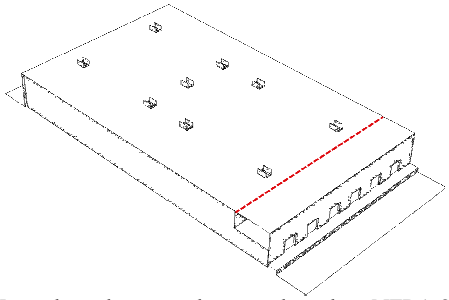

Figure 2. Natural smoke control system based on NFPA 204.

3. Numerical analyses

Further optimisation of the system was possible through numerical analysis, employing CWE approach. Numerical studies were performed in ANSYS Fluent software (v14.5). In all of the scenarios the fire was modelled as volumetric heat and smoke source, with maximum HRR shown in table below. The growth of fire was linear – steady state results were investigated. When time to reach a certain parameter was estimated, the fire was modelled as growing exponentially, until the fire area is limited by firefighters or sprinkler operation. It was assumed that the smoke was produced in combustion of materials with average heat of combustion 20.00 MJ/kg. Smoke was modelled as a perfect gas with all physical properties as air, beside the specific heat which was constant at 1.00 kJ/kg. Following physical sub-models were used for the calculations:

- turbulence model – RNG k-ε,
- fire model – transient volumetric source of heat and smoke, without combustion
- radiation model – P1,
- heat transfer model, third type boundary condition.

The modelling was transient, and the assessment of SHEVs performance was done 5 minutes after the maximum HRR was reached, with the assumption the conditions are close to a steady state.

Total amount of 32 numerical analyses were performed, to compare the standard smoke control solutions with optimised one. Optimisation was based on a CWE study for 8 discrete wind angles and two wind velocities (4.67 and 10 m/s). For the most onerous angle (135°) the study was performed for 3 heat release rates (5, 10 and 15 MW) and 3 wind velocities (1, 4.67 and 10 m/s).

With CWE optimization approach, the system is modified, so it does include smallest amount of ventilators, that should theoretically allow safe evacuation and rescue operation conditions within the building in wind conditions. The designer must know though, that the CFD performed without any wind influence, can often lead to an overestimation of system performance, that may be much lower, once the wind is included in the analysis.

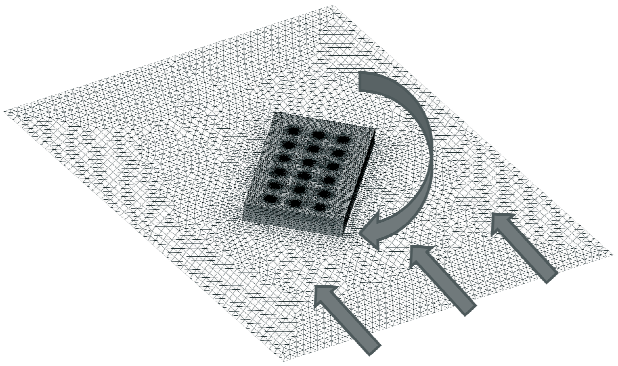

Figure 3. Numerical domain used in the analysis. The arrows indicate the wind direction, and the rotation of the numerical model within the domain to simulate oblique wind angles.

4. Results and discussion

In the case of tenant 1, that smallest optimised area of ventilators that is sufficient to provide required conditions for evacuation and rescue operations, is approx. 27 m². In case of PN-B 02877 approach, this value was 2*39.6 m² and in case of NFPA 204 it was 39 m². The optimised system had similar performance in the removal of the smoke from the reservoir. However, for all of the investigated systems at very high wind velocity (10 m/s), some mixing with air is observed and lower part of the building is filling slowly with low density smoke. Negative influence of wind is observed, especially in terms of non-uniform height of smoke layer throughout the building, and mixing between air and smoke in the lower layer. Overall performance of the optimized system may be considered on par with the performance of NFPA 204 design.

The results were obtained for three investigated fire sizes (5, 10 and 15 MW), they can be considered representative for the case of tenant 2.

It was also observed, that the results of numerical analyses differ significantly between cases with different wind velocity. This confirms the conclusions of previous study (Węgrzyński and Krajewski, 2017). At velocities 1,0 m/s and 4,67 m/s at the most onerous wind angle of 135°, the smoke was maintained in a well-defined smoke layer underneath the ceiling. The performance of the system was similar, to results of analyses without any wind effects. However, at wind velocity of 10 m/s, its effect was significant. The smoke layer has lost buoyancy in a large part of the building, which led to smoke gathering at the height of floor. This could affect the fire-fighting operations. More research is required in this field, in order to limit the effect of high wind velocities on the smoke control system performance (Węgrzyński, Krajewski and Kimbar, 2018). In case of extreme wind velocities, risk analysis should be performed in order to estimate the probability and consequences of an event of fire, in strong wind conditions.

5. References

NFPA 204 Standard for Smoke and Heat Venting. NFPA, 2015 Edition.

PN-B-02877 *Ochrona przeciwpożarowa budynków. Instalacje grawitacyjne do odprowadzania dymu i ciepła. Zasady projektowania*. PKN, 2001.

Thomas P.H., Hinkley P.L., Theobald C.R., Simms D.L. *Investigations into the flow of hot gases in roof venting*. Fire Research Technical Paper No 7. London: Her Majesty's Stationary Office, 1963.

Węgrzyński W., Krajewski G. *Influence of wind on natural smoke and heat exhaust system performance in fire conditions*. Journal of Wind Engineering and Industrial Aerodynamics, 164 (2017) 44–53. https://doi.org/10.1016/j.jweia.2017.01.014

Węgrzyński W., Krajewski G., Kimbar G. *A concept of external aerodynamic elements in improving the performance of natural smoke ventilation in wind conditions*. AIP Conference Proceedings 1922 (2018) 110006. https://doi.org/10.1063/1.5019109

Węgrzyński W., Krajewski G., Sulik P. *Case study 2 – production and storage building (Poland)*. 11th Conference on Performance-Based Codes and Fire Safety Design Methods. Warszawa: SFPE, 2016. https://doi.org/10.13140/RG.2.1.3677.4640

Węgrzyński W., Lipecki T. *Wind and fire coupled modelling—Part I: Literature review*. Fire Technology 54(5) (2018) 1405-1442. https://doi.org/10.1007/s10694-018-0748-5

Węgrzyński W., Lipecki T., Krajewski G. *Wind and fire coupled modelling—Part II: Good practice guidelines*. Fire Technology 54(5) (2018) 1443-1485. https://doi.org/10.1007/s10694-018-0749-4

Assessment of the possibility of using data from meteorological stations to determine thermal loads on scaffolding workers

Iwona Szer[1], Jacek Szer[2], Tomasz Lipecki[3]

[1]*Department of Building Physics and Building Materials, Lodz University of Technology, Poland, e-mail: iwona_s@p.lodz.pl*
[2]*Department of Building Physics and Building Materials, Lodz University of Technology, Poland, e-mail: jacek.szer@p.lodz.pl*
[3]*Department of Structural Mechanics, Lublin University of Technology, Poland, e-mail: t.lipecki@pollub.pl*

Abstract: The study evaluates the possibility of using data gathered from meteorological stations to determine thermal loads on people working on scaffoldings. For this purpose, the values calculated on the basis of data obtained from meteorological stations and from measurements performed in the surrounding of people working on scaffoldings were compiled and compared. The measurements were carried out on ten scaffoldings located in the Łódź and Lower Silesian voivodships, in the time period from February 2017 to September 2017. The results obtained at construction sites and meteorological stations were different, but statistical analyzes showed that they were correlated. Stronger correlation occurred for scaffoldings located in the Lower Silesian voivodship, while it was weaker for ones located in Łódź region.

Keywords: UTCI, scaffoldings.

1. Introduction

Work on scaffoldings requires increased physical effort, and in most cases it is carried out at a considerable height. In addition, employees are exposed to dynamically changing conditions of the external environment. This may result in reduction of motivation, concentration or psychomotor fitness (Traczyk and Trzebski, 2004), and as a consequence in the increase of the risk of appearance of dangerous situations leading to accidents. Therefore, an important issue is monitoring of the occurrence of adverse environmental conditions to which a construction worker may be exposed. There are many methods for assessing the thermal comfort of humans in the external environment (Coccolo et al., 2016). This article uses a simplified indicator which assesses human thermal loads – UTCI (Universal Thermal Climate Index). It takes into account the combined effect of external temperature, air humidity and wind speed (Błażejczyk and Kunert, 2011).

2. Research methods

2.1. Data gathered from the Institute of Meteorology and Water Management – National Research Institute (IMGW-PIB)

In order to determine the relationship, the UTCI index calculated on the basis of measurements performed in the environment of people working on scaffoldings was compared with the UTCI based on data from meteorological stations obtained from IMGW-PiB. Chosen meteorological stations were located as close as possible to the research site. In all cases, the scaffoldings were located in the same city as the stations. Meteorological data were adjusted to the same days and hours at which the given scaffolding was examined.

2.2. Data gathered in in-situ measurements on scaffoldings

Measurements were carried out on scaffoldings located in the Łódź voivodship – marked as E and in the Lower Silesian voivodship – marked as D. The structures were tested from February to September 2017. For each scaffolding, tests were carried out during one working week. Three series of measurements were performed every day: the first from 8 a.m., the second from 11 a.m., the third from 3 p.m. Measurements in each series lasted about one hour and depended on the size of the scaffolding. (Błazik-Borowa and Szer J., 2016). Selected environmental parameters: air temperature, relative air humidity, (Szer I et al., 2017), atmospheric pressure, illuminance, wind speed (Jamińska-Gadomska et al., 2017), sound level (Jabłoński et al., 2017), dustiness were measured on scaffoldings. The measurements were made with the use of AMI310 multifunction device, to which climate moduli registering different environmental parameters were connected. The measurements were made in the middle of the platform span at the height of the employee's face. The wind speed was measured first in the direction perpendicular and next parallel to the façade of the building.

3. Research results

The minimum, maximum and average values of the simplified human thermal load assessment index (UTCI) calculated on the basis of temperature, relative air humidity and wind speed recorded during one week of testing are presented in Table 1.

The maximum value, equal to 50.0°C, was observed for the E20 scaffolding, which was tested at the end of August and beginning of September. The lowest value, equal to -0.5°C, was calculated for the D12 scaffolding which was tested on February.

Table 1. Universal Thermal Climate Index – UTCI.

Scaffolding	UTCI average	UTCI minimum	UTCI maximum
	[°C]	[°C]	[°C]
E12	19.6	0	44.4
E15	28.6	15.3	43.3
E16	21.6	2.7	34.5
E19	26.2	19.5	41.0
E20	28.2	19.9	**50.0**
D12	9.2	**-0.5**	20.0
D16	22.4	10.6	34.3
D17	29.2	10.1	43.0
D18	28.9	12.8	41.3
D20	34.2	28.8	41.8

In order to compare the values measured on scaffoldings with ones obtained from meteorological stations, for each day and for each time of the day, the human thermal loads assessment index (UTCI) was calculated.

Figure 1 presents the relationship between the UTCI index calculated on the basis of measurements made on scaffoldings and data from meteorological stations, respectively for the Łódź and Lower Silesian voivodships.

a)

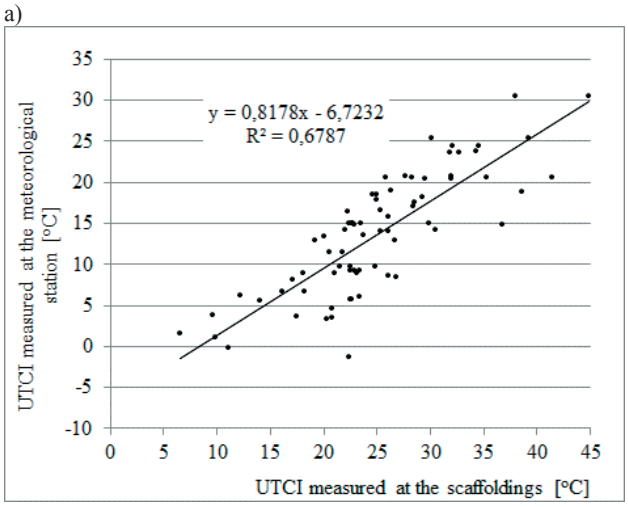

b)

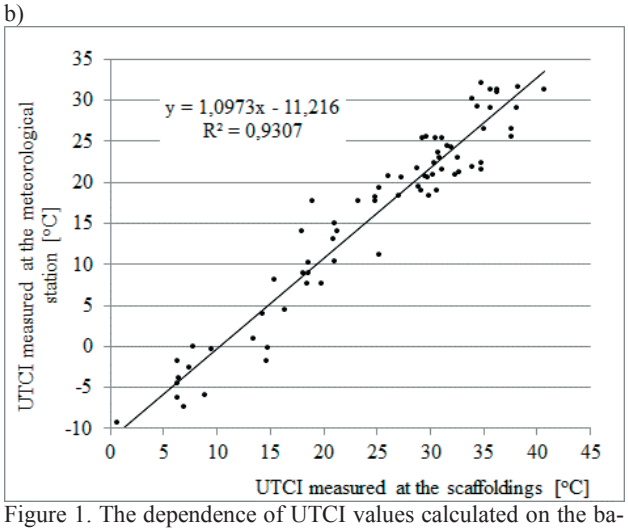

Figure 1. The dependence of UTCI values calculated on the basis of in-situ measurements on scaffoldings and respective meteorological station: (a) E12, E15, E16, E19, E20, (b) D12, D16, D17, D18, D20.

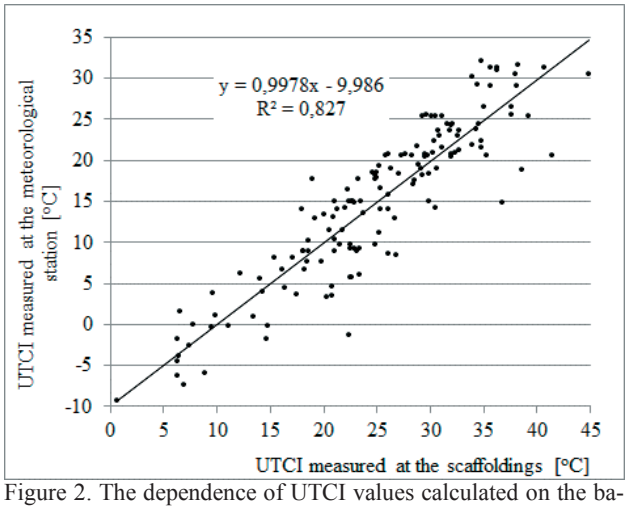

Figure 2. The dependence of UTCI values calculated on the basis of in-situ measurements on scaffolding and respective meteorological station; data for all scaffoldings.

The lowest slope of a straight line approximating results in Fig. 1 is observed for scaffoldings located in the Łódź voivodeship. In majority of cases structures were located in the city center. The air temperature, which is the main component of the UTCI indicator is always higher in the city center than the temperature outside the city. The value of the indicator is also influenced by the action of the building, including the reflection of solar radiation. A higher slope of approximating lines is observed for scaffoldings localized in the Lower Silesian voivodship. In this case most scaffoldings were located outside the city center, where the influence of buildings were less significant. To summarize, the relationship between UTCI calculated on the basis of measurements carried out on scaffoldings and meteorological stations for all structures is presented in Fig. 2.

4. Conclusions

The research has shown that the calculated values of the simplified index of human thermal loads – UTCI based on the measurements performed on scaffoldings and meteorological stations are correlated. Stronger correlation occurs for scaffoldings located in the Lower Silesian voivodship, while it is weaker for the results obtained for the Łódź voivodship due to the larger number of parameters affecting it. Using data measured at meteorological stations, it would be possible to determine the thermal loads acting on people working on scaffoldings. The paper presents test results for ten scaffoldings. Due to many factors affecting the UTCI index, among others, surrounding of the scaffolding, its height, the level of solar radiation reflection, the described results of tests can be the basis for indicating general dependencies. On the other hand, they cannot be use for the assessment of the quality of the relationships between values obtained on scaffoldings and meteorological stations. Therefore, studies on the working environment of people on scaffoldings should be developed.

5. Acknowledgments

The paper has been prepared as a part of the project supported by the National Centre for Research and Development within Applied Research Programme (agreement No. PBS3/A2/19/2015 "Modelling of Risk Assessment of Construction Disasters, Accidents and Dangerous Incidents at Workplaces Using Scaffoldings").

6. References

Błazik-Borowa E., Szer J., *Basic elements of the risk assessment model for the occurrence of dangerous events on scaffoldings*, Przegląd Budowlany 10 (2016) 24-29.

Błażejczyk K., Kunert A. *Bioklimatyczne uwarunkowania rekreacji i turystyki w Polsce*, Polska Akademia Nauk, 2011.

Coccolo S., Kämpf J., Scartezzini J.L., Pearlmutter D. *Outdoor human comfort and thermal stress: A comprehensive review on models and standards*, Urban Climate 18 (2016) 33-57.

Jabłoński M., Szer J., Szer I., Błazik-Borowa E., *Acoustic climate on scaffolding,* Materiały Budowlane 8 (2017) 32–34.

Jamińska-Gadomska P., Lipecki T., Bęc J., Błazik-Borowa E., *In-situ measurements of wind action on scaffoldings*, Proc. 7th EACWE, Liege, Belgium, 2017 (6 pages, USB, #179).

Szer I., Szer J., Cyniak P., Błazik-Borowa E., *Influence of temperature and surroundings humidity on scaffolding work comfort,* in Prevention of Accidents at Work, Taylor & Francis Group, 2017.

Traczyk Z. Trzebski A. *Fizjologia człowieka z elementami fizjologii klinicznej i stosowanej*. PZWL, Warszawa, 2004.